Final Report WY-2105F

State of Wyoming Department
of Transportation

SHRP2 Implementation Assistance Program (IAP)—Round 4

Concept to Countermeasures—Research to Deployment Using the SHRP2 Safety Data

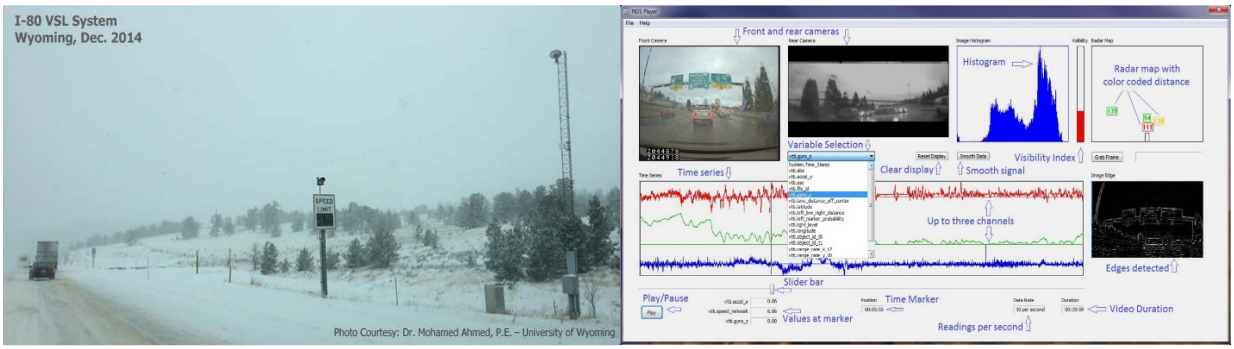

Driver Performance and Behavior in Adverse Weather Conditions: Microsimulation and Variable Speed Limit Implementation of the SHRP2 Naturalistic Driving Study Results - Phase 3

Prepared by:
Mohamed M. Ahmed, Ph.D., P.E.
Williams and Person Professor & WY Excellence Chair

Anik Das, Ph.D., P.E.
Md Nasim Khan, Ph.D., P.E.
Britton Hammit, Ph.D., P.E.
Elhashemi Ali, Ph.D.

October 2021

Phase 3 Final Report

From
Department of Civil and Architectural Engineering
University of Wyoming
1000 E. University Avenue, Department 3295
Laramie, Wyoming 82071
Telephone: (307) 766-5550
mahmed@uwyo.edu

U.S. Department of Transportation
Federal Highway Administration

American Association of State Highway and Transportation Officials
AASHTO
The Voice of Transportation

Transportation Research Board
of the National Academies
TRB

Disclaimer and Notices

This document is disseminated under the sponsorship of the Wyoming Department of Transportation (WYDOT) in the interest of information exchange. WYDOT assumes no liability for the use of the information contained in this document. WYDOT does not endorse products or manufacturers. Trademarks or manufacturers' names appear in this report only because they are considered essential to the objective of the document.

Quality Assurance Statement

WYDOT provides high-quality information to serve Government, industry, and the public in a manner that promotes public understanding. Standards and policies are used to ensure and maximize the quality, objectivity, utility, and integrity of its information. WYDOT periodically reviews quality issues and adjusts its programs and processes to ensure continuous quality improvement.

Working in Partnership

The second Strategic Highway Research Program (SHRP2) is a partnership of the Federal Highway Administration (FHWA), the American Association of State Highway and Transportation Officials (AASHTO), and the Transportation Research Board (TRB).

Copyright

Creative Commons:

Technical Report Documentation Page

1. Report No. WY-2105F	2. Government Accession No.	3. Recipient's Catalog No.	
4. Title and Subtitle Driver Performance and Behavior in Adverse Weather Conditions: Microsimulation and Variable Speed Limit Implementation of the SHRP2 Naturalistic Driving Study Results - Phase 3		5. Report Date October, 2021 6. Performing Organization Code	
7. Author(s) Mohamed Ahmed, Ph.D., P.E. (orcid.org/0000-0002-1921-0724) Anik Das, Ph.D. (orcid.org/0000-0003-4674-5334) Md Nasim Khan, Ph.D. (orcid.org/0000-0001-5996-091X) Britton Hammit, Ph.D. (orcid.org/0000-0002-8859-9075) Elhashemi Ali, Ph.D. (orcid.org/0000-0001-7643-7143)		8. Performing Organization Report No.	
9. Performing Organization Name and Address Department of Civil & Architectural Engineering University of Wyoming 1000 E. University Avenue, Dept. 3295 Laramie, Wyoming 82071		10. Work Unit No. (TRAIS) 11. Contract or Grant No. RS08217	
12. Sponsoring Organization Name and Address Wyoming Department of Transportation 5300 Bishop Blvd, Bldg 6100 Cheyenne, WY 82009-3340		13. Type of Report and Period Covered October, 2021 14. Sponsoring Agency Code SHRP2 - WYDOT	
15. Supplementary Notes Project Champions: Vince Garcia, FHWA Lead: Abdul Zineddin			
16. Abstract The negative impact of adverse weather conditions on traffic safety and operation is the primary focus of many studies. However, in-depth investigations of driver behavior and performance during adverse weather at a trajectory level using naturalistic driving data are limited. Over the years, researchers have utilized aggregate traffic and weather data to investigate their impact on roadway network operations and safety; however, these data might not represent the actual driving environment at a trajectory level. The novel approaches presented in this report, could fill existing gaps by investigating the safety and operational impacts of human behavior in conjunction with other factors related to weather, traffic, and roadway geometry via disaggregate trajectory-level data available through the Second Strategic Highway Research Program (SHRP2), Naturalistic Driving Study (NDS) and Roadway Information Databases. First, parametric and non-parametric models were utilized to better understand different behavioral factors, including lane-keeping, lane changes, gap acceptance, and speed selection, in adverse weather conditions. Findings from the behavioral investigation could be integrated into Weather-responsive Active Traffic Management (ATM) to disseminate safety messages in adverse weather conditions. Afterward, a unique radar-vision algorithm was developed to process trajectory-level data from instrumented vehicles to continuously predict driving states and estimate driving events using trips from the SHRP2 NDS. Subsequently, emphasis has been provided on developing reliable, accurate, and efficient machine learning-based lane change detection and prediction models through a data fusion approach considering different data availability. Additionally, essential indicators of near-crashes and the zone of interest for surrogate measures of safety were identified and thoroughly investigated. The lack of studies investigating driver behavior in adverse weather conditions stem from the fact that weather identification using video data is a daunting task. Therefore, several cost-effective and reliable detection systems were developed to detect trajectory-level weather information at a road-surface level in real-time using cutting-edge machine and deep learning techniques. Through crowdsourcing, real-time weather information can be integrated with Traffic Management Centers (TMCs) via Connected Vehicle Technologies. Finally, findings from the SHRP2 NDS were leveraged to develop Weather-based Microsimulation models to assess the safety and operational performance of ITS-based countermeasures on Wyoming freeways including Variable Speed Limit systems and the Wyoming Connected Vehicle Pilot Program. This study unlocked new horizons and potentials in conducting adverse weather-related research utilizing the NDS data, providing unprecedented opportunities to improve the reliability and effectiveness of safety and operational countermeasures.			
17. Key Words Naturalistic Driving Study, SHRP2, Driver Behavior and Performance, Road Weather Management, Speed Selection, Lane Keeping, Lane Change, Gap Acceptance, Car following, Radar-Vision, Machine Learning, Artificial Intelligence, Surrogate Measures of Safety, Image Processing, Deep Learning, Feature Selection, Microsimulation, Variable Speed Limit, Wyoming, Microsimulation, Connected Vehicles, Big-Data Analytics		18. Distribution Statement 	
19. Security Classification (of this report) Non-Classified	20. Security Classification (of this page) Non-Classified	21. No. of Pages 260	22. Price

Metric Conversion Factors

SI* (MODERN METRIC) CONVERSION FACTORS

APPROXIMATE CONVERSIONS TO SI UNITS

Symbol	When You Know	Multiply By	To Find	Symbol
		LENGTH		
in	inches	25.4	millimeters	mm
ft	feet	0.305	meters	m
yd	yards	0.914	meters	m
mi	miles	1.61	kilometers	km
		AREA		
in^2	square inches	645.2	square millimeters	mm^2
ft^2	square feet	0.093	square meters	m^2
yd^2	square yard	0.836	square meters	m^2
ac	acres	0.405	hectares	ha
mi^2	square miles	2.59	square kilometers	km^2
		VOLUME		
fl oz	fluid ounces	29.57	milliliters	mL
gal	gallons	3.785	liters	L
ft^3	cubic feet	0.028	cubic meters	m^3
yd^3	cubic yards	0.765	cubic meters	m^3
	NOTE: volumes greater than 1000 L shall be shown in m^3			
		MASS		
oz	ounces	28.35	grams	g
lb	pounds	0.454	kilograms	kg
T	short tons (2000 lb)	0.907	megagrams (or "metric ton")	Mg (or "t")
		TEMPERATURE (exact degrees)		
°F	Fahrenheit	5 (F-32)/9 or (F-32)/1.8	Celsius	°C
		ILLUMINATION		
fc	foot-candles	10.76	lux	lx
fl	foot-Lamberts	3.426	$candela/m^2$	cd/m^2
		FORCE and PRESSURE or STRESS		
lbf	poundforce	4.45	newtons	N
lbf/in^2	poundforce per square inch	6.89	kilopascals	kPa

APPROXIMATE CONVERSIONS FROM SI UNITS

Symbol	When You Know	Multiply By	To Find	Symbol
		LENGTH		
mm	millimeters	0.039	inches	in
m	meters	3.28	feet	ft
m	meters	1.09	yards	yd
km	kilometers	0.621	miles	mi
		AREA		
mm^2	square millimeters	0.0016	square inches	in^2
m^2	square meters	10.764	square feet	ft^2
m^2	square meters	1.195	square yards	yd^2
ha	hectares	2.47	acres	ac
km^2	square kilometers	0.386	square miles	mi^2
		VOLUME		
mL	milliliters	0.034	fluid ounces	fl oz
L	liters	0.264	gallons	gal
m^3	cubic meters	35.314	cubic feet	ft^3
m^3	cubic meters	1.307	cubic yards	yd^3
		MASS		
g	grams	0.035	ounces	oz
kg	kilograms	2.202	pounds	lb
Mg (or "t")	megagrams (or "metric ton")	1.103	short tons (2000 lb)	T
		TEMPERATURE (exact degrees)		
°C	Celsius	1.8C+32	Fahrenheit	°F
		ILLUMINATION		
lx	lux	0.0929	foot-candles	fc
cd/m^2	$candela/m^2$	0.2919	foot-Lamberts	fl
		FORCE and PRESSURE or STRESS		
N	newtons	0.225	poundforce	lbf
kPa	kilopascals	0.145	poundforce per square inch	lbf/in^2

*SI is the symbol for the International System of Units. Appropriate rounding should be made to comply with Section 4 of ASTM E380.
(Revised March 2003)

Table of Contents

List of Figures

List of Tables

List of Acronyms

AADT	Average Annual Daily Traffic
AASHTO	American Association of State Highway and Transportation Officials
ABS	Antilock-Braking System
ACC	Adaptive Cruise Control
AdaBoost	Adaptive Boosting
ADAS	Advanced Driver Assistance Systems
ADHD	Attention Deficit Hyperactivity Disorder
AES	Autonomous Emergency Braking
AIC	Akaike Information Criterion
AMS	Analysis, Modeling, and Simulation
ANN	Artificial Neural Network
ASWM	Average Silhouette Width Method
ATIS	Advanced Traveler Information System
ATM	Active Traffic Management
AUC	Area Under Curve
AV	Autonomous Vehicles
AVI	Automatic Vehicle Identification
AWP	All-Weather Paint
BF	Basis Function
CA	Cluster Analysis
CACC	Cooperative Adaptive Cruise Control
Caltrans	California Department of Transportation
CAN	Controller Area Network
CART	Classification and Regression Tree
CAS	Collision Avoidance Systems
CAT	Cooperative Automated Transportation
CAV	Connected and Autonomous Vehicle
CCTV	Closed-Circuit Television
CFA	Confirmatory Factor Analysis
CIE	International Commission on Illumination
CMF	Crash Modification Factors
CNDD	Commercially Collected NDD
CNN	Convolutional Neural Network
CORSIM	CORridor SIMulation
CTRE	Iowa State University Center for Transportation Research and Education
CV	Connected Vehicles
CV–VSL	Connected Vehicle-Based Variable Speed Limit

CVO	Commercial Vehicle Operation
CWS	Collison Warning System
DAS	Data Acquisition Systems
DBS	Dynamic Brake Support
DGPS	Differential Global Positioning System
DMS	Dynamic Massage Signs
DNN	Deep Neural Network
DOT	Department of Transportation
DRAC	Deceleration Rate to Avoid Collision
DSRC	Dedicated Short Range Communication
DT	Decision Tree
DTLB	Distance to the Lane Boundary
EFA	Explanatory Factor Analysis
FA	Factor Analysis
FARS	Fatality Analysis Reporting System
FC	Fully Connected
FFS	Free Flow Speed
FHWA	Federal Highway Administration
FOT	Field Operational Test
FRA	Federal Railroad Administration
FV	Following Vehicle
GCV	Generalized-Cross-Validation
GEH	Geoffrey E. Havers
GIS	Geographic Information System
GLCM	Gray Level Co-occurrence Matrix
GPS	Global Positioning System
GPU	Graphics Processing Unit
HAR	Highway Advisory Radio
HCM	Highway Capacity Manual
HMI	Human-Machine Interface
HOG	Histogram of Oriented Gradients
HPMS	Highway Performance Monitoring System
HSIS	Highway Safety Information System
HUD	Head-up Display
IAP	Implementation Assistance Program
ISS	Intelligent Safety Systems
K-NN	K-Nearest Neighbor
LBP	Local Binary Pattern

LCV	Lane-changing Vehicle
LD	Loop Detector
LDW	Lane Departure Warning
LiDAR	Light Detection and Ranging
LOS	Level of Service
LR	Logistic Regression
LSTM	Long Short-Term Memory
LV	Lead Vehicle
MANOVA	Multivariate Analysis of Variance
MARS	Multivariate Adaptive Regression Splines
ML	Machine Learning
MPR	Market Penetration Rate
MSE	Mean Square Error
MUTCD	Manual on Uniform Traffic Control Device
MZSF	Maximum Z Score Among Shadow Features
NB	Naïve Bayes
NCAR	National Center for Atmospheric Research
NCDC	National Climate Data Center
NDD	Naturalistic Driving Data
NDS	Naturalistic Driving Study
NFOT	Naturalistic field operational test
NHTSA	National Highway Traffic Safety Administration
NOAA	National Oceanic and Atmospheric Administration
OBU	On-Board Units
PAM	Partitioning Around Medoids
PCA	Principal Component Analysis
PDO	Property Damage Only
PET	Post Encroachment Time
PII	Personally Identifiable Information
RALPH	Rapidly Adapting Lateral Position Handler
ReLU	Rectified Linear Unit
RF	Random Forest
RID	Roadway Information Database
RMSE	Root Mean Square Error
RNN	Recurrent Neural Network
ROC	Receiver Operating Characteristic Curve
RSLC	Road Surface Luminance Curve
RSS	Residual Sum of Squares

RVD	Radar Vehicle Detection
RWIS	Roadway Weather Information System
SAR	Synthetic Aperture Radar
SCE	Safety-critical Event
SDLP	Standard Deviation of Lane Position
SEM	Structural Equation Modeling
SGB	Stochastic Gradient Boosting,
SHRP2	Second Strategic Highway Research Program
SMoS	Surrogate Measures of Safety
SVM	Support Vector Machine
TIM	Traveler Information Messages
TMC	Traffic Management Center
TTC	Time to Collision
USDOT	United States Department of Transportation
UW	University of Wyoming
V2I	Vehicle-to-Infrastucture
V2V	Vehicle-to-Vehicle
VDOT	Virginia Department of Transportation
VIF	Variance Inflation Factor
VMS	Variable Massage Sign
VMT	Vehicle Miles Travelled
VSL	Variable Speed Limit
VTTI	Virginia Tech Transportation Institute
WRMS	Weather Responsive Management Strategies
WRTM	Weather Responsive Traffic Management
WYDOT	Wyoming Department of Transportation
XGBoost	eXtreme Gradient Boosting

Chapter 1. Introduction

Motor vehicle crashes are considered one of the significant causes of morbidity and mortality, and they cause more deaths than most human diseases every year. According to the National Highway Traffic Safety Administration (NHTSA), about 94 percent of crashes are directly related to driver behavior. Moreover, human error is estimated to be the primary factor in more than 85 percent of crashes (*1*). Human errors while driving could be exacerbated by adverse road weather conditions due to poor visibility, slippery roadways, and a significant reduction in driver speed perception. According to the Federal Highway Administration (FHWA), adverse weather is responsible for around 21 percent of vehicle crashes, 19 percent of injury crashes, and 16 percent of fatal crashes each year in the United States (US) (*2*). A study by Andrey et al. concluded that weather-related factors could increase traffic fatalities and injuries by 25 percent and 45 percent, respectively (*3*). Another study reported that a one-unit reduction in visibility in snowy weather could increase the crash risk by 88 percent (*4*). A recent pile-up crash involving over 100 vehicles on Interstate-80, Wyoming, caused the death of three people and the closure of the interstate for two days (*5*). Although different studies quantified the impact of adverse weather on crashes differently, the overall trend from these studies indicates that the crash risk increases substantially during inclement weather. In addition, traffic speed, volume, and capacity can be reduced by 64 percent, 44 percent, and 27 percent, respectively, due to inclement weather (*2*).

Drivers' behavioral inconsistency in adverse weather can be predicted through driver behavior models, which requires high resolution and reliable driving data. However, safety researches are mostly based on aggregated traffic data from spot sensors, weather data from weather stations, historical crash data from police reports, and other similar sources (*6, 7*). Although these data have greatly contributed to the understanding of the contributing factors affecting crash occurrence and impacting roadway safety, one of the major limitations of using such data are that driver performance and behavior are considerably missing. In addition, the aggregate nature of such data is unable to provide insights at a trajectory level; i.e., what happened before, during, and after critical safety events. Currently, the most commonly used approaches for investigating driver behavior are simulator studies, instrumented car studies, self-report studies, and analysis of crash statistics. These methods have greatly contributed to the understanding of road user behavior and other crash-related factors. However, they have several limitations. For instance, driver behavior in a simulator or in a controlled environment may not properly represent the actual behavior in normal driving conditions. More specifically, driver behavior and performance might be biased, and they may not behave naturally, as they do in real life. Exclusive trajectory-level Naturalistic Driving Study (NDS) data collected by the second Strategic Highway Research Program (SHRP2) can overcome the above-mentioned limitations. This unique dataset provides an unprecedented opportunity for researchers to analyze driver performance and behavior through numerous amounts of representative natural driving data, by compiling a wide variety of traffic and environmental conditions. The SHRP2 NDS data make it possible to gather fundamental data on how people drive; how they avoid crashes, navigate, maintain speed; stay within their lane; control the vehicle; and how these vary according to age, experience, driver state, driver condition, and other roadway and environmental factors. The SHRP2 is the largest study on naturalistic driving behavior to date in the US. Between 2010 and 2013, the SHRP2 program has monitored approximately 3,100 participant drivers and produced over 33,000,000 travel miles from 3,800 vehicle-years of driving (*8, 9*). The SHRP2 collected a total of about t

petabytes of NDS data from six states around the US, including Florida, Indiana, New York, North Carolina, Pennsylvania, and Washington, as shown in Figure 1. In addition, a complementary database—Roadway Information Database (RID)—was constructed to provide context for NDS trips. The RID contains roadway, traffic operations, environmental, and other information corresponding to the most-travelled roadways traversed by the NDS participants *(13)*. The creation of these SHRP2 databases presents researchers an unmatched opportunity to advance current understandings of driving behavior and performance.

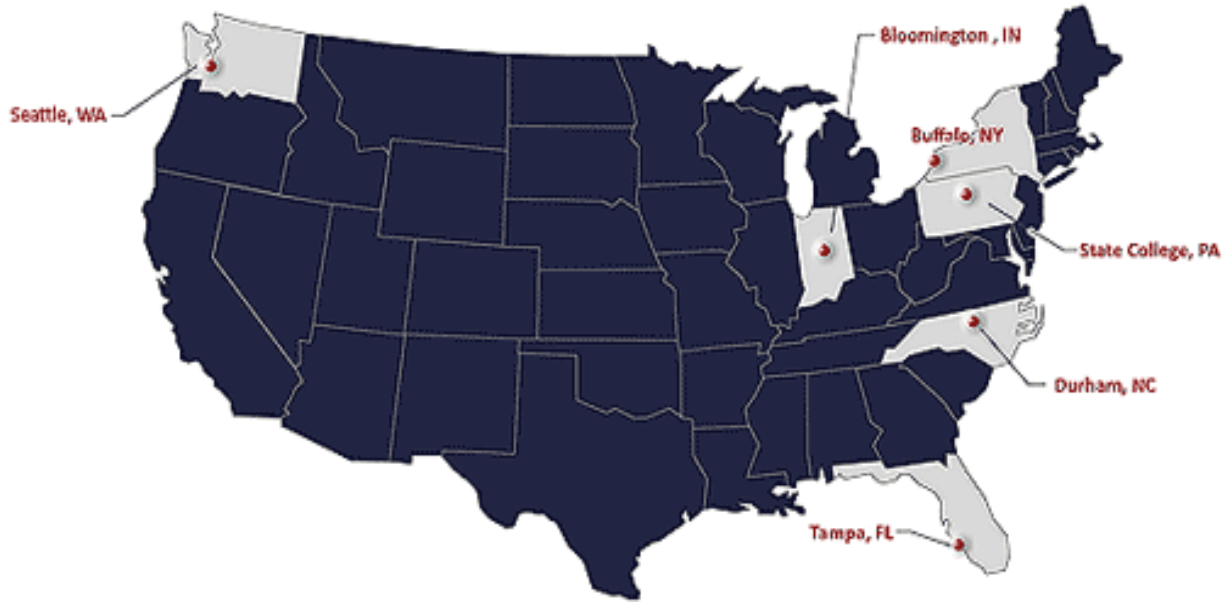

Figure 1 NDS Data Collection Sites *(10)*

As part of the SHRP2 Implementation Assistance Program (IAP), the Wyoming Department of Transportation (WYDOT) established a project to investigate the impact of adverse weather conditions on driving behavior for the purpose of establishing practical countermeasures to improve the safety, efficiency, and reliability of the Wyoming transportation network during harsh winter seasons. This project is expected to produce an updated variable speed limit (VSL) algorithm for the existing weather-dependent VSL corridors in Wyoming. In addition, the increased understanding of driving behavior in adverse weather conditions is expected to improve the accuracy of weather-related microsimulation modeling.

The SHRP2 IAP comprised three phases; this report presents the findings from the third project phase. The following section provides an overview of the Wyoming IAP objectives and research questions for Phase 3, summarizes previous findings from Phase 1 and Phase 2, and outlines the remainder of the report.

Project Objectives

The main objectives of the Wyoming SHRP2 IAP project are to utilize the SHRP2 NDS and RID databases to understand driver behavioral responses in adverse weather, and leverage the findings towards the development of Active Traffic Management (ATM) systems and feasible countermeasures that can be implemented by WYDOT to improve the reliability of the transportation network during adverse weather conditions. In order to achieve the aforementioned research objectives, the following research questions have been addressed in Phase 3:

- Can driver behavior (e.g., speed selection, car-following, lane keeping, lane change, and gap acceptance) during inclement weather conditions be characterized efficiently from the NDS data?
- Can the SHRP2 NDS video data be effectively used to develop a cost-effective trajectory-level weather detection system in real-time?
- What are the most appropriate surrogate measures for weather-related crashes that can be identified using the NDS data?
- Can human factors be effectively integrated to update the existing weather-dependent VSL control algorithm used by WYDOT for their interstate VSL systems and to assist in conceptualization of a Connected Vehicle-based VSL (CV-VSL) system?
- Can we improve guidance related to microsimulation modeling of adverse weather conditions, and generate a "base model" to represent driving behavior in adverse weather conditions for evaluating road weather connected vehicle applications to be used in the Wyoming Connected Vehicle (CV) Pilot project impact assessments?

The first goal in transitioning from Phase 2 to Phase 3 was to investigate additional driving behavior from the identified NDS trips occurring during adverse weather. The first phase allowed the collection of trips in various levels of precipitation based on activation of drivers' windshield wiper. In Phase 2, the research team introduced two additional data acquisition methods to collect significantly more trips. The developed data acquisition methodologies enabled the research team to develop more representative driver behavior models in Phase 3. Several driver behaviors, including speed selection, car-following, lane keeping, lane change, and gap acceptance, were thoroughly investigated and potential readily implementable countermeasures have been recommended. In addition, to gain further insights into driver lateral behavior this research also developed trajectory-level lane change detection and prediction models based on features from vehicle kinematics, machine vision, roadway characteristics, and driver demographics.

One of the vital purposes of Phase 3 was to develop a cost-effective trajectory-level weather detection system in real-time using the SHRP2 NDS video data and to explore their potential safety applications in Wyoming. For the first time, extensive data reduction steps were taken to identify and classify the various levels of adverse weather conditions to form a unique ground-truth dataset. Seven levels of weather conditions have been identified, including clear, light rain, heavy rain, light snow, heavy snow, distant fog, and near fog, and used to develop real-time weather detection system based on advanced machine learning and artificial intelligence techniques. Several recommendations have been provided to integrate the findings to the Wyoming roadways leveraging the existing roadside webcams. Real-time weather information could be shared with Traffic Management Centers (TMCs) utilizing crowdsourcing to aid in developing the next generation of traffic management and CV-VSL systems.

This research was then concentrated on detecting near-crash events on freeways using continuous naturalistic data and provided recommendations to enhance traffic safety, especially in CV environments. The research leveraged the SHRP2 NDS data for an early investigation of Surrogate Measures of Safety (SMoS) on freeways which revealed that trajectory-level vehicle kinematics data could be utilized to identify the contributing factors increasing the likelihood of near-crash events, especially in adverse weather. The finding could be used to define the interest zone of vehicle kinematics as indicators of near-crash events. The significant time zone was

determined to be the 11-seconds preceding the event timestamp using a parametric model and 23-seconds using non-parametric models. Therefore, the time zone of interest resulting from non-parametric models is more accurate in detecting near-crash events compared to the logistic regression model.

The ultimate goal in completing the third phase is to transfer the research outcomes into tangible and effective countermeasures that will improve the safety, operation, and efficiency of interstate roads during inclement weather conditions. The research team worked on translating raw vehicle kinematics, video feeds, roadway characteristics, and driver information into strategies that can be used to support and evaluate Weather-Responsive Traffic Management (WRTM) alternatives. The WYDOT was an early adopter of rural VSLs, and since implementation, has been seeking to refine control logic to automatically set speed limits. This research updated the existing VSL logic based on insightful findings from SHRP2 NDS related to driver behavior. In addition, this research contributed to the state-of-practice of microsimulation modeling by applying a methodology to use the SHRP2 NDS data to calibrate car-following models as a function of specific weather events. In addition, this study also suggested that the default parameters of microsimulation software, such as VISSIM, should be weather-specific to accurately develop Analysis, Modeling, and Simulation (AMS) tools for road weather CV applications. It is worth mentioning that the findings and baseline models developed in Phase 3 have been effectively used to test and evaluate the effectiveness of each CV application of the WYDOT CV Pilot Program.

Phase 1 Overview

Phase 1 of the Wyoming IAP project consisted of a proof-of-concept of the SHRP2 NDS and RID data that was intended to evaluate the feasibility of answering the research questions. Therefore, a small sample of NDS trips was queried from the SHRP2 NDS database, aiming to identify trips related to adverse weather conditions and matching trips occurring in clear weather conditions. Phase 1 data acquisition focused on precipitation events and queried trips from only two of the six SHRP2 sites; Washington and Florida. Trips occurring in precipitation were identified by tracking the windshield wiper status of the vehicles and extracting trips with active windshield wipers. In addition, a matching protocol was established in this phase to identify additional trips taken by the same driver on the same route in clear conditions.

Manual data reduction was performed in the first project phase to gain familiarity with the SHRP2 NDS data and suggest procedures for automating various elements of the process. The most time-consuming process involved manual video observation to classify weather conditions for each trip; therefore, the Wyoming research team began the development of the Wyoming NDS Visualization and Reduction software. This software provided an effective platform for viewing NDS data using a convenient graphical user interface and initialized efforts to detect visibility levels from the front video camera.

The preliminary analysis of driver behavior focused on selected speeds, acceleration, headways, and lateral lane position. As part of this analysis, behavior distributions in different classifications of adverse weather and traffic flow conditions were shown to be different. For example, in free-flow conditions and heavy rainfall, driver speeds followed a Weibull distribution, while in free flow and clear weather conditions, driver speeds followed a normal distribution. Additional findings suggested that speed reductions were statistically significant in heavy precipitation, and an increase in the speed variability during precipitation events was

detected. Aggressive braking and acceleration events were evaluated and findings suggested that average deceleration was higher in clear weather conditions, when compared to matching adverse weather trips.

Another avenue of research aimed to maintain the continuity of a single driver, on a single day, during various weather conditions. Detailed evaluations of specific trips were conducted to analyze the behavior changes of an individual driver on a trip that contained series of weather conditions (e.g., the trip's weather condition was initially classified as light rain, in the middle changed to heavy rain, and at the end was classified as clear conditions). The findings from this analysis indicated the importance of segmenting each trip by weather condition to ensure accurate results.

In addition to evaluating NDS, trips using summary statistics, preliminary modeling efforts were conducted to identify speed selection tendencies in different weather conditions. An ordered probit logit model was used to classify speed behavior as a function of traffic, speed limits, surface conditions, and weather. Results from this model indicated that weather, speed limits, and traffic conditions were significant, with weather and traffic conditions played the largest role in determining drivers' speed selection.

Finally, a small sample of weather-related crash and near-crash events were analyzed to identify crash surrogate measures. Two vehicle dynamics variables were used as indicators for identifying a potential crash; acceleration/deceleration and yaw rate. Thresholds for these variables were identified from a review of the available crash and near-crash events. More information about Phase 1 findings can be found in Phase 1 Final Report published in 2015, WY-16/08F, Driver Performance and Behavior in Adverse Weather Conditions: An Investigation Using the SHRP2 Naturalistic Driving Study Data-Phase 1 (*11*).

Phase 2 Overview

The objective of Phase 2 of the SHRP2 IAP was to conduct a thorough analysis using a larger set of NDS trips to extract behavioral trends specific to a wide variety of weather conditions on freeways. These weather conditions included rain, snow, and fog from a diverse driver population from the six SHRP2 data collection sites. Phase 2 addressed different gaps in the knowledge by presenting innovative methods to identify and analyze weather-related naturalistic driving data to better understand driver behavior and performance in adverse weather conditions. An innovative methodology to effectively identify weather-related trips in real-time using vehicle wiper status and other complementary methodologies helped to identify naturalistic driving weather-related trips using external weather data sources. In addition, a semi-automated data reduction procedure was developed to process raw trip data files into a format that further analyses and modeling techniques could be easily applied.

In addition to the contributions in data extraction and reduction, preliminary analysis, as well as advanced modeling techniques, were utilized in this study. These analyses were used to explain the relationship between different levels of speed selection and lane keeping behaviors and a set of contributing factors including roadway characteristics, environmental and traffic conditions, and driver demographics on a trajectory level. These modeling techniques ranged from common parametric approaches such as binary logistic regression and ordinal logistic/probit regression models to more advanced non-parametric/data mining modeling techniques such as Classification and Regression Trees (CART) and Multivariate Adaptive Regression Splines (MARS).

The results from this phase suggest that both parametric and non-parametric modeling approaches are important to analyze driver behavior and performance. In fact, this phase attempted to maximize the benefits of the advantages of parametric models, such as the ability to interpret the marginal effects of various risk factors, as well as the advantages of using nonparametric models, including but not limited to the ability to provide high prediction accuracy, handling of missing values automatically, and their capability of handling large number of explanatory variables in a timely manner, which might be extremely beneficial specifically for assessing traffic operations and safety in real-time considering weather and traffic data to be directly fed into the model.

The results of the developed speed selection models revealed that among various adverse weather conditions, drivers were more likely to reduce their speed in snowy weather conditions compared to other adverse weather conditions. Specifically, the odds of drivers reducing their speeds were 9.29 times higher in snowy weather conditions, followed by rain and fog with 1.55 and 1.29 times compared to clear conditions, respectively. In addition, variable importance analysis using CART method revealed that weather conditions, traffic conditions, and posted speed limits are the three most important variables affecting driver speed selection behavior. Moreover, the results of the developed lane-keeping models revealed that drivers in heavy rain conditions were more likely to have worse lane-keeping performance compared to clear weather conditions. More information about Phase 2 findings can be found in Phase 2 Final Report published in 2018, WY-18/05F, Driver Performance and Behavior in Adverse Weather Conditions: An Investigation Using the SHRP2 Naturalistic Driving Study Data-Phase 2 (*12*).

Report Organization

The remainder of this report presents the findings from Phase 3 of the Wyoming IAP project. The report is organized as follows:

- Chapter 2 - This chapter investigates driver behavior, including lane keeping, aggressive lane changing characteristics, gap acceptance, and speed selection, in clear and adverse weather conditions utilizing several statistical and data mining techniques.
- Chapter 3 - This chapter describes the development of data processing algorithms for trajectory-level data from instrumented vehicles to continuously predict driving states and estimate state transition events using trips from the SHRP2 NDS data.
- Chapter 4 - This chapter develops reliable and efficient lane change detection and prediction models considering features from available data sources through a data fusion approach. Several machine learning algorithms were trained, validated, tested, and comparatively analyzed based on different sets of features.
- Chapter 5 - This chapter presents the detection of surrogate measures of safety in adverse weather conditions.
- Chapter 6 - This chapter described the development of an in-vehicle weather detection system that can provide trajectory-level weather information in real-time. The system utilized the SHRP2 NDS video data and was based on advanced machine learning, deep learning, and image processing techniques.
- Chapter 7 - This chapter describes the integration of SHRP2 NDS findings to develop weather-based microsimulation models and to assess the safety and operational

performance of the WYDOT CV Pilot Program and the existing weather-based VSL system.

- Chapter 8 - This chapter provides summary and key findings, as well as recommendations for future research and practical applications.

Chapter 2. Driver Behavior Investigation

Driver behavior, surface conditions, vehicle performance, and visibility are negatively affected by adverse weather conditions, such as fog, rain, snow, ground blizzards, slush, and strong winds (*13–15*). Inclement weather conditions are major issues regarding safety as they contribute greatly to reduce visibility, which is one of the leading causes of crashes. Almost every year adverse weather causes a significant amount of fatalities in the US (*16, 17*). According to NHTSA data, weather contributed to 22 percent of vehicle crashes, 19 percent of crash injuries, and 16 percent of crash fatalities, between 2005 and 2014 (*18*). A previous study concluded that total injuries and fatalities increased by 25 percent on snowy days in the UK (*19*). Another study revealed that traffic collisions increased by 75 percent and related injuries increased by 45 percent due to precipitation compared to the normal conditions on Canadian roadways (*3*).

Literature Review

Lane Keeping Ability

The impact of adverse weather on safety and operation have been investigated in previous studies. Compared to other adverse weather conditions, fog is considered one of the most dangerous because of its irregular nature that can surprise drivers (*20*). Driving in fog can be critical and risky for all drivers due to reduced visibility. Poor visibility in fog caused several crashes over different years (*2, 21, 22*). A study on roadways in the UK found that injury crashes in heavy fog increased by 16 percent (*23*). Besides, researchers concluded that fog related crashes resulted in more severe injuries compared to clear conditions (*24, 25*).

Most of the previous studies on driver behavior in foggy weather conditions have been conducted using driving simulators. A study on longitudinal driver behavior concluded a significant decrease in acceleration and substantial increase in distance to the leading vehicle due to fog (*26*). The study of Kang et al. examined the effects of reduced visibility from fog and concluded that drivers tended to maintain a decent distance headway under the heavy fog conditions (*27*). Additionally, several previous simulated studies have investigated the effects of human factors on driving behavior in fog. A study investigated the effect of fog on distance perception and showed that people overestimated distance by 60 percent in foggy conditions (*28*). A study concentrated on the effects of driving experience on behavioral compensation due to fog found that experienced drivers drove at higher speeds in clear conditions, and showed a significant reduction in speed due to affected visibility compared to novice drivers (*29*). A previous study concluded that older drivers may have greater crash risk due to decreased ability to detect imminent collision events in fog (*30*). Another study examining car following performances suggested that during heavy fog, older drivers maintained a headway that was 21 percent less than younger drivers (*31*). In addition, it was found that the reason behind shorter headways in fog was to maintain better visual contact with the leading car (*32, 33*).

Reduced visibility due to fog affects safe driving behavior by obscuring the details of the environment and decreasing contrast (*34*). Due to the lower contrast, drivers are unable to perceive the necessary information from the roadway. Failure of recognizing this information can affect lateral control of driver (*33*). One of the lateral driver behaviors that can be highly associated with the run-off-road crashes is lane-keeping ability. A recent study revealed that run-off-road crashes contribute to an average of 57 percent of motor vehicle traffic fatalities occurred each year, where a major portion of these crashes occurred at nighttime and inclement weather conditions (*35*). Therefore, it is worth investigating driver lane-keeping performance in

inclement weather (foggy weather in this study) considering the contribution of poor lane keeping in run-off-road crashes.

Lane-keeping performance has been studied in the literature from driver distraction or reduction of visibility standpoints. A study conducted by Engström et al. examined the effect of visual and cognitive demand on lane-keeping performance, and found that lane-keeping performance was decreased by visual demand (*36*). Another study investigated driver inattention on lane-keeping performance and concluded that driver inattention, eyes-off-road, significantly decreased lane-keeping ability (*37*). Furthermore, the study of Barham et al. noted that reduced visibility was the main reason for the inconsistent and uncertain lateral position of drivers, which adversely affected lane-keeping performance (*38*). Using naturalistic driving study data, some recent studies found that adverse weather significantly decreased driver lane-keeping ability (*39–41*).

While previous studies used traditional parametric model to examine driver behavior, including lane-keeping ability (*37*, *39*, *40*, *42*, *43*), numerous data mining techniques have been utilized in prior studies (e.g., Decision Tree (DT), Random Forest (RF), Atrificial Neural Network (ANN), Factor Analysis (FA), Cluster Analysis (CA), MARS, etc.) because of their advantages over parametric models in many aspects (*41*, *44–48*). The association rules mining is one of the most popular and commonly used data mining techniques in transportation research; however, its use lied mainly in identifying contributing factors in crashes. Geurts et al. utilized association rule mining to identify accident patterns and characteristics in black spots (*49*). Pande and Abdel-Aty used an association rules algorithm to discover indirect association in crash data (*50*). Another study employed association rules in analyzing accident data of Iranian Railways to discover and explore hidden relationships and patterns among the data (*51*). A study focused on identifying crash contributory factors at urban roundabouts utilized association rules to explore the interdependences between these factors (*52*). A study conducted by Das and Sun applied association rules to investigate the pattern of traffic crashes under rainy weather conditions (*53*). In another study, association rules were utilized to discover patterns from vehicle-pedestrian crash database (*54*). Association rules technique has been attracted many attentions in recent years and in different fields including market basket analysis, medical record analysis, product recommendation and other fields to discover unknown patterns (*55–57*).

Lane Changing Characteristics based on Aggressiveness

Several studies have analyzed lane-changing behavior in different ways using different dataset. Data from instrumented vehicle were used in a study to identify the differences in lane-changing types during congested and uncongested traffic. The study categorized drivers into different groups (very conservative, somewhat conservative, somewhat aggressive, and very aggressive) based on their lane-changing characteristics (*58*). Another study of lane-changing behavior performed by Sun and Elefteriadou on urban streets also categorized drivers according to their lane-changing characteristics based on the personal background data, in-vehicle driver behavior and trajectory data (*59*). A study conducted by Wang et al. investigated the discretionary lane-changing characteristics using Next-Generation Simulation trajectory dataset and found that lane-changing duration followed a lognormal distribution and decreased with the navigation speed. In addition, they found no significant difference in lane-changing durations between left-to-right and right-to-left lane changes (*60*). A microscopic simulation study of four lane-changing strategies (speed leading, speed leading with overtaking, lane leading, and traffic leading) on traffic flow characteristics concluded that different lane-changing strategies might have various impact on the distribution of lane flow and freeway capacity. The study concluded

that number of lane-changing events will be decreased during higher densities in all strategies (*61*). Even though these studies utilized different dataset in examining lane-changing behavior, very few studies observed this behavior in a naturalistic setting. Lee et al. conducted the first naturalistic lane-changing analysis regarding frequency, duration, urgency, and severity of lane-changing with reference to maneuver type, direction, and other classification (*62*). Chen et al. used the 100-car NDS data in their study and found that frequency and time-to-collision (TTC) in naturalistic lane-changing events varied by vehicle speed (*63*). Another study conducted by Chen et al. predicted lane-changing maneuvers by developing an adaptive method from vehicle kinematics data based on the same dataset. The study concluded that drivers initiated steering maneuver for a lane-changing event within five seconds of lane crossing (*64*).

Although many studies investigated lane-changing characteristics using different parameters, few studies have specifically used lane-changing durations. A comprehensive examination of naturalistic lane-changing observed 8,667 lane changes from 16 participants with a mean duration of 9.07 s (*62*). The study conducted by Hill et al. collected 726 completed lane changes that were performed by 46 participants in an instrumented vehicle, and found the lane-changing durations ranged from 2.30 s to 13.8 s in addition to a mean of 5.48 s (*58*). Similarly, another study collected 282 lane changes from 16 participants who drove an instrumented vehicle. The study found the range of lane-changing durations varied from 3.41 s to 13.62 s with a mean of 6 s (*65*). Similar to the instrumented vehicle studies, Salvucci et al. identified average lane-changing duration of 5.14 s where 11 participants used a driving simulator (*66*). In another study, based on the trajectory dataset, Toledo et al. found the lane-changing duration ranged from 1 to 13 s with a mean of 4.6 s from the 1,790 identified lane changes (*67*). Overall, these studies suggested that range of lane-changing durations for cars varies widely from a minimum 1 s to a maximum 14 s. The probable reason for these variations might be the use of different datasets in different studies. For instance, trajectory-level data collected from driving simulator or instrumented vehicle studies are different from naturalistic driving. In addition, number of participants and definition of lane-changing event are also varied among various studies. These all contribute to the significant variations of lane-changing durations in several studies.

Driver aggressiveness is a crucial factor in microsimulation modeling, which is not currently incorporated in most of the microsimulation lane-changing models. There is a lack of studies that investigated the impact of foggy weather conditions on driver behavioral inconsistency in lane-changing decisions. Hence, it is essential to analyze driver behavioral aspects of lane-changing situations (e.g., aggressive lane changing) in order to calibrate realistic microsimulation lane-changing models in foggy conditions.

Gap Acceptance Behavior

A driver has to consider several factors while changing a lane, including speed, position of the vehicle, vehicle(s) in the target lane, as well as different vehicular characteristics, geographical characteristics of the roadway, and other factors, including weather and traffic characteristics (*68*). In order to execute a lane-changing maneuver, drivers assess the adjacent gap in the target lane, i.e., they evaluate the lead and lag gaps. The lane-changing decision is determined based on the availability of a safe gap in the target lane. Driver's inaccurate gap judgment and failure to accept a necessary safety gap after initiating a lane-changing maneuver might introduce high-risk driving maneuvers and could eventually result in a lane-changing crash (*68*). Therefore, gap acceptance is one of the critical elements of lane-changing analysis.

Different approaches for analyzing lane-changing gap acceptance can be found in the literature. Ahmed proposed a systematic approach for modeling lane-changing behavior using a discrete choice framework, where a gap acceptance model was utilized to characterize the execution of lane-changing maneuvers. Ahmed concluded that several important factors, including gap length, relative speed, distance remaining to the point at which lane change must be completed, etc., affect drivers' gap acceptance behavior (*69*). Toledo et al. modeled lane-changing gap acceptance as a binary choice problem by comparing the available space gaps with the critical gaps (minimum acceptable gap). They assumed that an available gap (i.e., lead and lag gap) was acceptable, if it was greater than the critical gap (*70*). Hill and Elefteriadou analyzed the lane-changing behavior on freeways by collecting data on drivers' desire speed, lane-changing duration, and gap acceptance, and found that drivers were more likely to accept smaller lag gaps during congested traffic conditions (*58*). Lee et al. developed a probability model for discretionary lane-changing maneuver (i.e., a maneuver that is intended to improve the perceived driving condition) in highways and found that both relative velocity and relative lead gap are the main criteria for discretionary lane-changing maneuvers and have similar positive influences on the choice probability model (*71*). In another study, Wang et al. developed multilevel mixed-effects linear models to examine the influencing factors of lane-changing gap acceptance and found that acceptance of lead and lag gaps were significantly affected by several factors, including environmental variable, vehicle type, and kinematic parameters (*72*).

In recent years, the use of numerous nonparametric techniques has increased due to their advantages over the traditional parametric techniques in investigating driver behavior (*41*, *73*, *74*). MARS is becoming one of the most popular nonparametric approaches in transportation fields. However, researchers mostly used this technique to develop crash prediction models and to identify crash-contributing factors. Haleem et al. utilized MARS model to develop crash modification factors for urban freeway interchange influence areas (*75*). Park and Abdel-Aty assessed the safety effects of multiple roadside treatments by estimating CMF using the MARS model (*76*). In another study, the MARS model was utilized to predict rear-end crashes at unsignalized intersections (*77*). A study focused on the analysis of freeway accident applied the MARS model to explore the effects of non-behavioral factors, including roadway geometric characteristics, traffic factors, and environmental conditions on the frequency of freeway accidents (*78*). Another study conducted by Gaweesh et al. applied the MARS model to develop crash prediction models for a case study of Wyoming Interstate 80 (*79*). Apart from the crash analysis perspective, the MARS model has been recently utilized in other transportation fields (e.g., traffic flow prediction, vehicular emission prediction, fuel consumption estimation, etc.) to model complex relationships and interactions (*80–82*).

Speed Selection Behavior

The effects of adverse weather on driver speed behavior have been investigated in previous studies. FHWA reported 5 to 40 percent, 3 to 13 percent, and 3 to 16 percent reduction in average speed attributable to snow, light rain, and heavy rain, respectively (*18*). The Highway Capacity Manual (HCM) stated 5 to 64 percent and 1 to 7 percent reduction in speed in heavy snow and rain, respectively (*4*). Based on traffic and weather data on the Metro freeway in the Twin Cities (St Paul and Minneapolis Minnesota), the study of Agrawal et al. (*83*) concluded that during light rain, and heavy rain, the free-flow speeds were reduced by 2 to 4 percent, and 4 to 7 percent, respectively. In another study, Rakha et al. (*84*) analyzed the impact of inclement weather on traffic stream behavior and reported free-flow speed reduction up to 19 percent and 9

percent due to snow and rain, respectively. In another study, Hogema et al. (*85*) observed the driving behavior of a 12 km long road segment on the A16 Motorway, in the Netherlands, for more than two years and found 8 to 10 kph speed reduction because of the poor visibility caused by fog. The study in Liang et al. (*86*) found similar results with a speed reduction of 8 kph due to the presence of fog on the roadways. Another study conducted by Perrin Jr. et al. (*87*) quantified the impact of wet pavement on free-flow speed. This study reported a 10 percent reduction in speeds due to wet surfaces, 13 percent due to wet and snowy surfaces, 25 percent due to wet and slushy surfaces, and 30 percent due to slushy surfaces.

Data Reduction and Preparation

Lane Keeping Ability

Utilizing the developed method, as described in Chapter 2, the research team collected fog-related NDS trips with their matched trips in clear conditions. Afterward, manual video verifications were conducted in order to filter out the trips that occurred in clear weather conditions. The next step of data reduction procedure was to reduce the dimensionality of the NDS data by selecting the most relevant time-series variables of interest. Subsequently, the received NDS trips were segmented into 1-minute time interval to preserve the consistent weather conditions within a single trip (*12*, *88*, *89*). This step also involved manual video observation and annotation of 1-minute environmental and traffic conditions. To maintain consistency and eliminate subjectivity in the manual video annotation process, video reviewers were trained comprehensively with several sample images and detailed written descriptions. Also, manual post verification was conducted by external reviewers. Figure 2, Figure 3, and Figure 4 exhibit sample images of heavy fog, distant fog, and clear weather that were provided during the manual annotation process.

Figure 2 Heavy Fog.

Figure 3 Distant Fog.

Figure 4 Clear Weather.

In this study, 124 trips in foggy weather conditions with their corresponding 248 trips in matched clear weather (i.e., 2 clear trips:1 foggy weather trip) were randomly selected and reduced for analyzing the lane-keeping behavior. The selected NDS trips involved 62 drivers who drove the same vehicle and same routes in both fog and clear weather conditions on freeways. These 62 driver ages ranged from 16 to 79 with a significant number of drivers in age group 30-34, and gender was mainly balanced among age groups. In total, 7,147 1-minute segments were reduced from the selected NDS trips. Once the non-freeway segments were removed, 5,584 1-minute segments that are equivalent to nearly 93 hours of driving time and around 8,196 traveled km in freeways were considered for the final analysis. Afterward, roadway characteristics provided in the RID database and driver demographics provided in the SHRP2 administrated survey questionnaires were linked with each 1-minute segment to create a final modeling dataset.

Lane Changing Characteristics Based on Aggressiveness

There were 214 trips in foggy weather conditions, with their corresponding 214 trips in matched clear weather, were reduced and randomly selected from the acquired NDS trips for analyzing the lane-changing behavior. The selected 214 trips involved 125 drivers (57 male and 68 female) who drove the same vehicle and same freeway routes in both fog and clear weather conditions, and aged between 16 to 89 years with a significant number of drivers in age group 20 to 24. The overall process from data reduction to analysis for investigating lane changing behavior is illustrated in Figure 5. Identifying lane-changing events in the reduced one-minute segmented

aggregate files was a challenging and a time-consuming task. To effectively identify lane-changing events occurring in fog and clear weather conditions; an interactive data visualization and reduction tool was developed. This tool has the capability of synchronizing the forward and rear camera videos with the time-series variables of interest (*11*). Lane position offset variable from the time-series data was used to identify lane-changing events and compute the duration of each lane-changing event. The variable is estimated from the distance to the left or right of the center of the lane and center of the vehicle based on machine vision techniques (*90*). Using the data visualization and reduction tool, and lane position offset variable from time-series data, all lane-changing maneuvers were manually identified in each one-minute segment from the reduced aggregated files.

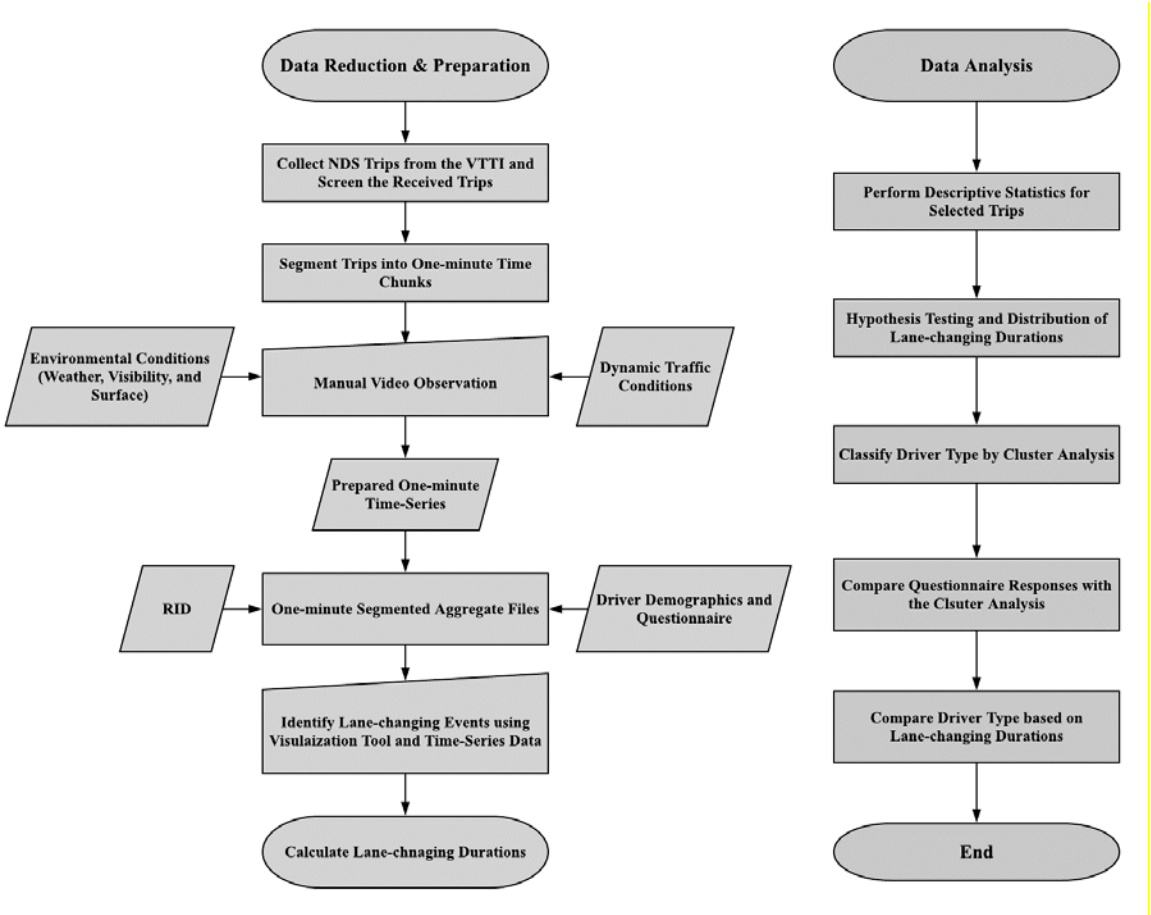

Figure 5 Summary of Data Reduction and Analysis Process

During the manual identification of lane-changing events, different maneuver types were identified based on a previous study by Lee et al. (*62*). Subsequently, the duration of each lane-changing event was calculated from the plot of lane position offset with time, as shown in Figure 6. In this figure, a lane-changing event is shown in a trip that traversed in foggy conditions on Interstate 5, in Washington.

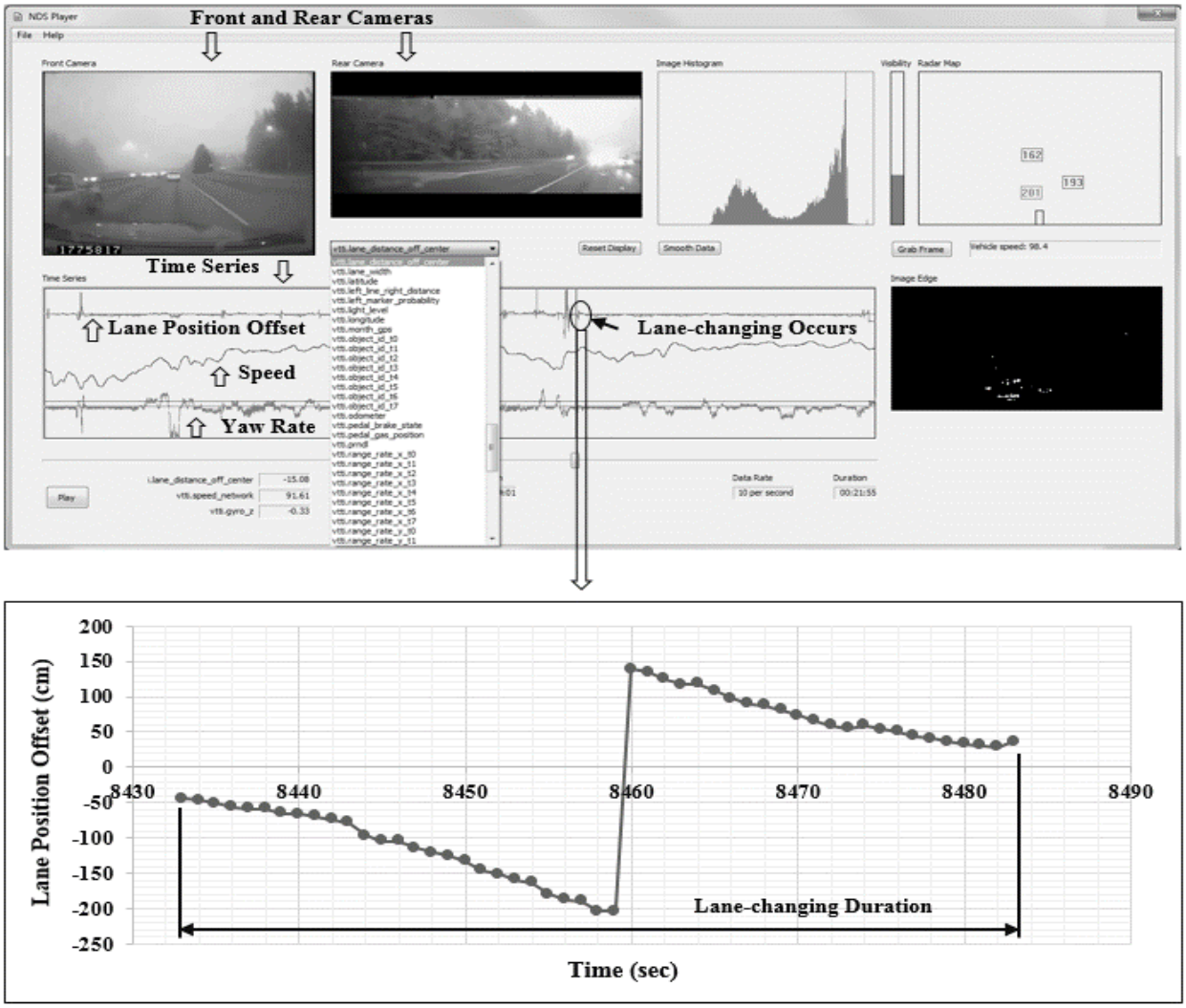

Figure 6 Identification of Lane-Changing Maneuvers from NDS Data (Trip ID: 52637998, I-5, Washington)

Gap Acceptance Behavior

DAS-equipped NDS vehicles had only radar data from a front-mounted radar. Considering the fact that front-mounted radar cannot detect the presence of a lag vehicle (i.e., the vehicle behind the NDS vehicle's lane), it is not possible to consider the NDS vehicle as a subject vehicle for gap acceptance analysis. Therefore, in order to investigate the lane-changing gap acceptance behavior, the vehicles adjacent to the NDS vehicle's lane were considered as the LCV in this study; where NDS vehicle served as a FV and provided the opportunity to analyze gap acceptance behavior of the vehicle (i.e., LCV) in front of it, as shown in Figure 7. Figure 7 demonstrates a lane-changing event in a trip performed by an LCV in clear weather conditions.

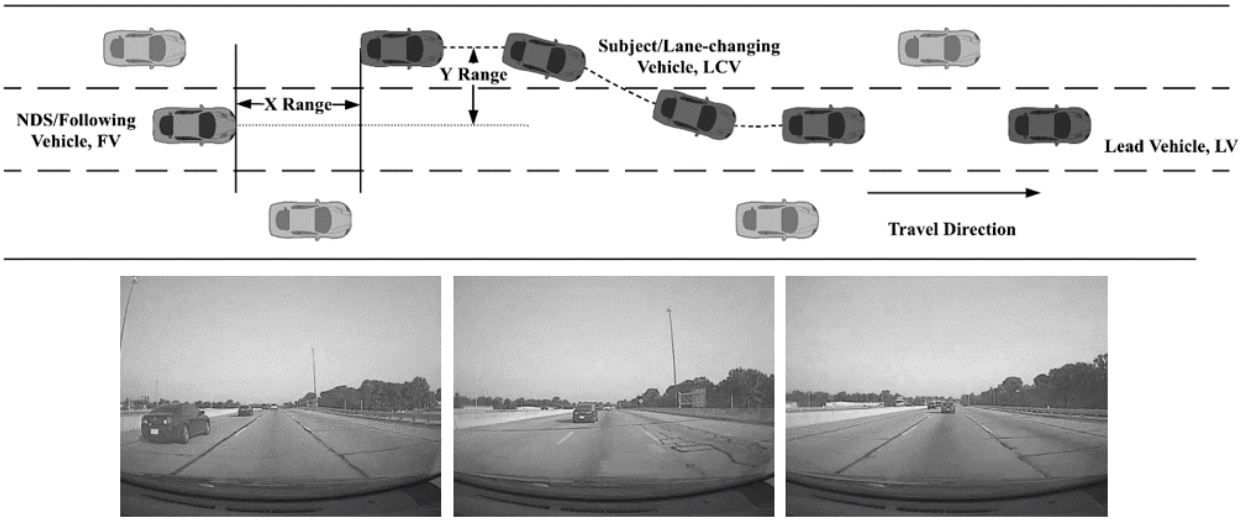

Figure 7 Typical Lane-changing Event

It is worth mentioning that authors had only access to data of LCV recorded by the NDS vehicle's front radar. In fact, gap acceptance analysis requires a lot of data processing for the front-mounted NDS radar data since these data are not readily available in the SHRP2 NDS data. Additionally, working with radar data is not straightforward because of its noisy nature and the limited distinction between detected object categories. Moreover, several NDS trips might exist with missing radar data or other erroneous values. Therefore, an effective algorithm was needed to be developed for processing radar data efficiently. This study developed an automatic algorithm to identify the lane-changing event and corresponding parameters for analyzing gap acceptance behavior. In order to develop the algorithm, the following steps were considered:

1. Some received NDS trips had missing radar data. NDS trips with missing radar data were imputed using *fillmissing* function of MATLAB, where missing data were imputed through linear interpolation of non-missing neighboring values (*91*). It is worth mentioning that no imputations were made if more than 10 percent of data were missing and those data were discarded from the algorithm.
2. Afterward, radar data were smoothed with *smoothdata* function of MATLAB using 'movemedian' method. The method helped to reduce the periodic trends in the data due to some outliers (*92*).
3. The presence of potential LCV on the nearest lane was determined considering the following criteria. The algorithm proceeded further only if the first criterion was met.
    - $If\ |Y_{lcv}| > |Y_l|$, potential LCV is on the nearest lane with respect to the NDS vehicle
    - $If\ |Y_{lcv}| < |Y_l|$, potential LCV is on the NDS vehicle's lane.

    Where, Y_{lcv}= left/right lateral distance between potential LCV and FV

    Y_l= distance from vehicle centerline to inside of left/right side lane marker based on a vehicle-based machine vision technique (*90*)
4. In order to ensure FV (i.e., NDS vehicle) did not move in a lateral direction, i.e., changed a lane, corresponding events were eliminated. The lane-changing maneuver of FV was identified using lane position offset variable from the NDS data. A threshold of ±100 cm

lateral shift (i.e., left and right) in the position of a FV was considered as a lane-changing maneuver (*41*). Figure 8 shows a sample of lane-changing maneuver (left to right) with lane position offset value above 100 cm and the peaks in the figure represent the occurrence of lane-changing maneuver of the FV. As can be seen in Figure 8, the value of lane position offset started to increase indicating that FV started to move laterally from left to right of the lane center until the value reaches a maximum point. A jump was then occurred representing the FV reached the far right of the driver's adjacent lane.

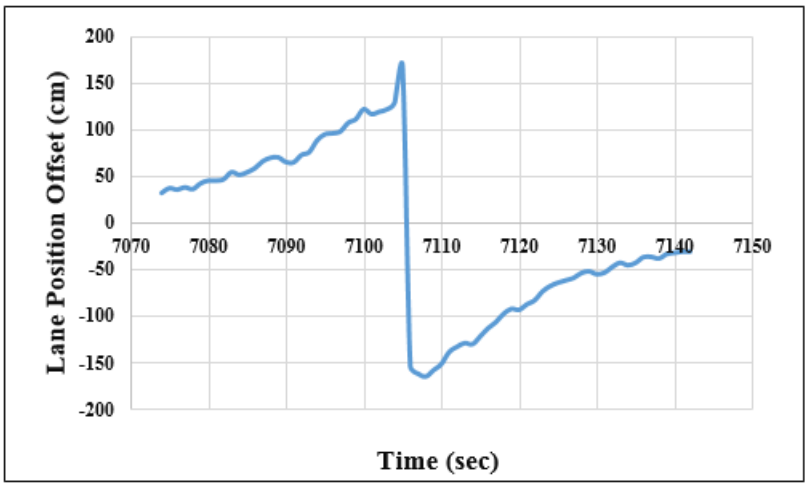

Figure 8 Demonstration of Automated Identification Process of FV's Lane-Changing Maneuver Using Lane Position Offset

5. The presence of lead vehicle (LV) on the NDS vehicle's lane was ensured considering the following criteria.

    - $If\ |Y_{lv}| < |Y_l|$, LV is on the NDS vehicle's lane
    - $If\ |Y_{lv}| > |Y_l|$, LV is not on the NDS vehicle's lane

    Where, Y_{lv}= left/right lateral distance between LV and FV

    These criteria were checked for all possible Y ranges. The velocity of LCV and FV (more than 1 meter/seconds were checked in this step in order to ensure that the two vehicles are in motion (*72*).

6. The local maximum (peak) of the Y range of potential LCV (i.e., identified in Step 3) was determined using *findpeaks* function of MATLAB. The peak is defined as the starting point of a lane-changing event.

7. Every local peak of the Y range was checked up to a 20 s period. Based on the literature, the maximum duration of lane-changing maneuver can vary up to 15 seconds. Therefore, 20 seconds was conservatively selected to capture all the lane-changing events. Additionally, a gradual reduction of Y range was considered to identify a lane-changing event. The end of the lane-changing event was determined when the Y range was close to zero. As an example, Figure 9 exhibits the Y range of a lane-changing scenario. The starting point of the lane-changing event is shown in A in the figure. Once the lane-changing event was initiated, the LCV's Y range started to decrease and approached to zero. When the LCV's Y range

touched the first zero value, it was considered the completion of lane-changing event. This point is the end of lane-changing event and is denoted as B in Figure 9. The time required for the LCV to travel from A to B was defined as the lane-changing duration.

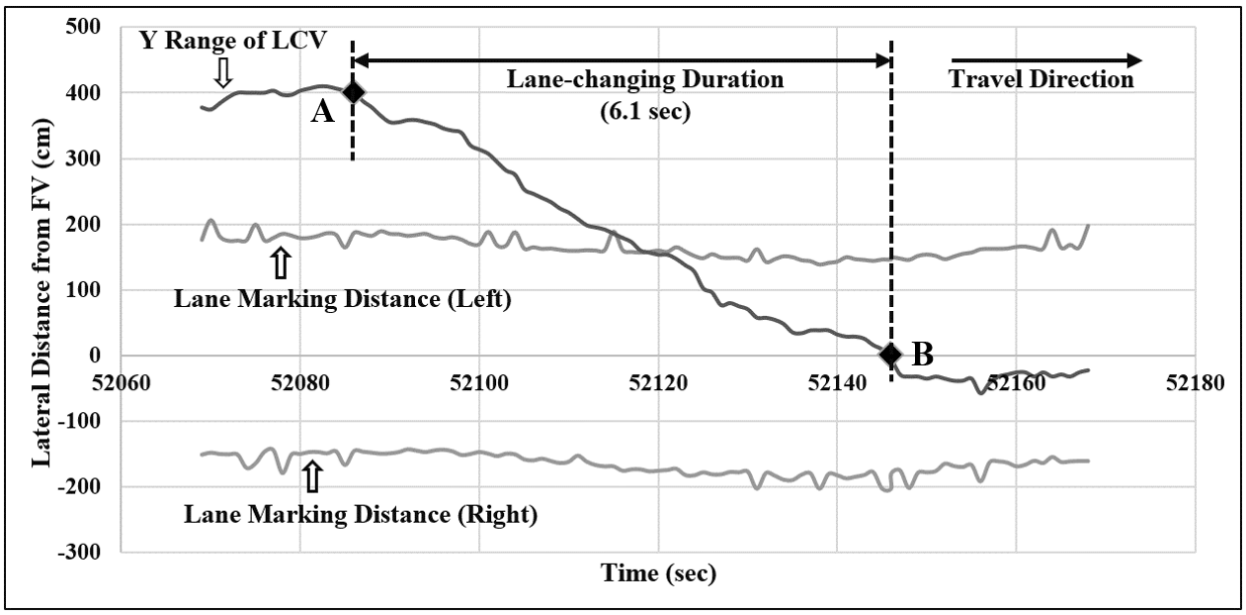

Figure 9 Y Ranges of a Lane-Changing Event

8. Once the lane-changing event was identified, lead and lag gaps were calculated. This study defined distance in terms of time rather than space, as time represents better driver behavior compared to space. The LCV is concerned with sufficient time for a safe lane-changing maneuver with corresponding travel speed. Therefore, time gaps provide better representation than distance gaps (*93*). The gaps were calculated when the LCV started its movement laterally from the current lane to the desired lane. Lead gap was denoted as the time taken to traverse the longitudinal distance between LV and LCV. On the contrary, lag gap represented the time taken to traverse the longitudinal distance between FV and LCV (*72*).
9. The identification algorithm (Step 1 to 8) repeated for the entire received NDS trips automatically in the MATLAB environment. In addition, a database was developed after extracting the necessary parameters for gap acceptance. The overall methodology used for automatic identification of lane-changing events has been shown in Figure 10.

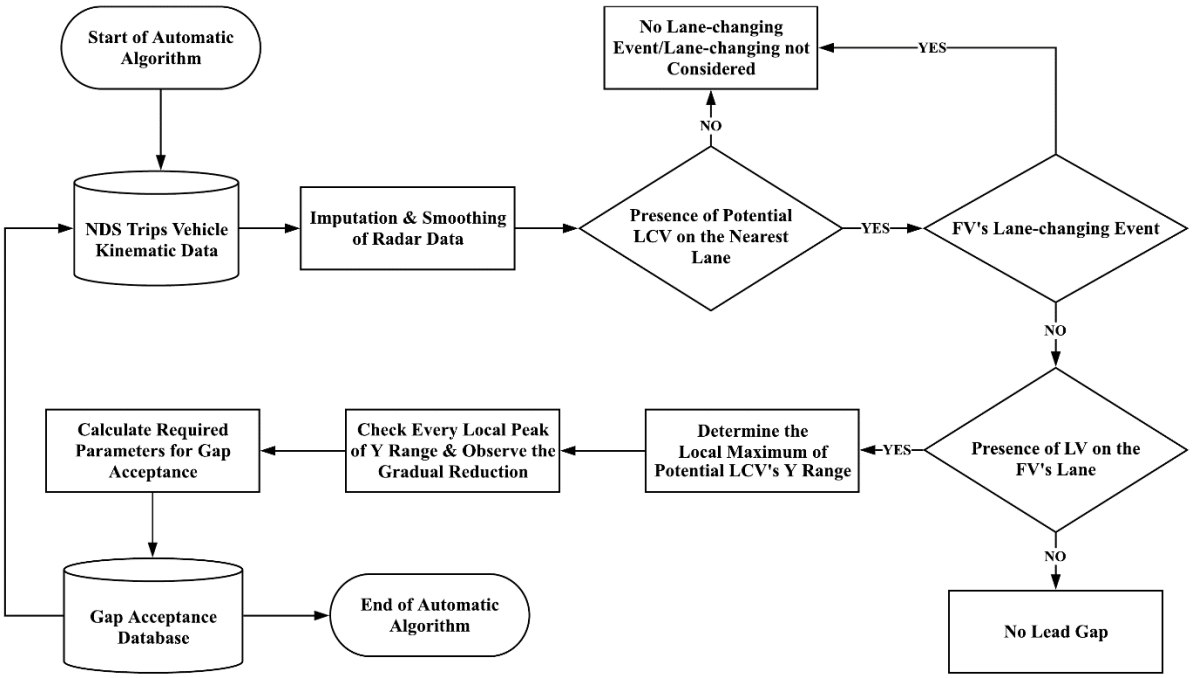

Figure 10 Automatic Algorithm for Identifying Lane-Changing Events Using Radar Data

After developing the automatic algorithm, all identified lane-changing events were manually verified using the Wyoming NDS Visualization and Reduction Tool (*12*, *94*). This step involved manual video observation and annotation of environmental conditions (i.e., weather, surface, and visibility), traffic states, and lane-changing maneuver types for each extracted lane-changing event within a single trip. In this study, 361 trips were randomly selected and considered for analyzing gap acceptance behavior. In total, 599 lane-changing events were verified and reduced from the selected NDS trips using the data visualization and reduction tool. Afterward, roadway characteristics provided in the RID database were linked with each lane-changing event to create a final modeling dataset.

Speed Selection Behavior

As mentioned earlier, the collected NDS trips had mainly three kinds of data: a) time-series data containing the information related to vehicle kinematics, b) survey questionnaires responses of the NDS drivers containing data related to driver demographics, and c) video data of the roadways. Expectedly, weather and traffic conditions were found to be inconsistent throughout the NDS trips. Therefore, first, the times series data were divided into 1-minute segments. Subsequently, the average vehicle kinematics were calculated over the 1-minute chunks, and driver demographics data were added to each 1-minute segment. Next, weather and traffic conditions were collected from manual video observation and added to the 1-minute segments. The traffic condition was grouped into two categories: free-flow considering Level of Service (LOS) A and B; and mixed-flow/congested-flow considering LOS C to F. The weather was categorized into four categories: clear, rain, snow, and fog, based on the following criteria.

- Clear: Excellent visibility; dry/wet/snowy road surface; road sign, marking, and surroundings are clearly visible.
- Rain: Raindrops are visible; wet road surface; affected visibility.

- Snow: Snowflakes are visible; snowy road surface; affected visibility.
- Fog: The horizon is undefinable; dry/wet/snowy road surface; affected visibility.

Finally, the RID data were also merged into each 1-minute segment using the ArcGIS software. A total of 10,046, 2,023, 1,231, and 2,026 1-minute segments in clear, rain, snow, and fog, respectively, were identified following the data reduction process.

The speed selection behavior was considered as the response variable in the models and grouped into four categories: 1) more than 5 mph above the speed limit, 2) between 0 to 5 mph above the speed limit, 3) between 0 to 5 below the speed limit, and 4) more than 5 mph below the speed limit. These intervals were selected based on the fact that for practical applications, such as VSL, speeds are usually incremented by 5 mph. Figure 11 shows the graphical representation of the response variable (*95*).

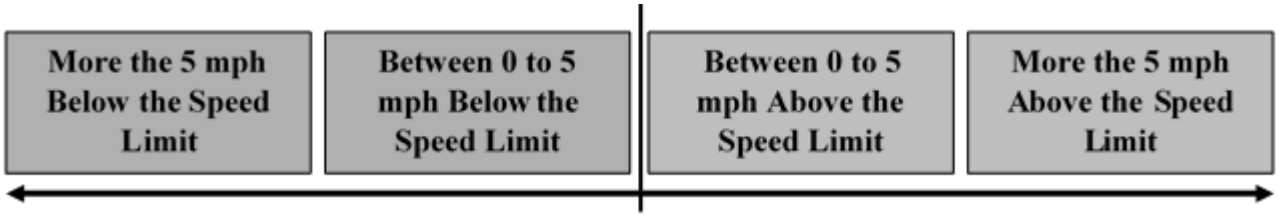

Figure 11 Graphical Representation of the Response Variable of the Speed Selection Models

The remaining variables are explanatory variables, including environmental variables, traffic conditions, driver demographics, and roadway factors. Table 1 shows a summary of the variables used in the speed selection models. Note that the same variables were used to calibrate both the association rules mining and the ordered logit model.

Table 1 Overview of the Selected Variables

Variable	Description	Levels	Frequency	Percentage
Response Variable				
Speed Selection	Percent speed reduction above or below the speed limit	1 = More the 5 mph above the speed limit	4765	31.1
		2 = Between 0 to 5 mph above the speed limit	3946	25.1
		3 = Between 0 to 5 below the speed limit	2081	13.6
		4 = More than 5 mph below the speed limit	4534	29.6
Explanatory Variables				
Weather	Predominant weather conditions in 1-min video observation	1 = Clear	10046	65.5
		2 = Rain	2023	13.2
		3 = Snow	1231	8
		4 = Fog	2026	13.2
Visibility	Predominant visibility conditions in 1-min video observation	1 = Not Affected	11192	73.0
		2 = Affected	4134	27.0
Surface	Predominant surface conditions in 1-min video observation	1 = Dry	11941	77.9
		2 = Wet	2285	14.9
		3 = Snowy/Icy	1100	7.2
Traffic Condition	Predominant traffic conditions in 1-min video observation	1 = Free Flow	8896	58.0
		2 = Mixed Flow	6430	42.0
Speed Limit	Predominant speed limit conditions in 1-min min video observation	1 ≤ 60	10328	67.4
		2 > 60	4998	32.6
Curve	Presence of curve in 1-min segment	1 = No curve	9994	65.2
		2 = Curve	5332	34.8
Number of lanes	Average number of lanes in 1-min segment	1 ≤ 2 lanes	7217	46.5
		2 > 2 lanes	8199	53.5
Gender	The gender the participant	1 = Female	7849	51.2
		2 = Male	7411	48.8
Age	The age group corresponding to the driver's birthdate	1 = Young (≤ 25 years)	6103	39.8
		2 = Middle (25 - 65)	7705	50.3
		3 = Old (≥ 65)	1518	9.9
Marital Status	The participant's marital status	1 = Single	5862	38.2
		2 = Married	8056	52.6
		3 = Other (Divorced, Widow)	1408	9.2
Driver Mileage Last Year	The approximate number of miles the participant drove last year	1 ≤ 10,000 miles	3412	22.3
		2 = 10,000 to 20,000 miles	9406	61.4
		3 ≥ 20,000 miles	2508	16.4
Driving Experience	Number of years of driving experience	1 < 10 years	33.5	33.5
		2 ≥ 10 years	66.5	66.5
Vehicle Class	The participant's vehicle class	1 = Passenger Car/SUV	12378	84.0
		2 = Minivan/Pick-up	2448	16.0

Methodology

As discussed earlier, the primary emphasis of this study was to investigate the impact of adverse weather on driver behavior by employing several statistical techniques, including parametric, non-parametric, clustering, and data mining approach. The details of the used methods are described in the following section.

Ordinal Logit Regression

An ordered logistic model can provide relationship between a response variable and explanatory variables. A logistic model has several advantages, such as it can handle non-linear effect and interaction terms *(38-39)*. In addition, predictor variables in logistic model do not have to be normally distributed or have equal variance in each group *(40)*. Moreover, the model result can be interpreted very easily by odds ratio *(41-42)*. Logistic regression modeling has been utilized in previous traffic safety and operation studies *(30)* and *(43)*. The ordinal logit model is a regression model for the ordinal dependent variable. This model uses cumulative probabilities up to a threshold, which makes the whole range of ordinal categories binary at that threshold (*96*). In this study, the driver behavior (i.e., speed selection and lane keeping ability) were considered as the response variable. The log of the probabilities of response variable can be expressed using the following equation.

$$logit[P(Y \leq j)] = log\frac{P(Y \leq j)}{1-P(Y \leq j)} = log\frac{\pi_1 + \ldots\ldots + \pi_j}{\pi_{j+1} + \ldots\ldots + \pi_c} = \alpha + \beta x_i, \qquad j = 1, \ldots\ldots, c-1$$

Equation 1

Where, $P(Y \leq j) = \pi_1 + \ldots\ldots + \pi_j$ is the cumulative probabilities of a response variable level less than or equals to j associated with a vector of explanatory variables x_i for NDS driver i , c is the number of possible outcomes ($c = 4$ in this study), α is a vector of cutoff points for the model, and β is a vector of the regression coefficient.

Association Rules Mining

Data mining technique focuses on identifying valuable information from large datasets. The process involves machine learning, statistical techniques, and database management systems to discover this valuable information in the form of associations, interesting patterns, and significant structures. Data mining techniques can be classified into two groups, descriptive and predictive. The descriptive data mining technique demonstrates the general properties of the data and illustrates the dataset in a compact way. On the contrary, the predictive approach attempts to anticipate the behavior of the new dataset (*97*).

Association rule is a popular descriptive data mining approach and a commonly used rule-based machine-learning method for discovering interesting relations of variables in large databases. The technique is intended to uncover obscured patterns in an itemset (a set of environmental, traffic, roadway geometry, and driver demographic factors in this study) that occur together or alone in a given event (i.e., a measure of lane-keeping performance in this study) using several algorithms. Among different algorithms, Apriori algorithm, introduced by (*98*), is one of the most widely used algorithms to mine association rules. The Apriori algorithm applies level-wise search for mining frequent itemsets. The study utilized Apriori algorithm of association rules to explore key association factors in driver lane-keeping performance.

Before explaining the method, a set of definitions needs to be provided, $I = \{i_1, i_2, \ldots i_3\}$ be a set of items and $D = \{t_1, t_2, \ldots, t_n\}$ be a set of database lane-keeping performance information called transaction. Each lane-keeping performance information in D contains a subset of the items in I.

An association rule can be defined as A → B, where, A, B ⊆ I and A ⋂ B = ∅ (*99*). Here, A is called the antecedent or left-hand-side (LHS), and B is consequent or right-hand-side (RHS) (*54*). It is worth mentioning that the interference made by an association rule does not suggest direct causation. Rather it implies the strong association between the antecedent and consequent of the rule.

Mining Interesting Rules

Various measures of significance and interest are used to select interesting rules. Among them, support, confidence, and lift are the most commonly used. The support of an association rule is defined as the percentage of lane-keeping performance (i.e., percentage of transaction) in the entire dataset covered by the rule (*100*). Equation 2 represents the support of association rule (A → B)

$$\text{Support, } s(A \rightarrow B) = \frac{\sigma\,(A \cap B)}{N} \qquad \text{Equation 2}$$

Where $\sigma\,(A \cap B)$ = Number of rules with particular lane-keeping performance (i.e., poor or good lane-keeping) where both A and B are present. N is the total number of lane-keeping performance.

The confidence of an association rule, c(A → B) can be measured as the percentage of lane-keeping performance (i.e., transaction) containing A that also contains B (*101*). The equation of confidence can be expressed as follows:

$$\text{Confidence, } c(A \rightarrow B) = \frac{s(A \rightarrow B)}{s(A)} \qquad \text{Equation 3}$$

However, an association rule A → B needs to satisfy the following constrains:

$$\text{Support, } s(A \rightarrow B) \geq minsup \qquad \text{Equation 4}$$

$$\text{Confidence, } c(A \rightarrow B) \geq mincon\,f \qquad \text{Equation 5}$$

Where, *minsup* and *mincon f* are the minimum support and minimum confidence, respectively.

Considering minimum support is important to find out a particular significant item in the dataset. A more popular and practical measure to rank the found rules is lift (*102*). The lift can be expressed as a measure of the deviation of the support of the whole rule from the support expected under independence given the support of antecedent and consequent (*100*). In other words, the lift of a rule is the ratio of the confidence of the rule and its expected value. The lift of an association rule, l(A → B) can be calculated as:

$$\text{Lift, } l(A \rightarrow B) = \frac{s(A \rightarrow B)}{s(A) \times s(B)} \qquad \text{Equation 6}$$

Where s(A) and s(B) denotes the support of an antecedent and a consequent. A lift value of 1 indicates the independence of the antecedent and consequent. A lift value greater than 1 suggests the positive independence (i.e., antecedent and consequent appear more often together than expected) between antecedent and consequent, whereas a lift value less than 1 suggests the negative independence (i.e., antecedent and consequent appear less often together than expected) (*103*) (*49*).

K-means Clustering

A clustering technique was adopted to classify driver into different categories based on their number of discretionary lane-changing events per mile and speed differences (i.e., difference

between mean speed and posted speed limit) while driving on freeways. Cluster analysis is a data-mining tool for identifying several driver behaviors and has been used successfully in various transportation research (*104–106*). Previous studies used the K-means clustering approach to classify drivers into groups (*59*, *104*, *107*). In this study, K-means cluster method was utilized to identify driver aggressiveness in fog and clear weather conditions. Drivers were classified into different categories based on feature X; where X is defined as:

X = [number of discretionary lane-changing events, and speed differences] Equation 7

K-means clustering is a type of unsupervised learning that is used to solve clustering problems. This method aims to classify a given dataset through a certain number of groups represented by the variable k (*108*). Using a predetermined number of clusters, the K-means clustering method partitions the observations into k clusters. In the k clusters, each observation is assigned to the cluster whose mean is closest to its value. The algorithm works through an iterative process to allocate each data point to one of the k groups according to the provided features (*109*). The required number of iterations may vary from a few to several thousand depending on the number of clusters and patterns, and the input data distribution (*110*). Euclidean metric is used in K-means algorithm for computing distance between points and cluster centers (*111*). The main goal of K-means algorithm is to minimize within-cluster sum of squares that is shown in the following equation.

$$\arg min_S \sum_{i=1}^{k} \sum_{Xj \in Si} ||Xj - \mu i||^2 \quad \text{Equation 8}$$

Where X_j (j = 1, 2…, n) are the set of observed data which includes the number of discretionary lane-changing events and speed differences in the perspective of this study. Si (i = 1, 2…, n) are the set of clusters k and μ_i represents the mean of cluster S_i.

The determination of the number of clusters is very crucial. Although there is no perfect method for determining the exact value of k, a number of heuristics are available for choosing the optimal number of clusters (*109*, *112*). In this study, different statistical measures (e.g., pseudo F statistics, Cubic Clustering Criterion (CCC), etc.) were considered to find out the optimal number of clusters for different groups in fog and clear weather conditions (*113*).

Multivariate Adaptive Regression Splines (MARS)

MARS is a nonparametric piecewise multivariate regression technique introduced by Friedman and can be used to model complex relationships among variables (*114*). In the MARS model, the space of independent variables is split into several regions separated by knots. Then it fits a spline function that consists of several polynomial basis functions (BF) between these knots smoothly. The general form of the MARS model is shown in the following equation (*41*, *76*, *77*, *114*).

$$\hat{y} = b_0 + \sum_{m=1}^{M} b_m + BF_m(x) \quad \text{Equation 9}$$

Where, $\hat{y}$ is the predicted response variable (i.e., lead and lag gap in this study), b_0 is the coefficient of constant BF, b_m is the coefficient of the basis function number (m), $BF_m(x)$ is the basis function number (m) for the independent variable x, and M is the total number of BFs.

There are two main phases to fit a MARS model. The first phase is the model generation that is composed of two stages, forward-stepwise regression selection technique, and the backward-stepwise elimination process. The second phase is the model selection. In the forward-stepwise selection stage, an initial model starts with a constant only. BFs are developed using equation 1

and added to the model in several regions of the independent variables. Afterward, the model searches for significant variable-knot combination, and the model improvement is assessed. The interactions are also introduced in this stage to improve the model fit. The search process is repeated until the best variable-knot combination is identified (*41*, *75*, *76*, *115*).

In the backward-stepwise elimination stage, the model identifies a BF with the lowest contribution and eliminate based on the residual sum of squares (RSS) criteria, as provided in equation 2 (*79*). After refitting the model, the model again identifies a BF to eliminate using the same criteria. The elimination process is repeated until all the BFs have been removed. The final results of the elimination process is a different series of candidate models (*115*).

$$RSS = \sum_{i=1}^{n}(y_i - \hat{y})^2 \quad \text{Equation 10}$$

The second and final phase to fit a MARS model is the model selection phase. The selection of the final model is based on the generalized-cross-validation (GCV) criterion or closeness between the training mean square error (MSE) and the test MSE. It is worth mentioning that a penalty for the model complexity is applied for the GCV criterion. The penalty is based on the degrees of freedom charged per each developed knot (*77*, *79*).

$$GCV(M) = \frac{1}{n}\frac{\sum_{i=1}^{n}(y_i-\hat{y})^2}{(\frac{1-C(M)}{n})^2} \quad \text{Equation 11}$$

$$C(M) = M + dM \quad \text{Equation 12}$$

Where, n is the number of lane-changing events, y_i is the lead/lag gaps for observation i, C (M) is the complexity penalty function, d is the defined cost for each BF optimization.

Results and Discussions

Lane Keeping Ability

Descriptive Statistics

After reducing the 372 NDS trips considered in this study, in total 7,147 one-minute segments (2,549 segments in fog, and 4,598 segments in matched clear weather) were reduced for further analysis. Once non-freeway segments were removed, 5,587 segments (1,912 segments in fog, and 3,675 segments in matched clear weather) were considered in developing the lane-keeping ordered logistic regression model. As mentioned earlier, weather conditions were not consistent within a single trip *(34)*. Therefore, considering the entire clear trip as a matched to a fog weather trip would not provide accurate results. Therefore, it is necessary to identify the exact matching routes that traversed in fog and corresponding clear trips. A GIS-based procedure was developed and utilized to identify exact corresponding traversed routes in matched trips in clear weather conditions, as shown in . After matching trips spatially, in total 5,398 one-minute segments (1,867 segments in fog, and 3,531 segments in matched clear weather) were considered for preliminary analysis. Table 2 breaks the categorization of these 5,398 one-minute segments into two different traffic states (free-flow and non-free-flow). Free-flow conditions indicated those conditions, when NDS driver has a leading vehicle existing at least in one lane but not affected by other vehicles, or has no leading vehicle in any lanes. Non-free-flow conditions considered other conditions when NDS drivers were affected by ambient traffic *(34)*. The summary statistics for the number of one-minute segments, total travel time, the length of routes along with their matching clear trips are provided in Table 2. A total of 5,398 one-minute

segments in clear and foggy weather conditions contained a total of 8,335 km of freeways and traveled over 89.97 hours in the six NDS states.

Table 2 Summary Statistics of NDS Trips (One-Minute Segment)

	Weather Condition	Heavy Fog	Matched Clear	Distant Fog	Matched Clear	Total
Free-flow Condition	**No of One-Minute Segment**	241	539	717	1467	**2964 one-minute segments**
	Total Duration (hr)	4.02	8.98	11.95	24.45	**49.40 hr**
	Total Length (km)	418.59	973.72	1260.29	2637.26	**5289.86 km**
Non-Free-flow Condition	**No of One-Minute Segment**	271	405	638	1120	**2434 one-minute segments**
	Total Duration (hr)	4.52	6.75	10.63	18.67	**40.57 hr**
	Total Length (km)	340.35	542.85	750.54	1411.11	**3044.85 km**
Total	**No of One-Minute Segment**	512	944	1355	2587	**5398 one-minute segments**
	Total Duration (hr)	8.54	15.73	22.58	43.12	**89.97 hr**
	Total Length (km)	758.94	1516.57	2010.83	4048.37	**8334.71 km**

It is worth mentioning that precise matching between trips occurred in foggy conditions and their corresponding matched clear trips was required to account for confounding factors in the preliminary analysis, this is not the case for the ordered logistic regression. From 5,398 one-minute segments, 2,964 one-minute segments in free-flow condition were considered for the preliminary analysis. As an example, a traversed route in fog on I-4, Florida, is shown in Figure 12 along with two matching trips to illustrate the procedure of eliminating non-matching segments in GIS.

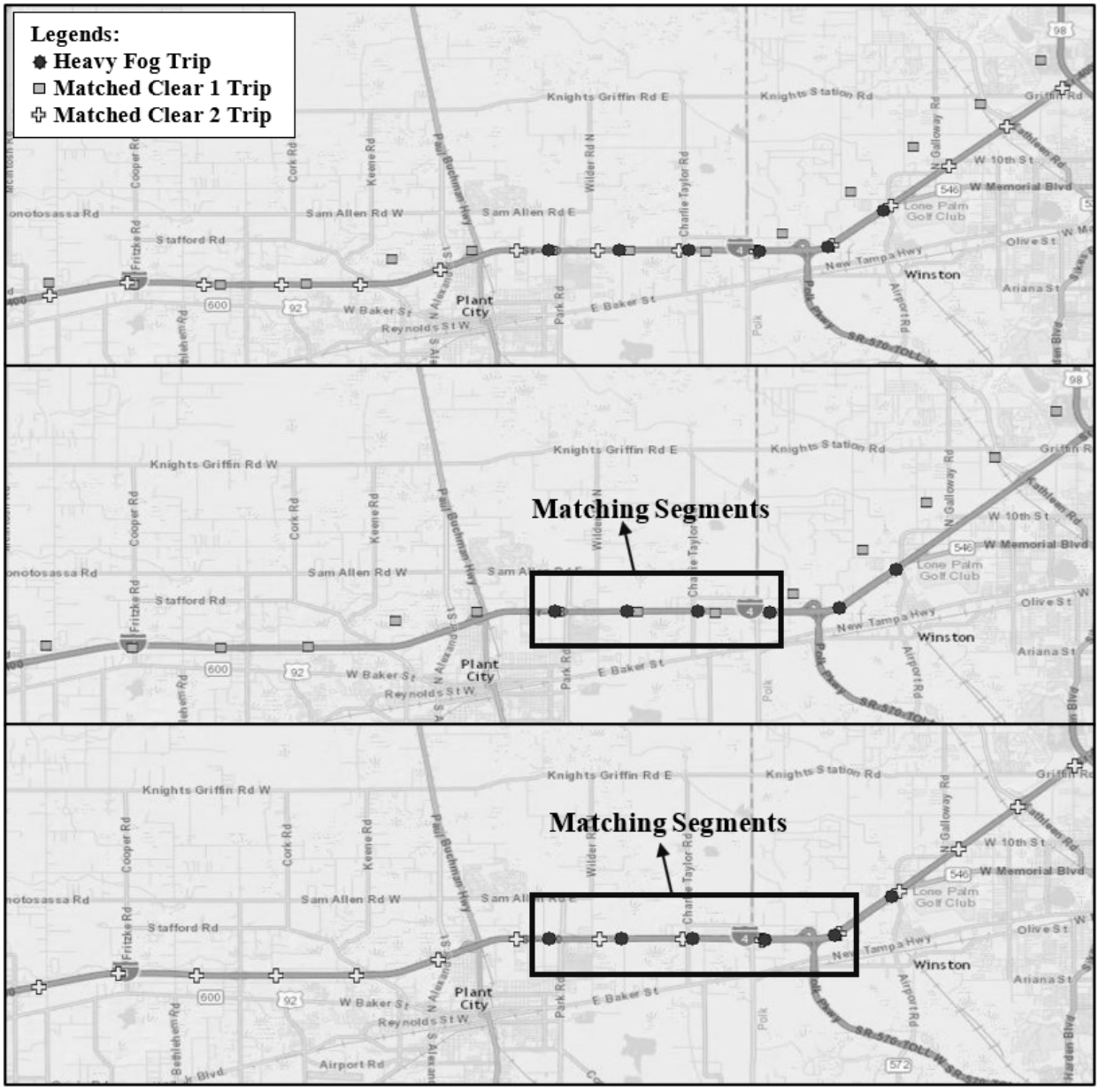

Figure 12 Identification of Matching Segments of Heavy Fog and Corresponding Clear Trips (I-4, Florida)

Preliminary Analysis

As mentioned earlier, in total 2,964 one-minute segments in free-flow conditions in heavy and distant fog with their matched clear trips were considered in the preliminary analysis. Table 3 shows descriptive statistics and various statistical tests for the variables of interest for fog and their corresponding matched clear in free-flow condition. To understand the magnitude of the difference between fog and clear weather, Cohen's d effect size was used. According to the Cohen's d test, d=0.2 can be considered as "small" effect size, 0.5 indicates "medium" effect size, and 0.8 defines a "large" effect size *(35)*.

The reported lane offset variable in the NDS was estimated based on machine vision. Lane offset can be considered as an indication of intended (lane change) or unintended deviation from the lane *(36).* As can be seen in Table 3, a t-test indicated that average lane offset to the left was significantly higher in clear weather conditions compared to heavy fog conditions, whereas average lane offset to the left in distant fog had no significant difference compared to their matched clear trips. However, no significant difference in average lane offset to the right between heavy and distant fog were found compared to their respective matched clear weather trips. Lane offset variability was significantly higher in clear weather trips compared to heavy fog but no significant difference in lane offset variability was found in distant fog and clear trips. The minimum and maximum value of lane offset indicated that drivers change multiple lanes during clear weather conditions compared to a single lane change in heavy fog conditions. .

Preliminary analysis indicated that average speed in heavy fog under free-flow conditions was significantly lower (5.28 km/hr) than in clear weather. However, the average speed in distant fog under free-flow conditions was found to be 2.3 km/hr lower than in clear weather. This might be due to the fact that distant fog has a tangible effect on driver performance. It was also found that speeds had a higher variability during clear weather conditions compared to heavy fog under free-flow conditions. This could be explained by the fact that drivers tend to increase their speeds more in clear weather conditions, which results in higher speed variability. However, speeds had higher variability during distant fog compared to clear conditions under free-flow conditions.

The acceleration/deceleration variable was tested, and ±0.3g acceleration/deceleration rates were set as a threshold to identify aggressive braking/acceleration events (37). However, all acceleration/deceleration were found to be within (-0.3g, +0.3g) range resulting in the recognition of zero aggressive braking events. The preliminary analysis demonstrated that no significant variability in average acceleration were recognized between heavy and distant fog compared to their respective matched trips in clear. Average acceleration in clear conditions was found to be significantly higher than heavy fog conditions. However, no significant difference was observed between average acceleration in distant fog and clear weather conditions.

Table 3 Preliminary Analysis for the NDS Instrumented Vehicle in Fog & Free-Flow Condition

	Statistical Test	Free-flow Condition							
		Heavy Fog		Matched Clear		Distant Fog		Matched Clear	
Lane Offset (Positive is offset to the right of lane center)		Pos.	Neg.	Pos.	Neg.	Pos.	Neg.	Pos.	Neg.
	Average (cm)	13.219	-17.816	17.396	-22.175	14.650	-19.729	13.874	-19.245
	SD	11.452	11.819	18.220	27.033	16.879	17.511	17.610	17.496
	Min. (cm)	0.078	-44.828	0.194	-345.241	0.096	-162.728	0.007	-236.298
	Max. (cm)	51.447	-0.762	105.864	-0.008	106.087	-0.041	126.381	-0.053
	Median (cm)	10.937	-14.202	11.763	-15.524	9.315	-14.921	8.251	-13.902
	Results of Statistical Test	• No significant difference between average lane offset to the right in heavy fog and clear weather. • Average lane offset to the left is significantly higher in clear weather. • Lane offset variability is significantly higher in clear weather.				• No significant difference found			
Speed		Speed	% Speed Reduction	Speed	% Speed Reduction	Speed	% Speed Reduction	Speed	% Speed Reduction
	Average (km/hr)	103.403	-3.332	108.686	-7.327	105.974	-4.139	108.274	-7.399
	SD	11.303	9.154	13.928	11.820	12.720	11.533	11.330	9.399
	Min. (km/hr)	63.625	-24.789	50.125	-42.627	38.649	-45.274	53.690	-42.104
	Max. (km/hr)	124.296	41.601	137.942	48.079	133.952	65.685	133.097	44.154
	Median (km/hr)	105.991	-4.538	109.784	-8.640	107.342	-5.137	108.723	-7.764
	Results of Statistical Test	• Average speed is 5.28 km/hr lower in heavy fog. • Speed variability is significantly higher in clear weather. • Proportion of violation ≥ 10 km/h above the speed limit is significantly higher in clear weather.				• Average speed is 2.3 km/hr lower in distant fog. • Speed variability is significantly higher in distant fog. • No significant difference between the proportion of speeding ≥ 10 km/h in distant fog and clear weather.			
Acceleration / Deceleration		Acc.	Dec.	Acc.	Dec.	Acc.	Dec.	Acc.	Dec.
	Average (g)	0.013	-0.013	0.016	-0.012	0.015	-0.017	0.016	-0.016
	SD	0.015	0.015	0.016	0.014	0.013	0.016	0.013	0.015
	Min. (g)	0.000	-0.061	0.000	-0.067	0.000	-0.070	0.000	-0.067
	Max. (g)	0.082	0.000	0.079	0.000	0.065	0.000	0.072	0.000
	Median (g)	0.008	-0.008	0.011	-0.006	0.011	-0.011	0.013	-0.011
	Results of Statistical Test	• Average acceleration is significantly higher in clear weather. • No significant difference between average deceleration in heavy fog and clear weather. • No significant difference between acceleration/deceleration variability in heavy fog and clear weather. • No acceleration/deceleration was found higher/lower than ± 0.3g.				• No significant difference found.			

Modeling Lane-keeping Ability-Parametric Approach

SDLP was considered as the categorical dependent variable for investigating lane-keeping ability in fog. SDLP is a widely used in assessing lane-keeping performance *(34)* and *(44)*. A general value of SDLP for normal driving was found to be 20 cm in previous studies *(45-46)*. Some studies used SDLP value of about 31 cm for driving on curved roads *(47)*. Therefore, SDLP was considered in three levels including below 20 cm, between 20 and 30 cm (moderate-lane keeping ability) and greater than 30 cm (considered poor lane keeping).

The explanatory variables used for the modeling consist of information extracted from the questionnaires, including driver characteristics (gender, education, marital status, driver mileage last year, driving experience, etc.), roadway characteristics (presence of curve, number of lanes, posted speed limit, etc.), environmental characteristics (weather, visibility, and surface

conditions), and traffic conditions. Table 4 shows the selected variables for developing the lane-keeping model.

Table 4 Variable Descriptions

Variable	Description	Type	Levels
Response Variable			
SDLP	Distance to the left or right of the center of the lane based on machine vision	Ordinal	1=Below 20 cm
			2=20-30 cm
			3=More than 30 cm
Explanatory Variables			
Environmental Characteristics			
Weather Conditions	Predominant weather conditions in 1-min video observation	Categorical	1=Clear
			2=Distant Fog
			3=Heavy Fog
Surface Conditions	Predominant surface conditions in 1-min video observation	Binary	1=Dry
			2=Wet
Visibility	Predominant visibility conditions in 1-min video observation	Binary	1=Affected
			2=Not Affected
Traffic Characteristics			
Traffic Condition	Predominant traffic conditions in 1-min video observation	Binary	1=Free-flow(A-B)
			2=Non-Free-flow(C-F)
Driver Characteristics			
Lane Change	Predominant lane change maneuver in 1-min video observation	Binary	1=Lane Change Occurs
			2=No Lane Change Occurs
Gender	The gender the participant identifies with	Binary	1=Male
			2=Female
Education	The highest completed level of education of the participant	Categorical	1= High school diploma or G.E.D.
			2= Some education beyond high school but no degree and College degree
			3= Some graduate or professional school, but no advanced degree (e.g., J.D.S., M.S. or Ph.D.) and Advanced degree (e.g., J.D.S., M.S. or Ph.D.)
Marital Status	The participant's marital status	Categorical	1=Married
			2=Single
			3=Other (Divorced, Widow(er), Unmarried Partners)
Driver Mileage Last Year Details	The approximate number of miles the participant drove last year	Binary	1=Less than 12,000
			2=Equal or greater than 12,000
Driving Experience	Number of years driving experience	Binary	1=Less than or equal 10 years
			2=More than 10 years
Roadway Characteristics			
Speed Limit	Predominant speed limit in 1-min video observation	Categorical	1=<55 mph
			2=(55-60) mph
			3=(65-70) mph
Presence of Curve	Presence of curve in 1-min segment	Binary	1=Curve
			2=Tangent
Number of Lanes	Average number of lanes in 1-min segment	Quantitative	-

To confirm the suitability and fitness of the models, the log likelihood ratio and the pseudo R^2 were used. The multicollinearity issue was assessed by calculating the Variance Inflation Factor (VIF). VIF is a measure of the amount of multicollinearity in a set of multiple predictor variables. A VIF between 5 to 10 means the predictors are highly correlated. A VIF above 10 indicates the highest correlation and the regression coefficients are considered as poorly

estimated *(48)*. The VIF value of all the predictor variables used in the model fell below 3, excluding any multi-collinearity issue. Table 5 shows the results of the model. Only statistically significant variables were retained in the final model.

Table 5 Ordered Logistic Regression Model for Lane-Keeping Ability in Different Weather Conditions

Parameter		DF	Estimate	Standard Error	Wald Chi-Square	Pr>Chi Sq	Odds Ratio	95% Confidence Interval	
Intercept	3	1	-1.5823	0.5093	9.6537	0.0019	-	-	-
Intercept	2	1	0.5724	0.5066	1.2765	0.2585	-	-	-
Weather Condition	Clear	-	-	-	-	-	-	-	-
	Heavy Fog	1	0.4265	0.2102	4.1171	0.0425	1.532	1.015	2.313
Surface Condition	Dry	-	-	-	-	-	-	-	-
	Wet	1	1.1963	0.2889	17.1474	<.0001	3.308	1.878	5.828
Visibility	Not Affected	-	-	-	-	-	-	-	-
	Affected	1	0.3140	0.1257	6.2460	0.0124	1.369	1.070	1.751
Traffic Condition	Free-flow	-	-	-	-	-	-	-	
	Non-Free-flow	1	-0.1339	0.0695	3.7116	0.0540*	0.875	0.763	1.002
Speed Limit	Below 55 mph	1	-	-	-	-	-	-	-
	55-60 mph	1	-1.2354	0.4725	6.8355	0.0089	0.291	0.115	0.734
	65-70 mph	1	-0.8429	0.4732	3.1734	0.0748*	0.430	0.170	1.089
Lane Change	No Lane Change Occurs	-	-	-	-	-	-	-	-
	Lane Change Occurs	1	4.3828	0.0878	2491.5222	<.0001	80.061	67.403	95.095
Gender	Male	-	-	-	-	-	-	-	-
	Female	1	-0.4627	0.0892	26.8849	<.0001	0.630	0.529	0.749
Education	High School	-	-	-	-	-	-	-	-
	Advance Degree	-	-0.2451	0.1421	2.9736	0.0846*	0.783	0.592	1.034
Marital Status	Single	-	-	-	-	-	-	-	-
	Married	1	-0.6855	0.1044	43.0920	<.0001	0.504	0.411	0.618
	Others (Divorced, Widow(er), Unmarried Partners)	1	-0.6513	0.1709	14.5197	0.0001	0.521	0.373	0.729
Drivers Mileage Last year	Below 12,000 miles	-	-	-	-	-	-	-	-
	Equal or Greater than 12,000 miles	1	-1.2537	0.5146	5.9358	0.0148	0.285	0.104	0.783
Driving Experience	Less than 10 years	-	-	-	-	-	-	-	-
	Equal or Greater than 10 years	1	0.4911	0.1195	16.8860	<.0001	1.634	1.293	2.065
Presence of Curve	Curve	-	-	-	-	-	-	-	-
	Tangent	1	-0.2621	0.0700	14.0278	0.0002	0.769	0.671	0.883
Number of Lanes		1	0.1018	0.0410	6.1557	0.0131	1.107	1.022	1.200
Weather × Gender	Heavy Fog, Female	1	-1.1873	0.2439	23.6969	<.0001	0.192	0.122	0.302
Driving Experience × Surface Condition	>10 years, Wet	1	-1.6208	0.4325	14.0438	0.0002	0.323	0.138	0.754
Speed Limit × Mileage Last Year	55-60 mph, ≥ 12, 000 miles	1	1.1480	0.5204	4.8663	0.0274	0.900	0.738	1.097
	65-70 mph, ≥ 12, 000 miles	1	1.1926	0.5217	5.2259	0.0223	0.941	0.762	1.161
Model Fit Statistics									
Likelihood Ratio Test: χ^2 = 4653.3440, DF = 23; P-value<0.0001 Score Test for the Proportional Odds Assumption: χ^2 = 147.9004, DF = 23; P-value<0.0001 Akaike Information Criterion (AIC) = 7224.590 Schwarz Criterion (SC) = 7390.281 -2LogL = 7174.590 R^2 = 0.5654, Max-rescaled R^2 = 0.6427									

**Significant at 90% confidence level*

It can be seen from Table 5 that visibility has a significant effect on driver lane-keeping behavior. The positive estimates of visibility indicated that SDLP was more likely to be higher in affected visibility conditions. This means drivers had worse lane-keeping ability, when visibility is affected. More specifically, drivers in reduced visibility conditions showed about 1.37 times higher SDLP, in comparison with drivers who were driving in good visibility conditions. The findings are in conjunction with existing literature *(28), (34),* and *(49)*. As expected, traffic conditions indicated a significant negative effect on SDLP. The negative sign depicts that drivers had less ability to change lane and better lane-keeping when traffic congestion increased. Specifically, the odds ratio of 0.875 depicted those drivers driving in free-flow conditions were 1.14 times more likely to have higher SDLP than drivers who were driving in congested traffic conditions.

As can be seen in Table 5, several driver demographics have a significant effect on lane-keeping behavior. Positive estimates of lane change described that SDLP was higher when the lane change occurred. Considering driver marital status, findings indicated that single drivers were 1.98 times (OR=0.504) more likely to have higher SDLP than married drivers. This is supported by the literature that single drivers showed more riskier driving behavior compared to other martial statuses *(50-51)*. Intuitively, lane-keeping ability on curves was found to be worse. Additionally, drivers with higher education showed better lane keeping compared to the relatively lower education categories.

Several interaction terms were included in the model to understand the effect of those variables together. The interactions between weather, gender, surface conditions, driving experience, speed limit, and driver mileage last year were found to have a significant effect on the lane-keeping ability. Considering the interaction between weather conditions and gender (OR=0.192), it was found that female drivers were 81 percent more likely to have better lane keeping in foggy conditions. Interaction between surface conditions and driving experience revealed that experienced drivers were 68 percent more likely to have better lane-keeping ability compared to inexperienced drivers when the surface condition was wet, exhibiting the cautious behavior of the experienced drivers (OR=0.323). Additionally, lane-keeping performance was found to be better for drivers who drove equal or greater than 12,000 miles last year compared to those drivers who drove less than 12,000 miles last year at speed limits between 55 mph to 70 mph.

Modeling Lane-keeping Ability-Non-Parametric Approach

Similar to the parametric approach, 5,584 1-minutes segments from 348 trips (i.e., 124 trips in fog and 248 trips in matching clear weather) were selected for modeling lane-keeping behavior utilizing association rules mining technique. These 5,584 1-minute segments contain various number of variables; however, thirteen categorical variables were selected based on prior studies (*39–41*), as shown in Table 6. In order to investigate factors that might have an impact on driver lane-keeping ability, the association rules mining was utilized in a supervised way. From these thirteen variables, SDLP was considered as the consequents of the supervised association rules mining in this study. This study utilized binary level of SDLP; less than or equal to 20 cm as good lane-keeping, and greater than 20cm means poor lane-keeping ability. The remaining 12 variables were considered as the antecedents. These antecedents can be interpreted as the potential confounding factors that contribute to the driver lane-keeping ability under different weather and traffic conditions. These variables include environmental, traffic, roadway geometry, and driver characteristics. Table 6 summarizes the descriptive statistics of the selected variables.

Table 6 Overview of Selected Variables

Variable	Description	Levels	Frequency	Percentage (%)
Consequent (Response Variable)				
SDLP	Distance to the left or right of the center of the lane based on machine vision	Poor Lane-keeping (>20 cm)	3558	63.72
		Good Lane-keeping (≤20 cm)	2026	36.28
Antecedents (Explanatory Variables)				
Environmental Characteristics				
Weather Conditions	Predominant weather conditions in 1-min video observation	Clear	4795	85.87
		Distant Fog	579	10.37
		Heavy Fog	210	3.76
Visibility	Predominant visibility conditions in 1-min video observation	Affected	664	11.89
		Not Affected	4920	88.11
Surface Conditions	Predominant surface conditions in 1-min video observation	Dry	5462	97.82
		Wet	122	2.18
Traffic Characteristics				
Traffic Condition	Predominant traffic conditions in 1-min video observation	Free-flow (LOS A&B)	2514	45.02
		Non-Free-flow (LOS C-F)	3070	54.98
Roadway Characteristics				
Presence of Curve	Whether the participants drove curve or tangent in 1-min driving	Curve	1668	29.87
		Tangent	3916	70.13
Speed Limit	Predominant speed limit in 1-min video observation	<= 60 mph (median of Speed Limit)	3018	54.05
		> 60 mph	2566	45.95
Freeway Number of Lanes	Average number of lanes in 1-min segment on the traversed freeway	<= 2 lanes	1491	26.70
		> 2 lanes	4093	73.30
Driver Characteristics				
Age	The participants' age	Young (< 25 years)	2174	38.93
		Middle (25-55 years)	3116	55.80
		Older (> 55 years)	294	5.27
Gender	The participant's gender	Male	3141	56.25
		Female	2443	43.75
Education	The highest completed level of education of the participant	Level=1 (High school diploma or G.E.D.)	445	7.97
		Level=2 (Some education beyond high school but no degree and College degree)	2857	51.16
		Level=3 (Some graduate or professional school, but no advanced degree (e.g., J.D.S., M.S. or Ph.D.) and Advanced degree (e.g., J.D.S., M.S. or Ph.D.))	2282	40.87
Driving Experience	Number of years driving experience	<= 10 years	2640	47.28
		> 10 years	2944	52.72
Driver Mileage Last Year Details	The approximate number of miles the participant drove last year	< 12,000 miles	1869	33.47
		=> 12,000 miles	3715	66.53

To get meaningful and significant results, minimum support and confidence need to be defined. Although several optimization algorithms can be applied to identify the minimum support and confidence, this study utilized several trial and error processes to set the optimum values of support and confidence, as recommended by a previous study (*54*). Low minimum support can increase the number of uninteresting rules, which make it difficult to interpret. Conversely, setting minimum support too high will generate less number of rules, which will fail to find some interesting rules and the inherent relationship among different itemsets. Therefore, the process of

trial and error was challenging to set the minimum threshold for support, as well as confidence. In addition, the number of itemsets is another factor to interpret the results. A rule is defined as a two-item rule, if there is a single antecedent and a single consequent in the rule. A three-item rule indicates that there are two antecedents and one consequent, or one antecedent and two consequents in the rule. In this study, the maximum length of association rules was set to four (i.e., four-item rule) for easier interpretation of the results (*53*).

The association rules were generated by using 'arules' package in R software (*100*)(*116*). As stated earlier, 13 different variables were selected, which corresponds to 29 items in total. The top ten frequent items in the dataset are Surface_Cond.=Dry, Visibility=Not Affected, Weather=Clear, Lane>2, Presence_of_Curve=Tangent, Driver_Mileage_Last_Year=>12,000, SDLP=Poor, Gender=Male, Age=middle, and Traffic_Condn.=Non-Free-flow. Figure 13 shows the item frequency plot graph.

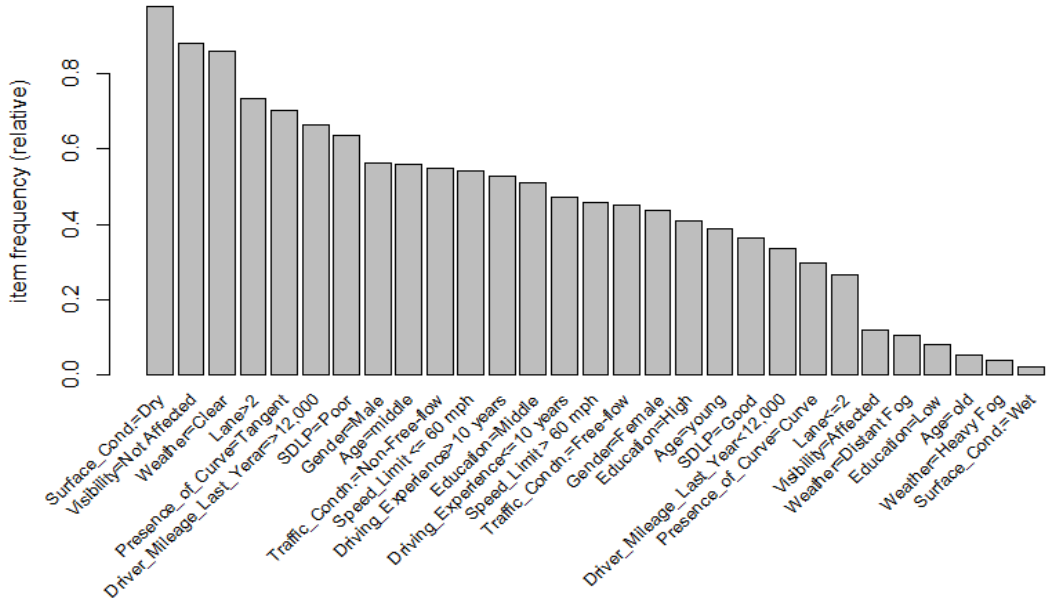

Figure 13 Item Frequency Plot of the Dataset

To generate association rules among the different characteristics (e.g., environmental, traffic, roadway geometry, and driver) in the database, Apriori algorithm was performed by keeping two levels of SDLP as consequents (i.e., SDLP=Poor and SDLP=Good). A higher value of lift in the rule indicates a stronger association between antecedent and consequent. As stated earlier, lift values greater than 1 indicate positive independence between antecedent and consequent. Therefore, rules were sorted according to the decreasing value of the lift, and minimum threshold of the lift was considered as 1. Table 7 shows the summary statistics of the extracted rules (after removing the redundant rules) where all the rules had lift value higher than 1. From Table 7, it can be seen that the range of lift value corresponding to the poor lane-keeping performance rules varied between 1.25 to 1.43, with a mean of 1.32. In contrast, the range of lift values from 1.24 to 1.73 was observed in the rules corresponding to good lane-keeping performance.

Table 7 Summary Statistics of Association Rules

Consequent Level	Number of Rules (Excluding Redundant Rules, Lift≥1)	Support			Confidence			Lift		
		Mean	Min.	Max.	Mean	Min.	Max.	Mean	Min.	Max.
1. Poor Lane-keeping (SDLP=Poor)	69	0.049	0.010	0.173	0.839	0.800	0.913	1.317	1.255	1.432
2. Good Lane-keeping (SDLP=Good)	85	0.085	0.030	0.193	0.499	0.450	0.628	1.376	1.241	1.731

Rules for Poor Lane-Keeping Performance

The association rules with poor lane-keeping performance as consequent were extracted from the generated rules. The minimum support and confidence were set at 1 percent and 80 percent , respectively. The number of rules obtained in this case was 84, and all of the rules had a lift value greater than 1. After removing the redundant rules, 69 rules were found.

The first 30 rules were listed in Table 8 by keeping the SDLP=Poor in consequent. The rules were ordered according to the decreasing values of the lift. From Table 8, it was observed that male drivers with driving experience less than or equal 10 years in non-free-flow traffic conditions (Rule 1: Driving_Experience<=10years, Gender=Male, Traffic_Condn.=Non-Free-flow => SDLP=Poor) produced highest lift value and were highly associated with poor lane-keeping performance (Support=6.93 percent , Confidence=91.27 percent , Lift=1.432). In addition, the effect of distant fog on driver poor lane-keeping performance was found in the second rule, indicating that the young drivers who were male and drove in distant fog conditions had higher propensity to have poor lane-keeping performance (Rule 2: Age=young, Gender=Male, Weather=Distant Fog => SDLP=Poor).

According to Table 8, it was also perceived that affected visibility was associated with poor lane-keeping performance in several rules (Rules 7-10, Rule 12, Rules 14-15, Rules 18-19, Rules 22-25, Rule 29). This finding is in conjunction with existing literature (*39–41*, *117*). For instance, the combined effect of higher speed limit, affected visibility, and distant fog on driver poor lane-keeping performance was found in Rule 7. (Speed_Limit > 60mph, Visibility=Affected, Weather=Distant Fog => SDLP=Poor). The rule can be expressed as (a) 1.56 percent of lane-keeping performances in the dataset occurred by drivers in speed limit above 60 mph with affected visibility under distant fog conditions and produced poor lane-keeping, (b) out of all lane-keeping performances in the dataset that occurred by drivers in speed limit above 60 mph with affected visibility under distant fog conditions, 87 percent were poor lane-keeping, (c) the proportion of poor lane-keeping performances that occurred by drivers in speed limit above 60 mph with affected visibility under distant fog was 1.37 times the proportion of poor lane-keeping performances in the overall dataset.

It is worth noting that male drivers were dominant in most of the rules for having poor lane-keeping performance. For instance, a rule indicates that the proportion of poor lane-keeping

performances involving with male drivers and affected visibility under distant fog conditions is almost 1.36 times the proportion of poor lane-keeping performances in the overall dataset (Rule 8: Gender=Male, Visibility=Affected, Weather=Distant Fog => SDLP=Poor). However, the generated rules indicated that male drivers had a worse lane-keeping ability than female drivers.

Additionally, the proportion of poor lane-keeping performance was found to be higher for more than two lanes in some of the rules. For instance, a rule indicates that drivers drove on more than two lanes freeways with affected visibility under distant fog condition were associated with poor lane-keeping performance (Rule 24: Lane>2, Visibility=Affected, Weather=Distant Fog => SDLP=Poor). Intuitively, the presence of curve was found to be an important factor for having a higher proportion of poor lane-keeping performance. The finding is consistent with the existing literature (*40*, *41*).

Table 8 Association Rules for Poor Lane-keeping Performance (First 30 Rules)

Rules	Antecedent	Consequent	Support (percent)	Confidence (percent)	Lift
1	{Driving_Experience<=10years, Gender=Male, Traffic_Condn.=Non-Free-flow}	{SDLP=Poor}	6.93	91.27	1.432
2	{Age=young, Gender=Male, Weather=Distant Fog}	{SDLP=Poor}	1.38	90.59	1.422
3	{Age=young, Gender=Male, Traffic_Condn.=Non-Free-flow}	{SDLP=Poor}	7.16	89.29	1.401
4	{Driving_Experience<=10 years, Gender=Male, Weather=Distant Fog}	{SDLP=Poor}	1.43	88.89	1.395
5	{Education=Middle, Gender=Male, Weather=Distant Fog}	{SDLP=Poor}	2.04	88.37	1.387
6	{Education=Middle, Gender=Male, Traffic_Condn.=Non-Free-flow}	{SDLP=Poor}	10.71	87.55	1.374
7	{Speed_Limit > 60mph, Visibility=Affected, Weather=Distant Fog}	{SDLP=Poor}	1.56	87.00	1.365
8	{Gender=Male, Visibility=Affected, Weather=Distant Fog}	{SDLP=Poor}	1.43	86.96	1.365
9	{Gender=Male, Traffic_Condn.=Non-Free flow, Visibility=Affected}	{SDLP=Poor}	2.02	86.92	1.364
10	{Driving_Experience>10 years, Lane>2, Visibility=Affected}	{SDLP=Poor}	2.78	86.59	1.359
11	{Driving_Experience<=10 years, Education=Middle, Gender=Male}	{SDLP=Poor}	10.40	86.59	1.359
12	{Driver_Mileage_Last_Year<12,000, Traffic_Condn.=Free-flow, Visibility=Affected}	{SDLP=Poor}	1.15	86.49	1.357
13	{Education=Middle, Gender=Male, Speed_Limit > 60 mph}	{SDLP=Poor}	10.66	86.48	1.357
14	{Age=middle, Lane>2, Visibility=Affected}	{SDLP=Poor}	3.21	86.47	1.357
15	{Lane>2, Visibility=Affected, Weather=Clear}	{SDLP=Poor}	2.70	86.29	1.354
16	{Age=young, Education=Low, Weather=Clear}	{SDLP=Poor}	1.00	86.15	1.352
17	{Education=Middle, Gender=Male, Presence_of_Curve=Curve}	{SDLP=Poor}	5.00	86.11	1.351
18	{Lane>2, Speed_Limit > 60 mph, Visibility=Affected}	{SDLP=Poor}	3.87	86.06	1.351
19	{Driving_Experience>10 years, Traffic_Condn.=Non-Free-flow, Visibility=Affected}	{SDLP=Poor}	1.33	86.05	1.350
20	{Gender=Male, Presence_of_Curve=Curve, Traffic_Condn.=Non-Free-flow}	{SDLP=Poor}	7.65	85.92	1.348
21	{Age=young, Education=Middle,Gender=Male}	{SDLP=Poor}	10.80	85.90	1.348
22	{Driving_Experience>10 years, Visibility=Affected, Weather=Distant Fog}	{SDLP=Poor}	1.31	85.88	1.348
23	{Gender=Male, Lane>2, Visibility=Affected}	{SDLP=Poor}	3.56	85.78	1.346
24	{Lane>2, Visibility=Affected, Weather=Distant Fog}	{SDLP=Poor}	1.90	85.48	1.342

Rules	Antecedent	Consequent	Support (percent)	Confidence (percent)	Lift
25	{Education=Middle, Gender=Male, Visibility=Affected}	{SDLP=Poor}	2.83	85.41	1.340
26	{Age=young, Education=Low}	{SDLP=Poor}	1.04	85.29	1.339
27	{Driving_Experience<=10 years, Education=Low, Gender=Male}	{SDLP=Poor}	1.04	85.29	1.339
28	{Driver_Mileage_Last_Year=>12,000, Education=Low, Gender=Male}	{SDLP=Poor}	1.04	85.29	1.339
29	{Age=middle, Driver_Mileage_Last_Year<12,000, Visibility=Affected}	{SDLP=Poor}	1.13	85.14	1.336
30	{Driver_Mileage_Last_Year=>12,000, Education=Middle, Gender=Male}	{SDLP=Poor}	12.30	85.02	1.334

Rules for Good Lane-Keeping Performance

The association rules with good lane-keeping performance as consequent were extracted from the generated rules. The minimum support and confidence were set at 3 percent and 45 percent , respectively. The number of rules obtained in this case was 119, and all of the rules had lift value greater than 1. After excluding the redundant rules, 85 rules were found.

Table 9 lists the first 30 rules by keeping the SDLP=Good in consequent, and the rules were ordered according to the decreasing values of the lift. As can be seen in Table 9, young female drivers who drove equal or more than 12,000 miles last year (Rule 1: Age=young, Driver_Mileage_Last_Year=>12,000, Gender=Female => SDLP=Good), produced highest lift value and were highly associated with good lane-keeping performance (Support=6.29 percent , Confidence=62.79 percent , Lift=1.731). The rule can be expressed as (a) 6.29 percent of lane-keeping performances in the dataset occurred by young female drivers who drove equal or more than 12,000 miles last year and produced good lane-keeping, (b) out of all lane-keeping performances in the dataset that occurred by young female drivers who drove equal or more than 12,000 miles last year, 62.79 percent were good lane-keeping, (c) the proportion of good lane-keeping performances that occurred by young female drivers who drove equal or more than 12,000 miles last year was 1,731 times the proportion of good lane-keeping performances in the complete dataset.

In addition, female drivers were found to be dominant in the antecedent part of the good lane-keeping performance. The findings are expected in comparison with the findings found in the rules for poor lane-keeping performance. However, the combined effect of female drivers who drove on a tangent was found to be dominant in some of the rules (Rule 8, Rule 12, Rule 15, and Rule 28). Among different age groups, younger drivers were found to be dominant in having good lane-keeping performance. The finding is consistent with a previous study (*41*). Moreover, drivers who drove equal or more than 12,000 miles last year were found to be a significant factor for having a higher proportion of good lane-keeping performance compared to drivers who drove less than or equal 12,000 miles last year.

Table 9 Association Rules for Good Lane-keeping Performance (First 30 Rules)

Rules	Antecedent	Consequent	Support (percent)	Confidence (percent)	Lift
1	{Age=young, Driver_Mileage_Last_Year=>12,000, Gender=Female}	{SDLP=Good }	6.29 percent	62.79 percent	1.731
2	{Age=young, Gender=Female, Speed_Limit <= 60 mph}	{SDLP=Good }	9.06 percent	59.25 percent	1.633
3	{Driver_Mileage_Last_Year=>12,000, Driving_Experience<=10 years, Gender=Female}	{SDLP=Good }	8.74 percent	58.87 percent	1.622
4	{Driver_Mileage_Last_Year=>12,000, Education=Middle, Gender=Female}	{SDLP=Good }	6.84 percent	56.43 percent	1.555
5	{Age=young, Gender=Female, Traffic_Condn.=Non-Free-flow}	{SDLP=Good }	6.81 percent	56.38 percent	1.554
6	{Age=young, Speed_Limit <= 60 mph, Traffic_Condn.=Free-flow}	{SDLP=Good }	5.14 percent	56.16 percent	1.548
7	{Driving_Experience<=10 years, Gender=Female, Speed_Limit <= 60 mph}	{SDLP=Good }	10.83 percent	55.76 percent	1.537
8	{Age=young, Gender=Female, Presence_of_Curve=Tangent}	{SDLP=Good }	9.51 percent	55.49 percent	1.529
9	{Education=Middle, Gender=Female, Speed_Limit <= 60 mph}	{SDLP=Good }	10.44 percent	55.31 percent	1.525
10	{Gender=Female, Speed_Limit <= 60 mph, Traffic_Condn.=Free-flow}	{SDLP=Good }	5.18 percent	55.15 percent	1.520
11	{Driver_Mileage_Last_Year=>12,000, Driving_Experience<=10 years, Speed_Limit <= 60 mph}	{SDLP=Good }	8.09 percent	54.99 percent	1.516
12	{Gender=Female, Presence_of_Curve=Tangent, Speed_Limit <= 60 mph}	{SDLP=Good }	9.33 percent	54.84 percent	1.512
13	{Age=young,Driver_ Mileage_Last_Year=>12,000, Speed_Limit <= 60 mph}	{SDLP=Good }	6.93 percent	54.51 percent	1.502
14	{Driver_Mileage_Last_Year=>12,000, Gender=Female, Speed_Limit <= 60 mph}	{SDLP=Good }	8.04 percent	53.45 percent	1.473
15	{Driving_Experience<=10 years, Gender=Female, Presence_of_Curve=Tangent}	{SDLP=Good }	11.57 percent	53.43 percent	1.473
16	{Driving_Experience<=10 years ,Gender=Female, Traffic_Condn.=Non-Free-flow}	{SDLP=Good }	8.51 percent	53.37 percent	1.471
17	{Age=young, Gender=Female, Lane>2}	{SDLP=Good }	9.29 percent	53.34 percent	1.470
18	{Education=Middle, Speed_Limit <= 60 mph, Traffic_Condn.=Free-flow}	{SDLP=Good }	5.28 percent	52.87 percent	1.457
19	{Driving_Experience<=10 years, Speed_Limit <= 60 mph, Traffic_Condn.=Free-flow}	{SDLP=Good }	5.62 percent	52.86 percent	1.457
20	{Presence_of_Curve=Tangent, Speed_Limit <= 60 mph, Traffic_Condn.=Free-flow}	{SDLP=Good }	6.12 percent	52.62 percent	1.450
21	{Age=young, Gender=Female, Surface_Cond.=Dry}	{SDLP=Good }	12.41 percent	52.58 percent	1.449
22	{Age=young, Education=Middle, Gender=Female}	{SDLP=Good }	11.98 percent	52.31 percent	1.442
23	{Driving_Experience<=10 years, Gender=Female, Lane>2}	{SDLP=Good }	11.52 percent	52.11 percent	1.436
24	{Age=young, Gender=Female}	{SDLP=Good }	12.48 percent	52.09 percent	1.436
25	{Driver_Mileage_Last_Year=>12,000,Gender=Female,Traffic_Condn.=Free-flow}	{SDLP=Good }	5.68 percent	51.80 percent	1.428
26	{Driver_Mileage_Last_Year=>12,000, Education=Middle, Speed_Limit <= 60 mph}	{SDLP=Good }	6.64 percent	51.67 percent	1.424
27	{Gender=Female, Speed_Limit <= 60 mph, Surface_Cond.=Dry}	{SDLP=Good }	12.48 percent	51.59 percent	1.422
28	{Education=Middle, Gender=Female, Presence_of_Curve=Tangent}	{SDLP=Good }	11.21 percent	51.57 percent	1.421
29	{Age=young, Presence_of_Curve=Tangent, Speed_Limit <= 60 mph}	{SDLP=Good }	7.56 percent	51.34 percent	1.415
30	{Gender=Female, Speed_Limit <= 60 mph}	{SDLP=Good }	12.89 percent	51.21 percent	1.411

Visualization of Extracted Rules for Lane-Keeping Performance

Examining all the rules generated for poor and good lane-keeping performances is not a feasible option. Therefore, a visible representation of the rules is needed. The results of the association rules can be visualized by using the 'arulesViz' package of R software. Grouped balloon plots are used to visualize the relationship between the representative group of antecedents and consequent of all the rules. The plot can be drawn by keeping antecedent groups as columns and consequents as rows. Figure 14 and Figure 15 illustrate grouped balloon plots of association rules generated for poor and good lane-keeping performance. The size of the balloon represents support values and the color indicates the lift values. The rules for poor and good lane-keeping performance can be easily identified based on high lift and high support groups in Figure 14 and Figure 15.

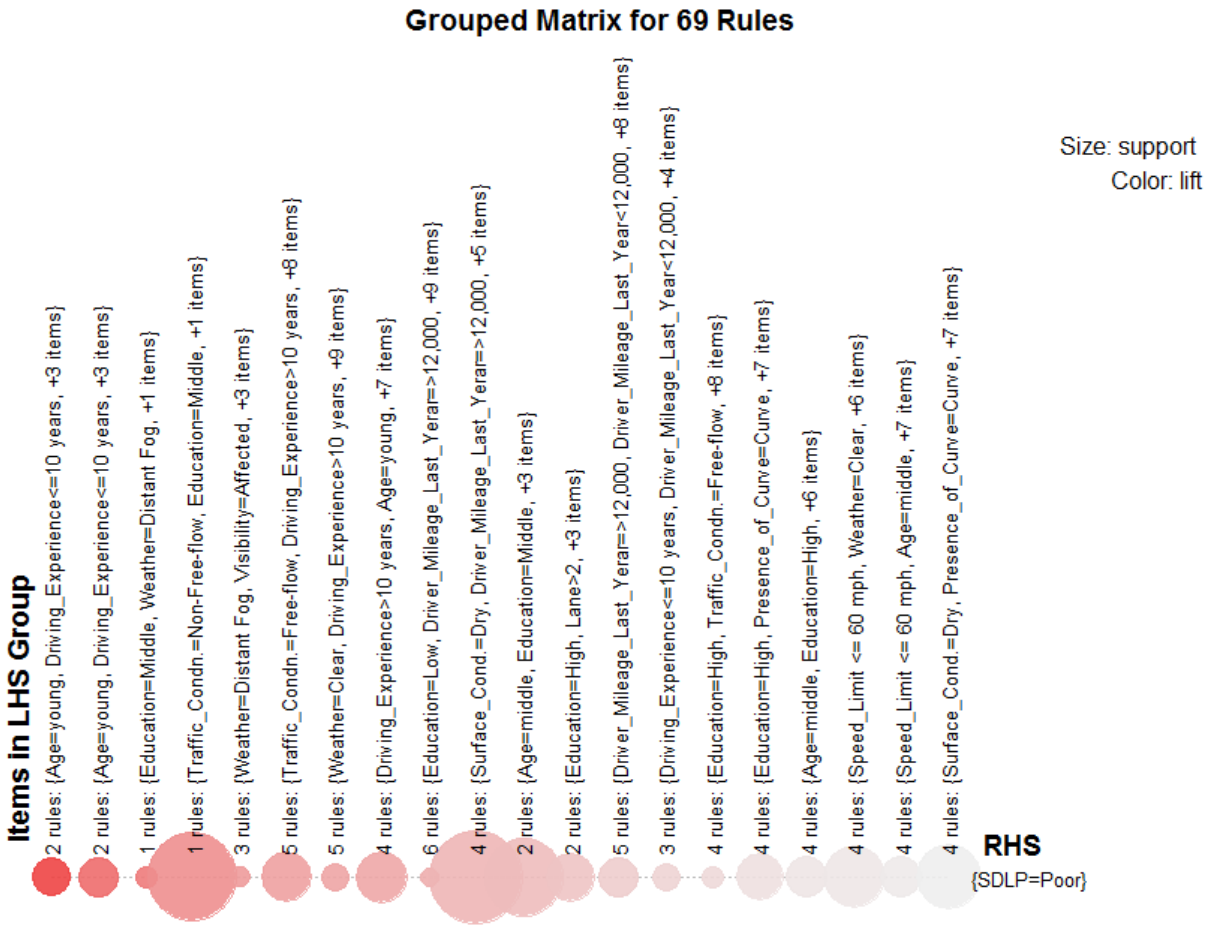

Figure 14 Grouped Balloon Plot of the Generated Rules for Poor Lane-Keeping Performance

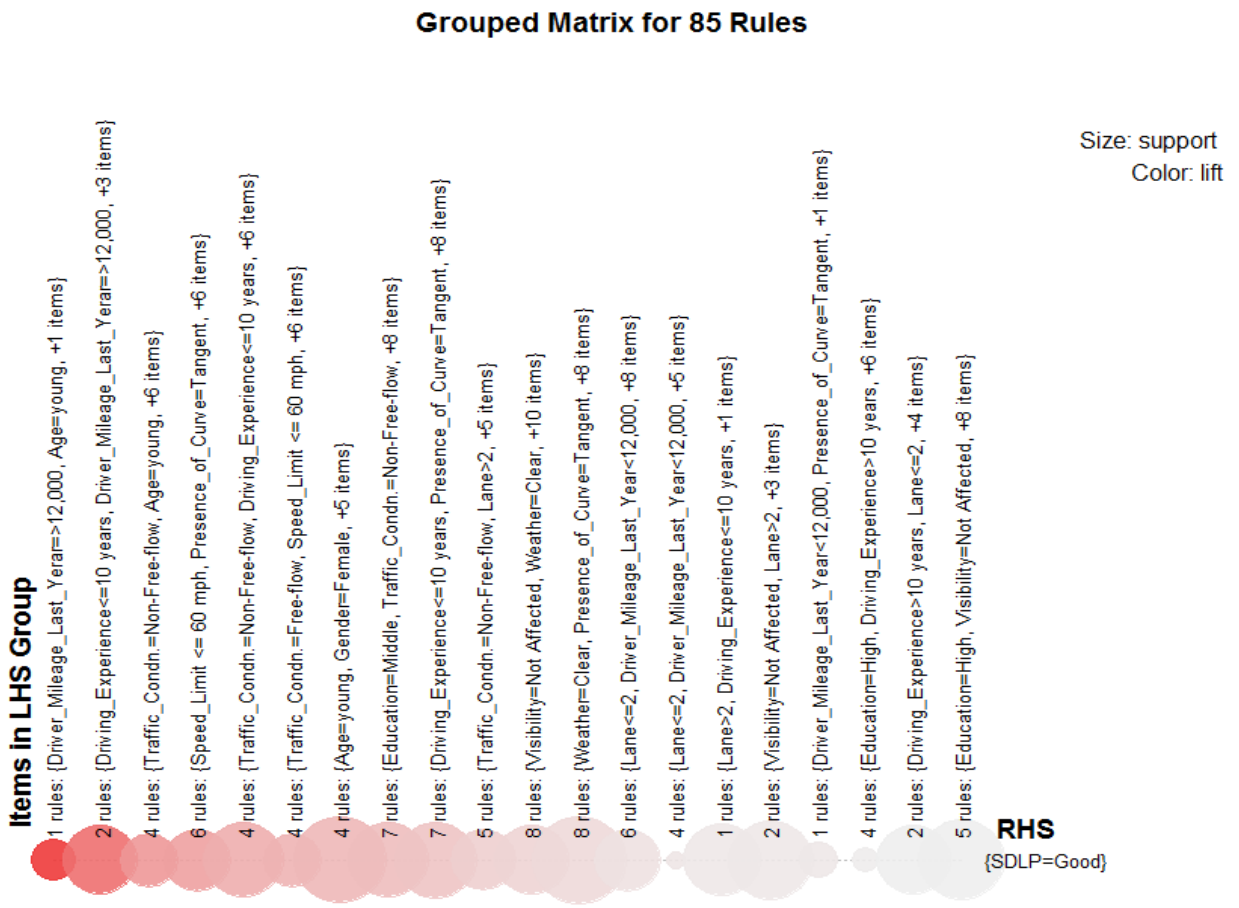

Figure 15 Grouped Balloon Plot of the Generated Rules for Good Lane-Keeping Performance

In addition to the grouped balloon plots, scatter plots were generated to visualize the relationship among lift, support, and confidence in the rules generated from poor and good lane-keeping performance. Figure 16 shows the scatter plots of the rules for poor and good lane-keeping performance with support and confidence values on the x-axis and y-axis, respectively. One scatter point denotes an association rule. The color of scatter points represents the lift value of each rule. It can be seen from Figure 16 and Figure 17 that most of the rules for poor lane-keeping performance are located close to the minimum support threshold. However, a number of rules are located in-between the support value of 0.05 to 0.1 for good lane-keeping performance. In general, Figure 16 and Figure 17 give an overview of the distribution of support and confidence in the extracted rules set for each of the lane-keeping performance.

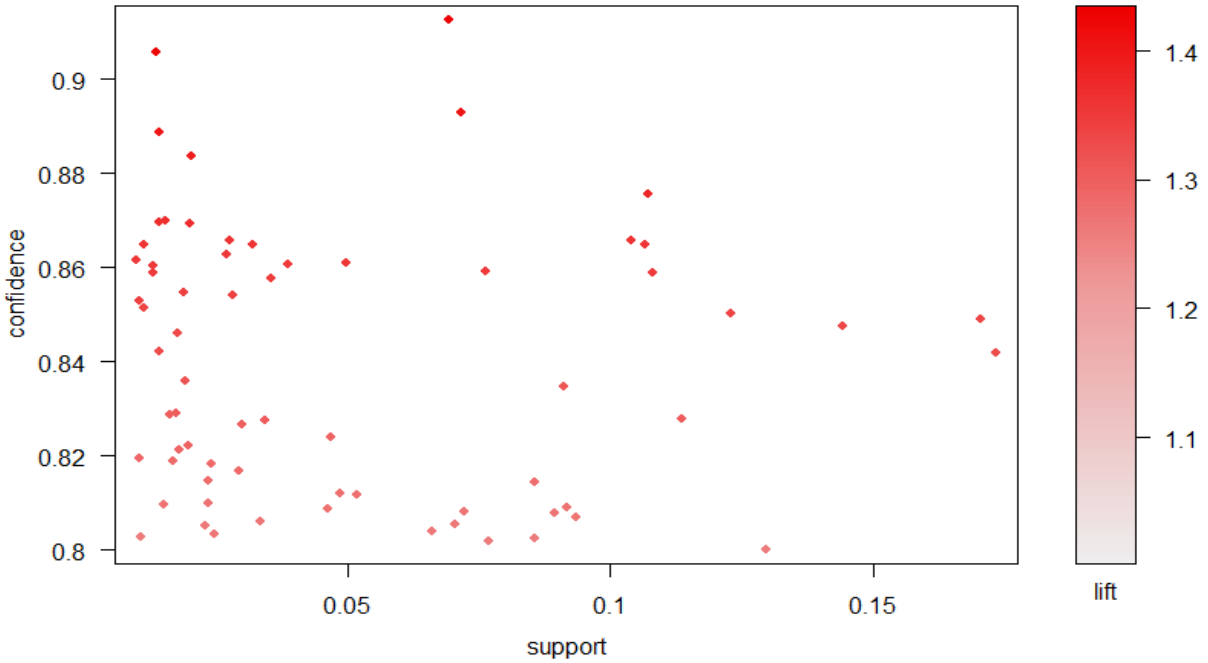

Figure 16 Scatter Plot of the Generated Rules for Poor Lane-Keeping Performance

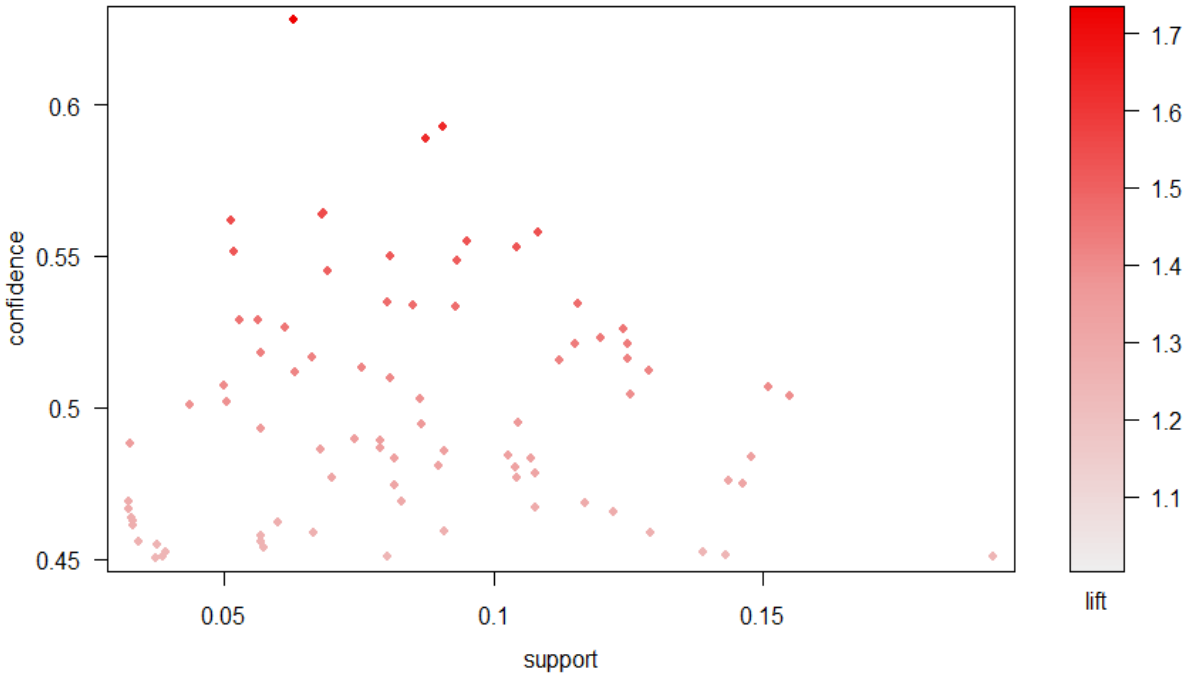

Figure 17 Scatter Plot of the Generated Rules for Good Lane-Keeping Performance

Lane Changing Characteristics Based on Aggressiveness

Descriptive Statistics

As stated earlier, 214 trips in fog and their corresponding matched clear weather conditions were considered for this study to analyze lane-changing maneuvers and identify driver types. In total, 537 lane changes in fog (92 in heavy fog and 445 in distant fog) and 1,163 lane changes in matched clear weather conditions (i.e., same driver, vehicle, and route) were identified from the considered trips. Based on the literature, six categories of lane-changing maneuvers were distinguished from video observations, where each maneuver was associated with the motivation for that particular maneuver (*62*). For instance, maneuver of slow lead vehicle indicated that driver changed their lane to pass or overtake a slower lead vehicle to maintain a constant speed. The description of each maneuver type is given in Table 10.

Table 10 Lane-Changing Maneuver Types and Description

Lane-changing Maneuver Type (Identified from the Video)	Type of Lane-changing	Description
Slow Lead Vehicle	Discretionary	Change lane to pass/overtake a slower lead vehicle so the NDS vehicle could maintain speed
Return	Discretionary	Change lane to return to drivers preferred lane
Enter	Mandatory	Change lane to enter the roadway
Exit/Prepare to exit	Mandatory	Change lane to exit/prepare to exit
Added Lane	Discretionary	Change lane due to the addition of a lane
Other Reasons	Discretionary	Change lane for other reasons or no noticeable reason found

It is worth mentioning that some of the reasons were identified in 'Other Reasons' maneuver type. Sometimes, driver changed lanes due to sudden change in visibility while going through tunnels or at night. In addition, lane changing occurred due to merging roadway, driving on curves, sun glare, or sudden merge of another vehicle in the NDS drivers' lane. However, of these 537 lane changes in fog, 37 lane changes (4 in heavy fog and 33 in distant fog) were identified as mandatory 'Enter' and 'Exit' maneuver. Similarly, among 1,163 lane changes in clear weather conditions, 77 lane changes were distinguished as 'Enter' and 'Exit' maneuver. Therefore, the final dataset were prepared by excluding mandatory 'Enter' and 'Exit' lane changes to capture only driver discretionary lane-changing characteristics. After removing mandatory lane-changing events, in total, 88 lane changes in heavy fog, 412 lane changes in distant fog, and 1,086 lane changes in matched clear weather were considered for further analyses. Table 11 shows the summary statistics of the total number of lane-changing events with the total number of drivers traveled in different traffic conditions under fog and matched clear weather. In addition, Table 11 provides mean number of lane-changing events per mile, total number of one-minute segments, total traveled time, and total length of traversed routes of the NDS trips considered for the study.

Table 11 Summary Statistics of Lane Changes in NDS Trips Considered

Weather Condition	Traffic Condition	Total No of Drivers	No of Lane-changing Events					Mean No of Lane-changing Events/mile	Total No. of One-minute Segments	Total Traveled Durations (hr)	Total Traveled Lengths (miles)
			Maneuver Types								
			1	2	3	4	Total				
Heavy Fog	Free-flow	27	11	8	-	19	38	0.26	165	2.75	178.33
	Mixed-flow	27	34	-	-	14	48	0.42	144	2.40	129.64
	Unstable-flow	6	1	-	-	1	2	0.36	19	0.32	5.30
	All LOS	40	46	8	0	34	**88**	0.30	328	5.47	313.27
Distant Fog	Free-flow	76	57	25	1	82	165	0.32	491	8.18	540.97
	Mixed-flow	89	130	17	3	83	233	0.39	882	14.7	778.75
	Unstable-flow	31	8	-	-	6	14	0.49	209	3.48	65.19
	All LOS	104	195	42	4	171	**412**	0.40	1582	26.37	1384.93
Matched Clear Weather	Free-flow	99	218	58	6	201	483	0.34	1445	24.08	1612.44
	Mixed-flow	102	362	47	6	104	519	0.38	1560	26	1484.67
	Unstable-flow	48	68	3	-	13	84	0.45	517	8.62	187.00
	All LOS	113	648	108	12	318	**1086**	0.35	3522	58.7	3279.54

Note: 1 = Slow lead vehicle, 2 = Return, 3 = Added Lane, 4 = Other Reasons

As can be seen from Table 11, number of lane-changing events in unstable flow conditions were quite low compared to the other two traffic conditions in both fog and clear weather. In heavy traffic conditions (e.g., LOS E&F), it is quite natural to perform minimal number of lane changes because of the limited number of gaps between vehicles. Therefore, inferring necessary characteristics for lane changing and exploring driver classification in this condition may not provide meaningful results. Considering this fact, data analysis were conducted based on free-flow and mixed-flow conditions.

Findings from Hypothesis Testing

In order to have a better understanding of driver lane-changing behavior in fog and clear weather under different traffic conditions, several hypotheses were tested for different scenarios in terms of their number of lane-changing events per mile and lane-changing durations. The hypotheses tested in this study were based on a study by Hill et al., however, this study extended the analysis to foggy weather conditions (*58*). All the tests were conducted for the drivers who drove in both heavy fog and clear weather as well as distant fog and clear weather using paired t-test at a 95 percent confidence level. Table 12 shows the results of the hypothesis tests performed.

Table 12 Results of Hypotheses Testing for the Fog and Clear Weather in Different Traffic Conditions

Hypothesis	Heavy Fog vs. Clear Weather	Distant Fog vs. Clear Weather
	Results of t-test	Results of t-test
1. Is there any significant difference in mean number of lane-changing events per mile between fog and clear weather in free-flow conditions?	t=1.318 P= 0.1061	t=1.638 P=0.0541
2. Is there any significant difference in mean number of lane-changing events per mile between fog and clear weather in mixed-flow conditions?	t=2.769 **P<0.001**	t=0.385 P=0.3508
3. Is there any significant difference in mean lane-changing durations between fog and clear weather in free-flow conditions?	t=0.426 P=0.3386	t=0.715 P=0.2389
4. Is there any significant difference in mean lane-changing durations between fog and clear weather in mixed-flow conditions?	t=2.907 **P<0.001**	t=1.515 P=0.0675
5. Is there any significant difference in mean durations of the free-flow lane changes to the left between fog and clear weather?	t=0.27 P=0.3959	t=1.867 **P<0.001**
6. Is there any significant difference in mean durations of the free-flow lane changes to right between fog and clear weather?	t=0.188 P=0.4269	t=0.94 P=0.1761
7. Is there any significant difference in mean durations of the mixed-flow lane changes to the left between fog and clear weather?	t=1.18 P=0.1276	t=1.589 P=0.0585
8. Is there any significant difference in mean durations of the mixed-flow lane changes to right between fog and clear weather?	t=1.064 P=0.303	t=0.838 P=0.2027

A paired t-test revealed that there was no significant difference in any of the group for hypothesis 1, which indicated that weather, had no effect on lane-changing maneuvers in free-flow conditions. According to hypothesis 2, the mean number of lane-changing events per mile in heavy fog was significantly higher than clear weather in mixed flow conditions. During adverse weather and mixed flow, different drivers choose different speeds depending on their ability, confidence, and familiarity with the roadway. Under limited visibility, specific drivers (e.g., young drivers) when stuck behind a slower vehicle they are more likely to change their lanes. Therefore, higher variability of speeds may lead to take more lane-changing maneuvers in heavy fog compared to clear weather under mixed-flow conditions. However, no significant difference in mean number of lane-changing events per mile between distant fog and clear weather were observed in mixed-flow conditions. The result of hypothesis 3 showed no significant differences in the mean lane-changing durations between fog and clear weather under free-flow conditions. The result was expected and suggested that during free-flow conditions, drivers in different weather conditions would take nearly the same durations for lane changing. The test result of hypothesis 4 showed that the mean lane-changing durations in heavy fog were significantly higher than clear weather in mixed-flow conditions. This might be due to the fact that drivers were more cautious while changing lanes in heavy fog than in clear weather in the presence of more ambient traffic (*67*). However, no significant differences were observed in mean lane-changing durations between distant fog and clear weather in mixed-flow conditions. The results of hypothesis 5 and 6 for heavy fog seems reasonable and suggested that drivers took nearly the same duration to change lanes in each direction (i.e., left and right) regardless of weather conditions. This result was also supported by the literature (*58*). According to the results of hypothesis 7 and 8, there were no significant differences between the mean durations of mixed-flow lane changes to the left and right in both fog and clear weather. This could be explained by the fact that drivers tried to be more cooperative because of potential frequent vehicle conflicts in mixed-flow conditions (*118*).

Lane-Changing Duration Distribution

Examining the number of lane-changing events and the distributions of lane-changing durations is important to incorporate drivers' naturalistic behavior on freeways in microscopic lane-changing models calibration and validation. Current microsimulation models consider lane-changing as an instantaneous event (*58*, *67*, *119*). For instance, CORSIM (CORridor SIMulation®) uses a default value of three second for lane-changing (*120*). However, this study found that lane changing was not an instantaneous event rather the durations of lane-changing were different in different weather and traffic conditions. Therefore, it is necessary to derive the actual distribution of lane-changing durations considering weather and traffic conditions to improve the existing microscopic model algorithms. Considering this, the study explored several distributions of lane-changing durations in fog and clear weather under free-flow and mixed-flow conditions. Different distributions of lane-changing durations were examined and fitted (e.g., Normal, Lognormal, Weibull, and Gamma) to identify common trends. Figure 18 exhibits the distributions of lane-changing durations in heavy fog, distant fog, and matched clear weather under free-flow and mixed-flow traffic conditions. From the NDS data used in this study, it was found that lane-changing durations follow a lognormal distribution in fog (heavy and distant) and matched clear weather under free-flow conditions. The similar trend was also found for the distribution of lane-changing durations in heavy fog and matched clear weather under mixed-flow conditions. However, gamma distribution was found to fit better the lane-changing durations in distant fog under mixed-flow conditions. As can be seen in Figure 18, the lane-changing duration observed in this study ranges from 1.69 to 15.87 s with a mean of 4.86 to 5.47 s, which is in line with the literature (*58*, *66*, *67*).

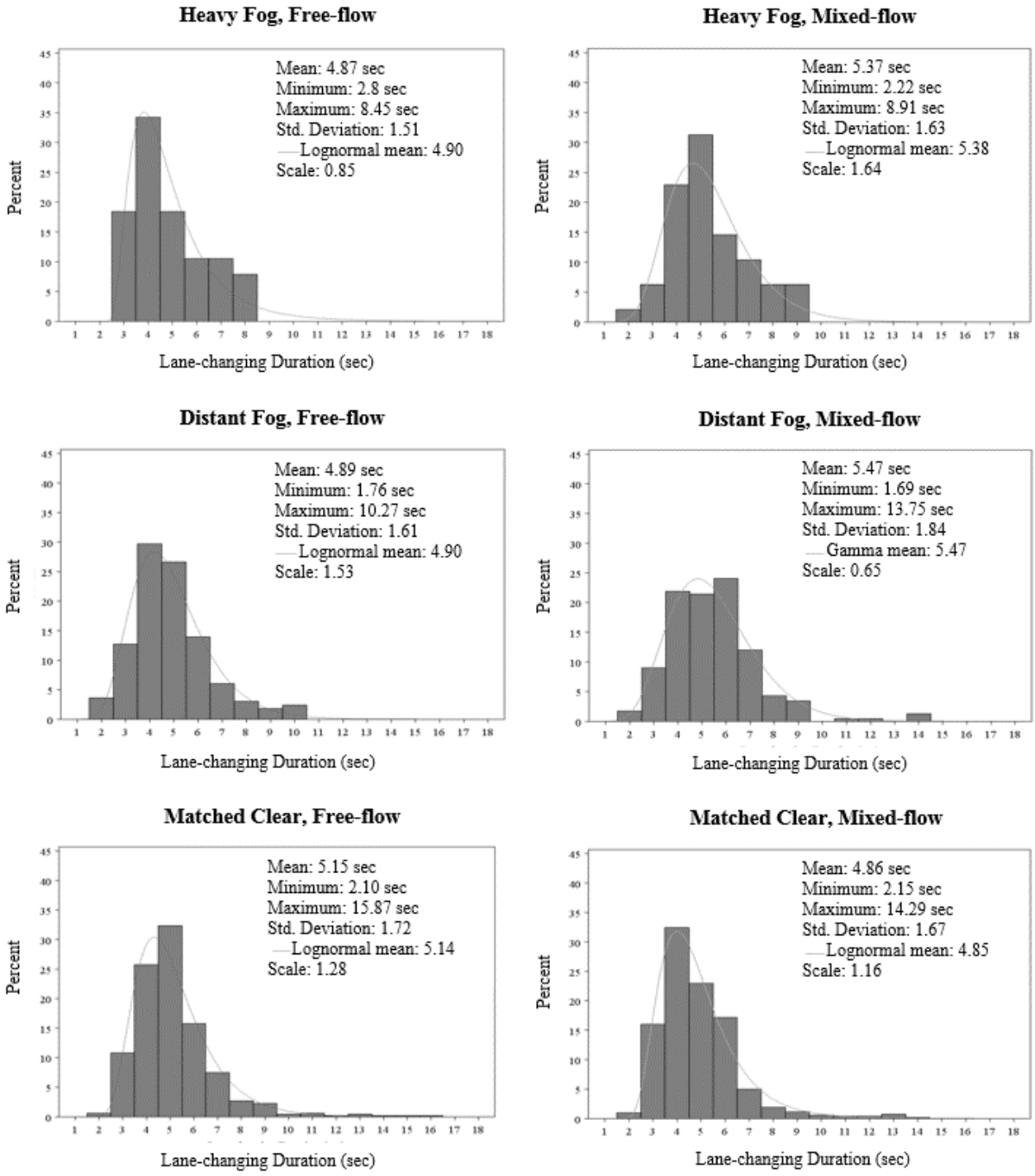

Figure 18 Fitted Distribution of Lane-Changing Duration in Fog and Clear Weather Under Free-Flow and Mixed-Flow Condition

Cluster Analysis for Identifying Driver Type

Although drivers' aggression is crucial for microsimulation modeling, most of the current microsimulation models do not have this parameter. Incorporating drivers' aggression in microsimulation models can make the model more realistic and practical. The driver type identified from the analysis of this study could be useful for calibrating and validating existing microsimulation lane-changing models. In this study, driver type was defined based on their aggressiveness while driving in four different traffic and environmental conditions as shown in Table 13. The main criteria for evaluating the aggressiveness of driver were the number of discretionary lane-changing events and speed differences from the speed limits. Several literatures showed the importance of these two parameters in determining aggressive driving behavior (*121–123*). The K-means cluster method was applied to the drivers who traveled in both heavy and distant fog and their matched clear weather under free-flow and mixed-flow conditions. The number of clusters was determined based on different test statistics, ease of interpretation of the analysis results, and potential practical implementation. The cluster analysis results revealed that two clusters were the most appropriate for the drivers corresponding to weather and traffic conditions 1, and three clusters were necessary for the drivers corresponding to weather and traffic conditions 2, as shown in Table 13. On the other hand, seven clusters were suitable for the drivers corresponding to weather and traffic conditions 3, and eight clusters were appropriate for the drivers corresponding to weather and traffic conditions 4. However, all the drivers were classified into two categories, conservative and aggressive, in order to compare their relationship in different foggy weather under various traffic conditions. In total, 13 and 17 drivers were identified corresponding to weather and traffic conditions 1 and 2, respectively. On the contrary, 48 and 63 drivers were identified corresponding to weather and traffic conditions 3 and 4, respectively.

The characteristics of the driver type for each foggy weather condition, in addition to their corresponding mean lane changing per mile and mean speed differences, are summarized in Table 13. For instance, the range of mean number of lane changing per mile for conservative drivers in all weather and traffic conditions varied between 0.281 to 0.557; whereas the mean number of lane changing per mile of aggressive drivers in all weather and traffic conditions ranged between 0.334 to 0.674. Conservative drivers in heavy fog under free flow conditions had lower mean number of lane-changing per mile compared to the conservative drivers in clear weather under free-flow conditions corresponding to weather and traffic conditions 1. Considering mean speed differences the range varied between -17.81 to 3.249 mph for conservative drivers. Conversely, all the mean speed differences for aggressive drivers were found to be positive. This indicated that aggressive drivers in all weather and traffic conditions drove 0.893 to 10.258 mph above speed limits.

Table 13 Characteristics of Driver Aggressiveness Type

Weather/Traffic Conditions		Driver Type	Number of Drivers	Percentage	Mean of Number of Lane-changes per mile	Mean Speed Differences
1	Heavy Fog/Free-flow	Conservative	5	38.46%	0.281	-0.634
		Aggressive	8	61.54%	0.663	6.907
	Clear/Free-flow	Conservative	11	84.61%	0.349	3.249
		Aggressive	2	15.39%	0.535	10.258
2	Heavy Fog/Mixed-flow	Conservative	4	23.53%	0.557	-17.61
		Aggressive	13	76.47%	0.674	0.951
	Clear/Mixed-flow	Conservative	4	23.53%	0.342	-7.979
		Aggressive	13	76.47%	0.334	3.361
3	Distant Fog/Free-flow	Conservative	25	52.08%	0.418	0.002
		Aggressive	23	47.92%	0.517	7.18
	Clear/Free-flow	Conservative	36	85.71%	0.346	2.464
		Aggressive	12	25.00%	0.539	9.822
4	Distant Fog/Mixed-flow	Conservative	22	34.92%	0.408	-17.810
		Aggressive	41	65.08%	0.472	0.893
	Clear/Mixed-flow	Conservative	18	28.57%	0.393	-12.450
		Aggressive	45	71.43%	0.442	2.680

The output of the cluster analysis is illustrated in Figure 19. As can be seen in Figure 19, aggressive drivers in all weather and traffic conditions had higher speed differences compared to conservative drivers. It was found that most of the drivers (i.e., aggressive and conservative) corresponding to weather and traffic conditions 1 and 3 drove above the speed limits. However, it was observed that all the conservative drivers corresponding to weather and traffic conditions 2 and 4 drove below the speed limits, whereas most of the aggressive drivers of the same weather and traffic conditions drove above the speed limits. Considering number of lane-changing events per mile, most of the aggressive drivers had higher number of lane-changing events compared to conservative drivers. For instance, the highest number of lane-changing events for aggressive drivers corresponding to weather and traffic conditions 1 was found to be 1. On the contrary, the highest number of lane-changing events for conservative drivers of the same weather and traffic conditions was found to be 0.59. In general, the cluster analysis result concluded that there were significant differences in number of lane-changing events and speed differences between aggressive and conservative drivers.

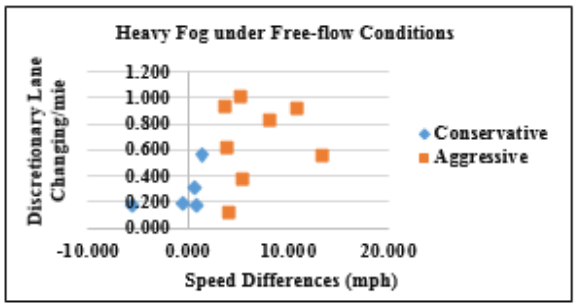

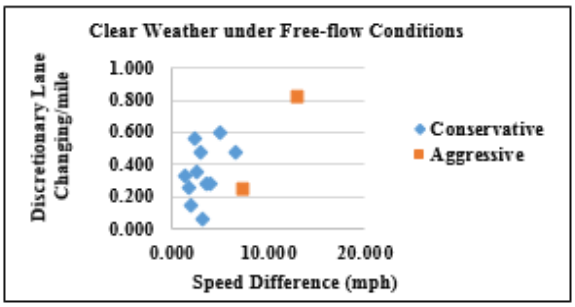

Weather and Traffic Conditions 1

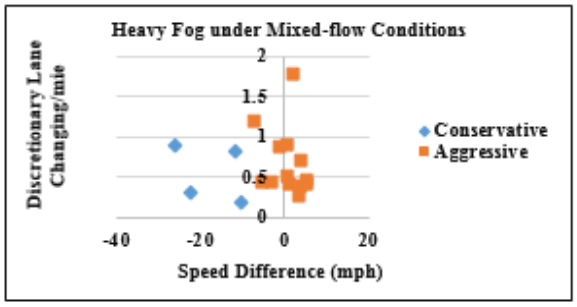

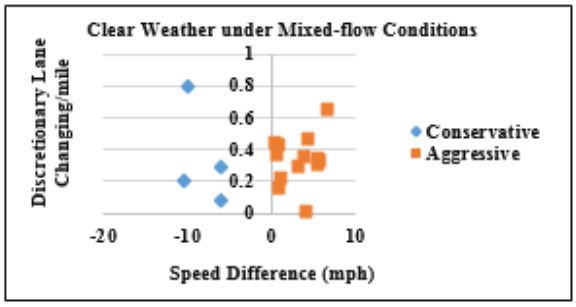

Weather and Traffic Conditions 2

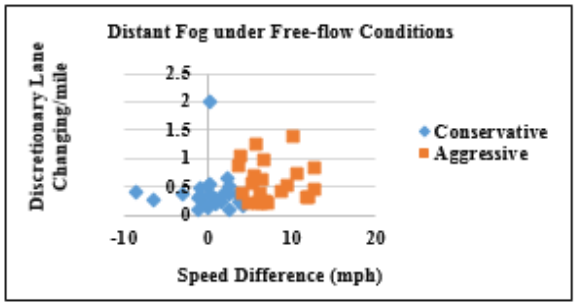

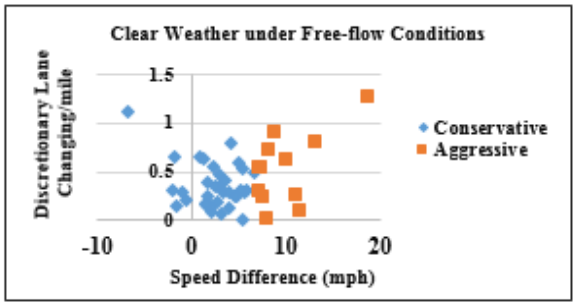

Weather and Traffic Conditions 3

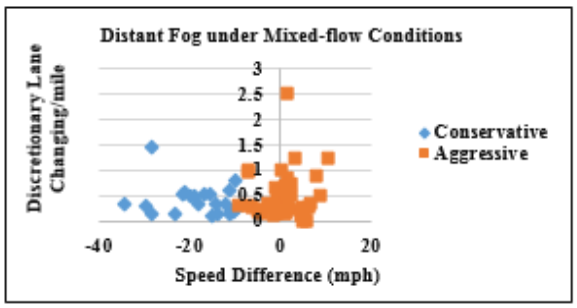

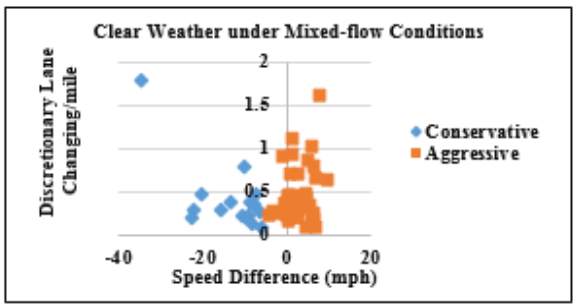

Weather and Traffic Conditions 4

Figure 19 Cluster Analysis Results

Comparison between SHRP2 Administrated Questionnaire Responses and Cluster Analysis

A comparison was made for evaluating the consistency of drivers stated preference responses with their actual behavior in real life. The results of the comparison would be useful to make a decision regarding whether survey questionnaires could be utilized in assessing driver lane-changing behavior in practice. The questions considered in this study, collected from the SHRP2 NDS questionnaire database, are related to drivers' risk-taking and risk perception behaviors. Based on the questionnaire responses, drivers were rated from 0 to 100 where 0 represents most conservative and 100 represents most aggressive with a cutoff value of 50. Drivers were defined as conservative if their scores ware equal to or less than 50, and aggressive if the scores were over 50. Four questions from the questionnaire corresponding to cluster parameters (i.e., lane changing and speed differences) were selected for the comparison. Each of the questions was given 25 points. For example, question 1 shown in Table 14 had seven response levels ranging from 1 to 7, where 1 is the lowest risk and 7 is the highest risk level. In between 1 to 7, the weights of other options were assigned based on their hierarchy. The same procedure was adopted for the other three questions. Table 14 shows the selected questions with their response levels.

Table 14 SHRP2 Administrated Questionnaire and Response Levels

Questions	Response Levels
1. "Drive at your normal speed during bad driving conditions, like road construction, rain, ice, or snow?"	From 1 to 7: 1-No Greater Risk 4-Moderately Greater Risk 7-Much Greater Risk
2. "Drive 10-20 mph over speed limit?"	From 1 to 7: 1-No Greater Risk 4-Moderately Greater Risk 7-Much Greater Risk
3. "Drive more than 20 mph over speed limit?"	From 1 to 7: 1-No Greater Risk 4-Moderately Greater Risk 7-Much Greater Risk
4. "Become impatient with a slow driver in the fast lane and pass on the right?"	From 1 to 6: 1-Never 2-Hardly Ever 3-Occasionally 4-Quite Often 5-Frquently 6-Nearly All the Time

Table 15 provides a sample of the comparison of questionnaire responses with cluster analysis corresponding to drivers in weather and traffic conditions 1. In addition, summary statistics of all weather and traffic conditions are provided in Table 16. Although the same driver may behave differently in various fog and clear weather conditions, some significant findings could be concluded. According to Table 16, responses of drivers in weather and traffic conditions 1 related to foggy weather reflected their actual driving while their responses to survey questionnaires did not match their real-life behaviors in clear conditions. In addition, during the free-flow conditions, drivers' responses related to foggy weather were more consistent with survey questionnaires compared to their responses in clear weather. Moreover, during the mixed-

flow conditions, majority of the drivers' responses were consistent with the survey questionnaires. For instance, the questionnaire responses of about 71 percent of drivers in weather and traffic conditions 2 matched with their real-life behavior.

Table 15 Sample of the Comparison of Questionnaire Responses and Cluster Analysis for Drivers in Weather and Traffic Conditions 1

Driver ID	SHRP2 Administrated Questionnaire Responses				Scoring	Heavy Fog					Clear Weather				
						Quantitative Responses		Driver Type		Comparison	Quantitative Responses		Driver Type		Comparison
	Q.1	Q.2	Q.3	Q.4		Speed Difference (mph)	Lane-changing/mile	From Questionnaire Response	From Cluster Analysis		Speed Difference (mph)	Lane-changing/mile	From Questionnaire Response	From Cluster Analysis	
695399	5	5	7	2	63.333	4.143	0.12	A	A	Yes	3.487	0.289	A	C	No
972860	5	4	7	2	59.167	0.882	0.169	A	C	No	7.495	0.249	A	A	Yes
811180	3	3	4	3	39.167	8.192	0.82	C	A	No	6.67	0.483	C	C	Yes
181169	6	4	6	3	64.167	0.735	0.311	A	C	No	2.084	0.142	A	C	No
415396	7	4	7	1	62.500	5.329	0.995	A	A	Yes	5.116	0.599	A	C	No
502426	3	2	6	5	53.333	-0.606	0.189	A	C	No	13.021	0.822	A	A	Yes
977738	7	7	7	1	75.000	3.883	0.609	A	A	Yes	2.415	0.558	A	C	No
235517	4	4	5	3	51.667	-5.675	0.175	A	C	No	2.615	0.357	A	C	No
788793	7	7	7	1	75.000	11.006	0.909	A	A	Yes	3.237	0.069	A	C	No
775082	5	5	7	2	63.333	13.377	0.545	A	A	Yes	3.046	0.476	A	C	No
816791	4	4	7	2	55.000	1.492	0.56	A	C	No	1.72	0.253	A	C	No
668733	5	5	8	2	67.500	3.771	0.941	A	A	Yes	1.344	0.326	A	C	No
220974	5	6	7	3	72.500	5.559	0.364	A	A	Yes	4.007	0.29	A	C	No

Table 16 Summary of the Comparison of Questionnaire Responses and Cluster Analysis for Drivers in Different Weather and Traffic Conditions

Weather/Traffic Conditions		Number of Drivers	Number of Drivers Consistent with Questionnaire Response and Cluster Analysis	Percentage of Drivers' Consistency (%)
1	Heavy Fog/Free-flow	13	7	58.33%
	Clear Weather/Free-flow	13	3	23.08%
2	Heavy Fog/Mixed-flow	17	12	70.59%
	Clear Weather/Mixed-flow	17	12	70.59%
3	Distant Fog/Free-flow	48	21	43.75%
	Clear Weather/Free-flow	48	14	29.17%
4	Distant Fog/Mixed-flow	63	39	61.90%
	Clear Weather/Mixed-flow	63	41	65.08%

Lane-Changing Durations Based on Driver Type

After classifying drivers into two categories using K-means (i.e., aggressive and conservative), this study compared two different driver types based on their mean lane-changing durations in fog and clear weather under free-flow and mixed-flow conditions, respectively. Figure 20 displays the mean lane-changing durations by driver type in different fog and clear weather under various traffic conditions. It was observed that, lane-changing durations of all conservative drivers ranged from 4.77 to 5.85 s. In contrast, lane-changing durations of all aggressive drivers varied between 4.20 to 5.61 s. This concluded that aggressive drivers had wider range of lane-changing durations compared to conservative drivers.

Meanwhile, it was observed that most of the conservative drivers had longer lane-changing durations than aggressive drivers, whereas conservative and aggressive drivers in distant fog corresponding to weather and traffic conditions 4 had nearly the same duration. This indicated that sometimes mixed flow conditions in foggy weather may affect driver decision-making behavior in lane-changing maneuvers (*124*). In addition, conservative drivers in heavy fog conditions (weather and traffic conditions 1 and 2) had longer lane-changing durations than in clear weather. Similar trend was found for the aggressive drivers corresponding to those weather and traffic conditions. The findings concluded that reduced visibility caused by heavy fog conditions resulted in longer lane-changing durations for both driver types compared to clear weather.

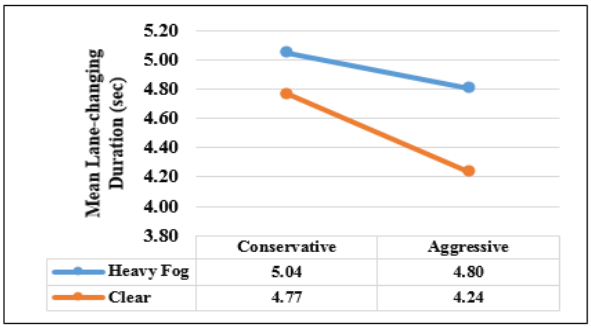

Weather and Traffic Conditions 1

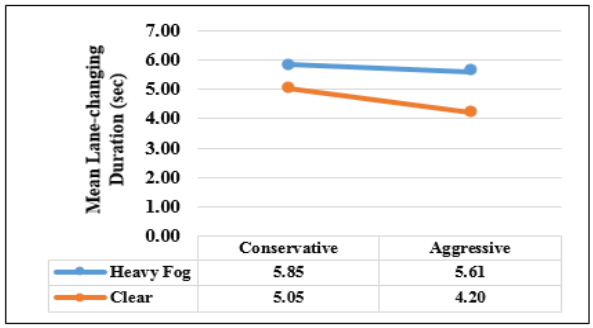

Weather and Traffic Conditions 2

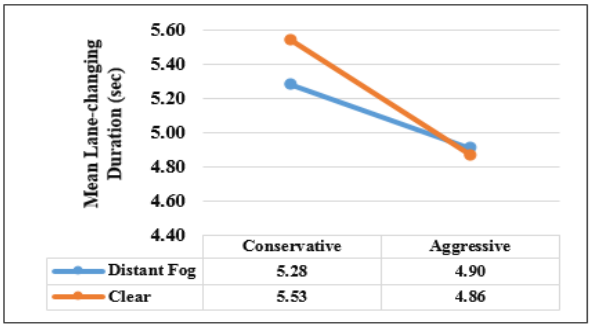

Weather and Traffic Conditions 3

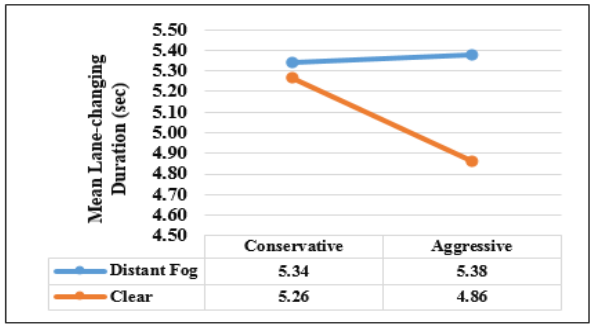

Weather and Traffic Conditions 4

Figure 20 Mean Lane-Changing Durations by Driver Type

Gap Acceptance Behavior

Gap Acceptance Characteristics

This study investigated the characteristics of lead and lag gaps in freeways in order to determine different features and trends of gap acceptance behavior. Although the lead and lag gaps are assumed to follow a lognormal distribution in the literature, naturalistic behavior might change the assumption (*125*). Different distributions of gap acceptance including, lognormal, gamma, Weibull, exponential, etc. were examined. The distributions were compared using Akaike Information Criterion (AIC) for goodness of fit. From the considered lane-changing event dataset, it was revealed that gamma distribution fitted the best for lead gaps. On the contrary, lag gaps followed a lognormal distribution. Figure 21 demonstrates the distributions of lead and lag gaps.

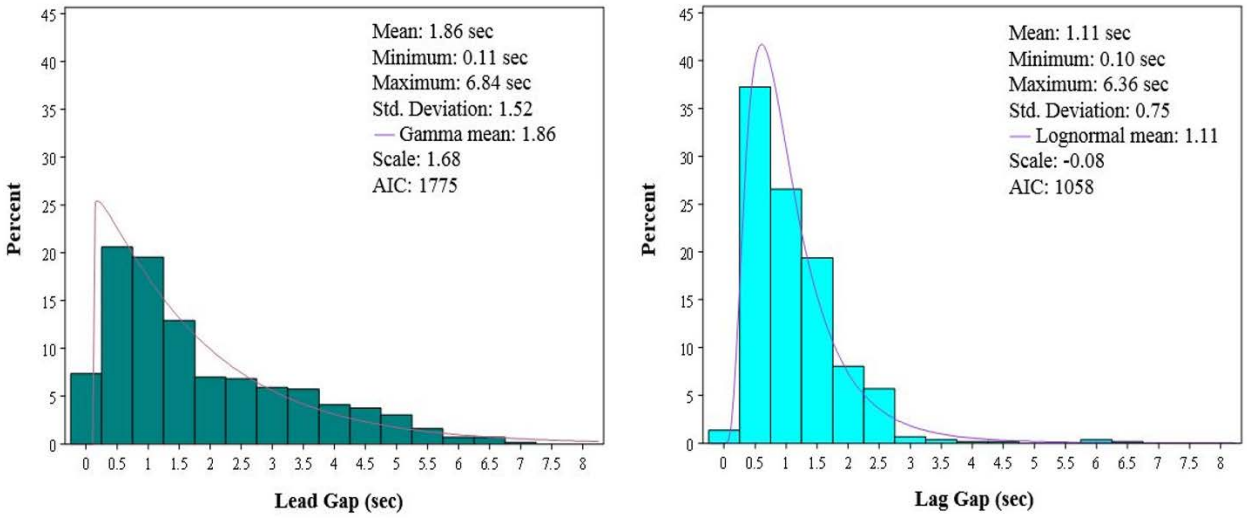

Figure 21 Fitted Distribution of Lead and Lag Gaps

As can be seen in Figure 21, the range of the lead gaps varied between 0.11 to 6.84 sec, with a mean of 1.86 sec. In contrast, the range of lag gaps varied from 0.10 to 6.36 sec. It is worth noting that the corresponding statistics of lead gaps (i.e., mean and maximum) are relatively higher than those of lag gaps. This suggested that LCV drivers accepted shorter headways in front of FV, whereas, they maintained larger headway behind the LV. This might be due to the fact that drivers were more dependent on mirrors while determining lag gap. Therefore, their perception of lag gap might not be reliable in comparison with the lead gap (*126*).

Modeling Gap Acceptance Behavior

As mentioned earlier, 599 lane-changing events were considered for modeling gap acceptance behavior using MARS model. The dependent variables in the models are lead and lag gaps, which were extracted from the developed automatic lane-changing event identification algorithm. The explanatory variables are the potential contributing factors that might have impact on gap acceptance behavior including, traffic flow parameters, environmental characteristics, roadway and motivation characteristics. The variables were selected based on their importance on gap acceptance behavior and previous studies (*70, 72*). Table 17 summarizes different variables used to set for lead and lag gap models.

Table 17 Variables Descriptions for Gap Acceptance Models

Variable	Description	Type	Source
Response Variables (Unit)			
Lead Gap (s)	Time taken to traverse the longitudinal distance between LV and LCV	Continuous	Developed Gap Acceptance Database
Lag Gap (s)	Time taken to traverse the longitudinal distance between FV and LCV	Continuous	Developed Gap Acceptance Database
Explanatory Variables (Abbreviation) (Unit)			
Traffic Flow Parameters			
Minimum Rear Headway (RH) (m)	Minimum distance between LCV and FV that was available after a lane-changing event	Continuous	Developed Gap Acceptance Database
FV Acceleration (FV Acc.) (g)	Following vehicle's acceleration during lane-changing event	Continuous	Developed Gap Acceptance Database
LCV Speed (LCV Sp.) (kph)	Lane-changing vehicle's speed during lane-changing event	Continuous	Developed Gap Acceptance Database
LCV Acceleration (LCV Acc.) (g)	Lane-changing vehicle's acceleration during lane-changing event	Continuous	Developed Gap Acceptance Database
LV Speed (LV Sp.) (kph)	Lead vehicle's speed during lane-changing event	Continuous	Developed Gap Acceptance Database
LV Acceleration (LV Acc.) (g)	Lead vehicle's acceleration during lane-changing event	Continuous	Developed Gap Acceptance Database
Relative Speed ($RS(V_{LCV} - V_{LV})$) (kph)	Relative speed between LCV and LV during lane-changing event	Continuous	Developed Gap Acceptance Database
Relative Speed ($RS(V_{LCV} - V_{FV})$) (kph)	Relative speed between LCV and FV during lane-changing event	Continuous	Developed Gap Acceptance Database
Traffic Conditions (TC)	Traffic conditions during lane-changing event	Categorical (1=Free-flow, 2=Non-free-flow)	Video Observation
Environmental Characteristics			
Weather Conditions (WC)	Weather conditions during lane-changing event	Categorical (1=Clear, 2=Others (Rain, Snow, and Fog)	Video Observation
Roadway Characteristics			
Curve Radius (R) (ft)	Curve radius during lane-changing event	Continuous	Roadway Information Database (RID)
Speed Limit (SL) (mph)	Speed limit during lane-changing event	Continuous	Roadway Information Database (RID)
Number of Freeway Lanes (Lanes)	Number of lanes during lane-changing event	Continuous	Roadway Information Database (RID)
Motivation Parameters			
Lane-changing Type (LC Type)	Type of Lane-changing during lane-changing event	Categorical (1=Mandatory, 2=Discretionary)	Video Observation

This study utilized a nonparametric MARS model to investigate the factors affecting gap acceptance behavior. In order to better interpret the obtained model, the maximum number of interactions was set as two, as supported by previous studies (*41*, *79*). Several numbers of BFs were examined to identify the optimum maximum number of BFs for both models. The optimum maximum number of BFs selected was 30 based on the lowest root mean square error (RMSE) value (*79*). Two types of BFs were obtained from the developed MARS model; simple/elementary BFs and complex BFs. Simple BFs include only single variable and no interaction, while complex BFs allow interaction between variables (*115*).

MARS Model for Lead Gaps

MARS model for lead gap acceptance was developed using the explanatory variables provided in Table 17. Table 18 presents developed MARS model for lead gaps. The results of MARS model for lead gaps showed that several variables were involved in simple and complex BFs. As can be seen in Table 18, the explanatory variables did not have a single direction of impact on the lead gaps. As mentioned previously, the developed knots split the explanatory variables into several regions meaning that variables might have a different impact on lead gaps. For instance, BF5 and BF6 represents two complex BFs for the (RS($V_{LCV} - V_{LV}$)), where a knot is developed at a value of 8. Additionally, the two BFs interact with a single BF (BF3), where the knot is developed at a value of 76. The coefficient of BF5 has a positive value and BF6 has a negative value. The estimated parameters of BFs in Table 18 were significant at a 95 percent confidence level.

Table 18 MARS Model for Lead Gap Acceptance

BFs	Basis Function	Estimate	Standard Error	P-value
BF0	Constant	0.71332	0.24996	0.00452
BF2	(0, 58.3361 – (RS($V_{LCV} - V_{LV}$)))	Not Sig.	Not Sig.	Not Sig.
BF3	(0, RH- 76.096)	-2.53186	0.19669	0.00000
BF4	(0, 76.096 - RH)	Not Sig.	Not Sig.	Not Sig.
BF5	(0, (RS($V_{LCV} - V_{LV}$)) - 8.1244) × BF3	0.05268	0.00290	0.00000
BF6	(0, 8.1244 – (RS($V_{LCV} - V_{LV}$))) × BF3	-0.05042	0.00854	0.00000
BF7	(0, RH- 75.872) × BF2	0.04916	0.00438	0.00000
BF8	(0, 75.872 - RH) × BF2	0.00059	0.00017	0.00052
BF9	(TC in (1))	7.00157	0.95816	
BF12	(0, 45.202 – LV Sp.) × BF4	0.00341	0.00068	0.00000
BF15	(0, Lanes - 2) × BF9	-0.59407	0.12238	0.00000
BF17	(0, LCV SP.- 4.4691) × BF9	-0.03607	0.00707	0.00000
BF18	(0, (RS($V_{LCV} - V_{FV}$)) - 29.0629) × BF4	-0.00323	0.00059	0.00000
BF19	(0, 29.0629 - (RS($V_{LCV} - V_{FV}$))) × BF4	-0.00092	0.00031	0.00288
BF20	(0, LV SP.- 122.005) × BF9	-0.07589	0.02199	0.00061
BF21	(0, 122.005 – LV Sp.) × BF9	-0.03741	0.00887	0.00003
BF22	(0, (RS($V_{LCV} - V_{LV}$)) - 20.636) × BF9	-0.05338	0.02277	0.01948
BF23	(0, 20.636 – (RS($V_{LCV} - V_{LV}$))) × BF9	-0.09273	0.01823	0.00000
BF24	(0, (RS($V_{LCV} - V_{LV}$)) - 30.503)	0.17035	0.02964	0.00000
BF25	(0, 30.503 – (RS($V_{LCV} - V_{LV}$)))	Not Sig.	Not Sig.	Not Sig.
BF26	(0, RH- 92.48) × BF25	0.00426	0.00175	0.01550
BF29	(0, 83.0836 – LV Sp.)	-0.03610	0.01224	0.00336

According to Table 18, several complex BFs (i.e., interaction) are present in the lead gaps model. Therefore, both the main effect variable and the interaction term in the BF should be considered to interpret the interaction term. For example, the BF15 for the interaction of traffic condition and number of freeway lanes, the equation can be written as:

$$-0.59407 \times (0, \text{Lanes} - 2) \times (\text{Traffic\_Condition in (1)}) \qquad \text{Equation 13}$$

Considering the free-flow traffic conditions (i.e., BF9=1), the final estimate of the interaction would be -0.59407 representing that if the lane-changing event occurs in more than two lanes in freeway and free-flow traffic conditions, the lead gaps will be lower. The effects of other interactions could be explained in a similar approach.

In MARS model, the effect of a given explanatory variable on the response variable could be easily identified by using the *Rate of Impression Expression*. It is worth mentioning that insignificant BFs needed to keep in the final model in order to calculate *Rate of Impression Expression* for an explanatory variable (*41*, *79*). For instance, the effect of LV speed on the lead gaps can be identified considering several steps (*115*). First, all the BFs that involve with LV speed should be selected and combined. For example, the relevant BFs for the LV speed would be BF4, BF9, BF12, BF20, BF21, and BF29. Afterward, the knots of the LV speed (i.e., 45.202, 76.096, 83.0836, and 122.005) and set of intervals/ranges considering the knots should be identified. Subsequently, for each interval, the BFs that are associated with that particular interval should be selected. Next, the *Impact Expression* for each specific interval could be obtained from the MARS equation by selecting the associated BFs for the given interval. The *Rate of Impression Expression* for the LV speed can be determined from the first derivative of the *Impact Expression* with respect to the LV speed. Based on the *Rate of Impression Expression*, the direction of impact could be positive, negative, or no impact. Table 19 shows the *Rate of Impression Expression* for the LV speed on the lead gaps for each identified interval.

Table 19 Impact of LV Speed on Lead Gaps

Combined Impact of LV Speed: 0.00341× (45.202-LV Sp.) × (76.096-RH) – 0.07589 × (LV Sp.-122.005) × (TC in (1)) – 0.03741 × (122.005 - LV Sp.) × (TC in (1)) – 0.03610 (83.0836-LV Sp.)			
Interval/Range	**Impact Expression**	**Rate of Impression Expression**	**Direction(s) of Impact**
≤ 45.202	0.00341× (45.202-LV Sp.) × (76.096-RH) - 0.03741× (122.005 - LV Sp.) × (TC in (1)) – 0.03610 × (83.0836-LV Sp.)	-0.00341(76.096-RH) + 0.03741 × (TC in (1)) + 0.03610	+ve (0.07351) if RH ≥76.096 m in free-flow conditions +ve if 54.539<RH<76.096 m in free-flow conditions -ve if RH<54.539 in free-flow conditions
45.202 < LV Sp.≤ 83.0836	-0.03741 × (122.005 - LV Sp.) × (TC in (1)) – 0.03610 × (83.0836-LV Sp.)	0.03741 × (TC in (1)) + 0.03610	+ve (0.07351) in free-flow conditions
83.0836 < LV Sp.≤ 122.005	-0.03741 × (122.005 - LV Sp.) × (TC in (1))	0.03741 × (TC in (1))	+ve (0.03741) in free-flow conditions
> 122.005	-0.07589 × (LV Sp.-122.005) × (TC in (1))	-0.07589 × (TC in (1))	-ve (-0.07589) in free-flow conditions

As can be seen from Table 19, LV speed had a different rate of impact on lead gaps in four different intervals. It is also worth noting that the directions of impact of LV speed also depend on the minimum rear headway for the first interval (i.e., not more than 45 kph). For instance, the lead gaps would be increased for the minimum rear headway greater than or equal 76 m under free-flow traffic conditions considering the first interval. This is also true for any minimum rear headway value from 54.5 to 76 m. However, lead gaps would be decreased with any value of less than 54.5 m. According to Table 19, lead gaps would be increased with the value of LV speed ranging from more than 45 to 122 kph under free-flow conditions (i.e., second and third interval). Moreover, lead gaps would be decreased in free-flow conditions (fourth interval) for any LV speed of greater than 122 kph.

MARS Model for Lag Gaps

MARS model was developed for the given explanatory variables considering lag gaps as a response variable. The results of the developed MARS model for lag gaps are provided in Table 20. Similar to the lead gaps model, the explanatory variables had no single direction of impact on the lag gaps and nonlinear performance was distinguished for all explanatory variables. The estimated parameters of BFs in Table 20 were significant at a 95 percent confidence level.

Table 20 MARS Model for Lag Gap Acceptance

BFs	Basis Function	Estimate	Standard Error	P-value
BF0	Constant	1.68551	0.13865	0.00000
BF1	(0, LCV Sp. - 4.46912)	Not Sig.	Not Sig.	Not Sig.
BF2	(0, RH - 72.16) × BF1	-0.00139	0.00019	0.00000
BF3	(0, 72.16 - RH) × BF1	-0.00195	0.00017	0.00000
BF4	(0, RH - 72.16)	0.08951	0.01286	0.00000
BF5	(0, 72.16 - RH)	0.12498	0.01053	0.00000
BF7	(0, LCV Sp. - 64.3712) × BF5	0.00185	0.00022	0.00000
BF11	(0, R - 2127)	-0.00005	0.00002	0.00321
BF12	(0, 2127 - R)	-0.00007	0.00003	0.02670
BF13	(0, LCV Sp. - 102.268) × BF11	0.000006	0.00000	0.00156
BF14	(0, 102.268 - LCV Sp.) × BF11	0.00001	0.00000	0.00000
BF16	(0, 5 - Lanes) × BF5	-0.00875	0.00150	0.00000
BF18	(0, 4 - Lanes) × BF1	0.00342	0.00064	0.00000
BF19	(0, LCV Sp. - 84.3765)	-0.01428	0.00457	0.00191
BF20	(0, 84.3765 - LCV Sp.)	Not Sig.	Not Sig.	Not Sig.
BF21	(0, Lanes - 3) × BF20	-0.02436	0.00308	0.00000
BF23	(0, LCV Acc. - 0.121325)	-0.35226	0.08879	0.00009
BF25	(0, RH - 69.76) × BF19	0.00173	0.00036	0.00000
BF27	(0, FV Acc. + 0.0232) × BF1	-0.03813	0.01048	0.00031
BF29	(0, RS($V_{LCV} - V_{FV}$)- 3.35113) × BF20	-0.00062	0.00006	0.00000
BF30	(0, 3.35113 - RS($V_{LCV} - V_{FV}$)) × BF20	-0.01089	0.00321	0.00077

In addition, there are several complex BFs exist in the lag gap model. As discussed earlier, the effect of a particular explanatory variable on the lag gaps could be identified using the *Rate of Impression Expression*. For instance, the *Rate of Impression Expression* for the FV acceleration on the lag gaps is provided in the following equations.

Impact Expression: -0.03813 × (FV Acc. + 0.0232) × (LCV Sp. - 4.46912) Equation 14

Rate of Impression Expression: -0.03813 × (LCV Sp. - 4.46912) Equation 15

Direction(s) of Impact: +ve if LCV Sp. > 4.46912, Zero if else Equation 16

According to equations 7-9, it is observed that the effect of FV acceleration on lag gaps depends on the LCV speed. For instance, FV acceleration had a positive effect on lag gaps for LCV speed greater than 4.7 kph, whereas, FV acceleration had no effect on lag gaps for LCV speed less than or equal 4.7 kph.

Variables Importance for Lead and Lag Gap Models

Table 21 provides the relative variable importance for lead and lag gap models, which is one of the most important MARS model outputs. As can be seen in Table 21, relative speed between LCV and LV turned out to be the most important variable affecting lead gap acceptance behavior. This indicates that relative speed between LCV and LV play a significant role in lead gap acceptance. The finding is consistent with previous studies exhibiting the effect of relative speed between LCV and LV on lead gap acceptance behavior (*70*, *72*). In contrast, LCV speed was found to be the most important variable affecting lag gap acceptance behavior. Minimum rear headway was the second important variable influencing both gap acceptance behaviors. Additionally, traffic conditions were the third important variable that affects lead gap acceptance, which is also consistent with a previous study (*72*). Table 21 also reveals that LV and LCV speeds, relative speed between LCV and FV, and the freeway number of lanes are the additional contributing factors affecting lead gap acceptance behavior. However, relative speed between LCV and FV was the third important variable affecting lag gap acceptance followed by the freeway number of lanes, curve radius, LCV and FV accelerations. It is worth noting that the relative speed between LCV and FV was found to be one of the common important factors in both gap acceptance behavior, which is also supported by a previous study (*72*).

Table 21 Relative Importance of Variables for Lead and Lag Gap Models

Lead Gap		Lag Gap	
Variable	**Score**	**Variable**	**Score**
$RS(V_{LCV} - V_{LV})$	100	LCV Sp.	100
RH	78.80	RH	85.58
TC	16.76	$RS(V_{LCV} - V_{FV})$	55.81
LV Sp.	12.83	Lanes	44.83
LCV Sp.	10.04	R	34.83
$RS(V_{LCV} - V_{FV})$	9.81	LCV Acc.	18.81
Lanes	9.40	FV Acc.	16.21

Speed Selection Behavior

Preliminary Analysis

Several possible distributions, including Weibull, normal, and lognormal, were investigated for each weather condition. Note that speed distribution is required for proper calibration of microsimulation models and characterization of traffic state in different weather conditions (*95*). To select the appropriate distribution, Akaike Information Criterion (AIC) was used as a measure of fitness. The AIC of the Weibull, normal, and lognormal distribution were found to be 12,916, 13,002, and 13,324, respectively, for rainy weather conditions. Therefore, it can be concluded that Weibull distribution fits the speeds the best in rainy weather under free-flow traffic amongst other distributions. Speeds in snow and fog were also found to have a Weibull distribution based on AIC as can be seen in Figure 22. Interestingly, speeds in clear weather conditions were found to have a normal distribution under free-flow traffic, which is in line with the literature (*95*, *127*). Speed distributions in congestion/mixed traffic under various weather conditions were also investigated; however, no specific distribution was found in mixed traffic.

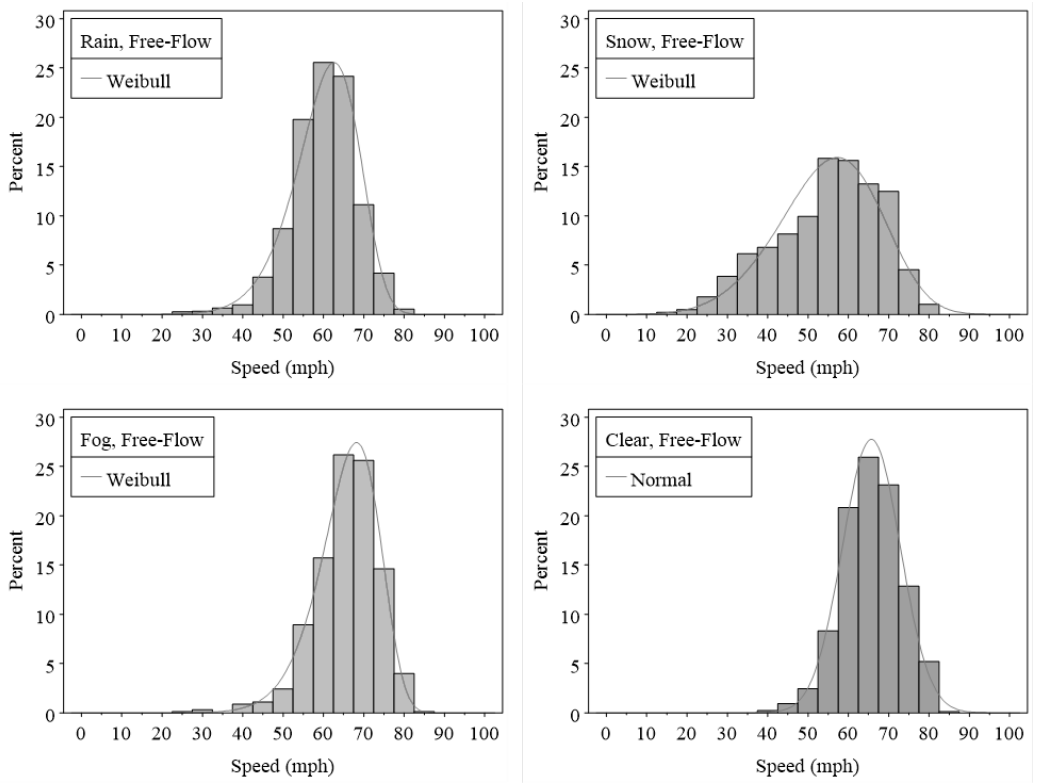

Figure 22 Distribution of Speeds in Rain, Snow, Fog, and Clear Under Free-Flow Condition

In addition, driver speeds in different weather conditions were also compared using Welch's t-test, as shown in Table 22. Only the trips in free-flow conditions were considered for this comparison since in congested flow; drivers are forced to reduce their speeds irrespective of weather conditions. Moreover, trips in adverse weather were matched with two trips in clear weather using ArcGIS software for the same driver, vehicle, and route. This was done to eliminate any potential bias due to different drivers' demographics and behaviors, vehicle characteristics, and roadway geometry. According to Table 22, speeds in rainy weather conditions were significantly lower than the speeds in clear weather conditions under free-flow

traffic. In addition, on average, driver speeds in rainy weather were 3.76 mph (5.95 percent reduction) less compared to their speed in matching clear weather trips. The speeds in snowy weather were also found to be significantly lower compared to speeds in matching clear trips. However, the negative effect of snow on driver speed was more significant than other adverse weather (e.g., rain and fog), since drivers reduced their speed by 10.49 mph (15.89 percent reduction) in snowy weather compared to their speeds in matching clear trips. Similarly, it was observed that drivers reduced their speeds by 2.64 mph (3.91 percent reduction) due to the presence of fog.

Table 22 Comparison of Speeds in Different Weather Under Free-flow Traffic

	Mean	SD	Min	Max	Speed Reduction	Welch's t-test
Rain	60.14	7.96	25.26	81.24	5.95 %	Speeds in rain are significantly lower than speeds in clear weather. t = -15.65, p-value < 2.2e-16
Matched Clear of Rain	63.90	6.83	41.14	85.41		
Snow	55.52	12.25	24.11	80.44	15.89%	Speeds in snow are significantly lower than speeds in clear weather. t = -30.93, p-value < 2.2e-16
Matched Clear of Snow	66.01	7.13	40.18	83.74		
Fog	64.93	8.18	24.02	83.23	3.91%	Speeds in fog are significantly lower than speeds in clear weather. t = -7.84, p-value = 9.2e-15
Matched Clear of Fog	67.57	7.07	40.02	85.71		

Association Rules Mining

Speed selection behavior, which had four levels, was considered as antecedent; and other variables related to traffic, environmental, roadway geometry, and driver demographics are considered as consequent. Association rules were generated for the levels of speed selection with other characteristics using 'arules' package in R® software. Since there were four levels of speed selection, 4 different sets of rules were generated for each of the levels. To get the optimum values of support and confidence, the trial and error process was utilized, as suggested by a previous study (*128*). In addition, the number of itemsets is another factor to be considered for proper interpretation of the results. A 2-item rule indicates that there are a single antecedent and a single consequent in the rule. Similarly, a 3-item rule indicates that there are two antecedents and one consequent or one antecedent, and two consequents in the rule (*74*). For this study, up to 4 rules were considered for appropriate and easily understandable interpretation of the results.

Rules for Speed Selection Level – 1 (More than 5 mph Above the Speed Limit)

The association rules considering speed selection level-1 as consequent were extracted and organized according to the decreasing lift value. After several iterations, the minimum support and confidence were set at 5 percent and 45 percent, respectively. Using these threshold values, the number of rules with a lift value greater than 1 was found to be 102. The top 25 rules for speed selection level-1 are listed in TABLE 3. It was found that novice drivers with experience of less than 10 years are highly associated with speeding in clear weather under free-flow traffic (support = 7.31 percent, confidence = 58.79 percent, lift = 1.891). The first rule with the highest lift value can be explained as follows: a) 7.31 percent of the speeds in the dataset occurred by

drivers with less than 10 years of driving experience in clear weather under free-flow traffic and produced speed selection level-1; b) out of all the speed selection levels in the dataset occurred by drivers with less than 10 years of driving in clear weather under free-flow traffic, 58.79 percent were speed selection level-1; and c) the proportion of speed selection level-1 by drivers with experience less than 10 years in clear weather under free-flow traffic was 1.891 times the proportion of speed selection level-1 in the complete dataset. According to Table 23, young drivers are associated with speed selection level-1, speeding more than 5mph above the speed limit, in several rules (Rule 9, Rule 12, Rule 23, and Rule 25). In addition, drivers with single marital status, and not affected visibility were also found to have an association with speed selection level-1 in several rules.

Table 23 First 25 Association Rules for Speed Selection Level-1

Rules	Antecedent	Support (percent)	Confidence (percent)	Lift
1	Driving Experience<10 years, Traffic=Free Flow, Weather=Clear	7.31	58.79	1.891
2	Driving Experience<10 years, Mileage Last Year= 10,000 to 20,000 miles, Traffic=Free Flow	5.77	57.21	1.840
3	Driving Experience<10 years, Traffic=Free Flow, Visibility=Not Affected	8.14	57.14	1.838
4	Marital Status=Single, Mileage Last Year= 10,000 to 20,000 miles, Traffic=Free Flow	5.94	57.02	1.834
5	Driving Experience<10 years, Surface=Dry, Traffic=Free Flow	8.57	56.96	1.832
6	Age=Young, Mileage Last Year= 10,000 to 20,000 miles, Traffic=Free Flow	5.93	55.36	1.781
7	Driving Experience<10 years, Gender=Female, Traffic=Free Flow	7.25	55.14	1.773
8	Driving Experience<10 years, Speed Limit<=60 mph, Traffic=Free Flow	6.37	55.11	1.773
9	Age=Young, Mileage Last Year= 10,000 to 20,000 miles, Weather=Clear	7.28	53.50	1.721
10	Driving Experience<10 years, Marital Status=Single, Traffic=Free Flow	8.35	53.49	1.720
11	Marital Status=Single, Mileage Last Year= 10,000 to 20,000 miles, Weather=Clear	7.31	53.49	1.720
12	Age=Young, Traffic=Free Flow, Weather=Clear	7.89	53.31	1.715
13	Curve=No, Driving Experience<10 years, Traffic=Free Flow	6.45	53.26	1.713
14	Driving Experience<10 years, Mileage Last Year= 10,000 to 20,000 miles, Weather=Clear	6.75	52.92	1.702
15	Marital Status=Single, Traffic=Free Flow, Weather=Clear	7.54	52.69	1.695
16	Driving Experience<10 years, Gender=Female, Weather=Clear	8.12	52.67	1.694
17	Marital Status=Single, Mileage Last Year= 10,000 to 20,000 miles, Visibility=Not Affected	7.67	52.06	1.674
18	Driving Experience<10 years, Mileage Last Year= 10,000 to 20,000 miles, Visibility=Not Affected	7.34	52.04	1.674
19	Driving Experience<10 years, Traffic=Free Flow	9.66	51.95	1.671
20	Gender=Female, Marital Status=Single, Traffic=Free Flow	7.18	51.45	1.655
21	Marital Status=Single, Traffic=Free Flow, Visibility=Not Affected	8.18	51.31	1.650
22	Marital Status=Single, Surface=Dry, Traffic=Free Flow	8.71	50.93	1.638
23	Age=Young, Surface=Dry, Traffic=Free Flow	9.15	50.83	1.635
24	Speed Limit<=60 mph, Traffic=Free Flow, Weather=Clear	11.06	50.81	1.634
25	Age=Young, Traffic=Free Flow, Visibility=Not Affected	8.61	50.79	1.634

Rules for Speed Selection Level – 2 (Between 0 to 5 mph Above the Speed Limit)

The association rules considering speed selection level-2 as a consequent were generated. After several trials, the minimum support and confidence were set at 3 percent and 33 percent , respectively. Once all the redundant rules with lift value less than 1 were eliminated, a total of 110 rules were found. The top 25 rules for this speed selection level according to the decreasing

order of lift value are listed in Table 24. It was found that male drivers in dry surface with mileage last year less than 10,000 miles were highly associated with speed selection level-2 (support = 7.31 percent, confidence = 58.79 percent, lift = 1.891) in dry road surface conditions. In addition, the effect of clear weather on selecting speed level-2 was found in several rules, including Rule 16, Rule 19, and Rule 20. Other antecedents that were found in several rules were young driver, single driver, and passenger car.

Table 24 First 25 Association Rules for Speed Selection Level-2

Rules	Antecedent	Support (percent)	Confidence (percent)	Lift
1	Gender=Male, Mileage Last Year<=10,000 miles, Surface=Dry	3.11	44.65	1.734
2	Gender=Male, Mileage Last Year<=10,000 miles, Visibility=Not Affected	3.09	43.76	1.699
3	Gender=Male, Mileage Last Year<=10,000 miles, Vehicle Class=Passenger Car/SUV	3.01	42.57	1.653
4	Age=Young, Gender=Male, Traffic=Free Flow	3.03	40.56	1.575
5	Age=Young, Mileage Last Year<=10,000 miles, Traffic=Free Flow	3.35	40.55	1.575
6	Marital Status=Married, Speed Limit>60 mph, Traffic=Free Flow	4.59	40.11	1.558
7	Lane<=2, Marital Status=Married, Speed Limit>60 mph	4.08	39.96	1.552
8	Age=Middle, Marital Status=Married, Speed Limit>60 mph	4.54	39.84	1.547
9	Marital Status=Single, Mileage Last Year<=10,000 miles, Vehicle Class=Passenger Car/SUV	3.51	39.56	1.536
10	Marital Status=Single, Mileage Last Year<=10,000 miles, Traffic=Free Flow	3.26	39.45	1.532
11	Gender=Male, Mileage Last Year<=10,000 miles	3.64	39.35	1.528
12	Age=Young, Mileage Last Year<=10,000 miles, Vehicle Class=Passenger Car/SUV	3.61	39.22	1.523
13	Mileage Last Year<=10,000 miles, Traffic=Free Flow, Visibility=Not Affected	4.31	39.03	1.516
14	Mileage Last Year<=10,000 miles, Surface=Dry, Traffic=Free Flow	4.31	39.03	1.516
15	Marital Status=Married, Speed Limit>60 mph, Surface=Dry	4.98	38.65	1.501
16	Marital Status=Married, Speed Limit>60 mph, Weather=Clear	3.55	38.55	1.497
17	Driving Experience=>10 years, Vehicle Class=Minivan/Pick-up	3.28	38.50	1.495
18	Marital Status=Married, Mileage Last Year= 10,000 to 20,000 miles, Speed Limit>60 mph	3.97	38.48	1.495
19	Mileage Last Year<=10,000 miles, Traffic=Free Flow, Weather=Clear	3.69	38.14	1.481
20	Mileage Last Year<=10,000 miles, Vehicle Class=Passenger Car/SUV, Weather=Clear	3.89	37.89	1.472
21	Mileage Last Year<=10,000 miles, Traffic=Free Flow, Vehicle Class=Passenger Car/SUV	4.14	37.72	1.465
22	Age=Middle, Speed Limit>60 mph, Traffic=Free Flow	4.58	37.70	1.464
23	Lane>2, Mileage Last Year<=10,000 miles, Surface=Dry	3.05	37.59	1.460
24	Mileage Last Year<=10,000 miles, Vehicle Class=Passenger Car/SUV, Visibility=Not Affected	4.59	37.55	1.459
25	Driving Experience=>10 years, Mileage Last Year<=10,000 miles, Surface=Dry	3.30	37.35	1.451

Rules for Speed Selection Level – 3 (Between 0 to 5 mph Below the Speed Limit)

The association rules with speed selection level-3 as consequent were extracted from the generated rules. The minimum support and confidence were set at 0.5 percent and 23 percent, respectively, which resulted in a total of 110 rules with lift values greater than 1. Table 25 listed the top 25 rules for the speed selection level-3 based on descending order of lift values. The highest lift value was found to be 2.425, representing the combined effect of old drivers, affected visibility, and roadways with a speed limit less than 60 mph on speed selection level-3. More

specifically, the proportion of selecting speed level-3 by old drivers on roadways with a speed limit less than 60 mph in affected visibility was 2.425 times the proportion of speed selection level-3 in the overall dataset. The old drivers were dominant in most of the rules for speed selection level-3. In addition, rainy weather was also found to have a significant association with speed selection level-3 in several rules including, Rule 3, Rule 6, Rule 8, Rule 9, Rule 11, Rule 12, Rule 14, Rule 15, and Rule 18. Additionally, affected visibility, wet road surface, female drivers were also found to have an association with speed selection level-3 in several rules as can be seen in Table 25.

Table 25 First 25 Association Rules for Speed Selection Level-3

Rules	Antecedent	Support (percent)	Confidence (percent)	Lift
1	Age=Old, Speed Limit<=60 mph, Visibility=Affected	0.70	32.92	2.425
2	Age=Old, Speed Limit<=60 mph, Surface=Wet	0.74	31.75	2.339
3	Age=Old, Speed Limit<=60 mph, Weather=Rain	0.68	31.23	2.300
4	Age=Old, Gender=Female, Mileage Last Year<=10,000 miles	0.70	31.21	2.299
5	Age=Old, Gender=Male, Mileage Last Year= 10,000 to 20,000 miles	0.76	30.05	2.213
6	Mileage Last Year<=10,000 miles, Speed Limit<=60 mph, Weather=Rain	0.88	29.35	2.161
7	Age=Old, Gender=Female, Speed Limit<=60 mph	0.72	29.21	2.151
8	Driving Experience=>10 years, Mileage Last Year<=10,000 miles, Weather=Rain	0.79	28.81	2.122
9	Gender=Female, Mileage Last Year<=10,000 miles, Weather=Rain	0.71	28.76	2.118
10	Age=Old, Lane<=2, Mileage Last Year= 10,000 to 20,000 miles	0.57	28.71	2.115
11	Lane<=2, Mileage Last Year<=10,000 miles, Weather=Rain	0.77	28.57	2.104
12	Mileage Last Year<=10,000 miles, Traffic=Free Flow, Weather=Rain	0.78	28.54	2.102
13	Age=Old, Surface=Wet, Visibility=Affected	0.71	28.39	2.091
14	Age=Old, Visibility=Affected, Weather=Rain	0.67	28.10	2.069
15	Marital Status=Married, Mileage Last Year<=10,000 miles, Weather=Rain	0.54	28.08	2.068
16	Driving Experience=>10 years, Gender=Female, Mileage Last Year<=10,000 miles	1.68	27.97	2.060
17	Age=Old, Gender=Female, Lane<=2	0.93	27.95	2.059
18	Mileage Last Year<=10,000 miles, Visibility=Affected, Weather=Rain	0.93	27.73	2.043
19	Age=Old, Lane<=2, Speed Limit<=60 mph	1.23	27.57	2.030
20	Age=Old, Mileage Last Year= 10,000 to 20,000 miles, Traffic=Free Flow	0.88	27.44	2.021
21	Age=Old, Marital Status=Married, Visibility=Affected	0.70	27.44	2.021
22	Age=Old, Mileage Last Year<=10,000 miles, Speed Limit<=60 mph	0.91	27.42	2.019
23	Marital Status=Others, Mileage Last Year<=10,000 miles	0.56	27.30	2.011
24	Age=Old, Lane<=2, Visibility=Affected	0.66	27.30	2.010
25	Driving Experience=>10 years, Mileage Last Year<=10,000 miles, Vehicle Class=Minivan/Pick-up	0.55	26.98	1.987

Rules for Speed Selection Level – 4 (More than 5 mph Below the Speed Limit)

The association rules with speed selection level-4 as consequent were generated using a minimum support and confidence level of 5 percent and 42 percent, respectively. A total of 105 rules with a lift value of more than 1 were found after removing all the redundant values. However, only the top 25 rules are reported in Table 26. As mentioned earlier, the speed selection level-4 represents a reduction in speed more than 5 mph below the speed limit. As expected, adverse weather condition, especially snowy weather, was found to have an association with speed selection level-4 in several rules. The highest association (support = 5.02 percent, confidence = 74.11 percent, lift = 2.505) was found for Rule 1 representing the

combined effect of snow weather and snowy road surface on driver speed selection level-4. This rule can be expressed as a) 5.02 percent of the speeds in the dataset occurred in snowy weather with the snowy road surface and produced speed selection level-3; b) out of all the speed selection levels in the dataset that occurred in snowy weather with the snowy road surface, 74.11 percent were speed selection level-4; and c) the proportion of speed selection level-4 in snowy weather with snowy road surface was 2.505 times the proportion of speed selection level-4 in the complete dataset.

Table 26 First 25 Association Rules for Speed Selection Level-4

Rules	Antecedent	Support (percent)	Confidence (percent)	Lift
1	Surface=Snowy, Weather=Snow	5.02	74.11	2.505
2	Surface=Snowy	5.10	71.00	2.400
3	Weather=Snow	5.68	70.67	2.389
4	Speed Limit<=60 mph, Traffic=Mixed Flow, Visibility=Affected	5.45	69.87	2.362
5	Traffic=Mixed Flow, Vehicle Class=Passenger Car/SUV, Visibility=Affected	5.08	67.07	2.267
6	Marital Status=Married, Mileage Last Year= 10,000 to 20,000 miles, Traffic=Mixed Flow	10.95	65.57	2.217
7	Age=Middle, Speed Limit<=60 mph, Traffic=Mixed Flow	11.77	65.10	2.201
8	Traffic=Mixed Flow, Visibility=Affected	6.02	64.64	2.185
9	Age=Middle, Marital Status=Married, Traffic=Mixed Flow	11.54	64.27	2.172
10	Gender=Male, Marital Status=Married, Traffic=Mixed Flow	9.60	63.89	2.160
11	Age=Middle, Mileage Last Year= 10,000 to 20,000 miles, Traffic=Mixed Flow	10.62	63.80	2.157
12	Age=Middle, Gender=Male, Traffic=Mixed Flow	9.43	63.03	2.131
13	Marital Status=Married, Speed Limit<=60 mph, Traffic=Mixed Flow	11.43	62.83	2.124
14	Age=Middle, Lane>2, Traffic=Mixed Flow	11.53	62.15	2.101
15	Lane>2, Marital Status=Married, Traffic=Mixed Flow	10.77	61.84	2.090
16	Driving Experience=>10 years, Mileage Last Year= 10,000 to 20,000 miles, Traffic=Mixed Flow	11.69	61.77	2.088
17	Driving Experience=>10 years, Speed Limit<=60 mph, Traffic=Mixed Flow	13.22	61.62	2.083
18	Age=Middle, Traffic=Mixed Flow, Vehicle Class=Passenger Car/SUV	13.13	61.33	2.073
19	Driving Experience=>10 years, Marital Status=Married, Traffic=Mixed Flow	12.71	61.20	2.069
20	Age=Middle, Curve=No, Traffic=Mixed Flow	9.57	61.03	2.063
21	Marital Status=Married, Traffic=Mixed Flow, Vehicle Class=Passenger Car/SUV	12.37	60.91	2.059
22	Gender=Male, Speed Limit<=60 mph, Traffic=Mixed Flow	10.28	60.53	2.046
23	Curve=No, Marital Status=Married, Traffic=Mixed Flow	8.93	60.37	2.041
24	Age=Middle, Driving Experience=>10 years, Traffic=Mixed Flow	13.77	60.11	2.032
25	Age=Middle, Traffic=Mixed Flow	13.87	59.91	2.025

Visualization of Extracted Rules for Speed Selection Behavior

The results were visualized using grouped balloon plot and scatter plot of the association rules. The grouped balloon plot can illustrate the relationship between the antecedent groups and the consequent of all the rules. The antecedent groups, also known as LHS, are arranged in rows and the consequent, also known as RHS, are arranged in the column as depicted in Figure 23 to Figure 26. The aggregated support and lift values are represented by the size and color of the balloons, respectively. The darker the shades of red, the higher the aggregated lift value, as well

as the larger the size of the balloon, the greater the aggregated support value. The rows are arranged based on the decreasing values of lift. Figure 23 illustrates that the most important group for speed selection level-1 consists of 1 rule which contains clear weather, drivers with less than 10 years of experience as well as one other item in the antecedent. Similarly, Figure 26 illustrates that the most important group for speed selection level-4 consist of snowy weather as well as snowy road surface condition.

Figure 23 Balloon Plot of the Generated Association Rules (Speed Selection Level 1)

Figure 24 Balloon Plot of the Generated Association Rules (Speed Selection Level 2)

Figure 25 Balloon Plot of the Generated Association Rules (Speed Selection Level 3)

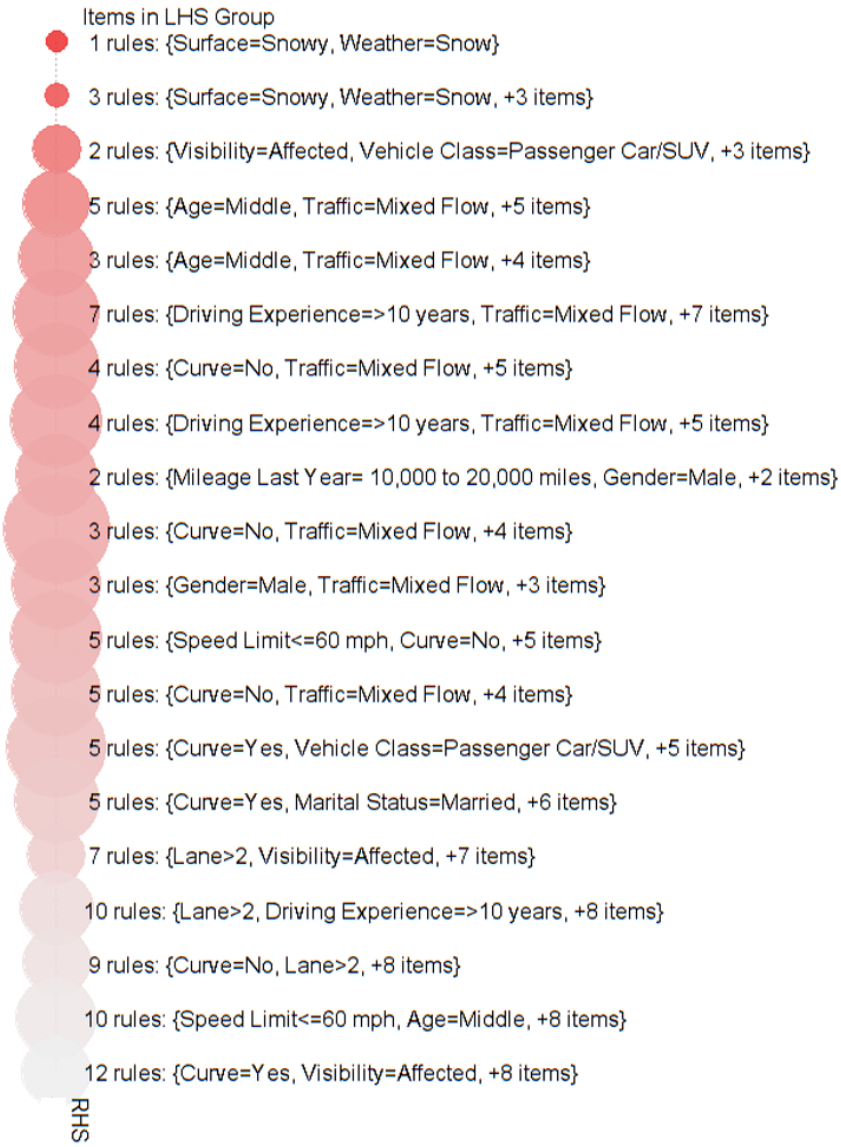

Figure 26 Balloon Plot of the Generated Association Rules (Speed Selection Level 4)

In addition, scatter plots were also created in order to illustrate the relationship among confidence, support, and lift in the associated rules for each of the speed selection levels. Note that important rules are generally clustered near the support/confidence border (*129*). Therefore, according to Figure 27 to Figure 30, the distribution of the generated rules can be considered as acceptable to achieve the study objective, since the majority of the points are located close to the support/confidence border. Most of the rules for the speed selection level-1 are clustered between the support value of 0.05 to 0.13 and up to 58 percent confidence with a maximum lift value of 1.9. On the other hand, most of the rules for speed selection level-4 are distributed between the support value of 0.05 to 0.02 and up to 74 percent confidence with a maximum lift value of 2.5.

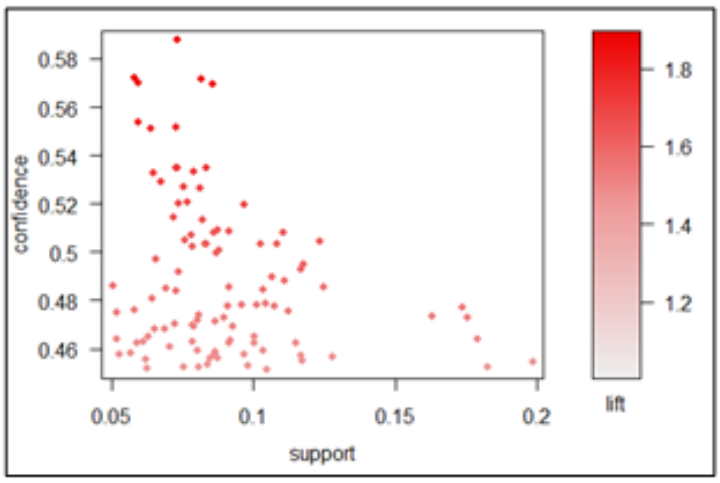

Figure 27 Scatter Plot of the Generated Association Rules (Speed Selection Level 1)

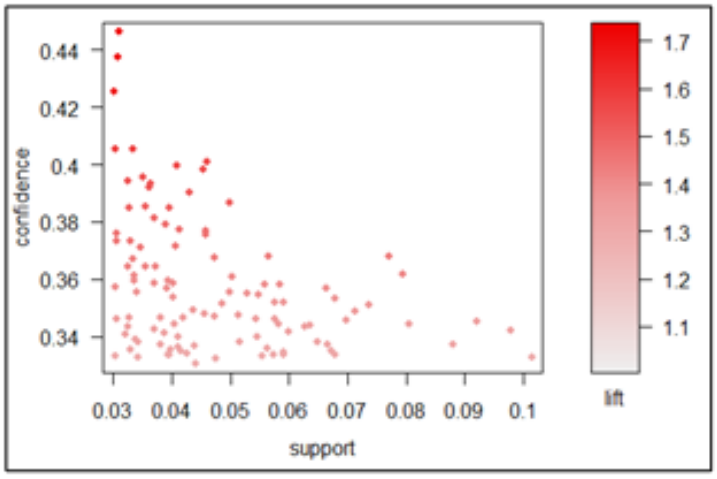

Figure 28 Scatter Plot of the Generated Association Rules (Speed Selection Level 2)

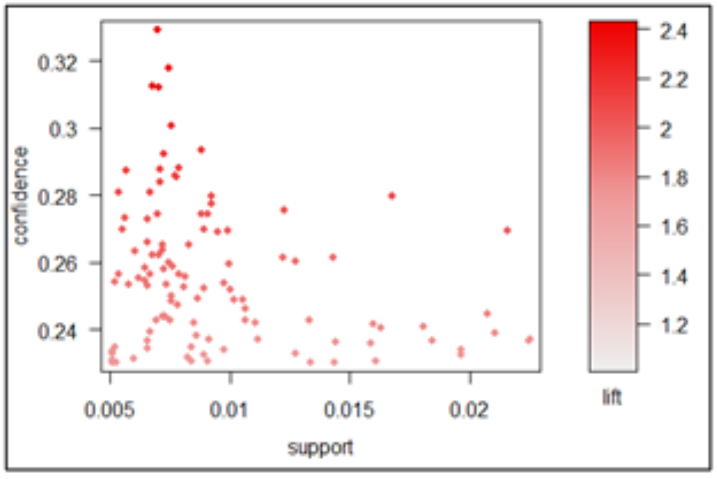

Figure 29 Scatter Plot of the Generated Association Rules (Speed Selection Level 3)

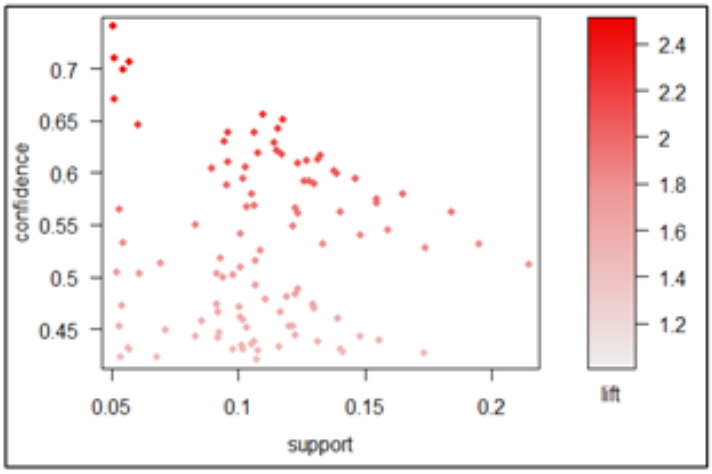

Figure 30 Scatter Plot of the Generated Association Rules (Speed Selection Level 4)

Ordered Logit Regression

In addition to the association rules mining approach, an order logistic regression model was also calibrated to investigate the effect of adverse weather on driver speed selection behavior. A total of 15,326 1-minute segments in different weather and traffic conditions were used in order to develop the model. Table 1 shows a summary of the variables used in the ordered logit model. Similar to the previous approach, the response variable was speed selection with four categories. Other variables related to driver demographics, roadway geometry, and environmental factor were considered as explanatory variables. The log-likelihood ratio was utilized to evaluate the fitness of the model. It was found that the overall explanatory variables had a statistically significant effect on the response at a 95 percent confidence level with a p-value less than 0.05 as can be seen in Table 27. To check any potential correlation, the variance inflation factor (VIF) was checked among all the explanatory variables, which revealed that all the variables had a VIF value less than 3. Note that, a VIF less than 10 indicates that there is no multicollinearity problem (*130*). Thirteen variables, as well as three interaction terms, were found to have a significant effect on the speed selection as can be seen in Table 27.

Table 27 Estimation of Ordered Logit Model for Speed Selection

Parameters		Estimate	Standard Error	Wald Chi-Square	P-value	Odds Ration	95% Confidence Interval	
Intercept		-2.229	0.062	1312.618	<.0001	0.108	-2.350	-2.109
Intercept		-1.463	0.060	593.235	<.0001	0.232	-1.580	-1.345
Intercept		-0.150	0.059	6.525	0.0106	0.861	-0.265	-0.035
Weather, (B = Clear)	Rain	0.372	0.102	13.332	0.0003	1.450	0.172	0.571
	Snow	1.521	0.142	115.337	<.0001	4.577	1.243	1.799
	Fog	0.572	0.049	137.124	<.0001	1.773	0.477	0.668
Surface, (B = Dry)	Wet	0.427	0.092	21.421	<.0001	1.532	0.246	0.607
	Snowy	1.080	0.143	56.783	<.0001	2.945	0.799	1.361
Visibility (B = Not Affected)	Affected	0.251	0.065	15.148	<.0001	1.286	0.125	0.378
Traffic, (B = Free-flow)	Mixed	1.649	0.037	1995.194	<.0001	5.202	1.577	1.721
Speed limit, (B ≤ 60 mph)	> 60 mph	0.146	0.036	16.896	<.0001	1.157	0.076	0.216
Curve, (B = No)	Yes	0.165	0.057	8.488	0.0036	1.180	0.054	0.276
Lane, (B ≤ 2)	> 2 lanes	-0.156	0.054	8.403	0.0037	0.855	-0.262	-0.051
Gender, (B=female)	Male	0.174	0.038	21.397	<.0001	1.190	0.100	0.248
Marital Status, (B = Single)	Married	-0.179	0.065	7.610	0.0058	0.836	-0.306	-0.052
	Others	-0.266	0.089	9.040	0.0026	0.766	-0.440	-0.093
Vehicle Class, (B = Passenger Car)	Minivan/Pick-up	-0.214	0.044	23.758	<.0001	0.807	-0.300	-0.128
Mileage Last Year, (B ≤ 10,000 miles)	10,000 to 20,000 miles	-0.494	0.042	137.515	<.0001	0.610	-0.577	-0.412
	≥ 20,000 miles	-0.873	0.053	270.968	<.0001	0.418	-0.977	-0.769
Driving Experience, (B < 10 Years)	≥ 10 years	0.574	0.067	74.266	<.0001	1.776	0.444	0.705
Age, (B = Young)	Middle	0.218	0.064	11.454	0.0007	1.244	0.092	0.344
	Old	0.432	0.080	29.168	<.0001	1.541	0.275	0.589
Curve*Driving Experience	Yes, ≥ 10 years	-0.184	0.069	7.139	0.0075	0.832	-0.319	-0.049
Visibility × Gender	Affected, Male	-0.660	0.072	83.250	<.0001	0.517	-0.802	-0.518
Lane × Marital Status	> 2 lanes, Married	0.458	0.069	44.389	<.0001	1.580	0.323	0.592
	> 2 lanes, Others	0.405	0.117	11.989	0.0005	1.499	0.176	0.634
Fit Statics Likelihood Ratio Test: $\chi^2 = 4707.467$, Df = 23, P-value < 0.001 Akaike Information Criterion (AIC) = 41202.310 -2 Log L = 41196.310								

B = Base Category

As expected, all the adverse weather conditions had a significant effect on speed selection behavior. It was found that drivers were more likely to choose lower speeds in adverse weather conditions. More specifically, the odds of drivers reducing their speeds were 1.45, 4.56, and 1.77 times higher in rain, snow, and fog, respectively, compared to their counterparts' speeds in clear weather. Note that, driving over the speed limit in adverse weather could be hazardous due to a significant reduction of available stopping sight distance. This study indicates that drivers reduced their speed to compensate for the negative effect of adverse weather. Other environmental factors, such as visibility and surface conditions, were also found to affect speed

selection significantly. Findings related to surface conditions revealed that the odds of drivers reducing their speeds in wet and snowy surfaces were 1.53 and 2.95 times higher compared to dry surfaces, respectively.

The traffic conditions were found to have a positive impact on speed reduction. Controlling all other factors, drivers are 5.2 times more likely to reduce their speeds in mixed traffic conditions compare to free-flow conditions. In addition, it was found that older drivers with age more than 65 years old were 1.54 times more likely to reduce their speed compared to the speeds of younger drives with age less than 25 years of age.

Considering the interaction terms, it was found that experienced drivers with more than 10 years of driving history were 17 percent less likely to reduce their speed on curves compared to drivers with an experience of fewer than 10 years and driving in straight segments. This result indicates that the experienced drivers are usually more confident to drive at higher speeds on curves compared to less experienced drivers (*127*).

Chapter 3. Radar-Vision Algorithms to Process Trajectory-Level Driving Data

Background

The investigation of driver behavior has been at the forefront of transportation research for decades. Research in this field examines trajectory-level driving data (e.g., speed, acceleration, and position) to characterize drivers' sophisticated and unique actions while operating a vehicle. It is critical that industry decision-makers understand the role of driver behavior on the safety, operations, and reliability of their transportation networks. While recognized as an important field of study, driver behavior is rarely considered by practitioners. This underrepresentation in practice is primarily due to limited consensus of the quantitative impacts that drivers' heterogeneous behaviors have on accurately forecasting traffic operations. Studies aiming to capture these quantitative effects have been limited by a deficit in high resolution trajectory-level driving data containing a substantial number of drivers in natural driving environments (*131–134*). Without a sufficient quantity of appropriate data, findings are ungeneralizable and outcomes cannot be included in practical decision support systems.

In recent decades, noteworthy advancements in the collection of trajectory-level data have been made. Among these data collection methods are aerial video footage, driving simulators, instrumented research vehicles (IRV), and naturalistic driving studies (NDS). Each data collection procedure has advantages and disadvantages associated with collection cost, background knowledge of driver characteristics, the quantity of driving data for particular roadways or driving environments, and the capacity to elicit and record natural driver responses. Among these, NDS enable the collection of large quantities of naturalistic trajectory-level data on a variety of roadways from a diverse set of drivers; this presents an unprecedented opportunity for the advancement of driver behavior research.

While a surplus of benefits is evident for using NDS data to examine driver behavior, one major impediment standing between data acquisition and data analytics is the substantial data processing required to transform the raw data into a usable format (*135*). In an effort to propel driver behavior research from its current plateau, this paper uses a sample of the second Strategic Highway Research Program (SHRP2) NDS data acquired from the Wyoming Department of Transportation's Implementation Assistance Program (IAP) project (*89*) to develop two algorithms that extract information about NDS trips using the collected radar data. The contributed algorithms automatically detect the driving state—defined by the presence of a downstream lead vehicle—and the transition events—the action that causes a change between two different driving states—from trajectory-level data. This effort serves as a foundation for the evaluation of driver heterogeneity among different driving populations and between different driving environments. The processed data can be used for driver behavior analytics, including the development, calibration, and validation of driver behavior models used in traffic simulation.

Literature Review

The SHRP2 NDS data have been available for six years. Previously, the Virginia Tech 100-Car NDS was conducted using a similar DAS (*136*). From the resulting database, multiple studies evaluated driving behavior for the purpose of developing and calibrating behavioral models. Sangster et al. applied eight drivers' data from the 100-Car NDS to calibrate four common car-following models (*137*). In processing these data, the authors identified multiple errors in the reported radar data that rendered systematic identification of car-following states (i.e., driving

states in which the subject vehicle is consistently following a lead vehicle) unreliable. The findings from their study provided guidance for the calibration of car-following models using naturalistic driving data and highlighted limitations in existing methods to process the data for widespread analyses (*137*).

Another study conducted by Higgs and Abbas evaluated the feasibility of automated segmentation and clustering of car-following behavior for the purpose of categorizing driving patterns (*138*). Using the data from twenty 100-Car NDS drivers, car-following states were automatically extracted using the following guidelines: (*i*) lead vehicle in same travel lane, (*ii*) following distance less than 120 meters, (*iii*) limited roadway curvature, (*iv*) speeds above 20km/hr, and (*v*) 30 seconds or more of continuous following behavior. From their study, Higgs and Abbas identified significant heterogeneity between drivers' behavior and discussed the need for a statistically significant sample size (i.e., number of drivers and amount of data per driver) to achieve meaningful results. They concluded that consideration of more drivers could result in the detection of more unique driving patterns (*138*).

Experience collecting and processing the 100-Car NDS were used to inform the development of the SHRP2 NDS. For instance, a data processing methodology was established to improve the usability of the SHRP2 NDS radar data. These procedures are reported in Reference (*139*) and summarized below for brevity.

- Reorganized data into an intuitive format.
- Corrected the time lag between data collection units.
- Merged objects to create continuous targets.
- Smoothed longitudinal range and range rate variables using a cubic spline.
- Computed lateral range and range rate variables.
- Identified and removed ghost targets.
- Estimated targets' direction-of-travel.
- Estimated targets' lane classification (relative to the subject vehicle)

Ultimately, each vehicle target was given a unique target identifier and the relative position of each target at each timestamp was updated. The position data were separated into (*i*) X distance, (*ii*) Y distance, (*iii*) rate of change in the X direction, and (*iv*) rate of change in the Y direction. The physical interpretation of the distance measurements is shown in Figure 31. Using these measurements, VTTI classified each target based on predicted travel direction and lane classification relative to the subject vehicle. This procedure resulted in a binary output for each target at each timestamp indicating whether or not the target is the current lead vehicle.

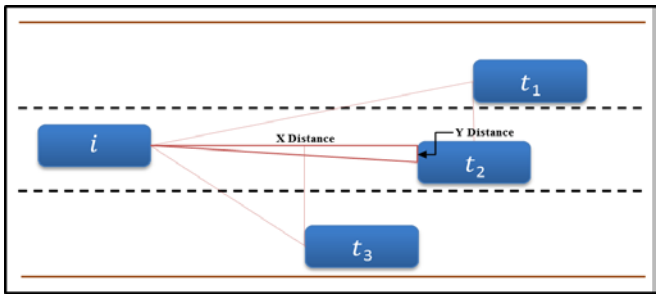

Figure 31 Processed Distance Measurements from Radar

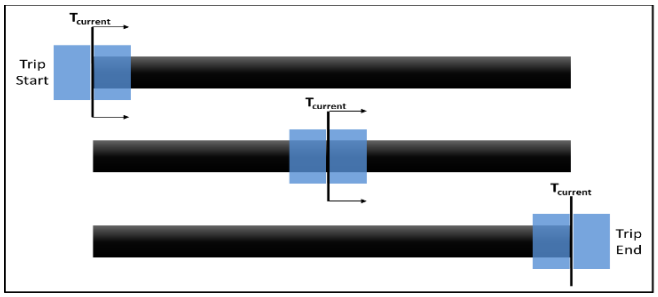

Figure 32 Iterative Smoothing Algorithm: Concept Diagram

While significantly better than the raw radar data, automatic identification of car-following using the processed radar data is restricted by inaccuracies in the classification of a target's lane. Use of the existing lane classification results produces a substantial number of false-negatives—that is, situations in which a target was denoted as *not* being a lead vehicle but actual conditions (as verified by the positional radar data and the front video) indicated that the target *was* the lead vehicle—and unreasonably short driving states caused by frequent shifts in target lane classifications. Therefore, the authors strived to build upon this effort by applying the processed radar measurements in a newly developed algorithm designed to reliably and continuously detect the presence of a lead vehicle throughout an NDS trip.

Driving State Detection & Event Classification

A fundamental component to analyzing driver behavior is identifying the driving environment. In this context, the driving environment is defined by external objects (e.g., other road users) and conditions (e.g., roadway configuration and weather conditions) that could impact driver behavior or vehicle performance. Advanced video processing techniques are currently being explored to infer some of these environmental conditions using SHRP2 NDS (*89*); however, these efforts are still ongoing and current progress has been limited by both the analytic complexity and the variability in video data quality. The research efforts discussed previously, as well as many other projects using NDS or other IRV data, developed algorithms to detect the immediate driving environment—the presence of a lead vehicle—from radar data (*137*, *138*). These algorithms are defined by thresholds (i.e., following distance, lateral offset, and speed) that are intended to ensure the following vehicle is continuously influenced by a single lead vehicle. Even with these defined thresholds, many previous studies are limited to a small sample of drivers with a small sample of trips because of the large processing effort needed to attain reliable outputs. The relevance of findings from even the most innovative analytic efforts are dependent on the size and diversity of their input data, which underscores the importance of generating systematic, reliable, and efficient algorithms to define the driving environment.

To address this need, the following algorithms were built to extract information about the driving environment from the internal and external sensor data, primarily from the forward-facing radar. Within the spectrum of "radar vision", the primary goal is to identify *driving states* in which the subject vehicle's radar detects (*i*) a downstream vehicle in the same travel lane (i.e., constrained driving scenario) or (*ii*) no vehicles in the downstream travel lane (i.e., unconstrained driving scenario). A new driving state is activated whenever the subject vehicle transitions between a constrained and an unconstrained driving state or when the target identified in a constrained state changes (i.e., a new lead vehicle is identified). Then, the procedure adds value to understanding these driving states by estimating the *driving events* that caused a transfer in driving state (e.g.,

lane change). The following definitions are provided to supplement the discussion in the subsequent sections.

- **Lead Vehicle**: a target is identified as a "lead vehicle" when it is traveling downstream of the subject vehicle in the travel lane—in this definition, no assumption is made regarding *if* or *when* the subject vehicle reacts to the presence of this lead vehicle.
- **Driving State**: current driving environment defined by the existence of a lead vehicle. The driving state can be either unconstrained with no lead vehicle or constrained with a lead vehicle. Each constrained driving state is distinguished by a unique target identifier.
- **Driving Segment**: collection of consecutive data points in which the driving state remains unchanged. For example, a driving segment could represent a continuous time period where no lead vehicle exists or where Target "A" exists.
- **Events**: describe the actions of the following or lead drivers that resulted in a change in driving state. These actions could include lane changes, approaching a lead vehicle, or separating from a lead vehicle.

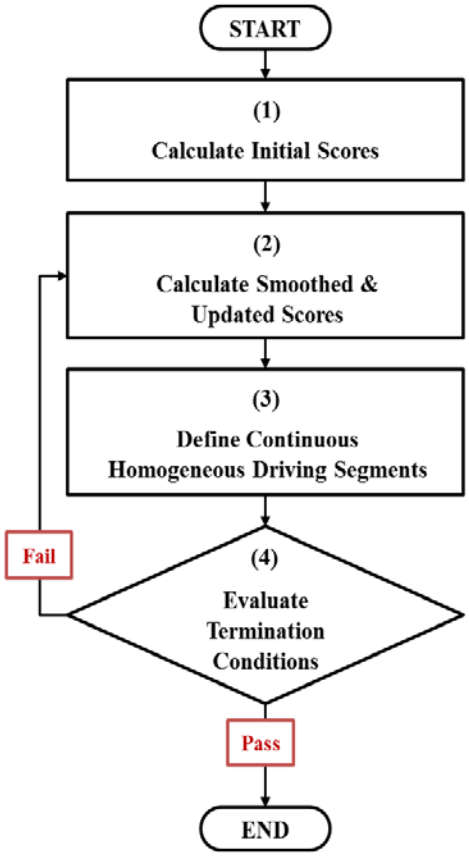

Figure 33 Iterative Smoothing Algorithm: Process Diagram

Iterative Smoothing Algorithm to Detect Driving State

The first algorithm was developed to determine the driving state at each time step and identify continuous segments of homogeneous driving states (e.g., 30 seconds following target A, 20 seconds with no lead target, 50 seconds following target B, etc.). An improvement to prior data processing efforts is achieved by estimating the driving state from *windows* of past and future radar data. This methodology involves greater computation power and larger memory storage;

however, it overcomes the limitations of instantaneous driving state predictions that are influenced by inherently noisy radar data. The general concept of the developed algorithm is shown in Figure 33. If the long rectangle is considered the flattened "video roll" of a particular trip, the algorithm generates a window of historic and future data surrounding each time step. Moving time step by time step through the trip (with a data recording frequency of 10 Hz), the algorithm estimates the driving state at each point. The driving state estimates are smoothed by repeating this process until termination conditions are reached.

The next sections discuss each step in the iterative smoothing algorithm, as shown in the process diagram illustrated in Figure 33. The following definitions are provided for reference in the discussion of the iterative smoothing algorithm.

Score: probabilistic value between [0, 1] assigned to each possible driving state at each time step indicating the probability of that specific driving state at that time step. For example, if the score for Target A is 0.9 and the score for No Lead Vehicle is 0.1, then there is an 90 percent chance that Target A is the lead vehicle and a 10 percent chance that No Lead Vehicle exists.

Initial Score: instantaneous score calculated using the radar data from a single time step.

Smoothed Score: score calculated from historic and future data windows for each target at each time step.

Updated Score: score calculated from a weighted average of the previous updated score in first iteration, this is the initial score—and the smoothed score for each target at each time step.

Score Matrix: matrix containing the probable driving state at each timestamp. The matrix is generated after the initial scores are calculated and is updated after each iteration of the smoothing algorithm.

Calculate Initial Scores

The first step in the iterative smoothing algorithm is to make an initial assessment of the probable driving state at each timestamp. The SHRP2 NDS radar unit is able to track up to eight targets at any given time (*139*); therefore, in this first step, the algorithm examines the data at each time step to calculate an initial score for each target at each timestamp. The probable driving state at each timestamp is then attributed to the driving state with the highest initial score; this information is stored in the score matrix.

The initial score is calculated using fuzzy set logic, which transforms explicit numeric inputs into the fuzzy domain, applies rules based on the derived fuzzy values, and transforms the results back into an explicit output. Fuzzy logic is appropriate when input noise or system uncertainty is easier to manage in a "fuzzy" domain than the "explicit" domain. When inferring driving state from radar measurements, both uncertainty and input noise are evident, making the detection of driving state an ideal candidate for a fuzzy logic solution. Figure 34 illustrates the developed methodology.

For every target at every timestamp, the relative position of the subject vehicle with respect to the target vehicle is input to the algorithm. Next, the fuzzification process transforms the explicit input values into fuzzy sets. The x-distance is converted into following distance with three fuzzy sets: close, moderate, and far distances. The y-distance is converted to represent the lateral lane offset with two fuzzy sets: in lane and not in lane. For each fuzzy set, membership functions

were developed to compute a degree of membership between [0, 1] that indicate how closely the input data match the described fuzzy set. Rather than using classical logic that requires crisp thresholds to classify data, fuzzy logic introduces flexibility and allows overlapping membership functions. In this way, a single input value can belong to one or more fuzzy sets at varying degrees of membership.

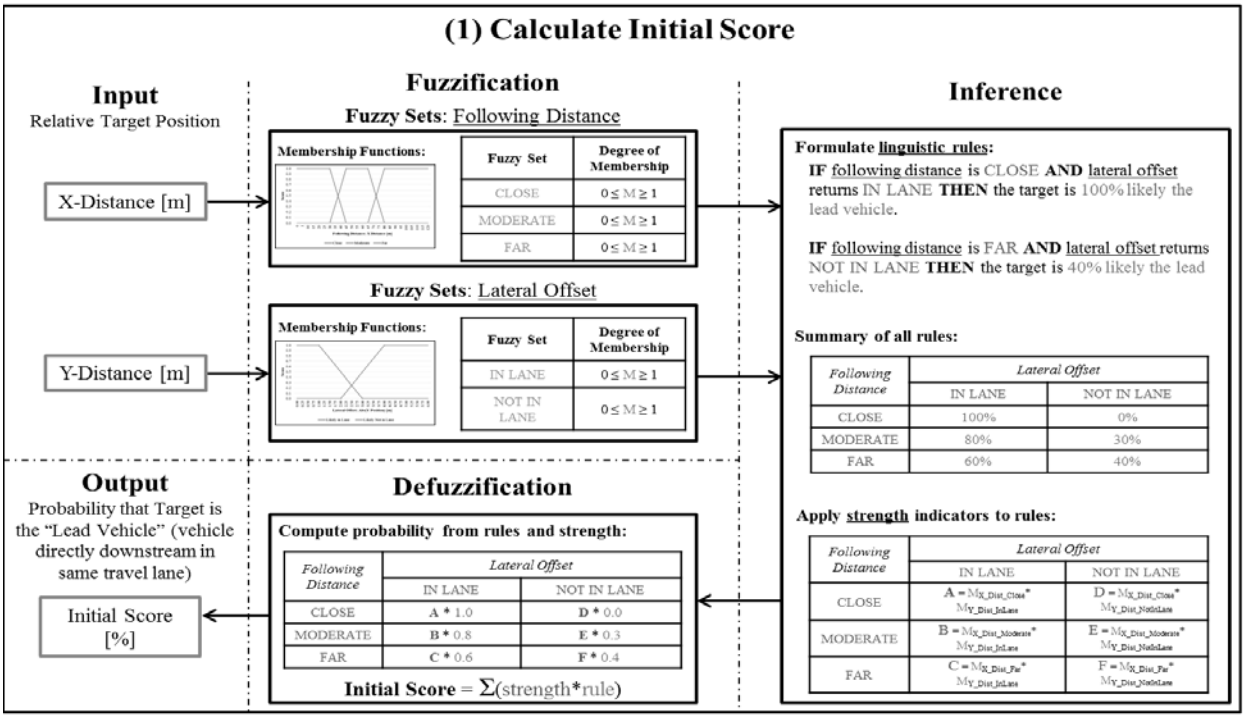

Figure 34 Initial Score Calculation

Once membership values are computed for each of the five fuzzy sets—close distance, moderate distance, far distance, in travel lane, and not in travel lane—the inference process begins. Inference processing, or rule evaluation, is central to knowledge-based decision-making. In the fuzzy domain, rules are developed linguistically expressed in an IF…THEN… format to describe dependencies between system inputs and system outputs. Six rules were developed that describe the driving state with each combination of lateral offset and following distance fuzzy sets; for example, IF following distance is **close** AND lateral offset returns **in lane** THEN the target is 100 percent likely the lead vehicle. The rules were formed considering the increasing level of uncertainty that arises with increased following distance, which is why greater confidence that a target is the lead vehicle is given to a target at a *far distance* that is *not in the travel lane*, compared with a target at a *moderate distance* that is also *not in the travel lane*. This increase in uncertainty at greater following distances stems from known radar precision limitations that amplify as objects' relative distance increases. Moreover, as the following distance decreases, greater certainty is available to determine whether a target is or is not the lead vehicle. This further explains why the likelihood that a target is the lead vehicle at a *close distance* is 100 percent when the target is *in the travel lane* and 0 percent when the target is *not in the travel lane*.

Finally, strength indicators are computed by multiplying membership values of corresponding fuzzy sets, as described in each linguistic rule. Using the rule definitions and strength values, the

defuzzification process computes the probability that the input target is the lead vehicle. This initial score is calculated as the sum of the product between each rule and corresponding strength value. Once initial scores are calculated for each target in a single timestamp, the initial score for "no lead vehicle" is calculated by subtracting the maximum initial score of all targets in that timestamp from one. For example, if at Time = 1, the score of Target A = 0.4, the score of Target B = 0.3, and the score of Target C = 0.6, the score for the "no lead vehicle" driving state = 1.0 – 0.6 = 0.4.

Calculate Smoothed & Updated Scores

After computing the initial scores, the iterative smoothing procedure begins with the calculation of smoothed and updated scores. Pseudocode, a graphic, and equations describing this procedure are given in Figure 35. Walking through the pseudocode, the first level of the algorithm iterates through each timestamp. Within each timestamp, the probable driving state is identified from the score matrix. Next, the probable driving states from windows of historic and future data immediately before and after the current timestamp are collected. Then, the algorithm loops through each possible driving state at that timestamp to calculate the smoothed and updated scores.

The smoothed score of a possible driving state is derived from the occurrence frequency and relative order of that driving state in the historic and future windows of probable driving states. To illustrate this concept, if the historic window of probable driving states at Time 10 = {no_lead, no_lead, no_lead, no_lead, target_a}, with the beginning of the list representing Time 5 and the end representing Time 9, and the current possible driving state is no_lead, then the historic frequency (f_H) and relative order (o_H) would be $f_H = 4/5$ (i.e., 4 occurrences of no_lead in window) and $o_H = 4/5$ (i.e., position of most recent no_lead in window is 4), respectively. These values are divided by the length of the historic list (length = 5) to normalize the output between [0, 1]. The final smoothed score is calculated with the frequency and order values from the historic and future windows, placing greater emphasis on frequency than order.

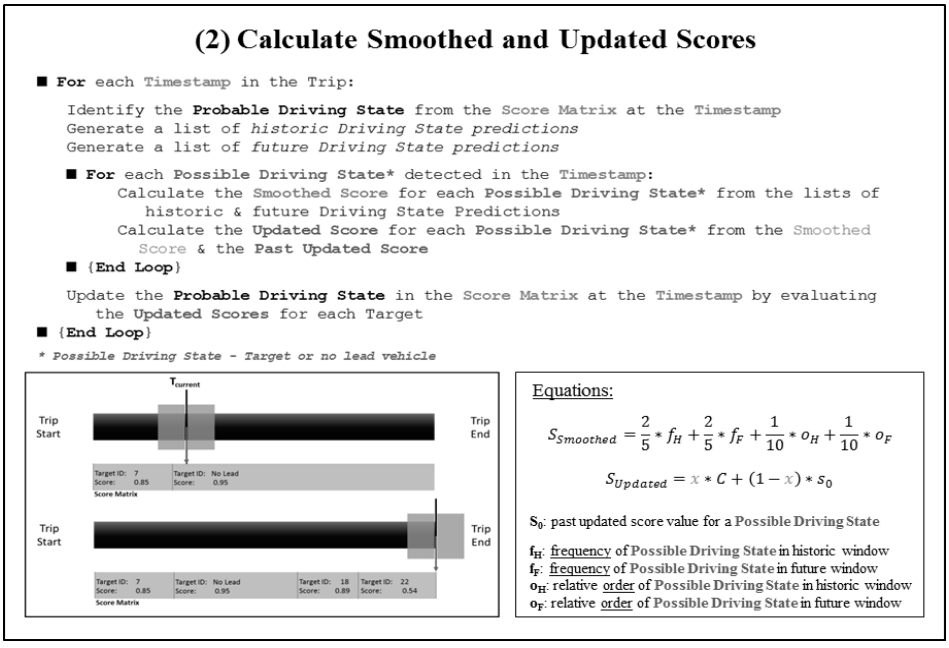

Figure 35 Smoothed & Updated Score Calculation

The updated score is computed as a weighted average between the smoothed score and the past updated score. In the first iteration, the past updated score is the initial score; however, after the first pass of the algorithm, the previously computed updated score is used. Once updated scores are computed for each possible driving state in the timestamp, the probable driving state—the state with the highest updated score—is identified and the score matrix is updated. The algorithm then repeats the procedures with the next time step until the trip is complete. For each pass of the algorithm, the window size is increased to facilitate controlled smoothing of the driving state prediction. In addition, the confidence weight given to the smoothed score is gradually decreased to reduce the risk of over-smoothing. The window size and confidence weights for each possible algorithm iteration are shown in Table 28.

Table 28 Algorithm Parameters

Algorithm Iteration	Window Size [sec]	Confidence Weight
1	3	12/18
2	4	11/18
3	5	10/18
4	6	9/18
5	7	8/18

Define Continuous Driving Segments

Once all updated scores are calculated and the score matrix is revised, the trip is segmented into homogeneous driving segments that reflect continuous time periods where a single driving state is detected. This concept is depicted in Figure 36. When picturing a trip as a storyboard or video feed, each block of time represents a continuous segment of free flow driving (i.e., no lead vehicle) or constrained driving (i.e., specific lead vehicle detected).

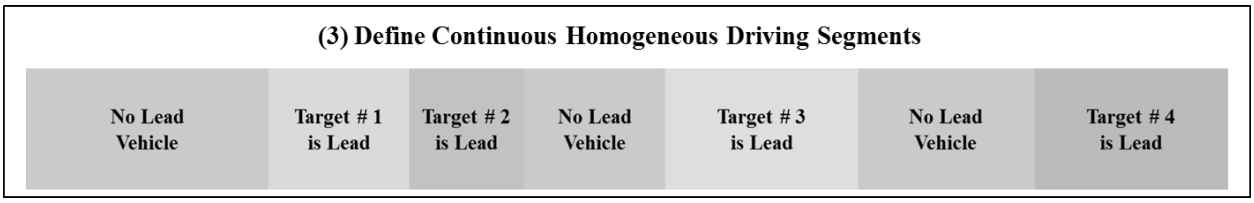

Figure 36 Example of Homogeneous Driving Segments

Evaluate Termination Conditions

After reviewing the homogeneous driving segments, termination conditions are evaluated to determine if another iteration of the algorithm is warranted and permissible. As previously described, the aim of this procedure is to smooth the transitions between continuous driving segments representing a single driving state to ensure that each segment accurately reflects the drivers' perceived environment. Therefore, the first termination condition verifies that each driving segment is longer than 1.1 seconds. This minimum threshold is regulated by the 85^{th} percentile perception time defined in Reference (*140*). The second termination condition prevents over-smoothing by limiting the number of allowable algorithm passes. Algorithm testing indicated that smoothing beyond five iterations delayed the algorithm's response in transitioning between driving states.

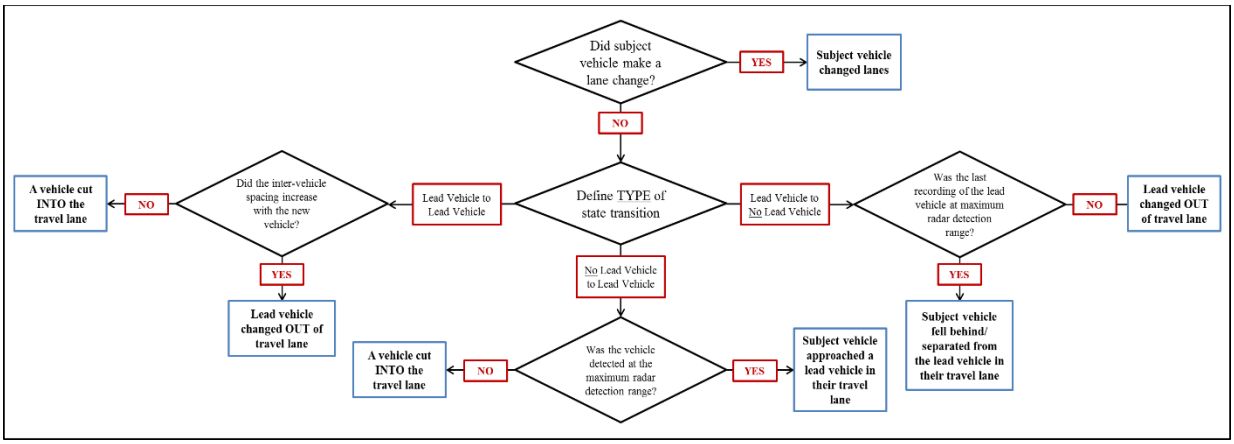

Figure 37 Decision Tree Algorithm

Decision Tree Algorithm to Estimate Events

To provide context for the transition between driving segments, a second algorithm was developed to estimate transition events. Each event is classified into five categories: (*i*) subject vehicle lane change, (*ii*) new vehicle cut-in (i.e., merged into travel lane), (*iii*) lead vehicle left travel lane (i.e., changed out of the lane ahead of subject vehicle), (*iv*) subject vehicle approached a slower moving vehicle, or (*v*) subject vehicle fell behind or separated from a faster moving vehicle. This is accomplished using decision tree logic shown in Figure 37.

Algorithm inputs include a window of radar data (i.e., position of the lead vehicle) and subject vehicle driving data (i.e., vehicle data collected from the CAN-Bus) describing the beginning and end of each driving segment. Each state transition, or decision point, is evaluated using a three second window of pertinent data from the end of the first segment and the beginning of the second segment. For example, a subject vehicle is determined to have made a lane change if the turn signal is active just before and after the transition. Following the decision tree logic illustrated in Figure 37, when a subject vehicle lane change is unlikely, the algorithm identifies the type of driving state transition (i.e., lead vehicle to lead vehicle, lead vehicle to no lead vehicle, or no lead vehicle to lead vehicle), as this distinction reduces the number of possible events. Depending on the type of transition, input data are used to evaluate specific questions related to the possible events. For example, if the transition had occurred between two lead vehicles, the algorithm uses the windows of radar data to determine if a new lead vehicle cut into the lane between the subject vehicle and the former lead vehicle or if the previous lead vehicle changed out of the lane and the subject vehicle picked up a new lead vehicle.

Final Output

Once the driving states are predicted by the iterative smoothing algorithm and each state transition event for the trip is estimated using the decision tree classification algorithm, a summary file is generated for the trip. As part of this summary, each driving segment is defined by its starting event, start and stop timestamps, duration, distance traveled, and summary statistics describing the subject vehicle and a lead vehicle (e.g., average speed, maximum deceleration, etc.), when applicable. A condensed sample of this output is shown in Table 29.

Table 29 Sample Output

Segment Number	Starting Event	Driving State	Segment Duration [sec]
1	start_recording	No Lead	3.8
2	sub_veh_LC	Target 1	26.8
3	sub_veh_LC	Target 2	11.8
4	lead_veh_LC_out	No Lead	17.5
5	sub_veh_approached	Target 3	14.6
6	lead_veh_LC_out	No Lead	38.5
7	sub_veh_approached	Target 4	14.2
8	lead_veh_LC_out	No Lead	16.7
9	sub_veh_approached	Target 5	7.8
10	sub_veh_separated	No Lead	123.9

Verification

As previously mentioned, the algorithm was constructed and verified using a sample of NDS data from the Wyoming SHRP2 NDS dataset. Verification and prediction accuracy was assessed from 74 NDS trips not used in algorithm generation that represents a variety of driving conditions, including daylight and night conditions, freeways and arterials, multiple lane configurations, and occasional work zones. Combined, these trips represent over 32 hours of driving. Manual video confirmation of algorithm results showed 96 percent accuracy in predicting driving states and 78 percent accuracy in estimating events in which correct driving states were predicted. Inaccuracies in driving state prediction resulted from missing or erroneous radar data, substantial roadway curvature, or confusing driving scenarios (e.g., collision on side of road). Alternatively, most event misclassifications occurred when a lead vehicle changed lanes at a far distance downstream.

To evaluate this algorithm's ability to achieve the original goal—which is to provide a continuous and reliable estimation of driving state to supplement existing data processing procedures implemented on the SHRP2 NDS—a comparison of homogeneous driving segments detected before and after algorithm deployment was conducted. One trip covering 28 km of freeway over 69 minutes was selected for the comparison; individual verification of driving state accuracy for this trip is 94 percent. The results in Table 30 produce evidence that the algorithm improved the continuity of the resulting driving segments by reducing the number of distinct driving segments by 79.5 percent and increasing the average duration of driving segments by 79.2 percent.

Table 30 Comparison of Driving State Detection

Comparison Factors	Raw & Post-Processed Radar Data	Developed Algorithm Post-Processing
Number of distinct driving segments	239	103
Average length of driving segments [sec]	17.3	40.0

Discussion

This study describes the development of data processing algorithms for trajectory-level data from instrumented vehicles to continuously predict driving states and estimate state transition events using trips from the SHRP2 NDS. The motivation for this work is to develop a systematic procedure that can characterize the driving environment to enable advancement in driver

behavior research by increasing the practicality of using a larger sample of trajectory-level data. The definition of a driving state was intentionally kept simple—either unconstrained with no detected vehicle downstream or constrained with a detected downstream vehicle assigned a certain target identifier. This vague definition allows researchers to mold more sophisticated definitions based on their specific project needs (e.g., distance and speed thresholds). For example, different types of car-following states or different components of car-following states (i.e., approach, continuous following, and separation) may be of interest and could be derived from the algorithm output. Another use case might focus on a driver's decision to make a discretionary lane change. Rather than requiring days of manual video observations to detect when a subject vehicle changed lanes after approaching a slower moving vehicle, the algorithm output could be structured to meet the specific research need and the data could be processed systematically to more efficiently analyze a larger sample size.

Planned algorithm enhancements include multiple layers of detection for identifying a subject vehicle lane change, such as the consideration of a vehicle's lane position—a variable determined by the SHRP2 NDS DAS to indicate the distance from lane center—that would improve estimation accuracy in situations in which drivers do not use their turn signals. Through the enhancement of this procedure, lane changes that don't result in a change in driving state could be detected (e.g., subject vehicle is traveling in the left lane with no lead vehicle and changes to the right lane—again with no lead vehicle ahead—which doesn't change the driving state). In addition, consideration of the subject vehicle's lateral acceleration will be applied in the computation of initial scores in the iterative smoothing algorithm for predicting driving state to account for roadway curvature and provide a better estimate of whether the lead vehicle is actually in the target lane. Lastly, a third algorithm will be introduced to estimate localized traffic congestion. Congestion levels will be assessed by the prevalence of additional radar targets (other vehicles) detected within a driving segment.

Many projects using the SHRP2 NDS data are currently in progress. One unique characteristic of the SHRP2 NDS is that a complementary geodatabase called the Roadway Information Database (RID) is available to provide context for the roadways traversed by NDS participants (*141*). The RID can be used to filter NDS trips based on roadway type, roadway configuration, or traffic control type. Additional information related to signage, speed limits, work zones, annual traffic counts, and weather events are also available.

In addition, as previously discussed, substantial value can be found in conducting detailed video processing; however, inconsistent video resolution, unpredictable visibility conditions, and intensive computational requirements have stinted the widespread use of these powerful algorithms. While the work presented in this paper focuses on the use of radar data to identify driving state, the authors are aware of the limitations caused by inherent radar noise and limited distinction between types of detected objects. Huge value could be realized through the fusion of "radar vision" and "video vision" to describe the driving environment of a SHRP2 NDS trip. When used in parallel, a much clearer picture of the driving environment would be produced at a higher confidence level than either process separately. Video vision could detect unique driving environments (e.g., work zones or adverse weather conditions) and confirm the existence of a lead vehicle, while radar data could provide accurate measurements and reliable detection when sunlight or precipitation inhibits video resolution.

Chapter 4. Detection and Prediction of Lane Change Maneuvers

Lane changes are one of the most frequent and complicated driving maneuvers occurring on roadways. According to the National Highway Traffic Safety Administration (NHTSA), lane change maneuvers were responsible for 543,000 motor vehicle crashes in the United States in 2018 (*142*). Fitch et al. reported that at least 60,000 people are injured annually due to lane change related crashes (*143*). Other studies concluded that 12.6 percent of all traffic accidents and 9.8 percent of crash fatalities are caused by lane change maneuvers (*144*). Therefore, driver lane change maneuvers need to be studied thoroughly considering its significance to roadway safety.

A lane change maneuver is one of the most commonly performed maneuvers, which takes place when a driver is in the process of moving the vehicle laterally from one lane to another. Lane change has been defined in different studies based on three criteria including explicit initiation and completion point, utilized data source, and required parameters (*145*). According to Toledo and Zohar, lane change event is defined as passing from one lane to immediate next lane. They defined the initiation point as a particular time instance when subject vehicle begins lateral movement, and the completion point is the time when the subject vehicle ends its lateral movement (*67*). The study of Tijerina et al. defined lane change maneuver as a separate decision and execution phase (*146*). In another study, Fitch et al. defined lane change as a driving maneuver that moves from one lane to another lane where both lanes have the same direction of travel (*143*).

Literature Review

Lane Change Detection

Different methods of lane change identification can be found in the literature. For instance, a study conducted by Bogard and Francher identified lane change using GPS data and used mainly path-curvature data to identify lane changes, where the process consisted of six steps (*147*). Miller and Srinivasan proposed a method to determine lane change maneuvers of heavy trucks using yaw rate. The study hypothesized that a lane change would produce a noisy-sine-wave-like yaw rate signal (*148*). Using the Next Generation Simulation (NGSIM) trajectory data, Thiemann proposed a smoothing algorithm and studied lane change dynamics. The study identified lane change using lane index that the vehicle is currently occupying, vehicle dimension, and vehicle position (*149*). In another study, Knoop et al. examined the number of lane changes as a function of the operational characteristics of the origin and target lane. They identified lane change using vehicle passing time, lane index, vehicle speed, and length from loop detector data (*150*). Koziol et al. suggested a lane change identification method using degree of curvature data. Several parameters were utilized to specify a lane change maneuver including the variation of the degree of curvature, the maximum and minimum values of the degree of curvature, the duration between the maximum and minimum degree of curvature, and the duration of the entire lane change (*151*). Another study utilized yaw rate and velocity to detect lane changes, turns, and curves on different road types (*152*). The lane change identification method proposed by Xuan and Coifman used vehicle lateral position acquired from the Differential Global Positioning System (DGPS) (*153*). A study conducted by Papathanasopoulou and Antoniou proposed a methodology based on temporary virtual lines to identify lane change maneuvers on mixed traffic trajectory data (*154*). Moreover, several subjective methods have also been used to identify lane change maneuver. In a study, lane

change maneuver was identified when the initiation and completion points of simulated multi-lane highway seemed apparent from experimenter's judgment (*66*). Another study conducted by Hanowski et al. used driver's pushbutton activation to identify lane changes while studying their fatigue (*155*). In general, it has been observed that most of the lane change identification methods are based on either data processing algorithms or subjective measures.

In addition, several studies utilized Machine Learning approach to detect lane change maneuvers. Yang et al. adopted Random Forest (RF) model for detecting lane changing decision and found the prediction accuracy of 85 percent, 91.3 percent, and 88 percent for no lane change, left change and right lane change, respectively, using the NGSIM data (*156*). A study focused on detecting imminent lane change maneuvers in connected vehicle environments and found 80 percent lane change detection accuracy using Artificial Neural Network (ANN) (*157*). Another study used Support Vector Machine (SVM) for detecting lane change intentions using instrumented vehicle and achieved accuracy close to 98 percent (*158*). A study conducted by Kumar et al. proposed SVM and Bayesian filtering algorithm for predicting lane change intention and concluded that the proposed algorithm was able to predict lane change on an average of 1.3 seconds before it occurs (*159*). A study concentrated on predicting driver's lane change decisions using a neural network model and found the accuracy of 94.58 percent and 73.33 percent for left and right lane changes, respectively (*160*).

Lane Change Prediction

Prediction of lane change maneuvers have been extensively studied in the literature utilizing different approaches and datasets. For instance, Schmidt et al. proposed a mathematical model for predicting lane changes using steering wheel angle in a driving simulator and found that the pre-steering action of the steering wheel angle is a good indicator to predict a lane change (*161*). Using vehicle sensor readings, Morris et al. developed a real-time on-road prediction system to provide the early notifications required for Advanced Driver Assistance Systems (ADAS), which is capable of predicting a driver's intention to change lanes up to 3s before the maneuver occurs (*162*). A study conducted by Toledo-Moreo and Zamora-Izquierdo combined position data from a set of low-cost GPS sensors with velocity measurement using an interactive multiple model and concluded that the model can predict lane changes in straight and curve road segments with a very short time (*163*). In addition, Naturalistic Driving Study (NDS) data have been utilized in previous studies to predict lane change maneuvers. Using 100-Car NDS data, Chen et al. developed an adaptive method from vehicle kinematics to predict lane-changing maneuvers and concluded that drivers started steering maneuvers for a lane change within 5s of the vehicle crossing the lane line (*164*). A study conducted by Leonhardt and Wanielik evaluated features for lane change prediction based on driving situation and driver behavior using naturalistic data and suggested that features associated with NDS vehicle's controls and movement are appropriate to predict the lane change maneuver (*165*).

With regard to methodological approaches, Machine Learning techniques have gained popularity because of their efficiency in solving several nonlinear and complex problems (*166–169*). Considering the promising performance of Machine Learning approaches, researchers have utilized these techniques to predict lane change maneuvers. Gao et al. adopted decision tree approach to predict lane change intention of an autonomous vehicle and found the highest prediction accuracy of 62.9 percent for 9s prediction horizon (*170*). Benterk et al. developed an approach based on Support Vector Machine (SVM) to predict lane change maneuvers of surrounding vehicles on highways and concluded that their proposed algorithm was able to

predict lane change on an average of 1.95s before the maneuver occurs with an accuracy of around 97 percent (*171*). Another study considered Random Forest (RF) method for predicting discretionary lane change decision behavior on freeway and obtained the prediction accuracy of 88 percent and 91 percent of right and left lane changes, respectively (*156*). A study conducted by Hou et al. combined Bayes classifier and decision tree to predict driver decisions on mandatory lane change and found the prediction accuracy close to 79 percent (*172*).

Data Acquisition and Processing

The SHRP2 NDS study focuses on understanding of drivers' interaction with and adaptation to the vehicle, traffic, roadway characteristics, and other environmental features (*173*). The NDS collected an unprecedented amount of data from more than 3,400 drivers in six US states including Florida, Indiana, New York, North Carolina, Pennsylvania, and Washington between 2010 and 2013 (*174*). These data include vehicle kinematics data (e.g., speed, acceleration, etc.); machine vision-based data (e.g., lane position offset); radar data (e.g., longitudinal and lateral position of the surrounding vehicles); and front and rear roadway views from four video cameras (*173*). The RID dataset was developed by the Center for Transportation Research and Education (CTRE) of the Iowa State University. The RID dataset include detailed roadway data, e.g., horizontal curvature, grade, cross-slope, shoulder type, lane information, and so on, of the six NDS states (*174*, *175*). A subset of the large SHRP2 NDS data were acquired from Virginia Tech Transportation Institute (VTTI) and utilized in this study. The SHRP2 NDS and RID datasets were linked in this study to detect lane change maneuver under different geographical and environmental conditions.

NDS trips that occurred in different weather conditions (i.e., clear, snow, rain, and fog) were collected using the two unique methodologies. The methodologies were developed by the research team and based on weather data from the National Climatic Data Center (NCDC) and weather-related crash locations. Both of the methods utilize a radius of five nautical miles to isolate all the extracted NDS trips occurred in different weather conditions (*12*, *74*, *167*, *176*). By using these processes, a large number of NDS trips in different weather conditions were received.

Lane Change Detection

From the received NDS trips, 400 trips (100 trips in each weather condition) were randomly selected and considered for detecting lane change maneuvers. The next step of the data processing was to aggregate time-series data based on lane change duration. Previous studies suggested that lane change durations vary from a minimum of 1 sec to a maximum 14 sec with a mean of 5 sec or 6 sec (*58*). To have an overall idea about the mean lane change duration of the dataset, 500 lane changes were identified from the NDS video data. The mean duration of the lane changes was found to be 6 sec, which is in line with the literature. Therefore, a moving window of 6 sec was selected for aggregating time-series data. Subsequently, roadway characteristics provided in the RID database and driver demographics provided in the SHRP2 administrated survey questionnaires were linked to create the final dataset. The dataset was then manually annotated using the Wyoming NDS Visualization and Reduction tool and categorized into two groups: lane change and no lane change (*11*, *12*). It is worth mentioning that accurate lane change annotation is essential for the appropriate training of Machine Learning models. A sample of 1,200 lane changes (300 lane changes from each weather condition) and 1,200 no lane changes were randomly selected for this study, which corresponded to 110 drivers with age ranged between 16 to 89 years of age with a significant number of drivers in age group 20 to 24

years. It is worth mentioning that the sampled data resampled the original distribution of the original SHRP2 NDS data.

Lane Change Prediction

A total of 377 trips in different weather conditions including clear, snow, rain, and fog were randomly selected and considered for predicting lane change maneuvers. The subsequent step was to develop a comprehensive dataset representing segments before lane changes and no lane changes. To effectively identify lane change events from the selected SHRP2 NDS trips and the corresponding time-series parameters during the event, the authors developed an automatic lane change identification algorithm using lane position offset parameters. Details about the development of the identification algorithm can be found in Das et al. (*166*). Once lane change events were identified, mean, standard deviation, minimum, and maximum of associated parameters (i.e., speed, longitudinal acceleration, lateral acceleration, yaw rate, and lane position offset) for each lane change event were extracted. Subsequently, all the lane changes were annotated manually utilizing the Wyoming NDS Visualization and Visibility Identification Tool (*12*). This study considered a random selection of 300 lane changes annotated from each weather condition (i.e., clear, snow, rain, and fog) which summed up to 1,200 lane changes in total.

Once the sample of 1,200 lane changes has been selected, the next step was to extract necessary data before the initiation of the event. In order to do that, a reasonable prediction horizon length (i.e., the time length at which the prediction is being made) should be defined, which allows for capturing continuous changes in vehicle kinematics along with other data from machine vision and roadway characteristics. Note that shorter prediction horizon length can capture substantial fluctuations in the parameters and therefore, can improve the prediction accuracy. In contrast, relatively longer prediction horizon length could be practical for human-driven vehicles, nonetheless, the prediction accuracy could be compromised. However, there is no specific threshold that defines the optimal prediction horizon length for predicting lane change maneuvers. This study considered a prediction horizon length of 5s based on the findings from previous studies (*164*, *166*). Consequently, a sample of 1,200 segments corresponding to “lane change within 5s” were extracted.

It is worth mentioning that non matched samples should be higher to some extent than the matched sample in developing ML models. Therefore, a sample of 2,400 segments representing “no lane change within 5s” were selected and combined with “lane change within 5s” segments (*166*). The combined dataset contained 141 drivers aged between 16–84 years, where a major proportion of drivers were young (i.e., between 20–24 years). As mentioned earlier, roadway geometric characteristics have been extracted from the RID and driver characteristics have been collected from the SHRP2 survey questionnaire responses. These two datasets were then merged to NDS data that makes a comprehensive final dataset.

Methodology

Machine Learning techniques were utilized to detect and predict lane change maneuvers considering four different categories of features from vehicle kinematics, machine vision, roadway characteristics, and driver demographics. First, relevant features were selected and then trained and validated using three different Machine Learning classifiers. Then, the accuracy of the trained models was tested using a new dataset. It is worth mentioning that 80 percent of data were utilized for training and validation, and the remaining 20 percent data were used for testing (*177*, *178*).

Feature Description for Lane Change Detection

Four time-series parameters including vehicle speed, longitudinal acceleration, lateral acceleration, and yaw rate were extracted and utilized as measures of vehicle kinematics to detect lane changes. The mean value of the vehicle kinematics may depend on several factors (i.e., speed limit, presence of curve, aggressiveness of driver, etc.) and might not be a good indicator of lane change maneuver. During the lane change process, the value of the vehicle kinematics varies significantly, irrespective of the mean value of the parameters. Therefore, to capture the variation of the kinematics during lane change maneuverer, standard deviation was utilized instead of mean value (*157*).

In addition to vehicle kinematics, standard deviation of lane position offset, which is based on machine vision, was also utilized. Lane position offset is estimated from the distance to the left or right of the center of the lane and center of the vehicle based on machine vision techniques (*179*). The variable is a good indicator of lane change maneuver. As recommended by a previous study, a threshold of ±100 cm lateral shift (i.e., left and right) in the position of a vehicle can be considered as a lane change maneuver (*41*). As an example, Figure 38 and Figure 39 represent sample of two-lane change maneuvers with lane position offset values above and below 100 cm. As can be seen in Figure 38, lane position offset value started to increase indicating that the vehicle started to move from left to right of the lane center. When the value reaches a maximum point, a jump occurred indicating that the vehicle reached the far right of the driver's adjacent lane. The same process occurred when driver changed lane from right to the adjacent left lane (Figure 39).

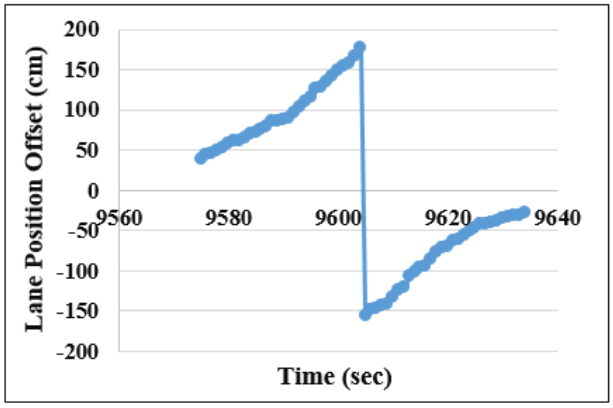

Figure 38 Illustration of Lane Change Maneuver Using Lane Position Offset (Lane Change to Right)

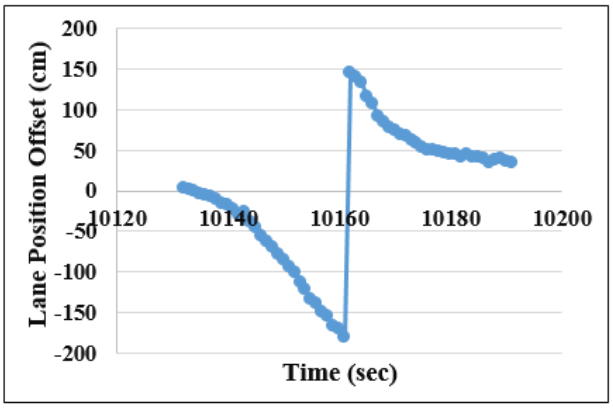

Figure 39 Illustration of Lane Change Maneuver Using Lane Position Offset (Lane Change to the Left)

Moreover, additional parameters from roadway characteristics and driver demographics were considered, as these features can influence lane change maneuver. The number of lanes and presence of curve/tangent from the RID as well as drivers' gender and age from the SHRP2 administrated survey questionnaires were selected as the detection parameters for training and validating Machine Learning models. The descriptive statistics of the selected features is shown in Table 31.

Table 31 Descriptive Statistics of the Selected Features

Features	Type	Mean	Median	Min	Max	Percentage	Source
Standard Deviation of Speed (mph)	Continuous	1.34	0.88	0	17.04	-	Vehicle Kinematics of NDS Time-Series Data
Standard Deviation of Longitudinal Acceleration (g)	Continuous	0.02	0.02	0	0.23	-	Vehicle Kinematics of NDS Time-Series Data
Standard Deviation of Lateral Acceleration (g)	Continuous	0.03	0.02	0	0.24	-	Vehicle Kinematics of NDS Time-Series Data
Standard Deviation of Yaw Rate (deg/sec)	Continuous	0.57	50.63	0.06	19.15	-	Vehicle Kinematics of NDS Time-Series Data
Standard Deviation of Lane Position Offset (cm)	Continuous	60.45	0.43	0	537.90	-	Machine Vision-based Data of NDS
Number of Lanes	Continuous	2.69	2	1	7	-	Roadway Information Database (RID)
Curve/Tangent	Categorical (Curve)	-	-	-	-	33.65%	Roadway Information Database (RID)
	Categorical (Tangent)	-	-	-	-	66.35%	
Gender	Categorical (Male)	-	-	-	-	46.97%	SHRP2 Administrated Survey Questionnaires
	Categorical (Female)	-	-	-	-	53.03%	
Age	Categorical (Young: <25 years)	-	-	-	-	25.00%	SHRP2 Administrated Survey Questionnaires
	Categorical (Middle: 25-44 years)	-	-	-	-	33.61%	
	Categorical (Old: >44 years)	-	-	-	-	41.39%	

The lane change detection analysis was performed in three steps. The first step included combined features based on vehicle kinematics, machine vision (i.e., lane position offset), roadway characteristics, and driver demographics (Category 1). This step investigated the performance of lane change detection models when all the data are available. Although lane position offset illustrates a significant pattern during the lane change process, it might not be available or might provide erroneous value during harsh weather conditions where lane markings are not visible. It is worth noting that during the data reduction process, extreme harsh weather was excluded from the Category 1 dataset, which contained machine vision-based data.

The subsequent step considered all the features except lane position offset, which was collected using machine vision algorithms (Category 2). Note that, this step considered all the weather

conditions, including extreme harsh weather. One of the major limitations of machine vision algorithm is that it might not work properly during extreme adverse weather including heavy snow. In addition, lane position offset parameter might not be readily available. Therefore, the second step investigated the performance of the models in the absence of machine vision-based feature.

The final step considered only vehicle kinematics-based features, which are readily available (Category 3). Similar to the second step, extreme harsh weather was considered in Category 3 features. It is worth mentioning that myriad of similar data to NDS will become available with the advent of Connected and Automated vehicle deployment. Hence, the main purpose of using only vehicle kinematics-based features was to check whether the trained models could detect the lane change maneuver with acceptable accuracy when other data are not available including roadway characteristics, driver demographics, and machine vision. This splitting of the data into three different steps will provide guidance to transportation researchers on what data should be collected for lane change detection models.

Relevant Feature Extraction for Lane Change Prediction

Table 32 summarizes the selected parameters/features associated with different data sources used for lane change prediction.

Table 32 Overview of the Selected Features

Features	Units	Description	Levels
Features associated with Vehicle Kinematics			
Speed (Mean, Standard Deviation, Minimum, Maximum)	mph	Vehicle speed from the roadway network	-
Longitudinal Acceleration (Mean, Standard Deviation, Minimum, Maximum)	g	Vehicle acceleration in the longitudinal direction versus time	-
Lateral Acceleration (Mean, Standard Deviation, Minimum, Maximum)	g	Vehicle acceleration in the lateral direction versus time	-
Yaw Rate (Mean, Standard Deviation, Minimum, Maximum)	deg/sec	Vehicle angular velocity around the vertical axis	-
Feature associated with Machine Vision			
Lane Position Offset (Mean, Standard Deviation, Minimum, Maximum)	cm	Distance to the left/right of the center of the lane and center of the vehicle based on Machine Vision	-
Features associated with Driver Characteristics			
Age	-	The age group corresponding to the participant's birthdate.	1 = Young (< 25 years)
			2 = Middle (25-55 years)
			3 = Old (> 55 years)
Gender	-	The participant's gender	1 = Female
			2 = Female
Education	-	The participant's highest completed level of education	1 = Low (High school diploma or G.E.D.)
			2 = Medium (Some education beyond high school but no degree and College degree)
			3 = High (Some graduate or professional school, but no advanced degree)
Marital Status	-	The participant's marital status	1 = Single
			2 = Married
			3 = Other (Divorced, Widow)
Driving Experience	-	The participant's number of driving years	2 = ≤ 10 years
			3 = > 10 years
Driver Mileage Last year	-	The approximate number of miles the participant drove last year	1 = < 10,000 miles
			2 = 10,000-20,000 miles
			1 = > 20,000 miles
Vehicle Class	-	The participant's vehicle class	1 = Passenger Car/SUV
			2 = Minivan/Pick-up
Features associated with Roadway Characteristics			
Presence of Curve	-	Whether the participants drove curve or tangent in the segment	1 = Curve
			2 = Tangent
Radius	Feet	Curve radius of the segment in which participants drove	-
Curve Length	Feet	Curve length of the segment in which participants drove	-
Speed Limit	mph	Speed limit of the segment	1 ≤ 60 mph

After the selection of features from different data sources, six sets of features were introduced from the final dataset as shown in Figure 40. Transportation researchers and practitioners always thrive on new data sources for real-life applications. Therefore, developing lane change prediction models through six feature sets will provide appropriate guidance to researchers on what optimum approach should be selected based on available datasets. This could also guide future NDS DAS design on which data would be required.

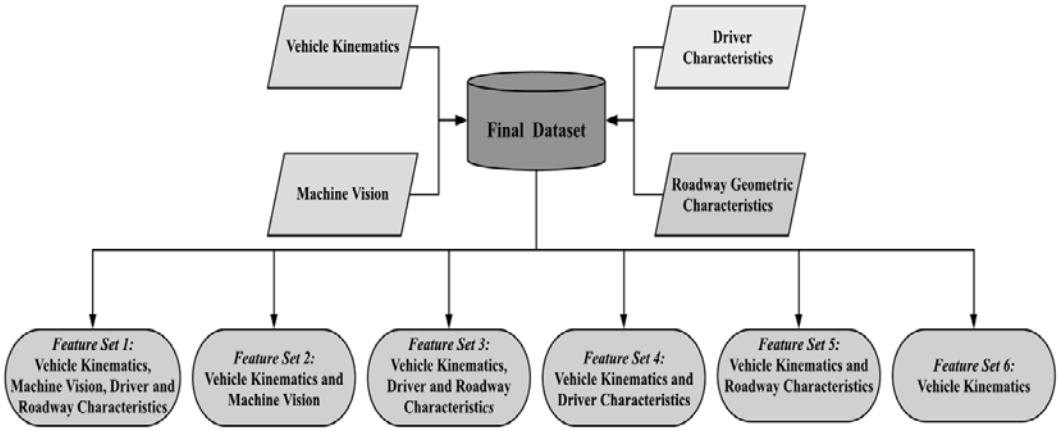

Figure 40 Illustration of Six Feature Sets

Relevant feature extraction is one of the initial steps of building ML models. If noisy/irrelevant features in the datasets are used directly into the model, the performance of the model could be degraded. Hence, the extraction of relevant features is necessary to improve the accuracy and reduce the computational complexity of the model. In order to extract relevant features for each feature set, Boruta feature selection algorithm was utilized in R® through a package called "Boruta". The algorithm works as a wrapper-based process around RF classification model. At the initial step, shadow features (i.e., a copy for each feature) are created and shuffled in order to reduce correlations and biases among the features. With the underlying RF model, the algorithm calculates maximum Z-score among shadow features (MZSF) and compares that with all the original features during each iteration. The features that have lower importance than MZSF are marked as unimportant and removed accordingly. Conversely, all the features that have higher importance than MZSF are marked as important. When the algorithm reaches its pre-specified RF runs or when all the features are tagged as important and unimportant, the algorithm stops (*180*). Figure 41 to Figure 46 show the final important features (i.e., inside grey box), unimportant features (i.e., inside purple box) along with the maximum, mean, and minimum Z-scores of a shadow feature (i.e., features outside the boxes) obtained from Boruta feature selection algorithm for each feature set.

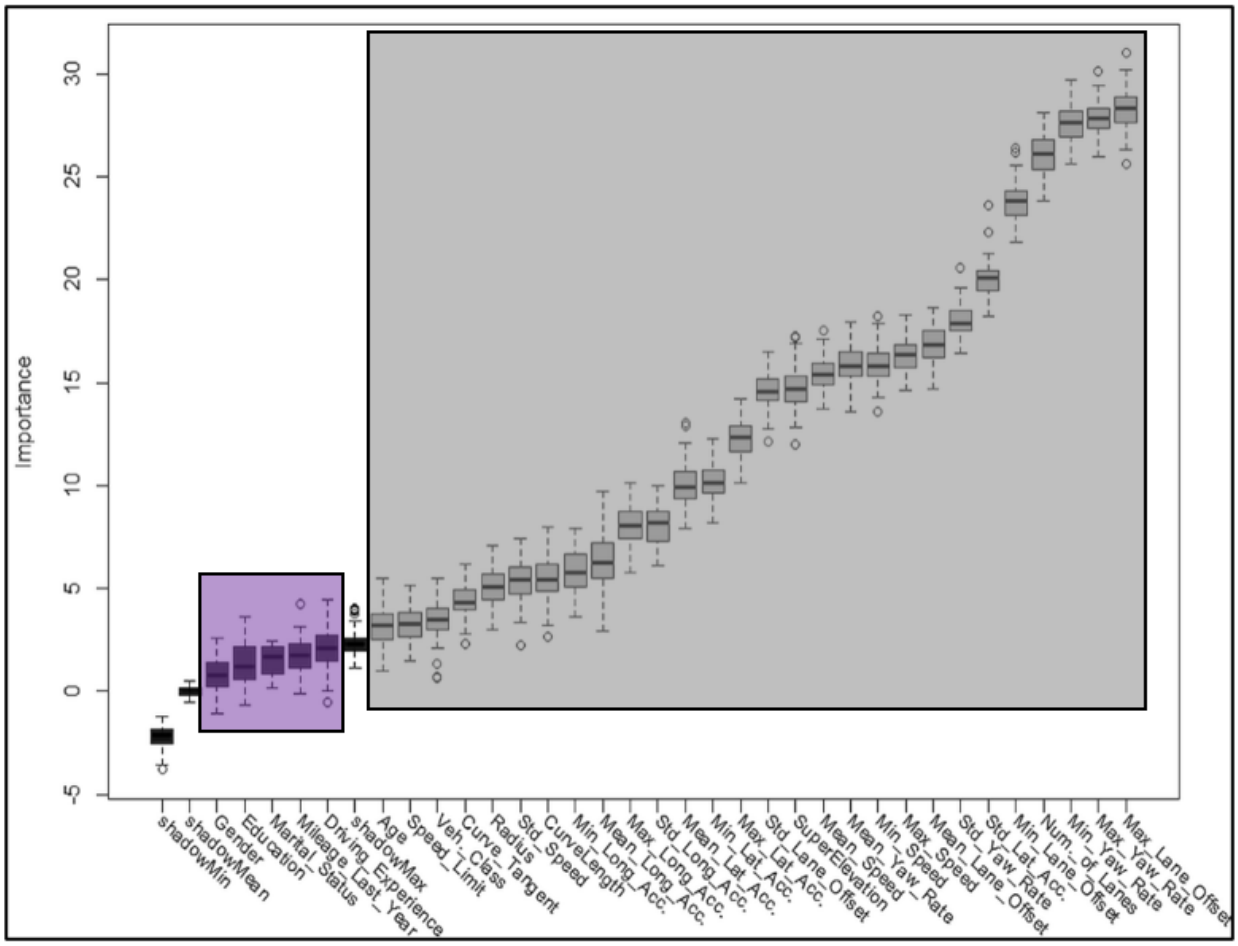

Figure 41 Box Plots of the Z-Scores Obtained from Boruta Feature Selection Algorithm (Feature Set 1)

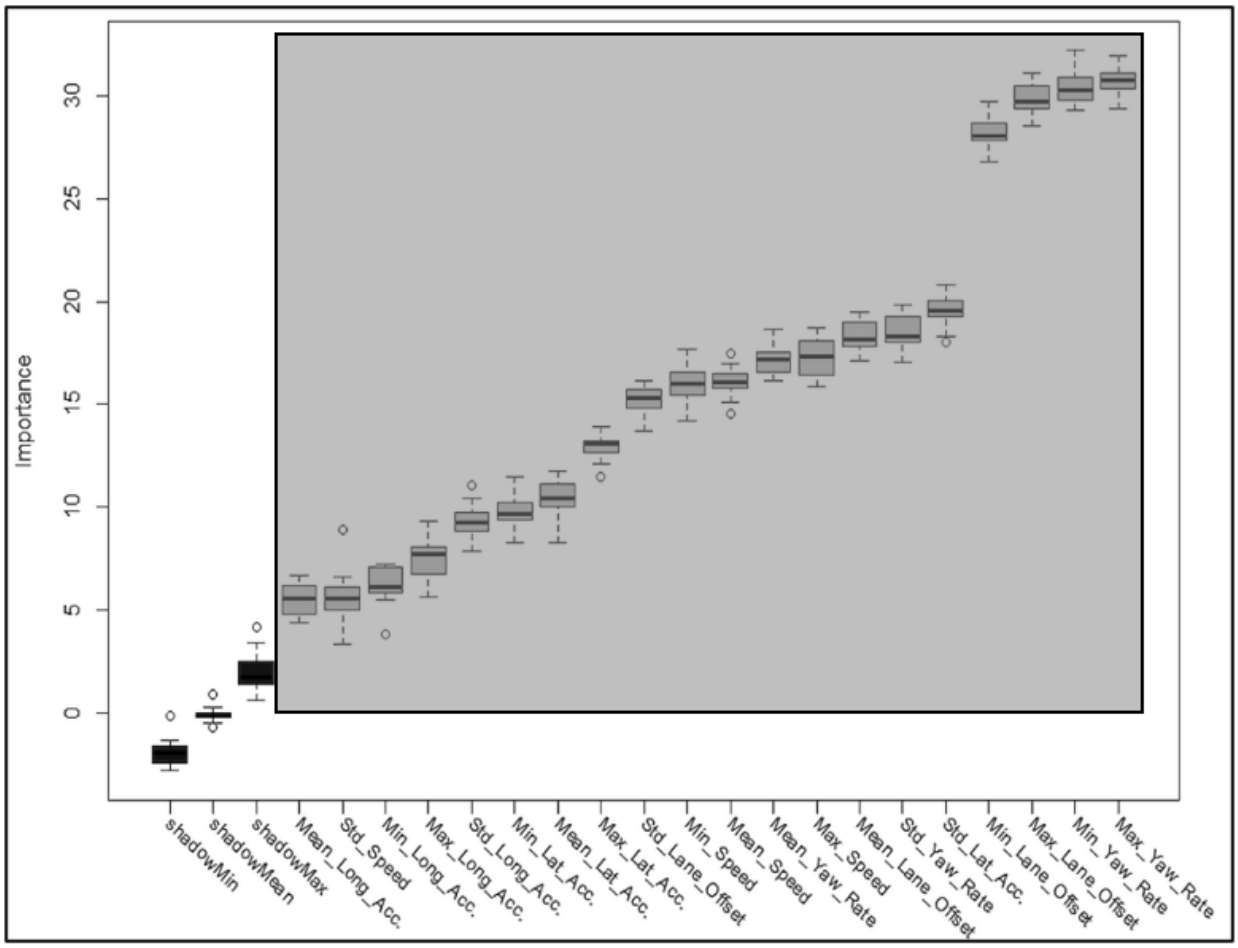

Figure 42 Box Plots of the Z-Scores Obtained from Boruta Feature Selection Algorithm (Feature Set 2)

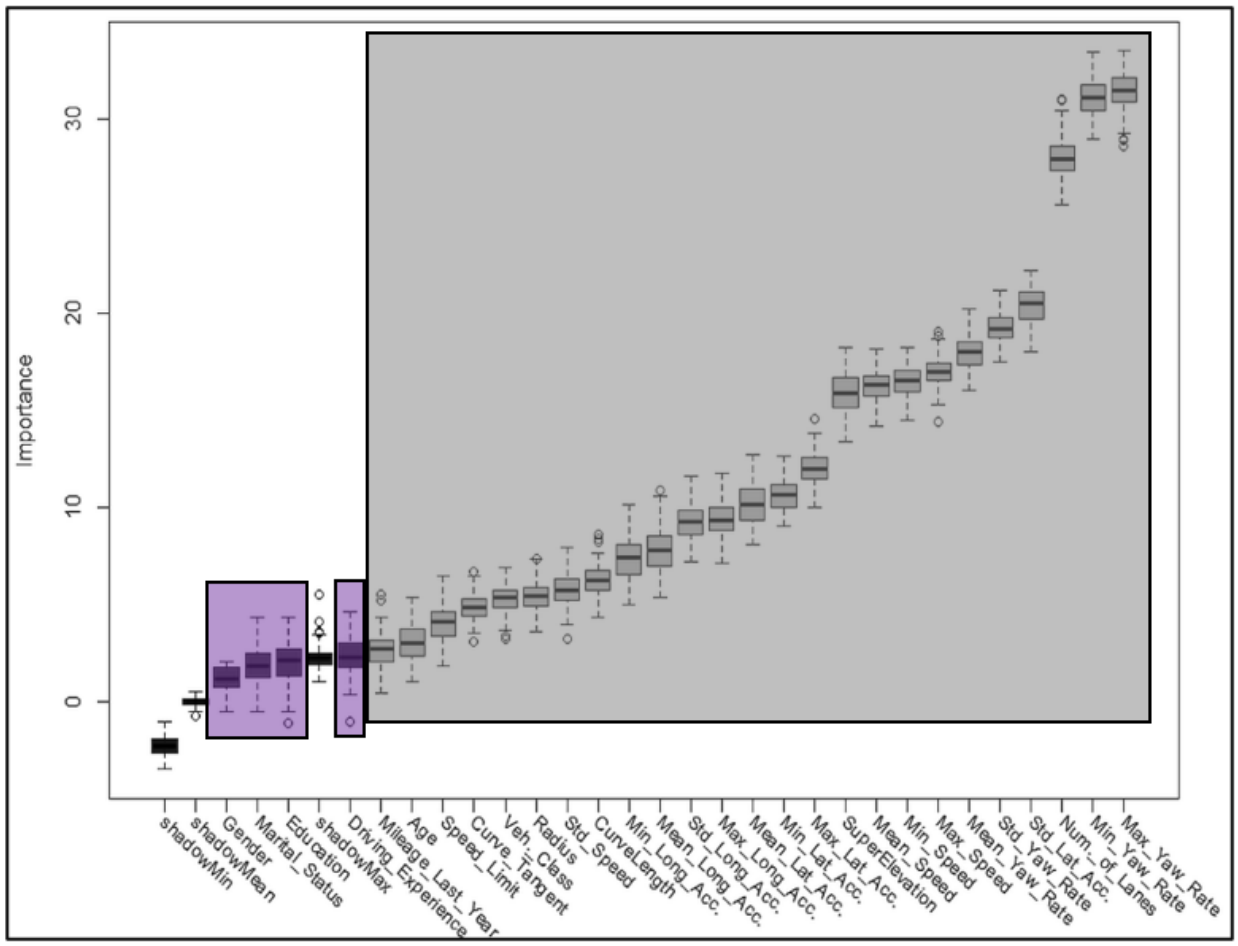

Figure 43 Box Plots of the Z-Scores Obtained from Boruta Feature Selection Algorithm (Feature Set 3)

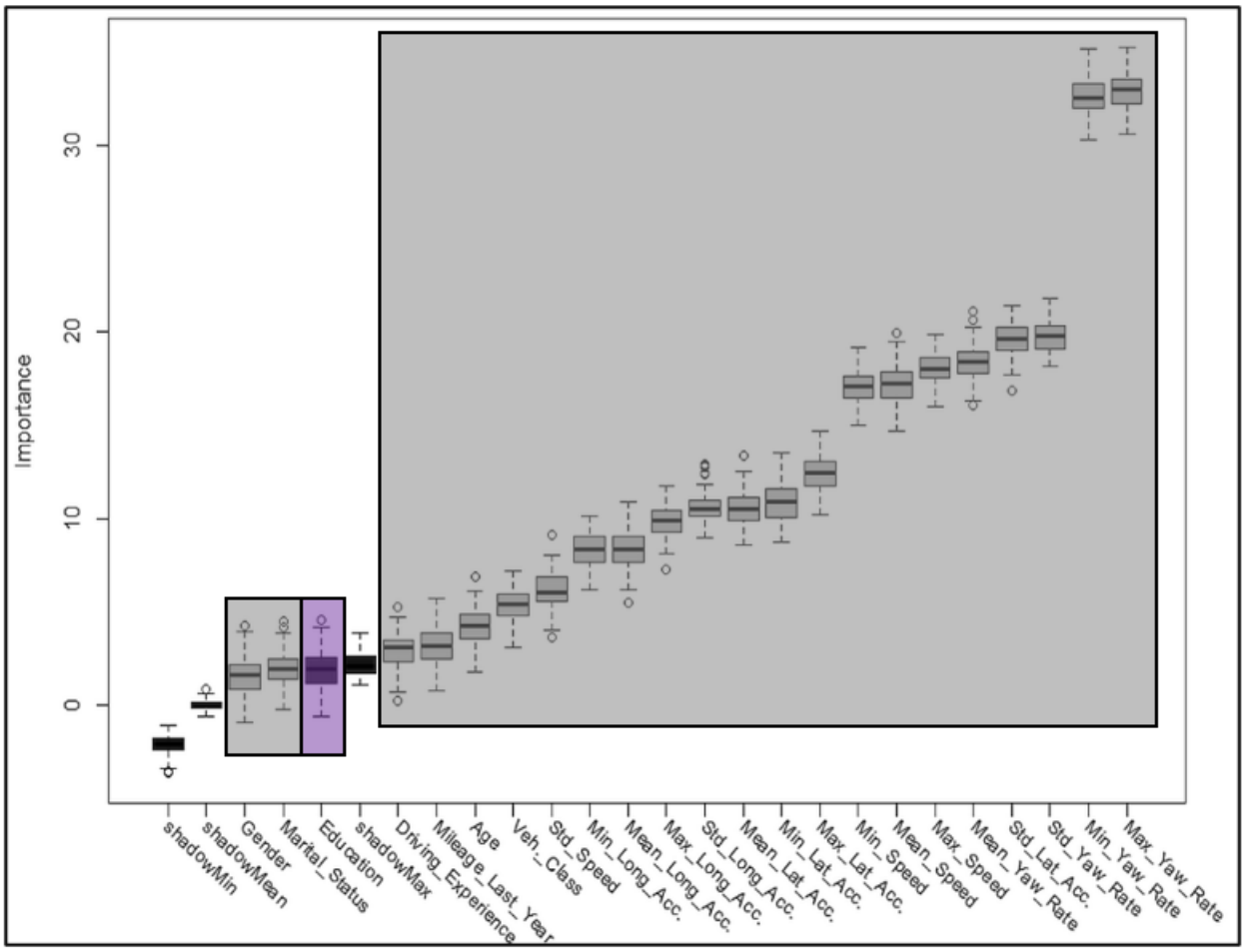

Figure 44 Box Plots of the Z-Scores Obtained from Boruta Feature Selection Algorithm (Feature Set 4)

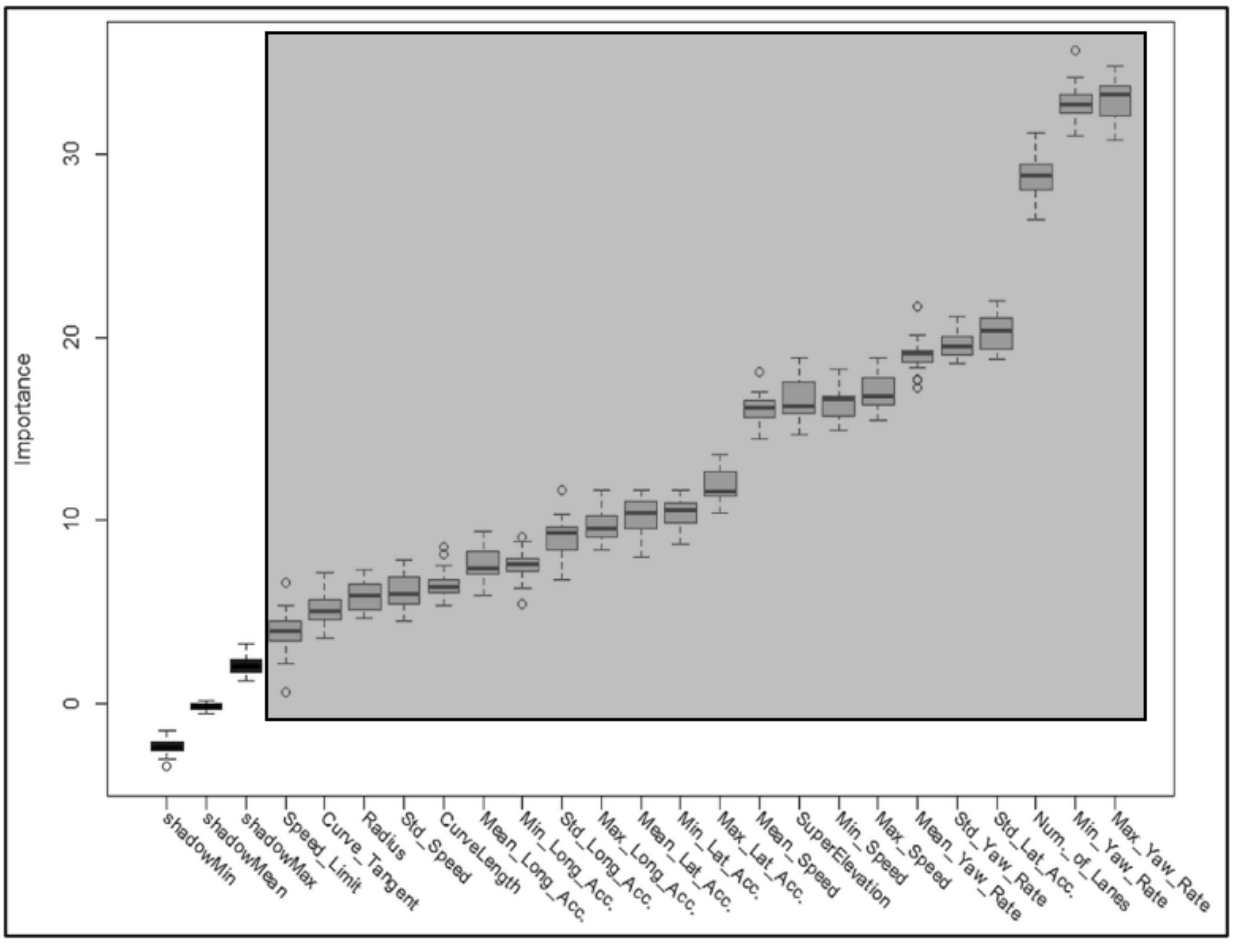

Figure 45 Box Plots of the Z-Scores Obtained from Boruta Feature Selection Algorithm (Feature Set 5)

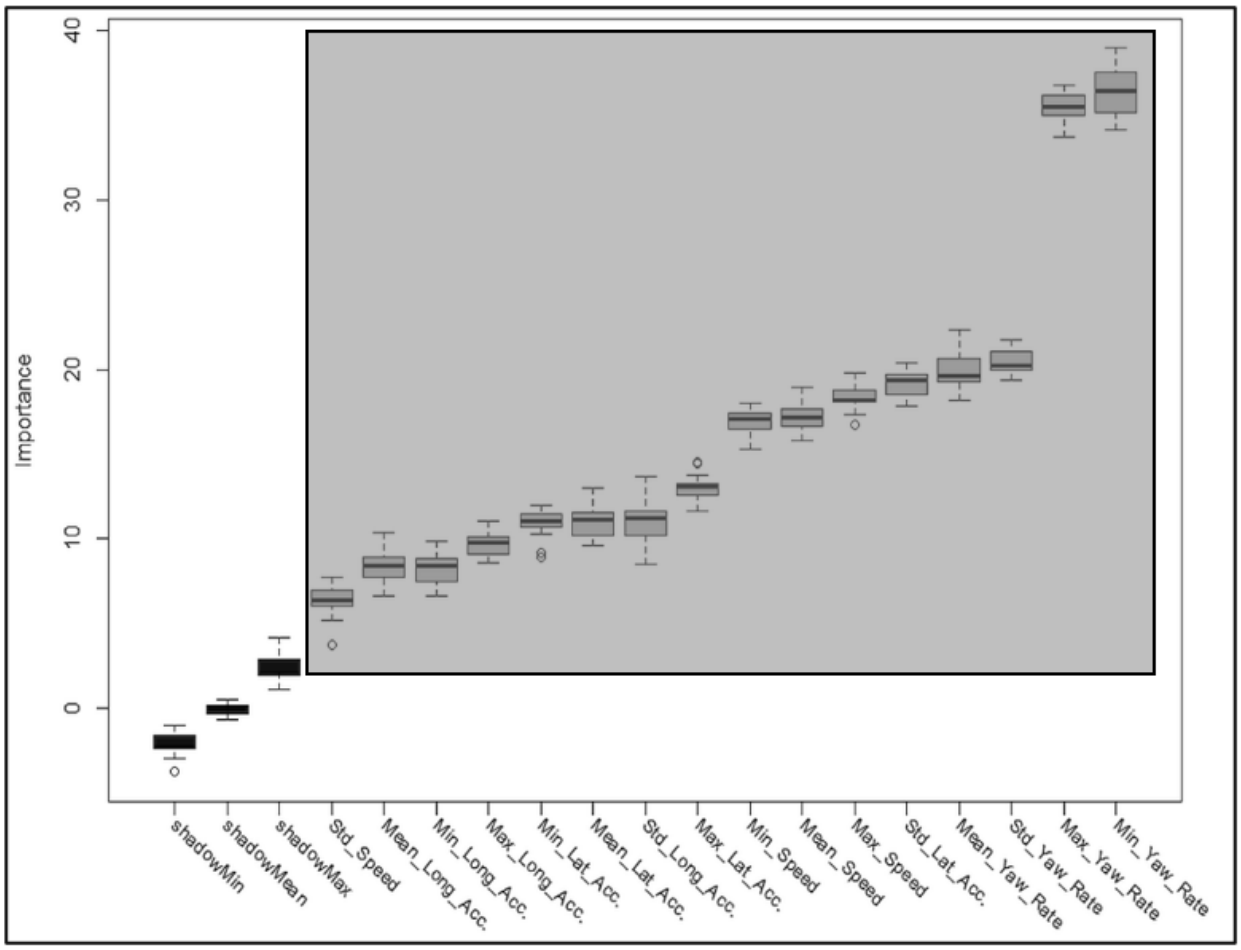

Figure 46 Box Plots of the Z-Scores Obtained from Boruta Feature Selection Algorithm (Feature Set 6)

Classification Algorithm

Several widely used Machine Learning classifiers were used to develop the lane change detection and prediction models. This section briefly describes the different Machine Learnig Algorithms.

CART is a type of supervised learning algorithm where a dataset is continuously split based on a certain parameter. There are two main components of CART- root node and leaf or terminal node. Root node contains all the data and locates at the top of the tree. Leaf node is the terminal node and refers to a classification or decision. The in-between nodes are called internal nodes. Splitting criterion is one of the vital components of a CART. The splitting decision is made based on some criteria (e.g., Gini index, information gain, etc.). The results provided by the CART are easy to explain. In fact, a complex CART model can be interpreted by simple visualization (*181*).

RF is a supervised ensemble learning algorithm that usually trained with a bagging technique. The algorithm comprises of multiple randomly selected decision trees. In RF, individual tree is built from a randomly selected subset of original training data and prediction results from each

tree are collected. Instead of using all features at each node, the RF considers a random subset of features to generate the best split. Such randomness enhances variety in the model, which improves the overall model accuracy. One of the main advantages of RF is its capability of preventing the overfitting problem (*182*).

XGBoost is one of the effective implementations of Gradient Boosting (GB) ensemble learning technique. GB produces a prediction model by combining weak learners (e.g., decision trees) into strong leaners, where weights are adjusted sequentially based on the information (i.e., errors) from the previous iteration. At every iteration, the arbitrary loss function (a measure of prediction ability) is minimized using gradient descent method to improve the model accuracy. XGBoost, on the other hand, considers a more precise estimation than the GB. Unlike the GB, XGBoost computes second-order gradient of the loss function, which provides supplementary information about obtaining minimum loss function and gradient direction. Moreover, XGBoost implements an additional regularized approach that can impose additional control over the model complexity and reduce the risk of overfitting. Hence, more accurate and better model performance is obtained (*166, 183*).

AdaBoost is a popular boosting algorithm developed for binary classification problems. The classifier combines weak classifier algorithms to form a strong classifier. The process starts with predicting original training dataset and providing equal weight to each observation. If the prediction is wrong in the first learning, it provides higher weight to observations, which have been predicted incorrectly. The learning process continues iteratively until a reasonable accuracy of the model is reached (*184*).

SVM is a supervised ML classifier that is based on the concept of separable optimum hyperplane and provides an approach to discrimination in which the hyperplane separates the data points into two classes in a high-dimensional space. In SVM, several kernel functions are used to convert data, which then can be utilized to build the hyperplane. The points that are relatively nearer to the hyperplane are known as support vector. The support vectors are used to maximize the possible margin (i.e., distance from the hyperplane to the closest data point) of the classifier and the most difficult points to classify (*166, 185*).

KNN is one of the most commonly used ML algorithms that classifies a new data point based on a similarity measure, which is called distance function. The classification is conducted by a majority vote to its neighbor. The accuracy of the KNN model might increase with the increase of k value (i.e., the number of nearest neighbors). However, the choice of k is very crucial in the KNN model and considered one of the most influential factors of prediction quality. The optimum k value should be selected in such a way that provides the appropriate balances between the bias and variance of the model (*186, 187*).

Naïve Bayes (NB) is a classification algorithm that can be used to train models for both binary and multi-class classification problems. The algorithm is based on a probabilistic model with conditional probabilities (i.e., Bayes Theorem). In NB, a probability can be computed based on the training data for every feature and every class. To classify a new feature, the probability of every feature corresponding to the different classes is computed initially and then the new feature is assigned to the class which has the maximum likelihood estimate. In addition, the probability distribution can be estimated for every feature and every class when continuous features are used and sufficient training data are not available to identify all feature probabilities accurately.

Because of the assumption of feature independence and the probability distribution estimation, the NB algorithm is computationally effective (*188*).

Artificial Neural Network (ANN) is information-processing system based on the neural structure of the brain. The system consists of a large number of interconnected neurons that arrange in layers (i.e., input, hidden, and output layers) and works in a unit to solve a particular problem. The ANN processes any given information one time and learn by matching their classification of the information with the actual known information classification. One of the main advantages of the ANN is that it does not need any assumption or prior knowledge of problem-solving. ANN is currently being used in a variety of fields for pattern recognition, machine transition, and image recognition (*160*, *189*).

Results and Discussions

Performance of the Lane Change Detection Models

The lane change detection models were developed using the "*caret*" package in R®. After splitting of data in three steps, Machine Learning algorithms were applied to train and validate the lane change detection models at every step. A 5-fold cross-validation technique was utilized to train and validate RF, SVM, and ANN models. Subsequently, a new test dataset was also utilized to test and evaluate the performance of the lane change detection models. It is worth noting that the testing dataset had never been used during training and validation of the Machine Learning models. The parameters of all the models were tuned in order to achieve the best performance. For the RF model, two parameters, i.e., the number of trees to grow (ntree) and the number of variables randomly sampled at each tree node (mtry) were tuned. For instance, it was found that ntree equals to 500 and mtry equals to 2 provided the best performance for the RF model used in Category 1. Similarly, the best SVM model after parameter tuning in Category 1 was based on radial kernel function, a cost and sigma value of 1 and 0.12, respectively. In addition, the feed-forward neural network with a single hidden layer was utilized to train and validate the ANN model. Based on parameter tuning, five hidden units and a weight decay value of 0.0004 were used for the ANN model in Category 1.

Category 1 – Fusing Vehicle Kinematics, Machine Vision, Roadway Characteristics, and Driver Demographics

The detection summary of the RF, SVM, and ANN models using features based on vehicle kinematics, machine vision, roadway characteristics, and driver demographics is shown in Figure 47 to Figure 49 in the form of a confusion matrix. The confusion matrix represents the percentages of the correctly and incorrectly classified lane change events. The highest overall detection accuracy of 91.5 percent and 88.9 percent was found for the RF model during validation and testing, respectively. As can be seen in the figures, the true positive rate of the RF model was about 93 percent during validation meaning that 93 percent of lane changes have been detected correctly. In fact, the RF model provided the highest true positive rate during validation. On the contrary, SVM model had the lowest true positive rate (86.7 percent) during validation. However, it was found that SVM model had the lowest true negative rate (91.2 percent) and the highest false positive rate (8.8 percent) during testing, which indicated that about 9 percent of no lane changes have been detected as lane changes. Similar to the validation, the highest true positive rate and the lowest false negative rate were found for the RF model for the test dataset.

To measure the classification performance of the Machine Learning models, the Receiver Operating Characteristic (ROC) curve was utilized. More specifically, Area Under the Curve (AUC) of a ROC plot can be used to evaluate the performance. An AUC value over 0.9 indicates high accuracy, in between 0.7 to 0.9 represents moderate accuracy, and values between 0.5 to 0.7 denote poor accuracy (*190*). Figure 47 to Figure 49 show the ROC curves of the RF, SVM, and ANN models for Category 1 features during validation. All the models had AUC value greater than 0.9, which indicates all the models detected lane change maneuver with high accuracy. However, the highest AUC value (0.959) was observed in the RF model. Considering the highest overall accuracy and the AUC value, RF model is the recommended model to be used for the Category 1 features.

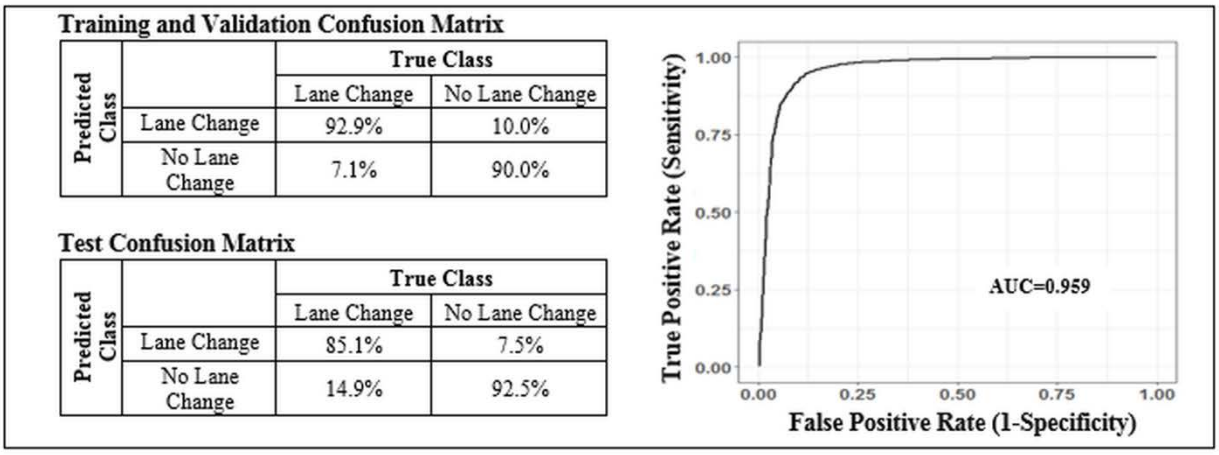

Figure 47 Detection Summary of the RF Model Using All Features

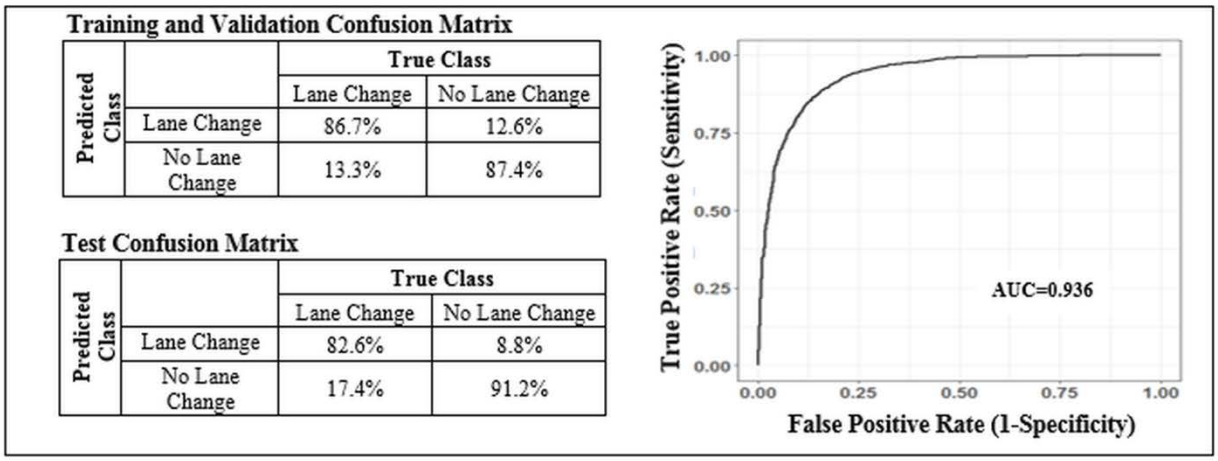

Figure 48 Detection Summary of the SVM Model Using All Features

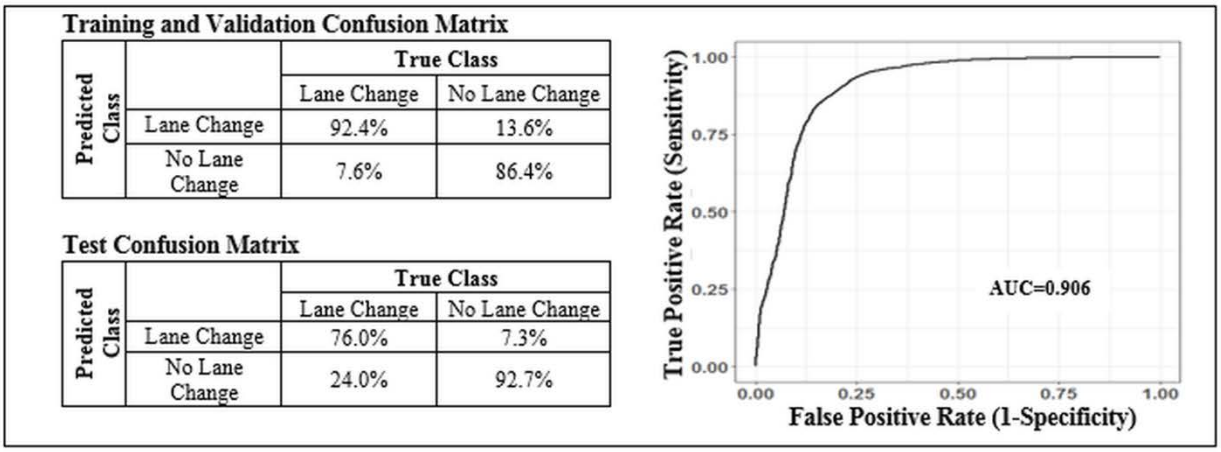

Figure 49 Detection Summary of the ANN Model Using All Features

Category 2 – Fusing Vehicle Kinematics, Roadway Characteristics, and Driver Demographics

The overall detection accuracy of the RF, SVM, and ANN models was found to be comparatively lower but still impressive using features based on vehicle kinematics from CAN-bus and external sensors, roadway characteristics, and driver demographics. Figure 50 to Figure 52 show the detection summary of the three models using confusion matrix. It was found that the RF classifier outperformed all other classifiers with a detection accuracy of 81.8 percent and 79.9 percent during validation and testing, respectively. In contrast, the lowest detection accuracy was found for the SVM model (80.5 percent during validation and 78.1 percent during testing). The highest true positive rate (84.5 percent) and the lowest false negative rate (15.5 percent) were found in the RF model during validation, which indicates that the model has accurately detected around 85 percent of lane changes. However, the lowest true positive rate (74.4 percent) and highest false negative (25.6 percent) was found in the ANN model during testing suggesting that around 26 percent of lane changes have been misclassified by the model. In addition, it was observed that RF and SVM had similar true positive rates during testing. According to the figures, the values of AUC of the trained models were found to be greater than 0.8, which indicates moderate accuracy. The finding pointed out that excluding the machine vision-based feature (i.e., lane position offset) did not significantly reduce the detection accuracy. Based on the evaluation results, the study suggested that the RF model would provide better lane change detection in presence of vehicle kinematics, roadway characteristics, and driver demographics.

Training and Validation Confusion Matrix

Predicted Class		True Class	
		Lane Change	No Lane Change
	Lane Change	84.5%	20.9%
	No Lane Change	15.5%	79.1%

Test Confusion Matrix

Predicted Class		True Class	
		Lane Change	No Lane Change
	Lane Change	75.4%	15.4%
	No Lane Change	24.6%	84.6%

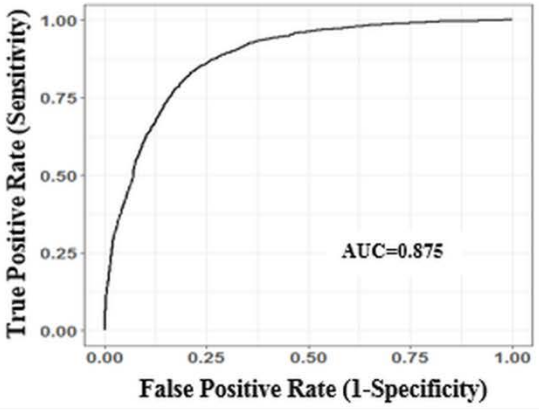

Figure 50 Detection Summary of the RF Model Using Category 2 Features

Training and Validation Confusion Matrix

Predicted Class		True Class	
		Lane Change	No Lane Change
	Lane Change	79.2%	18.1%
	No Lane Change	20.8%	81.9%

Test Confusion Matrix

Predicted Class		True Class	
		Lane Change	No Lane Change
	Lane Change	75.7%	19.8%
	No Lane Change	24.3%	80.2%

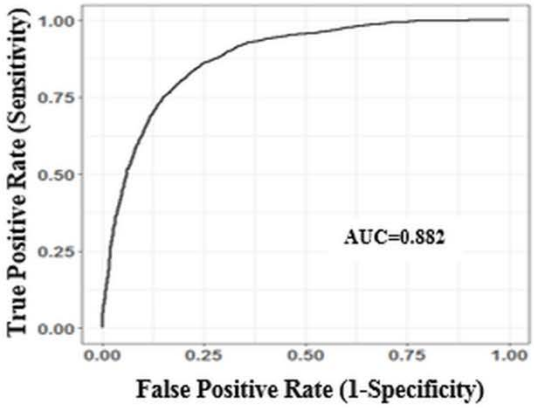

Figure 51 Detection Summary of the SVM Model Using Category 2 Features

Training and Validation Confusion Matrix

Predicted Class		True Class	
		Lane Change	No Lane Change
	Lane Change	83.7%	23.5%
	No Lane Change	16.3%	76.5%

Test Confusion Matrix

Predicted Class		True Class	
		Lane Change	No Lane Change
	Lane Change	74.4%	17.8%
	No Lane Change	25.6%	82.2%

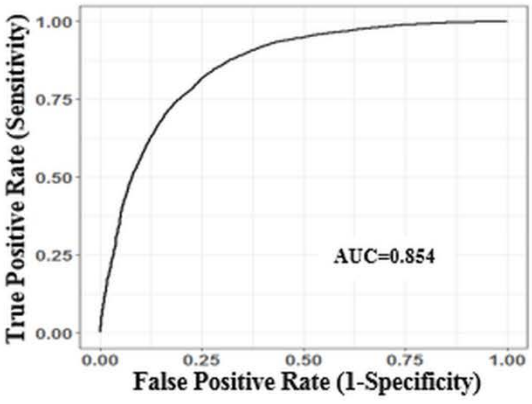

Figure 52 Detection Summary of the ANN Model Using Category 2 Features

Category 3 – Features Based on Vehicle Kinematics Only

Category 3 consists of features related to only vehicle kinematics (i.e., standard deviation of speed, standard deviation of longitudinal acceleration, standard deviation of lateral acceleration, and standard deviation of yaw rate). The detection summary of the Machine Learning models is shown in Figure 53 to Figure 55.

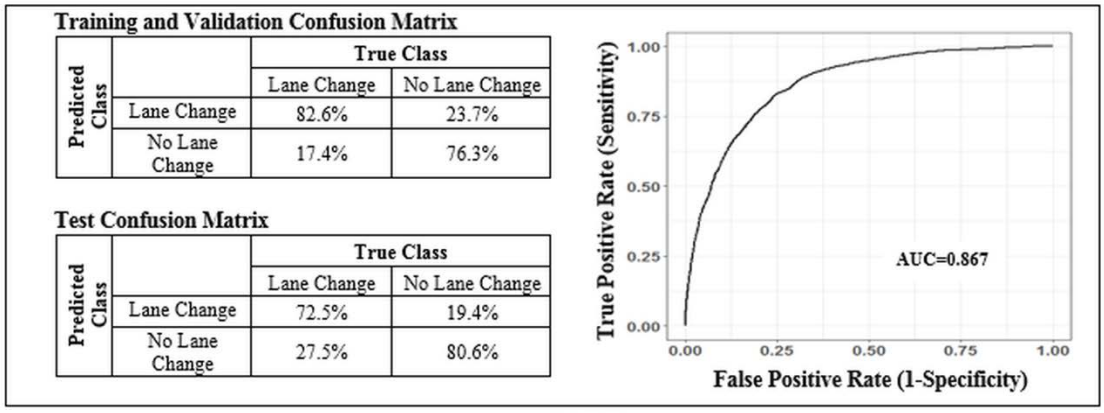

Figure 53 Detection Summary of the RF Model Using Vehicle Kinematics Features

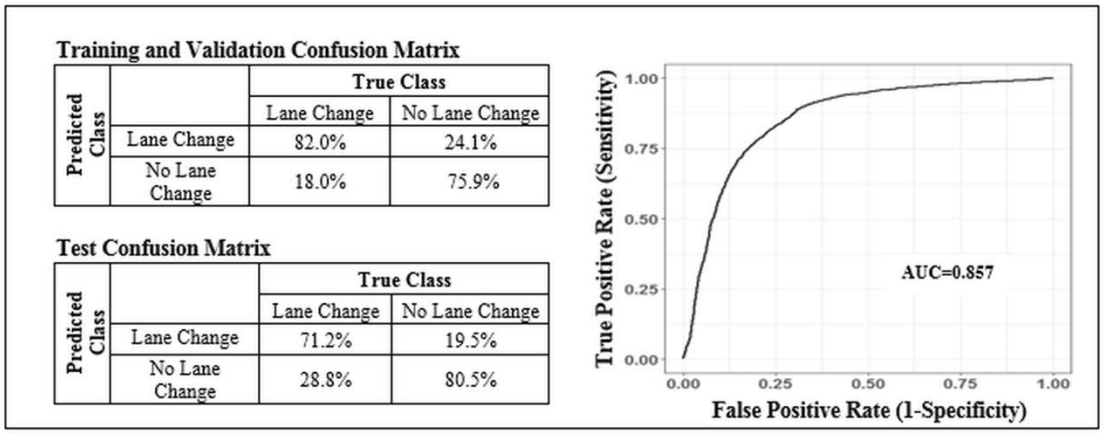

Figure 54 Detection Summary of the SVM Model Using Vehicle Kinematics Features

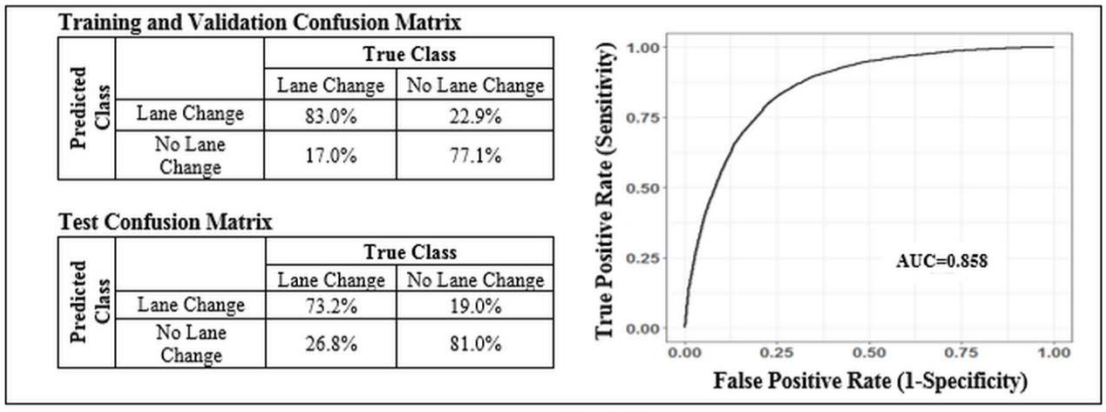

Figure 55 Detection Summary of the ANN Model Using Vehicle Kinematics Features

While the highest overall detection accuracy was observed in the ANN model (80.1 percent during validation and 77.1 percent during testing), the lowest detection accuracy was found for the SVM model (79 percent during validation and 75.7 percent during testing). The highest true positive rate (83 percent) and the lowest false negative rate (17 percent) was found in ANN model during validation indicating that 83 percent of lane change maneuvers have been detected correctly by the classifier. In addition, the ANN model had the lowest false positive rate (22.9 percent) and the highest true negative rate (77.1 percent) during validation. The result suggested that around 23 percent of no lane changes have been detected as lane changes. It is worth noting that ANN had similar results during testing. The overall AUC values corresponding to three models were found to be greater than 0.8. The finding indicated that the use of only vehicle kinematics based features could also produce moderate accuracy without including other features such as roadway characteristics or driver demographics. Considering the overall performance of all the Machine Learning models, the study suggested that the ANN model would provide better lane change detection when only vehicle kinematics are available.

Performance of the Lane Change Prediction Models

The ML based lane change prediction models were also developed using the "caret" package in R®. Once the dataset was split into six feature sets, ML classifiers were employed to train and validate the prediction models. The prediction models were trained and validated using five-fold cross-validation approach and then test dataset were utilized to comparatively evaluate the performance of the models. It is worth mentioning that parameters of all the models were tuned using the grid-search method to obtain the best performance (*191*). For the CART model, maximum depth of any node of the final tree (maxdepth) can be tuned. As an example, a value of 6 provided the best performance for the CART model used in Feature Set 6 (i.e., vehicle kinematics features). Considering the RF model, two parameters can be tuned-the number of variables randomly sampled at each tree node (mtry) and the number of trees to grow (ntree). It was found that the best combination for the "mtry" and "ntree" was found to be 20 and 200, respectively for the RF model in Feature Set 6. However, number of trees (nIter) parameter was tuned for AdaBoost model and found to be 50 for Feature Set 6. Similarly, a number of parameters including number of boosting iterations (nrounds), maximum tree depth (max_depth), shrinkage (eta), minimum loss reduction (gamma), and subsample ratio of columns (colsample_bytree) can be tuned for the XGBoost model. The best prediction performance was obtained for nrounds equals 150, max_depth equals 2, eta equals 0.4, gamma equals 0, and colsample_bytree equals 0.8 considering the Feature Set 6. In addition, two parameters, cost and sigma were tuned during the training of SVM model. A cost and sigma value of 1 and 0.13, respectively, were used for SVM model in Feature Set 6. Moreover, the best KNN model after parameter tuning in Feature Set 6 was based on maximum number of neighbors (kmax) value of 7 and Minkowski distance (distance) value of 2. Finally, two parameters, laplace correction (laplace) and bandwidth adjustment (adjust) were tuned during the training of the NB model and found to be 0 and 1, respectively, using the Feature Set 6.

Since the ML models were developed to predict lane change maneuvers, which is critical from safety and operation perspectives, the prediction accuracy cannot be the only measure to evaluate the performance of the models. The study utilized several performance measures to assess the performances of the classification algorithms including accuracy, recall/sensitivity, precision, and F1-score. Recall measures the capability of the model to find all "lane change within 5s" in the dataset, whereas, precision specifies the ability of the model to classify only "lane change

within 5s" as "lane change within 5s" with no false prediction. It is worth noting that a model might have high precision and low recall value or vice-versa. However, when the model has balanced with high recall and precision values, the best performance is obtained. This can be measured by the F1-score, which is the harmonic mean of precision and recall. A high F1-score indicates the model is balanced with high recall and precision values, therefore, the best prediction performance is attained (*168*). The accuracy, recall, precision, and F1-score were calculated using the following equations.

$$Accuracy = \frac{TP+TN}{TP+TN+FN+FP} \quad \text{Equation 17}$$

$$Recall = \frac{TP}{TP+FN} \quad \text{Equation 18}$$

$$Precision = \frac{TP}{TP+FP} \quad \text{Equation 19}$$

$$F1 - score = 2 \times \frac{Recall \times Precision}{Recall+Precision} \quad \text{Equation 20}$$

Where TP is the no. of correctly classified "lane change within 5s", TN is the no. of correctly classified "no lane change within 5s", FN is the no. of misclassified "lane change within 5s" as "no lane change within 5s", FP is the no. of misclassified "no lane change within 5s" as "lane change within 5s".

Table 33 shows the prediction summary of all ML models in terms of overall accuracy for six feature sets. As shown in Table 33, the overall prediction accuracy of lane change maneuvers ranged from 69.4 percent to 97.0 percent using Feature Set 1 (i.e., all features together) during validation. Considering only vehicle kinematics-based features (i.e., Feature Set 6), the prediction accuracy ranged from 65.7 percent to 97.3 percent. The findings indicated that only vehicle kinematics based features can predict lane change maneuvers with considerably high accuracy in comparison with other feature sets. However, it has been observed that the XGBoost model outperformed all other models in predicting lane change maneuvers with an outstanding accuracy of above 96 percent for all six feature sets. This is followed by the AdaBoost method, which produced overall accuracy ranging from 94 percent to 95.6 percent. Moreover, it was found that some models such as SVM, KNN, and NB did not achieve acceptable accuracy indicating the inability of those models to predict such maneuvers.

Table 33 Overall Accuracy Results of the Machine Learning Models for Six Feature Sets

Models	Overall Accuracy (%)											
	Feature Set 1		Feature Set 2		Feature Set 3		Feature Set 4		Feature Set 5		Feature Set 6	
	Validation (%)	Test (%)	Validation (%)	Test (%)	Validation (%)	Test (%)	Validation (%)	Test (%)	Validation (%)	Test (%)	Validation (%)	Test (%)
CART	87.3	86.4	87.2	86.4	87.1	86.4	87.2	86.4	87.1	86.4	87.2	86.4
RF	94.4	92.9	94.2	93.1	94.2	93.9	94.2	94.2	94.2	92.6	94.4	94.2
XGBoost	97.0	96.7	97.0	96.0	97.2	96.8	97.3	96.9	97.2	96.3	97.3	96.5
AdaBoost	95.6	94.3	95.2	95.0	95.3	94.7	95.3	95.3	95.2	94.3	95.6	94.0
SVM	72.6	71.4	69.9	69.9	71.7	69.6	69.9	68.5	70.9	69.0	68.7	68.9
KNN	69.4	67.9	67.4	64.6	69.3	67.6	67.4	65.0	70.0	66.0	65.7	61.3
NB	71.7	72.5	70.1	67.2	68.3	68.8	67.5	68.3	68.7	69.3	65.7	64.3

The recall values of all ML models for all feature sets are provided in Table 34. According to Table 34, XGBoost model resulted in the highest recall values compared to other models across six feature sets. This is consistent with the overall accuracy results obtained for the XGBoost model. In addition, the similar recall values of the XGBoost model exhibited the stable performance of the model considering all six feature sets in comparison with other models. However, the recall values of AdaBoost models were found to be comparatively lower than the XGBoost model but higher than other models for all six feature sets, which are followed by the RF and CART models. On the contrary, the SVM, KNN, and NB models showed a fluctuating performance with very poor recall values during validation and testing in six feature sets. Hence, the performance of these models makes them potentially unreliable to predict lane change maneuvers.

Table 34 Recall Results of the Machine Learning Models for Six Feature Sets

Models	Recall (%)											
	Feature Set 1		Feature Set 2		Feature Set 3		Feature Set 4		Feature Set 5		Feature Set 6	
	Validation (%)	Test (%)	Validation (%)	Test (%)	Validation (%)	Test (%)	Validation (%)	Test (%)	Validation (%)	Test (%)	Validation (%)	Test (%)
CART	62.6	59.8	61.7	59.8	63.0	59.8	61.7	59.8	63.0	59.8	61.7	59.8
RF	89.2	85.5	87.5	85.5	88.2	85.5	86.8	85.9	88.2	84.6	86.8	86.7
XGBoost	94.5	92.9	94.6	92.5	94.9	92.9	94.6	92.1	95.0	90.9	94.2	91.7
AdaBoost	91.3	89.2	89.7	89.2	90.4	89.6	90.1	89.2	90.4	87.1	90.1	86.3
SVM	33.4	33.6	24.5	26.6	31.7	29.5	23.4	22.4	29.3	28.6	15.8	17.8
KNN	49.1	51.5	43.2	49.0	46.1	45.6	39.3	36.1	48.1	46.1	39.2	37.8
NB	41.7	46.1	65.0	67.6	24.1	26.6	34.5	41.1	32.6	33.6	54.5	56.8

The precision results listed in Table 35 are consistent with the recall results for the XGBoost, AdaBoost, and RF models. Note that the highest precision values were achieved by the CART model for all six feature sets during validation and testing. The findings are different from the corresponding recall values of the model. While the CART model had the highest precision values, it had relatively lower recall values, as shown in Table 34. It indicated that the CART model missed a substantially higher percentage of "lane change within 5s" compared to other models such as XGBoost, AdaBoost, and RF models. As mentioned earlier, a model might have a high precision with a low recall. Therefore, F1-score is needed to make a decision regarding the overall prediction performance of the model. The precision values of the XGBoost model were found to be comparatively lower than the CART model; however, the values are higher than all other models. As can be seen in Table 35, the precision values of the XGBoost model ranged from 96.4 percent to 97.7 percent and 95.3 percent to 98.7 percent during validation and testing, respectively, across the six feature sets indicating that the model had the more balanced performance compared to other models. Similar to the accuracy and recall results, the precision values of the SVM, KNN, and NB models were relatively lower than the other models.

Table 35 Precision Results of the Machine Learning Models for Six Feature Sets

Models	Precision (%)											
	Feature Set 1		Feature Set 2		Feature Set 3		Feature Set 4		Feature Set 5		Feature Set 6	
	Validation (%)	Test (%)	Validation (%)	Test (%)	Validation (%)	Test (%)	Validation (%)	Test (%)	Validation (%)	Test (%)	Validation (%)	Test (%)
CART	98.7	99.3	99.8	99.3	97.4	99.3	99.8	99.3	97.4	99.3	99.8	99.3
RF	93.6	92.8	94.7	93.2	94.1	95.8	95.5	96.3	93.9	92.7	96.1	95.4
XGBoost	96.6	97.0	96.4	95.3	96.6	97.4	97.1	98.7	96.6	97.8	97.7	97.8
AdaBoost	95.1	93.5	95.8	95.6	95.2	94.3	95.7	96.4	95.1	95.5	96.4	95.4
SVM	68.2	63.8	62.2	61.5	65.5	59.2	62.7	57.4	63.6	57.5	61.8	62.3
KNN	54.5	52.1	51.3	47.2	54.6	51.9	51.4	47.0	55.8	49.1	48.2	41.4
NB	61.1	62.0	54.2	50.8	55.4	57.1	51.8	53.5	55.1	57.0	48.7	47.2

Table 36 demonstrates the F1-score results of the ML models for six feature sets. As expected, the XGBoost model achieved higher F1-scores compared to the other models with impressive F1-score values ranging from 95.5 percent to 95.9 percent for validation dataset and 93.9 percent to 95.3 percent for test dataset across the six feature sets. The results confirmed that the XGBoost model had a more balanced prediction performance followed by the AdaBoost, RF, and CART models.

Table 36 F1-score Results of the Machine Learning Models for Six Feature Sets

Models	F1 Score (%)											
	Feature Set 1		Feature Set 2		Feature Set 3		Feature Set 4		Feature Set 5		Feature Set 6	
	Validation (%)	Test (%)	Validation (%)	Test (%)	Validation (%)	Test (%)	Validation (%)	Test (%)	Validation (%)	Test (%)	Validation (%)	Test (%)
CART	76.6	74.6	76.3	74.6	76.5	74.6	76.3	74.6	76.5	74.6	76.3	74.6
RF	91.3	89.0	90.9	89.2	91.1	90.4	90.9	90.8	91.0	88.5	91.2	90.9
XGBoost	95.5	94.9	95.5	93.9	95.7	95.1	95.8	95.3	95.8	94.2	95.9	94.6
AdaBoost	93.2	91.3	92.6	92.3	92.7	91.9	92.8	92.7	92.7	91.1	93.2	90.6
SVM	44.8	44.0	35.2	37.1	42.7	39.3	34.0	32.2	40.1	38.2	25.2	27.7
KNN	51.6	51.8	46.9	48.1	50.0	48.6	44.5	40.8	51.7	47.5	43.2	39.5
NB	49.6	52.9	59.1	58.0	33.6	36.3	41.4	46.5	41.0	42.3	51.5	51.6

After evaluating all performance measures, it can be concluded that XGBoost model obtained the best and balanced performance in terms of accuracy, recall, precision, and F1-score for all six feature sets. A previous study also suggested that XGBoost provides better prediction performance because of its accuracy, execution speed, and scalability (*183*). Considering the overall prediction performance of the XGBoost model, the study recommended to use the model for predicting lane change maneuvers irrespective of feature set. However, the comparative evaluation indicated that the SVM, KNN, and NB models failed to capture the minimal changes of features in each feature set, which ultimately performed very poorly. In addition, it has been observed that the tree-based models performed better compared to SVM, KNN, and NB models, in general.

The detailed performance of the XGBoost model for six feature sets are presented in Figure 56 in the form of confusion matrix, which confirmed the aforementioned discussion. For instance, the true positive rate and false negative rate of the XGBoost model were found to be 94.2 percent and 5.8 percent, respectively, during validation considering the Feature Set 6 indicating that around 94 percent of "lane change within 5s" have been correctly classified by the model, while only 6 percent of "lane change within 5s" have been misclassified. The false positive rate of the model based on Feature Set 6 was found to be only 1.1 percent during validation, as shown in Figure 56. It is worth mentioning that the higher the false negative and false positive rates, the greater the associated risk since in such scenarios, AVs might not maneuver in an appropriate way, which might potentially increase the crash probability. However, similar performance of the XGBoost model for other feature sets was observed in both validation and testing. The Area Under the Curve (AUC) values associated with each feature set were found to be greater than 0.9 representing the high accuracy of the XGBoost model in predicting lane change maneuvers.

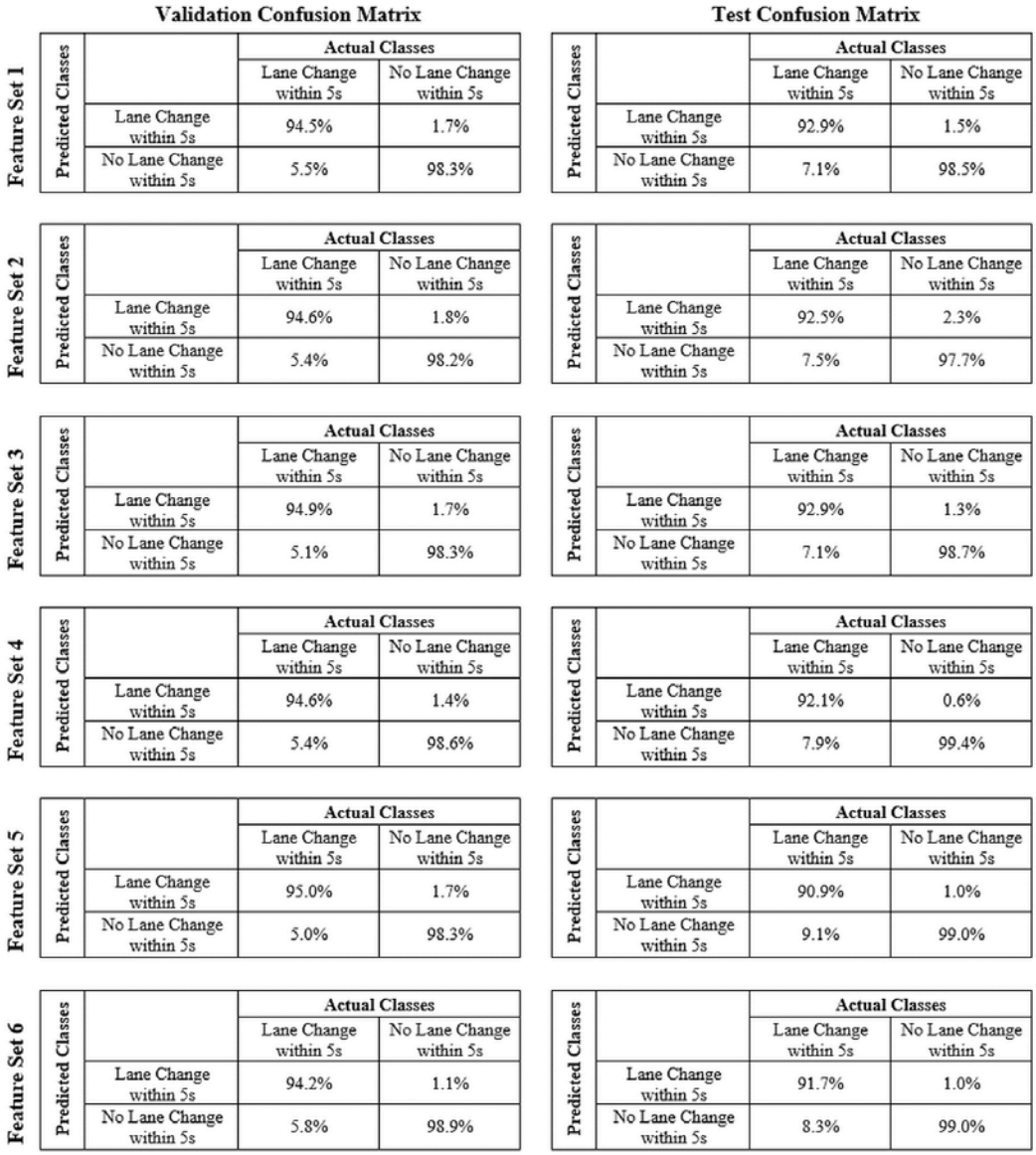

Figure 56 Confusion Matrices of XGBoost Model for Six Feature Sets

Chapter 5. Detection of Surrogate Measures of Safety in Adverse Weather Conditions

Literature Review

The use of traffic conflict techniques is one of the forms of non-crash data that can overcome the lack of crash data (*192*), (*193*), (*194*). Traffic conflict technique is based on observing SCEs on roadways based on the evasive maneuver, sudden braking, or sudden lane departure or occupancy that a driver does to avoid a crash (*194*), (*195*). Although this technique is not a new approach, it still has a number of issues in measuring traffic conflicts and in applying this technique to traffic safety analysis (*192*). Three main concerns associated with this technique are "the consistency in conflict definition," "the validity of the conflict technique," and "the reliability of conflict measurement" (*192*).

Numerous studies have tried to identify and apply Surrogate Measures of Safety to overcome the lack of adequate crash data. Some have identified traffic conflicts (*194*), (*196*), (*192*), critical events such as aggressive lane merging, speeding and running on red (*197*)). Other studies considered acceleration noise (*198*), time-integrated time-to-collision (*199*). Other surrogate measures include gap time, deceleration rate, encroachment time, initially attempted post-encroachment time, and proportion of stopping distance (*200*).

A leading new approach in the transportation field is to develop a technology that allows vehicles to be in continuous contact with each other, with infrastructure, and with handheld devices, named as CV. The CV is a new technology that is developed to help in improving traffic operation and enhance traffic safety. CV technology has the potential to address a majority of multi-vehicle crashes. The USDOT introduced the concept of road weather connected vehicle applications and services that aim to estimate the weather impacts on roadway, vehicles, and drivers (*201*). In addition, CV can provide assistance to transportation agencies in enhancing mobility, capacity, and transportation management (*202*), (*203*). The communication ability of CV can help in exchanging information related to the vehicle speed, position of CVs, and the relative position of surrounding vehicles that can help in estimating the traffic congestion level and to avoid crashes (*204*).

The relationship between the SMoS and CV can be illustrated through using the SHRP2-NDS data. This relationship would help in developing a connected vehicle-controlled algorithm. Another emerging question this study is trying to solve is what data should be collected from CV in the future so that SMoS analysis could be conducted. For instance, this could include using yaw rate for lane departure warning system and deceleration rate in a forward collision warning.

The SHRP2 has collected new and comprehensive data that will aid in understanding what happened before, during, and after crashes and near-crash events. This new data will enhance understandings of driver behavior, and factors contributing to traffic crashes. The SHRP2 data is classified into two massive databases; the Naturalistic Driving Study (NDS) database and the Roadway Information Database (RID) (*205*). The data include front and rear video records of the traveled roadways. Moreover, the NDS data contain vehicle speed, brake pedal activation, acceleration, yaw rate, etc. Information is also available from radar installed in the front of the NDS vehicle, the presence of alcohol, and seatbelt use among other factors. The importance of NDS data is illustrated by having unique real-time recordings for vehicle kinematics, radar data, GPS and network speed, brake pedal activation, along with front and rear video records. Real-

time data for driver behavior and performance can be estimated using the NDS datasets in different weather conditions (clear and adverse weather).

In 2010, a study collected new NDS dataset using six different equipped vehicles models to investigate driver behavior and vehicle performance, the relation between the instrumented 100-Car NDS vehicle and other vehicles, and the effect of driver demographics on traffic safety (*206*). Due to the limitations of the number of crashes collected and reported in the NDS data, the study used near-crash events as a surrogate measure for crash events. The study showed that the frequencies of contributing factors for crashes and near-crashes were related. Moreover, it concluded that due to the few numbers of crash events, utilizing near-crash events provided an appropriate number of samples to be used in a sound statistical analysis.

Therefore, this chapter intended to utilize the NDS data for an early investigation of SMoS on freeways that could be collected from CV in the future. Moreover, this chapter illustrated the effect of weather conditions on traffic safety by comparing vehicle kinematics of all near-crash events in the rain vs. clear condition. In addition, this chapter evaluated the SHRP2 NDS weather-related vehicle kinematics that will help in extending this work in the future by supporting the development of real-time CV applications requiring weather and roadway conditions input data.

Study Data

To help detecting near-crash events, the numbers of total events used in this study and reported in Dataset 1 were:

- 30 near-crash events in rainy weather and 58 matched normal driving trips; 2 near-crashes had only 1 normal driving matched event.
- 60 near-crash events in clear weather and 120 matched normal driving trips.

The time series NDS data were aggregated over 5-second, 10-second, 15-second, and 60-second time windows prior to the event timestamp (zero was used for the event timestamp). The aggregating of Dataset 1 over a fixed time period was important to store the data in a particular order with a reference point, which helped in comparing events with non-events. This also enabled the calculation of average, standard deviation, and coefficient of variation of vehicle kinematics. In this research, the time chunking was assumed and tested to determine which time aggregation would be more suitable to capture any changes in vehicle kinematics of the reduced data. The time chunking technique would be evaluated in the analysis and modeling step to choose the most appropriate time slice length.

Research Methodology

The research methodology was divided into the following parts:

- Identify essential indicators of near-crashes and the zone of interest for SMoS. This identification was carried out by considering each near-crash event as a unique scenario and comparing indicator values with their defined thresholds in previous studies. In this step, vehicle kinematics trajectories were utilized as input. This step aimed to show that the combinations of different vehicle kinematics were underlying factors for an event.
- Illustrate the effect of a change in weather conditions on near-crashes by comparing the results of all events in rainy weather conditions to events in clear weather conditions. Values of SMoS and the zone of interest of each indicator in rainy weather conditions were compared to the corresponding values in clear weather conditions. In addition,

this step would enhance the understanding of vehicle kinematics signatures and how rain could affect these signatures.

- Model the relation between SMoS and video reduced data using parametric statistical model (Binary Logistic Regression) and non-parametric statistical models (Decision Tree, k-Nearest Neighbor, and Deep Learning Artificial Neural Network) to detect near-crash on freeways. This step would help in understanding the important SMoS and environmental related factors that might increase near-crashes on freeways.

Statistical Models

Parametric and non-parametric statistical models were developed to detect near-crashes on freeways using the extracted data from video records and the NDS time series dataset. A Binary Logistic Regression model was used as a parametric detection model, non-parametric detection models such as Decision Tree Classification, k-Nearest Neighbors (k-NN) Classification, and Deep Learning Artificial Neural Network Classification, all were developed using the RapidMiner® software (*207*), (*208*).

Logistic Regression

Previous studies used logistic regression models to estimate crash severity and crash risk (*209*)(*210*); (*211*). In 2004, a study utilized stepwise logistic regression analysis to study the effects of environmental, district, human, vehicle, safety, and site factors on injury severity in vehicle crashes (*210*). Therefore, a binary logistic linear regression model was used to estimate the probability of having a near-crash event on a freeway. For the input data, different aggregation levels were attempted. The response variable (*Y*) had the value 1 if it was a near-crash event or a value of 0 for normal driving. Suppose Y has a Bernoulli distribution with probability of success (Y=1) given by $\pi = \pi(x, \beta)$. The following equation shows the general form of the logistic regression model with logit link where x is the vector of the predictor variables and β is the vector of regression coefficients (*212*).

$$\text{Logit}(\pi) = \log\left(\frac{\pi}{1-\pi}\right) = x'\beta \qquad \text{Equation 21}$$

A Stepwise selection was used to select a subset of the predictors that were important for detecting near-crash events. The selection method was based upon the p-value of the residual Chi-square score statistic using a significance level of 0.15 to enter and a significance level of 0.10 to stay (*213*).

Non-Parametric Models

Non-Parametric models have advantages over traditional statistical modeling. As non-parametric models do not need any certain assumptions between dependent and independent variables which are required in traditional statistical modeling. Also, non-parametric models are proficient of handling large data while traditional statistical techniques might have some limitations (*214*); (*215*); (*216*) (*217*). Therefore, non-parametric models have been employed in engineering and non-engineering fields. This study selected three supervised machine learning algorithms to achieve its objective. This section is explaining these three algorithms (*218*), (*214*), (*219*), (*208*), (*220*), (*221*).

Decision Tree (DT) is a supervised machine learning algorithm used to classify input data in a tree structure to detect a specific response (*220*). According to the response type, categorical or continuous, the DT works as a classification or regression algorithm. In this study, the DT was

used as a classification algorithm. This algorithm works by splitting predictors into nodes. Each node represents a splitting rule of one attribute. DTs contain root, splitting, and leaf nodes. The root node is the first node that the tree starts with, while the leaf node is the end node where the optimal split ends. Between the root node and the leaf node, the splitting process is done to divide nodes into two or more sub-nodes. The splitting process aims to create the highest homogeneity of nodes and sub-nodes before reaching the leaf node (*220*). The splitting of decision tree is based on a selected criterion. In general, there are five main splitting criteria each can be used in optimizing the split value. These five criteria are:

Information Gain: “The entropies of all the attributes are calculated and the one with the least entropy is selected for the split. This method has a bias towards selecting attributes with a large number of values.”

Gain Ratio: “A variant of information gain that adjusts the information gain for each attribute to allow the breadth and uniformity of the attribute values.”

Gini Index: “A measure of inequality between the distributions of label characteristics. Splitting on a chosen attribute results in a reduction in the average gini index of the resulting subsets.”

Accuracy: “An attribute is selected for splitting, which maximizes the accuracy of the whole tree.”

Least Square: “An attribute is selected for splitting, that minimizes the squared distance between the average of values in the node with regards to the true value.”

k-NN is a type of supervised machine learning algorithm where new data points get classified in a particular class based on a distance to its neighbor. There are two main disadvantages while using the k-NN classification. First, the k-NN is a lazy learner because it does not learn much from the training data (*222*). Second, its dependency on the selection of a “good value” for “k” (*222*). In k-NN classification, the k is representing the number of nearest neighbor data points that have the smallest distance from an example point. To select the value of k, it should not be a too small value, as the classification may be prone to overfitting because of noise in the training data. On the other hand, k value should not be a too large value, as the classification may miss-classify the test instance by including data points that are located far away from its neighbor. The selection of k value can be done through a trial and error method to achieve the highest model performance (*222*).

An Artificial Neural Network (ANN) is a supervised machine learning algorithm with a structure that was inspired by the human brain. ANN algorithms are used to uncover patterns in the dataset or to model a relationship between inputs and outputs (*223*). The structure of a neural network consists of a number of layers; each layer contains processing units called “neurons.” A neuron is used to receive and pass information before and after the data are manipulated using a “transfer function.” All neurons are connected to the neurons in the layers located immediately before and after to transfer data. At each neuron, each connection is associated with a specific weight used to compute a value for that neuron (*214*). To train a neural network, forward propagation and backward propagation are repeatedly used to adjust the value of the weights between each neuron. To start the training process, a set of randomly selected weights are assigned, and forward propagation is used to calculate resulting model proficiency. Then, based on the margin error of the output, the backward propagation adjusts the weights to decrease the error (*214*). One of the types of ANN is the Deep Learning ANN (*224*); (*221*). The terminology “Deep

Learning" is used to describe the presence of many hidden layers which are specified to analyze a complex problem (*225*). The Deep Learning ANN algorithm is selected to improve classification detection accuracy.

Non-parametric Models Structure

In this chapter, non-parametric models were developed according to the model structure and process as shown in Figure 57. The model structure was divided into four main steps: importing input data, selecting the target variable, operating a cross-validation operator, and finally the creation of output and results. The Cross-Validation operator was used to evaluate the accuracy of the developed model and how the model would perform using a subset of input data. The cross-validation operator is divided into two sub-processes: training and testing sub-process, and the input data was split into two sets. The training sub-process use one set of data to train the model. Then the testing sub-process use the other set of data to evaluate the model performance. The input data used in these models were based on 1-second and 5-second time slices, where each time slice would represent a separate trial.

For Decision Tree, the model was built based on targeting higher accuracy, as an attribute is selected for splitting the tree to maximize the accuracy of the whole tree. The maximal depth was selected as 20 after many trials to achieve the highest performance. While for k-NN, the k value was selected to be 10. This selection was based on running the algorithm many times with different k values and then choosing the k value with the best performance. The distance method used was Euclidean to calculate the distance between the unknown data point and the training data. However, for Deep Learning ANN, the number and size of hidden layers used in this model were 3 hidden layers, each with 50 neurons. The times the dataset should be iterated were set to be 10. Also, the "adaptive learning rate algorithm (ADADELTA)" was used in modeling steps, as it combines the benefits of "learning rate annealing" and "momentum training" to avoid "slow convergence."

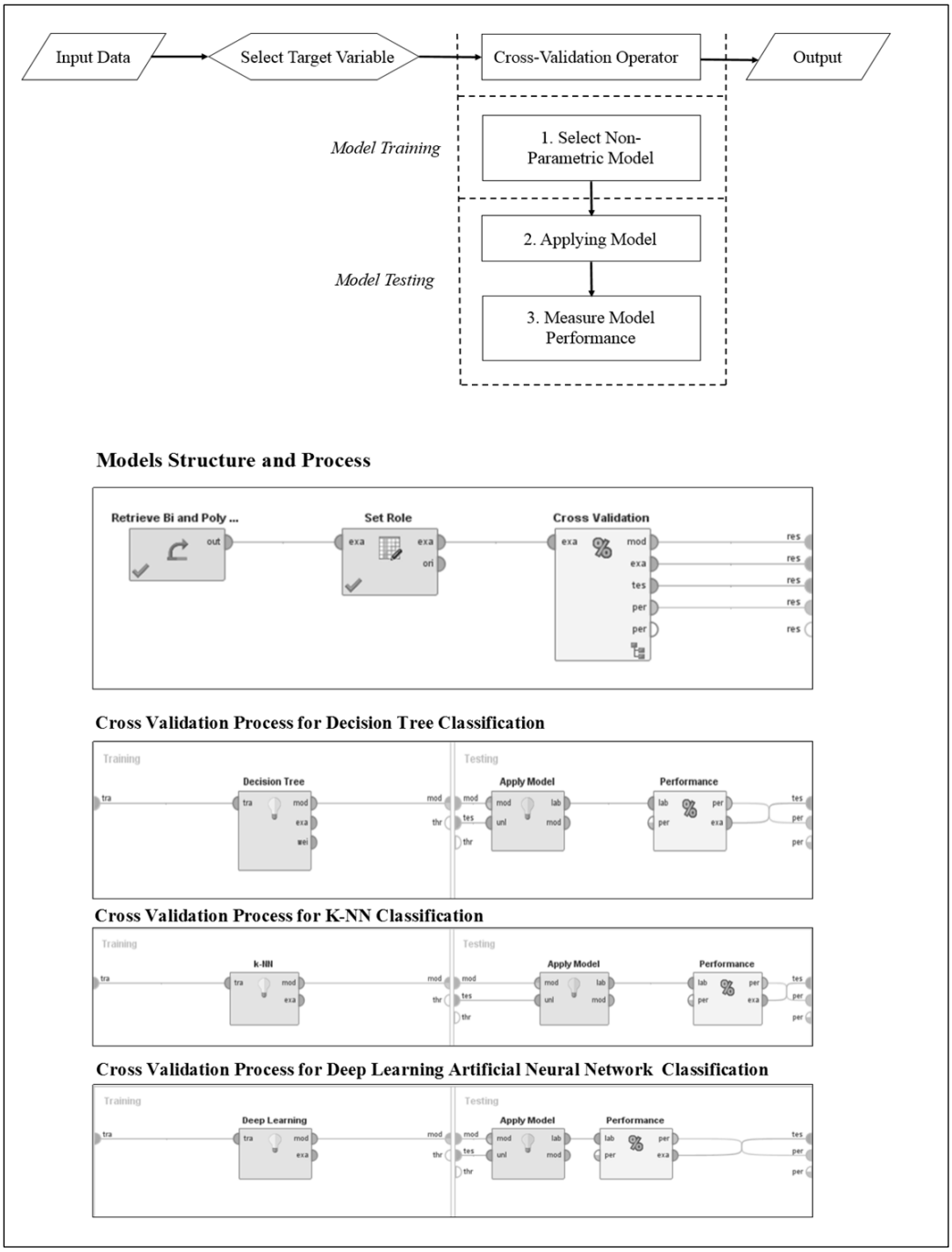

Figure 57 Non-Parametric Models Structures and Processes for All Time Slice Input Data

Data Analysis

Various SMoS for near-crash and matched events were plotted against the time as shown in Figure 58 to Figure 63. The data used in this step were aggregated using a 0.1-second aggregation level. The Figures show all the events and trips, in addition to the average, minimum and maximum trends. The reason for presenting the extremums of vehicle kinematics was to help in estimating the zone of interest of this vehicle kinematics that led to a near-crash occurrence (time window length and vehicle kinematic values). In these figures, the zero time represents the

timestamp of an event or a matched normal driving to an event. As the timeline has negative values representing the timeline before the event, and positive values representing the timeline after the event. Negative values of acceleration and deceleration rate represent deceleration rates, while positive values represent acceleration rates. A negative yaw rate means that the NDS vehicle was turning left, while a positive value indicates turning right.

Figure 58 to Figure 60 show a comparison between speed, acceleration and deceleration rate, and yaw rate for near-crash events in rainy weather conditions and events in clear weather conditions. Figure 58 shows that average speeds in clear weather conditions are higher than in the rain. However, clear weather events had a higher standard deviation of speed than in the rain. Figure 59 represents the difference between acceleration and deceleration rates in the rainy and clear weather. It was clear that the zone of interest in rainy weather conditions started 10 seconds before the events while the zone of interest in clear weather started within 5 seconds before the events. The maximum values of deceleration rate in clear weather condition were slightly higher than in rainy weather. Figure 60 shows the difference between the yaw rate in the rain and clear weather. The values of yaw rate were higher in clear weather than in rain weather around time zero (during the event). Thus, drivers in clear weather chose to change lanes more frequently than in the rain. The zone of interest for yaw rate in both weather conditions was too short during the event. Extreme yaw rates before and after an event due to a lane change or driving on a curve were eliminated from the data presented in the Figures.

In addition, and Figure 61 to Figure 63 summarize normal trips matched events in clear and rainy weather conditions. The reasons for using this visual comparison were to show:

- The vehicle kinematics signatures in normal trips regardless of driver behavior and freeway geometry.
- The wider range of acceleration and deceleration rate during events compared to normal matched trips.
- The extremes in yaw rate for normal trips matched to rain events were still higher than those trips matched to clear weather condition. This indicated that the reason behind the increase in yaw rate in rain events and their matched trips was due to the change in road geometry.
- The speed selection range is still not affected by having an event or not, but it is affected by weather conditions, traffic conditions, and road geometry.
- Figure 58 to Figure 63 show that the zone of interest for each indicator is not constant, but it might be defined using a statistical model through having significant variables within specific time slices before near-crash events timestamp.
- The last step in the data analysis was to show the difference in the average of speed, acceleration and deceleration rate, yaw rate between near-crash events and the normal matched trips. Figure 64 to Figure 66 show this comparison in the rain and clear weather. These figures show that during events, regardless of the weather condition, many vehicle kinematics changed and so can show an early surrogate measure of near-crashes. Moreover, the figures show the impact of weather condition on vehicle kinematics signature. These charts could be a guidance step towards an automation process of extracting different driving patterns.

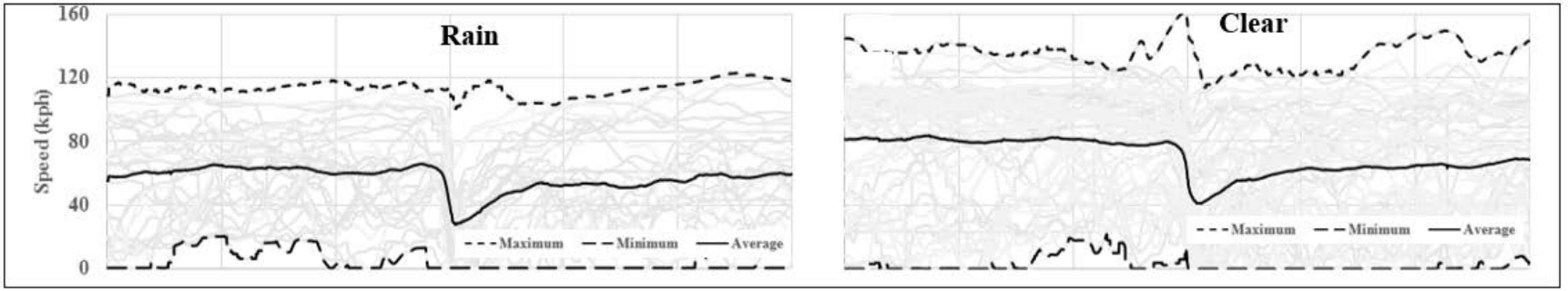

Figure 58 Speed Trajectories for Near-Crash Events in Rain and Matched Clear Weather

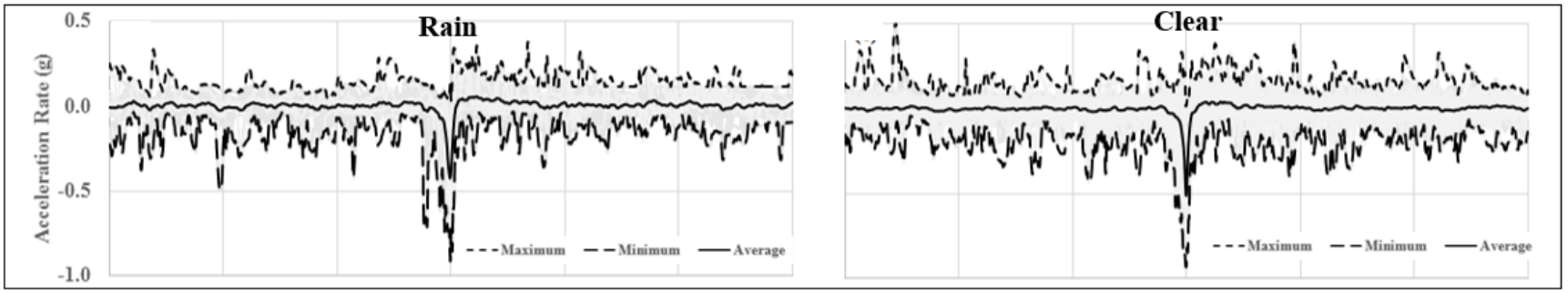

Figure 59 Acceleration and Deceleration Rate Trajectories for Near-Crash Events in Rain and Matched Clear Weather

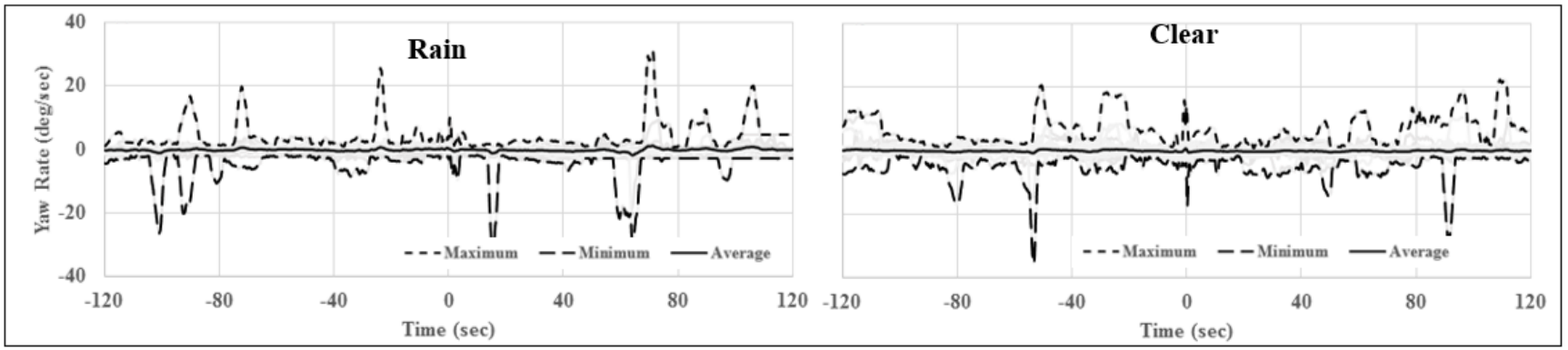

Figure 60 Yaw Rate Trajectories for Near-Crash Events in Rain and Matched Clear Weather

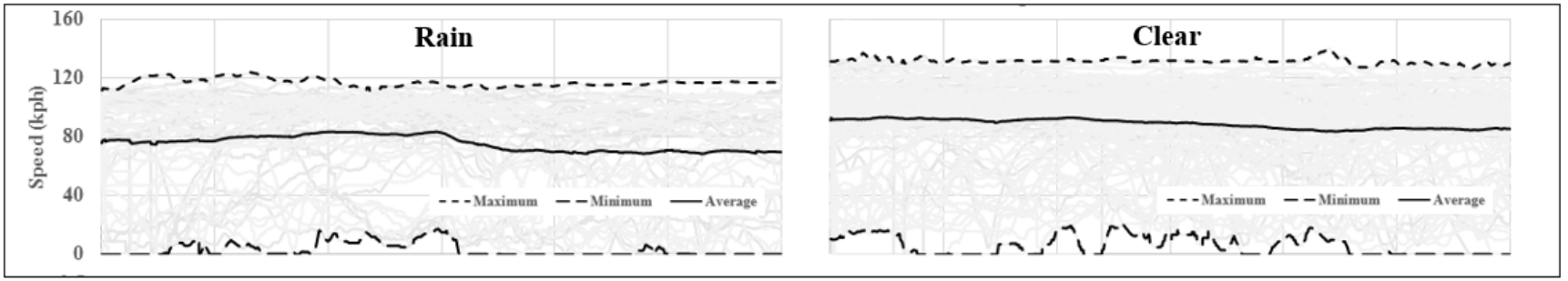

Figure 61 Speed Trajectories for Normal Trips Matched to Events in Rain and Clear Weather

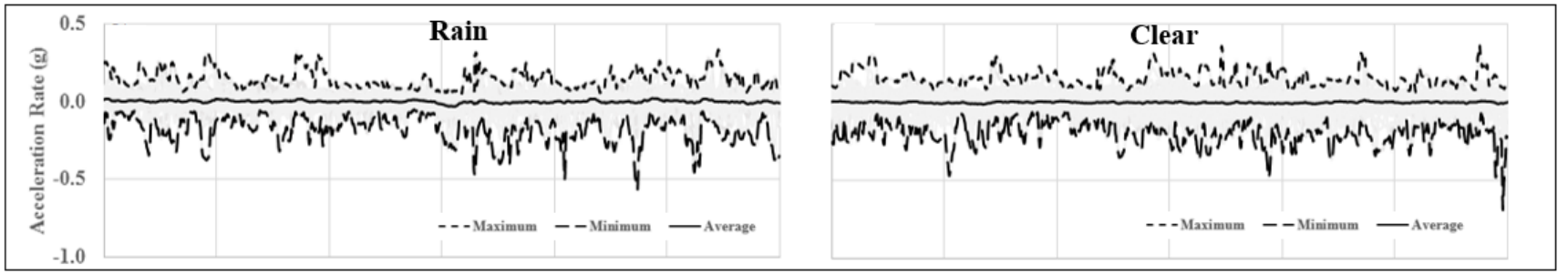

Figure 62 Acceleration and Deceleration Rate Trajectories for Normal Trips Matched to Events in Rain and Clear Weather

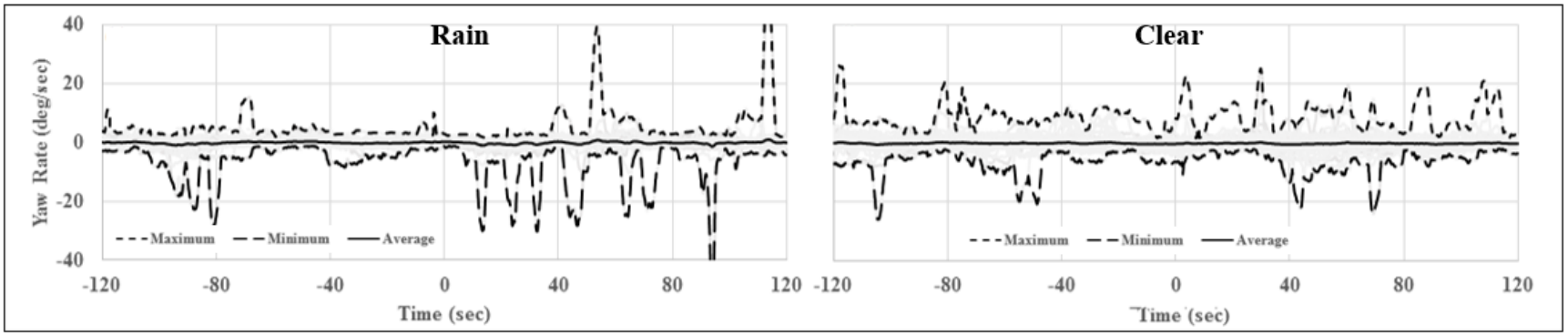

Figure 63 Yaw Rate Trajectories for Normal Trips Matched to Events in Rain and Clear Weather

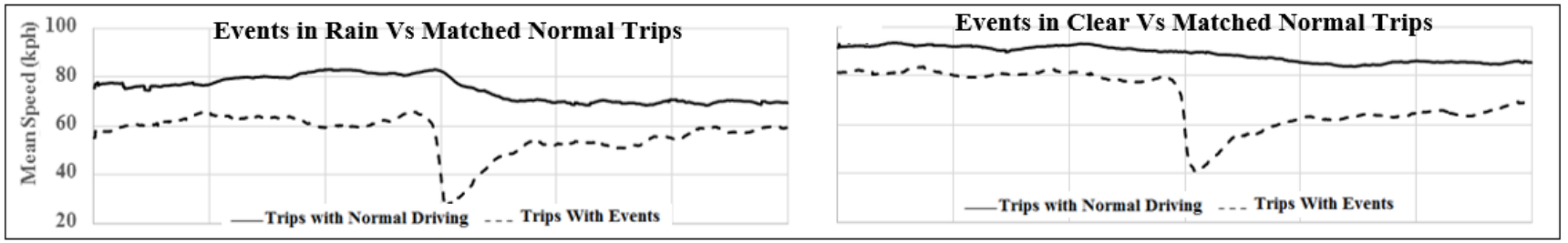

Figure 64 Comparison between Average Speed for Events in Different Weather Conditions with Normal Driving Trips

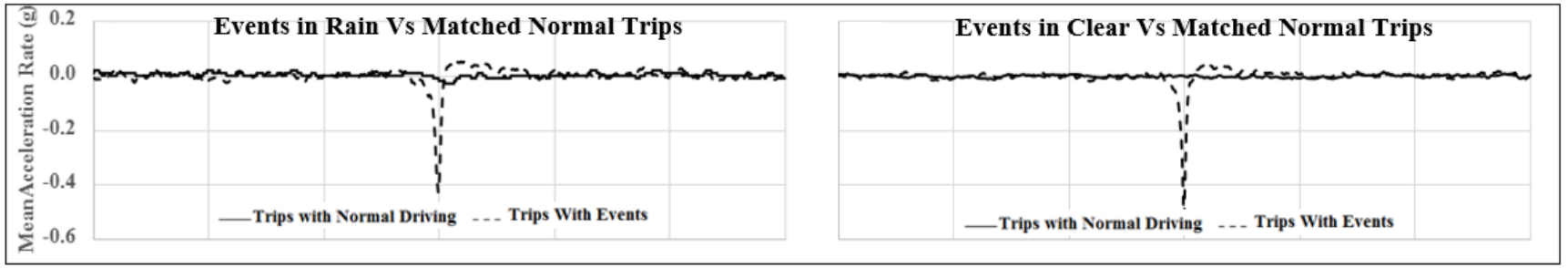

Figure 65 Comparison between Average Acceleration and Deceleration Rate for Events in Different Weather Conditions with Normal Driving Trips

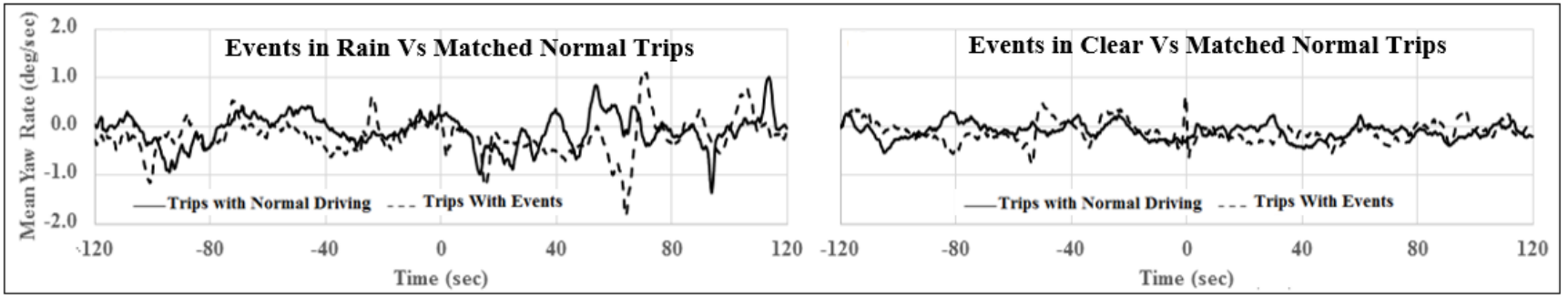

Figure 66 Comparison between Average Yaw Rate for Events in Different Weather Conditions with Normal Driving Trips

Table 37 provides statistical analyses for near-crash events in the rainy and clear weather conditions and their match normal trips. The aggregation level for the data used in the statistical analyses was a one second fixed moving time window. Two sample statistical comparisons were conducted of the indicators for near-crashes in the rain compared to clear weather conditions and for near-crashes compared to matched trips. One-sided t-tests, t(df), were used to test whether a population mean was lower than the other population mean assuming the population variances were unequal (*226*). One-sided F-tests, F(df1, df2), were used to test whether a population variance was lower than the other population variance (*226*). While a significance level of 0.05 was used in the comparisons, the sample sizes were large enough for small differences to be declared significant. Table 37 shows that the mean speed, mean acceleration and deceleration rate, and mean yaw rate were lower in rain events than clear events. The variation for acceleration and deceleration rate and yaw rate were higher in rainy weather than in clear weather. However, the variation for speed was lower in rainy weather than in clear weather. These results led to the conclusion that weather condition affected the crash indicators. Moreover, Table 37 explains the difference between events in different weather conditions and the normal matched trips. The variation of each indicator for different weather conditions was higher for the event trips. For rain weather conditions, the mean speed and the mean yaw rate were lower for the event trips. For clear weather conditions, the mean speed and mean acceleration and deceleration rates were lower for event trips.

Table 37 Statistical Analysis for the Near-crash Events and Matched Normal Trips

Statistical Tests	Events in Rain VS Event in Clear Weather		Events in Rain Weather VS Matched Normal Trips		Events in Clear Weather VS Matched Normal Trips	
	Rain Condition	Clear Condition	Events in Rain	Matched Trips	Events in Clear	Matched Trips
Speed (kph)						
Mean	56.64	70.54	56.64	75.5	70.54	88.96
Variance	59.2	119.31	59.2	27.08	119.31	9.75
t- test	Mean Speed was significantly lower in Rain t(4311) = 51.00		Mean Speed was significantly lower in Rain Events t(4216) = 99.52		Mean Speed was significantly lower in Clear Events t(2790) = 79.43	
F- test	Speed variability was significantly lower in Rain Events F(2400,2400) = 2.02		Speed variability was significantly higher in Rain Events F(2400,2400) = 2.19		Speed variability was significantly higher in Clear Events F(2400,2400) = 12.24	
Acceleration and Deceleration Rate (g)						
Mean	0.0017	-0.0014	0.0017	0.0023	-0.0014	0.0004
Variance	0.0015	0.0014	0.0015	0.0001	0.0014	0.0000
t- test	Mean Acc. and Dec. Rate was significantly higher in Rain Events t(4793) = 2.87		No significant difference between Mean Acc. and Dec. Rate for Events in Rain and their matched trips t(2493) = 0.68		Mean Acc. and Dec. Rate was significantly lower in Clear Events t(2493) = 2.39	
F- test	Acc. and Dec. Rate variability was significantly higher in Rain Events F(2400,2400) = 1.08		Acc. and Dec. Rate variability was significantly higher in Rain Events F(2400,2400) = 20.11		Acc. and Dec. Rate variability was significantly higher in Clear Events F(2400,2400) = 51.76	
Yaw Rate (deg/sec)						
Mean	-0.2097	-0.0955	-0.2097	-0.0633	-0.0955	-0.1009
Variance	0.1401	0.0471	0.1401	0.1162	0.0471	0.0248
t- test	Mean Yaw Rate was significantly lower in Rain Events t(3848) = 12.93		Mean Yaw Rate was significantly lower in Rain Events t(4756) = 14.17		No significant difference between Mean Yaw Rate for Events in Clear and their matched trips t(4384) = 0.97	
F- test	Yaw Rate variability was significantly higher in Rain Events F(2400,2400) = 2.98		Yaw Rate variability was significantly higher in Rain Events F(2400,2400) = 1.21		Yaw Rate variability was significantly higher in Clear Events F(2400,2400) = 1.89	

Modeling and Results

Parametric and non-parametric statistical models were developed to detect near-crashes on freeways using the extracted data from video records and NDS time series dataset. Where a Binary Logistic Regression model was used as a parametric detection model, non-parametric detection models were developed using RapidMiner® software (*207*), (*208*).

Modeling Steps

The modeling steps were:

1. Preparing time series dataset:
   The NDS data used in the statistical model had 3 percent missing values. The reasons for having missing values could be due to reporting issues for driver demographics while the

missing values for vehicle kinematics could be due to issues with the Data Acquisition System (DAS). The missing values were imputed using a Decision Tree imputation method in SAS® Enterprise Miner™ (*227*). The standard deviation and coefficient of variance for vehicle kinematics, with a fixed moving time window, were used as an input dataset for all models, with different aggregation levels of 1, 5, 10, 15, and 60-seconds. The standard deviation would help in capturing any change in vehicle kinematics over time.

2. Selecting effective time slice:
   The time length from the trip start-time till the near-crash timestamp was not constant over the whole events and their matched trips. In this study, time length should be identical to help to define the zone of interest for the SMoS. In addition, only time slices occurred on freeways and in daytime were considered in this study. Based on these limitations, the minimum time length that could fulfill the study limitations was found to be two minutes. After that, the data reduction step was performed as mentioned earlier. Finally, a verification step was performed by testing the performance of the logistic regression model and decision tree models using different time lengths as trial and error alternatives. The trial and error method used 120, 105, 90, 75, 60, 45, 30, and 15 seconds before the near-crash event timestamp. As five time slice lengths were assumed 1, 5, 10, 15, and 60-seconds, a binary logistic model was used to validate the time slice lengths using a trial and error technique.

   Results indicated that using time slices of length 1-second and 5-second could produce more reliable results, while other time slice lengths did not provide any important predictors. In addition, the results obtained from these trials indicated that important predictors were in the last 30 second before the near-crash timestamp. Therefore, the input data for all models would be classified into two main trials: the first trial would use a 1-second time slice, while the second trial would use 5-second time slice spanning only 30 seconds before the event timestamp.

3. Additional Input data:
   Response Characteristics (Event or Trip (EorT)), Driver Characteristics, Environmental Factors, and Traffic Flow Characteristics, all were added to the input data. These data were described in Table 38.

4. Developing parametric and non-parametric models.
   - Vehicle kinematics time slices (T) were numbered as follows:
   - The data were used from 30 seconds before the event (time slice number 90) till the event time slice T120.
   - For 1-second time slice length: T91, T92, T93, …, T118, T119, T120.
   - For 5-second time slice length: T95, T100, T105, …, T110, T115, T120

Table 38 Data Description

Variable	Symbol	Type	Levels	Frequency	Percentage
Response Characteristics					
Trip Type	EorT	Binary	Event = 1	90	33.58
			Normal Trip = 0	178	66.42
Driver Characteristics					
Gender	Sex	Binary	Male = 1	100	37.31
			Female = 0	168	62.69
Driver Age	Age	Ordinary	< 25 = 1	108	40.30
			25 - 64 = 2	149	55.60
			> 64 =3	11	4.10
Environmental Factors					
Weather Condition	WC	Binary	Rain = 1	50	28.09
			Clear = 0	128	71.91
Visibility Level	VL	Binary	Low Visibility = 1	54	20.15
			High Visibility = 0	214	79.85
Road Condition	RC	Binary	Wet = 1	41	15.30
			Dry = 0	227	84.70
Traffic Flow Characteristics					
Dynamics Traffic Status	DTS	Binary	Non-Free Flow = 1	181	67.54
			Free Flow = 0	87	32.46

Results of the Binary Logistic Regression Model

Table 39 shows the parametric model results from the variable selection procedure. The results indicated that the significant predictors, for a 1-second time slice, were the standard deviation of acceleration and deceleration rate six seconds before the event and one second before the event. In addition, results indicated the importance of the coefficient of variance for acceleration and deceleration rate eleven seconds before the event, and the coefficient of variance for yaw rate two seconds before the event. However, model results for a 5-second time slice were weather condition (WC), dynamic traffic status (DTS), visibility level (VL), and coefficient of variance of yaw rate before the event. The goodness of fit was assessed by the Hosmer and Lemeshow Goodness-of-Fit Test (*212*); (*213*). The p-value was equal to 0.49 and 0.77 for the 1-second and 5-second time slice length, respectively. These p-values provide indicates no evidence against a poor fit. The Area under the Receiver Operator Curve (ROC) provided a measure of the ability of the model to discriminate between trips resulting in a near crash and those trips that did not result in a near crash (*228*). The fitted models had an Area under the ROC equal to 0.98 and 0.71 for the 1-second and 5-second time slices, respectively. However, results of the binary logistic regression model using a 1-second time slice show enurmous values of standard errors for the standard deviation of acceleration and deceleration rate at time slice 106 and 120 seconds. The standard error is inversely proportional to the root square of sample size, so one of the reasons for having big values of the standard error is the small sample size. Another reason that might increase the standard error is the presence of high multicollinearity among the explanatory variables (*229*). However, results of the binary logistic model using a 5-second time slice show standard error associated with explanatory variables less than 1 and the sample size in case of the 5-second time slice is less than that in case of 1-second time slice. Therefore, having big standard errors and high odds ratios could be due to the high multicollinearity between the explanatory

variables. One of the suggested solutions is to use interactions between explanatory variables in addition to the main effects to avoid the multicollinearity (*230*). Accordingly, more trials were done using interactions between variables to achieve low standard errors in the binary logistic model. However, there was no significant change in the results. Based on these discussions on the model results, the utilization of 5-second time slice length could provide significant results with low standard error compared to the 1-second time slice.

Moreover, the model results indicated that the input data over different time slice durations would affect the accuracy of detecting near-crash events on freeways. As for the 5-second time slice, results demonstrated the contribution of weather conditions, visibility level, traffic flow characteristics, and the coefficient of variance of yaw rate in the last 5-second to a near-crash estimate on freeways. However, for the time slice length of 1-second, results showed that vehicle kinematics in the last 11 seconds before the near crash could help in detecting near-crash events on freeways. Based on the logistic regression model results, the 1-second time slice could detect near-crashes on the freeway using vehicle kinematics data only without considering any environmental factors and traffic conditions. This result can be used in CV applications to enhance traffic safety.

Table 39 Logistic Regression Estimates for Modeling Near-Crash Occurrence on Freeways

Variable	Coefficient	Standard Error	Wald Chi-Square	Significance	Odds Ratio	90% Wald Confidence Limits	
1-second Time Slice							
Intercept	-5.51	0.81	45.96	<.0001	-	-	-
Standard Deviation of Acc. and Dec. Rate, (T106)	39.31	16.89	5.41	0.02	>999.999	>999.999	>999.999
Standard Deviation of Acc. and Dec. Rate, (T120)	134.60	21.36	39.70	<.0001	>999.999	>999.999	>999.999
Coefficient of Variance of Acc. and Dec. Rate (T100)	0.24	0.10	5.84	0.02	1.27	1.08	1.50
Coefficient of Variance of Yaw Rate, (T118)	-0.40	0.20	4.23	0.04	0.67	0.48	0.92
5-second Time Slice							
Variable	**Coefficient**	**Standard Error**	**Wald Chi-Square**	**Significance**	**Odds Ratio**	**90% Wald Confidence Limits**	
Intercept	-1.79	0.30	34.88	<.0001	-	-	-
WC	1.37	0.34	16.37	<.0001	3.92	2.25	6.82
DTS	0.90	0.32	7.97	0.00	2.46	1.46	4.16
VL	0.76	0.33	5.29	0.02	2.15	1.24	3.70
Coefficient of Variance of Yaw Rate, (T120)	0.03	0.02	3.20	0.07	1.04	1.00	1.07

Results of Non-Parametric Models

Figure 67 shows the results of decision tree classification in a tree structure format to detect the occurrence of a near-crash event on a freeway. As “Std” refers to the standard deviation, “CV” is the coefficient of variance, “S” is the average speed, “A” is the acceleration and deceleration rate, and “Y” is the yaw rate at a certain time slice “T.” For example, “StdAT120” refers to the standard deviation of the acceleration and deceleration rate at time slice number 120, which is the timestamp of the event. Tree results using 1-second time slice indicate that the contribution of vehicle kinematics to near-crash detection was within the last 23 seconds prior to the event. The standard deviation of acceleration and declaration rate 1 second before the event was the

root node with a split value of 0.04g. While for a 5-second time slice of length, the weather condition, gender, and vehicle kinematics were the contributing factors to near-crash events within the last 20 seconds. In addition, weather condition was the root node and the splitting rule was based on the weather category (rain=1, clear=0). This indicates that the accumulation of the change in vehicle kinematics started 23 or 20 seconds before the event timestamp. In addition, using the decision tree algorithm in detecting near-crash events could provide early warnings to drivers starting from 23 or 20 seconds before the event. The application of this finding should balance between and imminent and normal situation, too many warnings might be annoying or distracting to drivers. The accumulation of another SMoS from vehicle kinematics at different time slices would help in defining an imminent situation. Finally, the thresholds for different vehicle kinematics, human factors, and environmental factors presented in the decision tree models could be used in updating CV applications.

Non-parametric models were compared based on the accuracy of the developed model to detect near-crash events. It is worth mentioning that all these models were trained using the cross-validation operator as mention previously in the model structure section. Table 40 shows models accuracy, specificity, and sensitivity associated with 1-second and 5-second aggregation levels. Results show a significant difference in accuracy based on the aggregation level. For example, the results of 1-second show that the Decision Tree model had the highest accuracy of 96 percent, followed by Deep Learning ANN with an accuracy equal 84 percent, and k-NN provided an accuracy equal to 81 percent. However, for 5-second, Deep Learning ANN had the highest accuracy of 85 percent, followed by Decision Tree model with an accuracy equal to 69 percent, then the k-NN model with an accuracy equal to 63 percent. The reason of having the lowest model accuracy using the k-NN algorithm is that the k-NN algorithm is a lazy algorithm as it has no real training phase, but it memorizes the training dataset instead (*231*). However, Decision Tree and Deep Learning ANN showed high accuracy in detecting near-crash on freeways using 1-second and 5-second time slices, respectively. Moreover, Deep Learning ANN showed almost the same results for different time slices. The Deep Learning ANN is superior model to detect a near-crash event on a freeway due to the presence of more hidden layers and the implementation of an adaptive learning rate algorithm that can improve the model accuracy.

a. Time Slice of 1-second Length

StdAT120 > 0.038
| CVAT103 > 15.477: 0 {1=0, 0=2}
| CVAT103 ≤ 15.477: 1 {1=81, 0=1}
StdAT120 ≤ 0.038
| StdAT119 > 0.059: 1 {1=7, 0=0}
| StdAT119 ≤ 0.059
| | StdAT97 > 0.000: 0 {1=0, 0=175}
| | StdAT97 ≤ 0.000: 1 {1=2, 0=0}

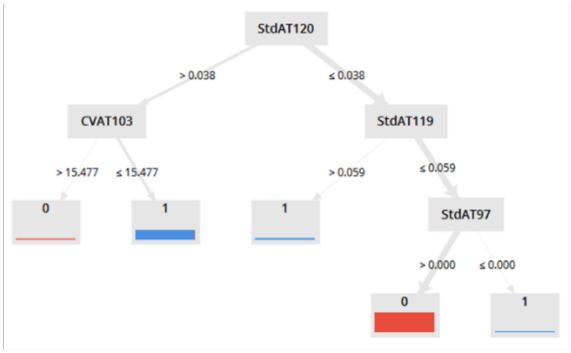

b. Time Slice of 5-seconds Length

WC = 0
| StdY100 > 0.085: 0 {1=50, 0=154}
| StdY100 ≤ 0.085
| | StdA100 > 0.025
| | | Sex = 0: 0 {1=0, 0=4}
| | | Sex = 1: 1 {1=2, 0=0}
| | StdA100 ≤ 0.025: 1 {1=8, 0=0}
WC = 1
| StdA120 > 0.030
| | CvY100 > 2.171: 0 {1=0, 0=3}
| | CvY100 ≤ 2.171
| | | CvS105 > 0.345: 1 {1=29, 0=4}
| | | CvS105 ≤ 0.345: 0 {1=0, 0=2}
| StdA120 ≤ 0.030: 0 {1=1, 0=11}

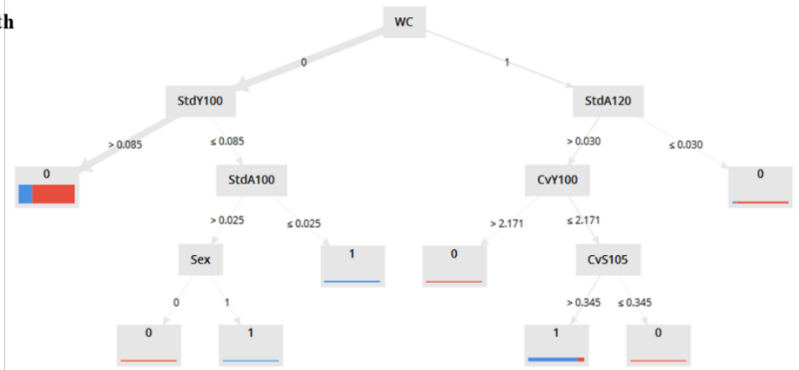

Figure 67 Results of the Decision Tree Classification Model

Table 40 Results of Non-Parametric Models for Detecting Near-Crashes

Non-Parametric Models	Time Slice Length	Overall Classification Rate	True Positive Rate	True Negative Rate	False Positive Rate	False Negative Rate
Decision Tree	1- Second	96%	93%	97%	3%	7%
	5- Seconds	69%	13%	97%	3%	87%
k-NN	1- Second	81%	49%	98%	2%	51%
	5- Seconds	63%	20%	85%	15%	80%
Deep Learning ANN	1- Second	84%	87%	83%	17%	13%
	5- Seconds	85%	93%	81%	19%	7%

Chapter 6. Weather Detection

Adverse weather events, such as snow, rain, fog, can directly impact roadway safety, by reducing the visibility and roadway surface friction, negatively affecting vehicle as well as drivers' performance, and potentially increasing required stopping sight distance. The Federal Highway Administration (FHWA) revealed that adverse weather is responsible for around 16 percent of fatal crashes, 19 percent of injury crashes, and 21 percent of Property Damage Only (PDO) crashes each year in the U.S. (*18*). Previous studies concluded that weather-related factors could increase traffic fatalities and injuries by 25 percent and 45 percent, respectively (*3*, *19*). Adverse weather conditions were also found to increase the risk of lane change (*232*) and secondary crashes (*233*). In addition, many studies have also concluded that driver behavior, including speeding, lane-keeping, and lane-changing behavior can also be negatively impacted by adverse weather conditions (*73*, *74*, *127*, *234*, *235*). However, the adverse effect of weather on roadway safety and operation can be effectively mitigated through the implementation of various safety systems, such as Variable Speed Limit (VSL) and Advanced Driving Assistance System (ADAS) (*236*). It is worth mentioning that all these systems require precise detection of weather conditions at the road surface level in real-time to operate appropriately.

Literature Review

Different approaches to image-based weather detection can be found in the literature. Previous studies have developed weather detection models based on different data sources and relying on various image processing techniques, computer vision algorithms, advanced modeling techniques, including machine learning and deep learning. The related works have been described in the following sections under three broad categories based on the source of data.

Weather Detection Using Fixed Sources

Many studies have used fixed data sources, such as Road Weather Information System (RWIS), Closed-Circuit Television (CCTV), to detect road weather and surface conditions. The study of Jonsson proposed a weather detection system based on the sensor data from RWIS combined with camera images. This study used Principal Component Analysis (PCA) to separate six road conditions, including dry, wet, snow, icy, and snowy with wheel tracks (*237*). Another study by the same author using the same data sources developed a weather detection algorithm capable of identifying dry, wet, snowy, and icy road conditions with an impressive detection accuracy ranging from 91 percent to 100 percent The study of Carrillo et al. also used similar data sources to develop a surface condition detection system utilizing several pre-trained deep learning models to detect bare, partial snow-covered, and full snow-covered pavement (*238*). Based on RWIS camera images, the study of Pan et al. leveraged several pre-trained Convolutional Neural Network (CNN) to detect four road conditions: bare, partially snow-covered, fully snow-covered, and not recognizable. This study achieved an accuracy of more than 97 percent using the ResNet50 architecture (*239*). Another study proposed a framework based on CCTV images to detect different situations, such as raining and non-raining scenes, daylight and night-time scenes, crowded and non-crowded traffic, and wet and dry roads. This study applied pre-trained neural network models via transfer learning and found an exact match ratio of 0.84. The study of Lee et al. analyzed the colors and edge patterns of the CCTV video to detect sunny, rainy, and cloudy conditions and achieved an overall accuracy of about 86 percent (*240*). Another study by the same research group developed an algorithm to estimate the amount of rainfall based on clustering techniques and found an accuracy of 80 percent (*241*). A study by Babari et al.

proposed a visibility estimation method based on gradient magnitude using roadside highway CCTV images and estimated the visibility with 30 percent error (*242*). Another study utilized CCTV images to develop road surface detection models with three categories, including clear, rain-wet, and snow. This study utilized a pre-trained CNN architecture, named VGG16, and achieved an overall detection accuracy of 77 percent (*243*). A recent study also used webcam images to develop weather and surface condition systems (*244*).

Weather Detection Using Open-Source Internet Images

The use of open-source internet images from various platforms, including Google, Flickr, Pixabay, and Yahoo, to develop weather detection models has also been explored in the literature. Ibrahim et al. proposed a new weather detection model, named WeatherNet, using Google images. The proposed WeatherNet was based on ResNet50 architecture and can detect clear, rain, and snowy weather condition with an overall accuracy of around 93 percent (*245*). Another study prepared a comprehensive image dataset, named Img2Weather, consisting of more than 180,000 images in an attempt to develop a weather detection system capable of classifying five weather types: sunny, cloudy, snowy, rainy, and foggy. This study achieved an accuracy of 70 percent using the Random Forest model (*246*). The study of Guerra et al. also created a dataset by extracting images from various platforms, including Creative Commons, Flickr, Pixabay, and Wikimedia Commons. This study proposed a novel algorithm based on CNN architecture and concluded that the proposed model can detect rain, fog, and snow with an accuracy of 80 percent (*247*).

Weather Detection Using Moving Sources

One of the major limitations of weather detection models based on fixed cameras and/or open-source images from the internet is that they cannot provide trajectory-level weather information at the road surface level. Therefore, many studies have used in-vehicle vision systems to detect weather conditions at road surface level. For instance, Pomerleau developed a weather detection system by estimating the reduction of contrast between consistent road features, such as lane markings, shoulder boundaries, and marks left by leading vehicles. The effectiveness of the weather detection system was tested using simulated fog images, as well as real-time images from in-vehicle cameras, which concluded that the system could identify reduced visibility caused by adverse weather conditions (*248*). Another study developed a weather detection system based on an in-vehicle vision system and AdaBoost classifier and found that the proposed system can classify sunny, cloudy, and rainy weather conditions with an accuracy of 96 percent, 89 percent, and 90 percent, respectively (*249*). Khan et al. extracted Local Binary Pattern (LBP) based features from snowy images and used three different classification algorithms to detect snow from an in-vehicle video camera (*167*). Another study by the same authors utilized the SHRP2 Naturalistic Driving Study (NDS) video data to develop a fog detection model based on various neural network architectures and found an overall detection accuracy of 97 percent in detecting two levels of fog (*250*). Qian et al. proposed a weather detection system based on dashcams and found 80 percent accuracy for clear and snow/ice-covered images and 68 percent for clear/dry, wet, and snow/ice-covered images (*251*). Another study used an inexpensive car-mounted video camera to capture images of the road surface at night-time, which was subsequently used to develop a detection model. They achieved an accuracy of 96 percent, 89 percent, and 96 percent in recognizing dry, wet, and snowy road conditions, respectively (*252*). Bronte et al. proposed a real-time fog detection system using an onboard low-cost black and white camera. Their system is based on two clues: estimation of the visibility distance, which is

calculated from the camera projection equations, and the blurring due to the fog (*253*). It is worth mentioning that most of the studies based on in-vehicle cameras or sensors require the presence of a consistent object in front of the vehicle. For instance, a weather detection method described in (*248*), requires road making, shoulder boundaries, tracks left by other vehicles. The fog detection system proposed in (*254*) requires a distinct object in the image. Some studies also used the horizon (*255*), and the road edge lines (*253*) to develop a weather detection system.

Data Acquisition and Preparation

The SHRP2 NDS video data were used in this study and were acquired from the Virginia Tech Transportation Institute (VTTI). To date, the SHRP2 is the largest study on naturalistic driving behavior in the US. Between 2010 and 2013. The SHRP2 collected a total of about 2 petabytes of NDS data from six states around the US, including Florida, Indiana, New York, North Carolina, Pennsylvania, and Washington. Participant vehicles were instrumented with a DAS. The DAS includes forward radar; four video cameras, including one forward-facing color wide-angle camera; accelerometers; vehicle network information; Geographic Positioning System (GPS); onboard computer vision lane tracking, plus other computer vision algorithms; and data storage capability (*173, 256*). For this study, only the video data of forward-facing color cameras were used.

Acquisition of the NDS video data and preparation of image dataset from the video data was a challenging and time-consuming task. To effectively extract video data of trips occurring in snowy weather conditions from the massive SHRP2 NDS dataset, two unique methods were developed. The first method used weather data from the National Climate Data Center (NCDC). To identify the potential location of trips occurring in snowy weather conditions, a buffer zone of 5 nautical miles (n.m.) around each weather station was defined as a zone of influence. This method was used in a previous study where snow-related crashes were predicted with an accuracy of about 60 percent (*257*). NDS trips were requested based on the daily weather information to identify all trips impacted by snowy weather. The second method utilized weather-related crashes to identify potential locations of trips occurring in snowy weather. This method considered each weather-related crash location as a center of the influence zone and similar to the previous method, a buffer zone of 5 nautical miles (n.m.) was used to identify trips occurred in snowy weather. More details about these methods can be found in (*12*). By using these processes, video data were received for trips occurred in adverse weather and their corresponding video data of trips in clear weather.

Snow Detection

After the acquisition of video data of adverse and clear weather from the VTTI, all the videos were observed manually to filter out the videos that did not occur in snowy weather. A new dataset of still images was created from the video data by extracting images from the videos at 12 frames per minute sampling rate. While higher sampling rates at 600 frames per minute seem reasonable for feature extraction of signs, signals, work zones, and other features, it might be too much and less efficient for weather conditions. For training models, the number of accurately annotated frames in various weather conditions is more important than a higher sampling rate. In addition, the videos used in this study represent trajectory-level data, meaning that all the videos were captured from a moving vehicle. Also, all the trips occurred at different locations. Hence, all the images are unique and none of the images are correlated.

Once the extraction of the images from the video data was completed, all the images were cropped at the bottom to remove the dashboard and to maintain consistency among the images, which results in an image pixel size of 350 widths and 250 heights.

The image dataset was then annotated manually and grouped into three categories: clear, light snow, and heavy snow. The snow was categorized based on the amount of visible snowflakes, surface conditions, and visibility. The selection for these two levels of snow has been inspired and is consistent with the levels provided in the Highway Capacity Manual (HCM), the Highway Safety Manual (HSM), and a wide body of literature in safety and operations. It is worth mentioning that most of the existing literature categorized levels of snowy weather based on quantitative measures. For instance, Agarwal et al. (*258*) categorized snow into four levels, including trace snow (≤ 0.05 in/hr.), light snow (0.06-0.1 in/hr.), moderate snow (0.11-0.5 in/hr.), and heavy snow (>0.5 in/hr.), based on the intensity of snowfall. Similarly, Weng et al. (*259*) grouped snow into three categories: heavy (>5 mm/hr.), medium (> 3mm/hr.), and light (> 0.7mm/hr.). However, categorizing levels of snow based on quantitative measures is not possible from the SHRP2 NDS video data. Hence, qualitative-based measures have been adopted and several criteria have been selected to define the levels of snowy weather as shown in Table 41 and sample images of weather conditions are shown in Figure 68. It is mentionable that the visibility was reported as clear if the video observers can clearly see and recognize road signs, markings, and roadside surroundings. On the other hand, visibility was categorized as affected if roadside surroundings (delineators, guardrail, etc.), road markings, and the horizon could not be seen clearly and the information on road signs is not readable. In order to maintain consistency in reducing video data, video observers were provided with comprehensive training.

Once the manual image annotation has been completed, the images were grouped into two datasets: training dataset and testing dataset. The training dataset consists of 8,000 images in each category which resulted in 24,000 images and is equivalent to 2,000 minutes of video data, whereas the testing dataset consists of 2,000 images in each category which resulted in 6,000 images and is equivalent to 500 minutes of video data. It is mentionable that the testing dataset has never been used during the training process.

Table 41 Classification of Weather from SHRP2 NDS Video Data

Weather	Criteria
Clear	• Clear visibility • Road signs, markings, and surroundings are clearly visible
Light Snow	• Snowflakes are visible • Little/No snow on the road surface • Clear/Affected visibility • Road markings and information on road signs and vehicles ahead could be recognized
Heavy Snow	• Snowflakes are clearly visible • Surface covered with snow • Affected visibility • Road markings and information on road signs and vehicles ahead could not be clearly recognized

Figure 68 Sample Images of Weather Condition from SHRP2 NDS Video Data

Fog Detection

In order to develop the fog detection system, the extracted images were grouped into three categories: clear and near fog and distant fog. It is worth mentioning that the classification of fog is not consistent in the literature. The National Oceanic and Atmospheric Administration (NOAA) classified fog into two categories back in 1949 (*260*). They classified fog as near if the visibility distance falls below 0.25 miles and light if the visibility distance is between 0.3 miles to 6 miles. In 1992, the South Carolina Department of Transportation (SCDOT) developed a low visibility warning system, where they defined fog as dense if the visibility falls below 300 feet and light if the visibility ranges between 300 feet to 900 feet (*261*). However, for this study, fog was classified into three categories including clear, near fog, and distant fog, using qualitative-based measures extracted from the NDS videos. The fog was classified based on the visibility of road markings, readability of road signs, roadside surroundings (delineators, guardrail, New Jersey barriers, etc.), and the horizon. The fog was reported as near fog during manual image annotation if the following conditions were observed:

- Few road markings in front of the NDS vehicle could be observed.
- Information on the road signs could not be read.
- Roadside surroundings and traffic ahead could not be clearly recognized.
- The horizon is undefinable.

On the other hand, the fog was classified as a distant fog if:

- Road markings and information on road signs could be easily recognized.
- Roadside surroundings and traffic ahead are visible.

- The horizon is undefinable.

Sample images of near fog and distant fog are shown in Figure 69.

Near Fog

Distant Fog

Figure 69 Sample Images of Weather Condition from SHRP2 NDS Video Data

Once the manual image annotation has been completed, the images were grouped into two datasets: training dataset and testing dataset. The training dataset consists of 8,000 clear weather images, 6,800 distant fog images, and 1,200 near fog images which resulted in 16,000 images and is equivalent to around 1333 minutes of video data. In addition, the testing dataset consists of 2,000 clear weather images, 1,700 distant fog images, and 300 near fog images which resulted in 4,000 images and is equivalent to around 333 minutes of video data. As near fog is a relatively rare environment condition, the number of near fog images are respectively less compared to other categories. The summary statistics of the data used in this study are shown in Table 42.

Table 42 Summary Statistics of Image Datasets

	Weather	Number of Images	Equivalent video Duration (min)
Training Dataset	Clear	8,000	666.67
	Distant Fog	6,800	566.67
	Near Fog	1,200	100
	Total	**16,000**	**1333.33**
Testing Dataset	Clear	2,000	166.67
	Distant Fog	1,700	141.67
	Near Fog	300	25.00
	Total	**4,000**	**333.33**

Adverse Weather Detection

Utilizing the above-mentioned methods, video data were collected considering the trips that occurred in adverse weather and their respective matched trips in clear weather. To confirm particular weather conditions (i.e., heavy snow, light snow), all the collected videos were manually observed and verified. In total, 217 trips in clear, 172 trips in snow, 204 trips in rain, and 168 trips in foggy weather were selected and considered for further analysis. Consequently, images were extracted at a sampling rate of 12 frames per minute from the videos of the selected NDS trips to create a database of images consisting of more than 20,000 images. Afterward, all the images were cropped at the bottom to discard the dashboard resulting in an image size of 250 × 200 pixels.

Once the extraction of images from the videos was completed, all the images were manually annotated and grouped into seven weather categories including clear, light rain, heavy rain, light snow, heavy snow, distant fog, and near fog. It is worth pointing out that manual annotation of images was a critical and time-intensive task. However, numerous criteria were fixed based on quantitative measures to define the weather categories in order to obtain precise annotation. In addition, the research team was provided with comprehensive training to remove any potential bias in the manual annotation process. Table 43 lists the criteria used during the annotation process and Figure 70 to Figure 73 illustrate the sample images of weather conditions (*234*). After the image annotation, a balanced number of images of 2,500 per category were randomly selected for the development of the weather detection model.

Table 43 Criteria for Image Annotation

Weather	Criteria
Clear	• Clear visibility • Road signs, markings, and surroundings are visible
Light Rain	• Raindrops are visible • Dry/ slightly wet road surface • Clear/Moderate visibility • Wiper at a low setting • Road markings and information on road signs and vehicles ahead could be recognized
Heavy Rain	• Raindrops are visible • Wet road surface • Affected visibility • Wiper at a high setting • Road markings and information on road signs and vehicles ahead could not be recognized
Light Snow	• Snowflakes are visible • Little/No snow on the road surface • Clear/Moderate visibility • Road markings and information on road signs and vehicles ahead could be recognized
Heavy Snow	• Snowflakes are visible • Surface covered with snow • Affected visibility • Road markings and information on road signs and vehicles ahead could not be recognized
Distant Fog	• Road markings and information on road signs could be easily recognized • Roadside surroundings and traffic ahead are visible • The horizon is undefinable
Near Fog	• Only a few road markings in front of the NDS vehicle could be observed • Information on the road signs could not be read • Roadside surroundings and traffic ahead could not be properly recognized • The horizon is undefinable

Figure 70 Sample Images of Clear Weather Conditions

Figure 71 Sample Images of Rainy Weather Conditions

Figure 72 Sample Images of Snowy Weather Conditions

Figure 73 Sample Images of Foggy Weather Conditions

Methodology

To determine snowy weather from the video data, machine learning techniques were used, which includes the extraction of features from the image datasets followed by the training of the extracted feature using different classifiers and finally testing the accuracy of the trained models using a new test dataset. It is worth mentioning that machine learning techniques have been extensively used in various fields of engineering for image classification, pattern recognition,

and text categorization (*262–264*). In addition, various deep learning techniques were also investigated to develop weather detection systems.

Feature Extraction

Two texture-based features including Grey Level Co-occurrence Matrix (GLCM) and Local Binary Pattern (LBP) was used as classification parameters.

Grey Level Co-Occurrence Matrix (GLCM)

GLCM is one of the most commonly used approaches of extracting texture features of an image and was developed by Haralick et al. in 1973 (*265*). The GLCM demonstrates how often a pixel value, p (i, j) in an image occurs with a specific relationship with its neighbor pixels. So, each element (i, j) of the matrix is the number of occurrences of the pair of pixels with values i and j.

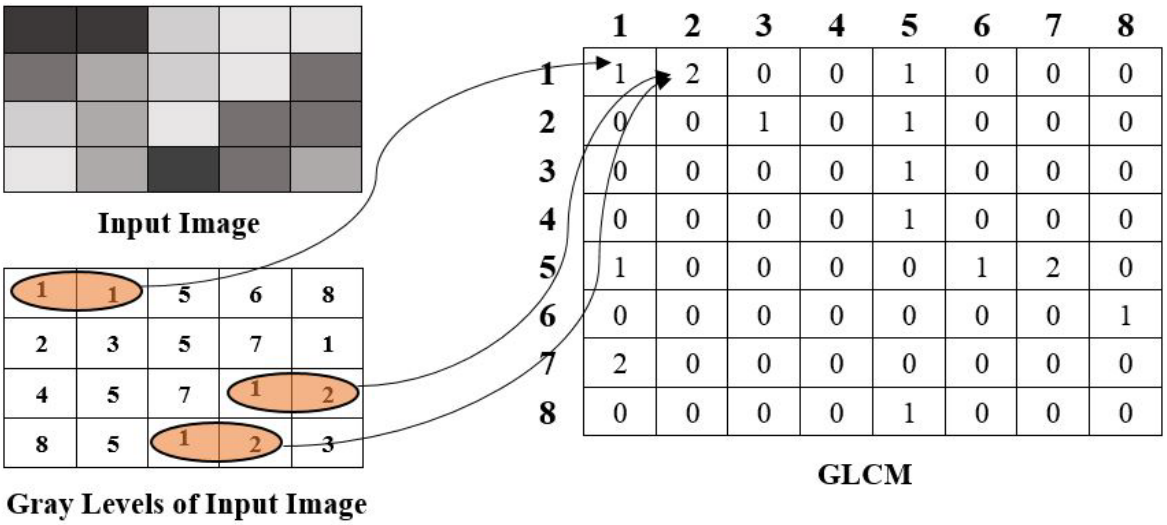

Figure 74 Example of Gray Level Co-Occurrence Matrix

The input image in Figure 74 consists of 20 pixels since the dimension of the image is 5 pixels × 4 pixels. Pixel is the smallest unit of an image. The input image has a total of 8 gray tones/levels ranging from 1 to 8. It is mentionable that the higher the gray levels the lighter the pixel. The dimension of GLCM depends on the number of grey levels. Since the input image has 8 gray levels, the GLCM matrix has 8 rows and 8 columns. In the GLCM matrix, element (1, 1) contains value one because the input image has only one instance where two pixels with value one occurred horizontally. Similarly, the element (1, 2) holds the value two because there are two instances where horizontally adjacent pixels have values one and two. It is mentionable that the grey images used in this study had 256 grey levels ranging from 0 to 255, where 0 represents black, 255 represents white, and any number in between represents different shades of gray.

For each image, a GLCM was constructed and from the GLCM four texture features, including contrast, correlation, energy, and homogeneity were extracted. All the computations were performed in a MATLAB environment.

Contrast measures the local grey level variation in the GLCM and can be defined using the following equation. The lowest possible value of the contrast is 0 which represents a constant image (*265*, *266*).

Contrast = $\sum_i \sum_j (i-j)^2 . p(i,j)$ Equation 22

Here, i and j are the horizontal and vertical cell coordinates, and p (i, j) is the grey level of the pixel located at coordinate (i, j) in the GLCM.

Correlation is a measure of gray pixel linear dependency with relative pixels in an image. The correlation ranges between 1 to -1, where 1 indicates maximum correlation and -1 indicates minimum correlations (*265*, *266*).

$$\text{Correlation} = \frac{\sum_i \sum_j (i \times j) p(i,j) - \mu_x \times \mu_y}{\sigma_x \times \sigma_y} \quad \text{Equation 23}$$

Here, i and j are the horizontal and vertical cell coordinates; p (i, j) is the gray level of the pixel located at coordinate (i, j) in the GLCM; μ_x and μ_y are the means relative to the horizontal and vertical component, respectively; and σ_x and σ_y are the standard deviations of the horizontal and vertical GLCM, respectively. μ_x, μ_y, σ_x, and σ_y can be described using the following equations.

$$\mu_x = \sum_{i=0}^{N-1} \sum_{j=0}^{N-1} i \times p(i,j) \quad \text{Equation 24}$$

$$\mu_y = \sum_{i=0}^{N-1} \sum_{j=0}^{N-1} j \times p(i,j) \quad \text{Equation 25}$$

$$\sigma_x^2 = \sum_{i=0}^{N-1} \sum_{j=0}^{N-1} p(i,j)(i - \mu_x)^2 \quad \text{Equation 26}$$

$$\sigma_y^2 = \sum_{i=0}^{N-1} \sum_{j=0}^{N-1} p(i,j)(i - \mu_y)^2 \quad \text{Equation 27}$$

Here, N is the number of gray levels in the image. It is mentionable that for each image, there was one unique GLCM. Therefore, a total of 8000 GLCM was constructed since the training dataset consisted of 8000 images and subsequently features were extracted from each GLCM separately.

Energy represents the sum of squared elements in the GLCM and is a measure of local uniformity of the texture and can be described using Equation 7. The value of energy ranges from 0 to 1, where 1 is for a consistent image (*265*, *266*).

$$\text{Energy} = \sum_i \sum_j p(i,j)^2 \quad \text{Equation 28}$$

The homogeneity represents the adjacency of the distribution of the elements in the GLCM. The value of the homogeneity ranges from 0 to 1, where 1 is for a diagonal matrix. The homogeneity can be described using equation 8 (*265*, *266*).

$$\text{Homogeneity} = \sum_i \sum_j \frac{1}{1 + (i-j)^2} p(i,j) \quad \text{Equation 29}$$

Before the training of the GLCM based models, boxplots were made to investigate the overall patterns of the GLCM features extracted from the image dataset as shown in Figure 75 to Figure 78, which indicates that the overall patterns and shapes of each category were different from one another.

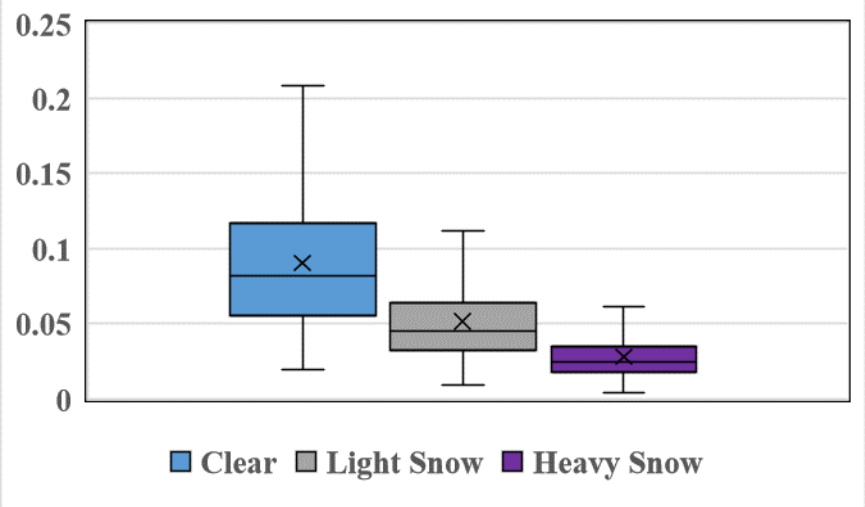

Figure 75 Boxplots of Contrast of Images

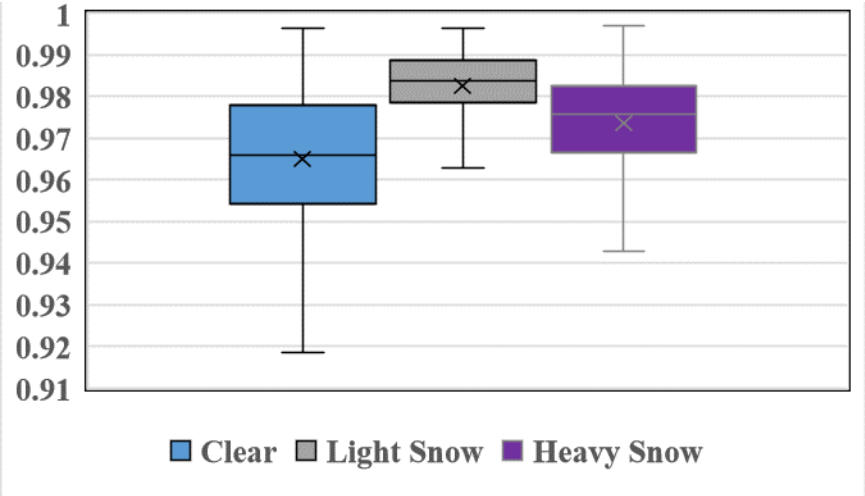

Figure 76 Boxplots of Correlation of Images

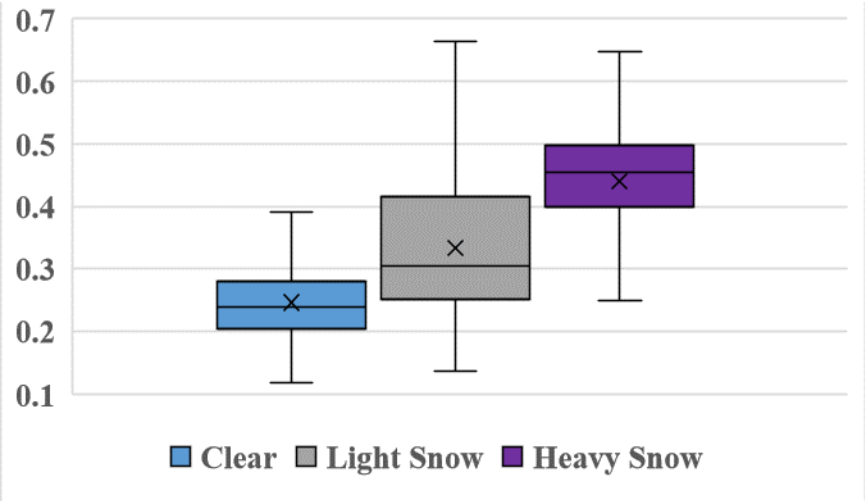

Figure 77 Boxplots of Energy of Images

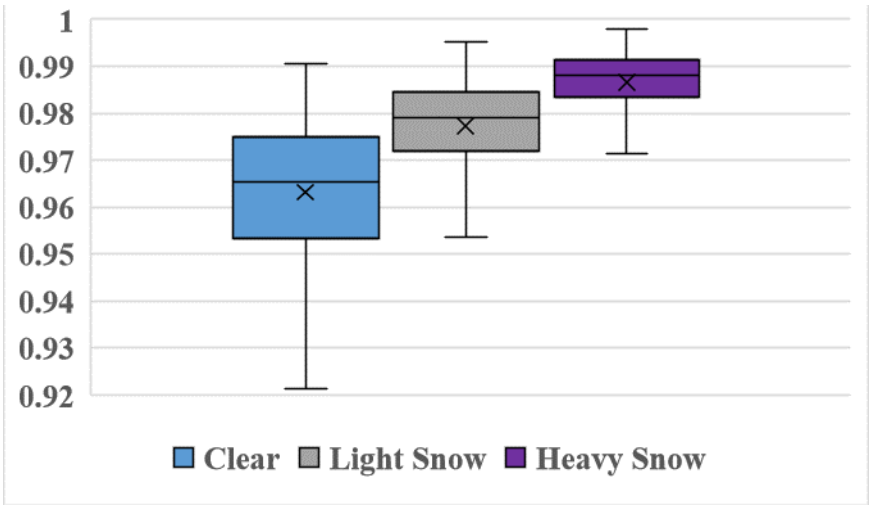

Figure 78 Boxplots of Homogeneity of Images

The range of contrast values of the clear image group varies between 0.02 to 0.22 with a mean value of 0.09. Conversely, the light snow image group has a much narrower range starting from 0.01 to 0.13 with a mean value of 0.05. Similarly, the contrast value of the heavy snow image group ranges between 0.004 to 0.06 with a mean value of 0.03. Considering correlation value, the clear image group has a wider range and lower mean compared to snow image groups. The range of correlation values of the clear image group varied between 0.96 to 1 with a mean value of 0.97 whereas the correlation value of the light snow image group ranges between 0.94 to 1 with a mean value of 0.98. The box plots of the other two GLCM texture features (e.g., Homogeneity and Energy) also exhibit similar kinds of variations in shapes and patterns as can be seen in Figure 75 to Figure 78. Overall, from the boxplots of the image dataset, it can be concluded that the GLCM features (i.e., contrast, correlation, energy, and homogeneity) can be used as significant classification parameters for training the machine learning models.

Local Binary Pattern (LBP)

Local Binary Pattern (LBP) is a powerful means of texture description and was developed by Ojala et al. (*267, 268*). The LBP operator computes a local representation of texture by comparing each pixel with its surrounding neighborhood of pixels. The original LBP algorithm operates on a fixed 3×3 neighborhood of pixels and assigns a level to each pixel of an image. Subsequently, the histogram of the levels can be used as a texture descriptor. Figure 79 illustrates the original LBP operator.

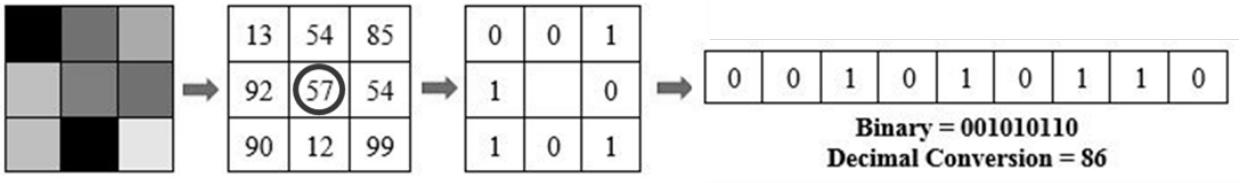

Figure 79 Demonstration of the Original Local Binary Pattern (LBP) Operator

Although the original LBP implementation can capture extremely fine-grained details using a fixed 3×3 neighborhood in an image, it cannot capture the details at varying scales. To overcome this problem, an extension of the original LBP was utilized in this study. To account for variable

neighborhood sizes, two parameters were introduced: the number of points P in a circularly symmetric neighborhood and the radius of the circle R. The LBP feature was then defined as:

$$LBP_{P,R} = \sum_{P=0}^{P=P-1} s(g_P - g_C)2^P \qquad \text{Equation 30}$$

$$s(x) = \begin{cases} 1, x \geq 0 \\ 0, x < 0 \end{cases}$$

Here, P is the number of points around the center pixels, R is the radius of the circle, g_c is the gray-scale value of the center pixel, and g_p is the grayscale value of a neighborhood pixel. Figure 80 shows an illustration of $LBP_{8,1}$ used in this study, in which 8 neighbor pixels are located on a circle of radius 1 around the center pixel. The numbers on the circle represent the grey levels of the 8 neighborhood pixels around the center pixel.

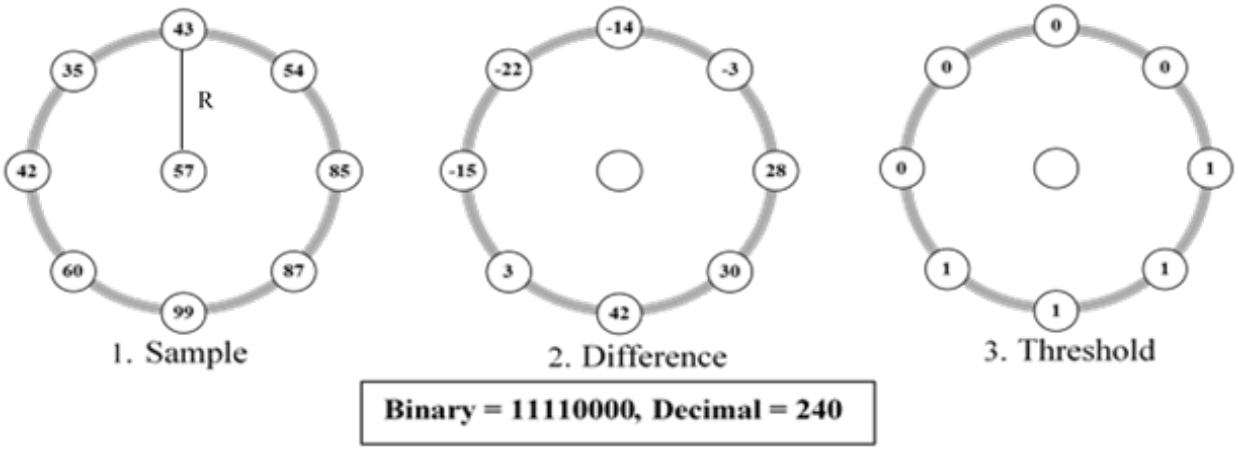

Figure 80 Demonstration of LBP Feature in a Local Neighborhood of an Image

Once the LBP was determined for each pixel of an image, it was grouped into two categories: uniform and non-uniform. An LBP is considered to be uniform if it has at most two 0-1 or 1-0 transitions. For example, the pattern 00001000 (2 transitions) and 10000000 (1 transition) are both considered to be uniform patterns since they contain at most two 0-1 and 1-0 transitions. Pattern 11001001 (4 transitions) and 01010010 (6 transitions) is not considered a uniform pattern since it has more than two 0-1 or 1-0 transitions. Subsequently, all the uniform patterns were assigned with separate labels and all the non-uniform patterns were assigned with a single label. Since (8,1) neighborhood was used in this study, there were a total of 256 patterns, 58 of which were uniform, which yielded 59 different labels (*269*, *270*).

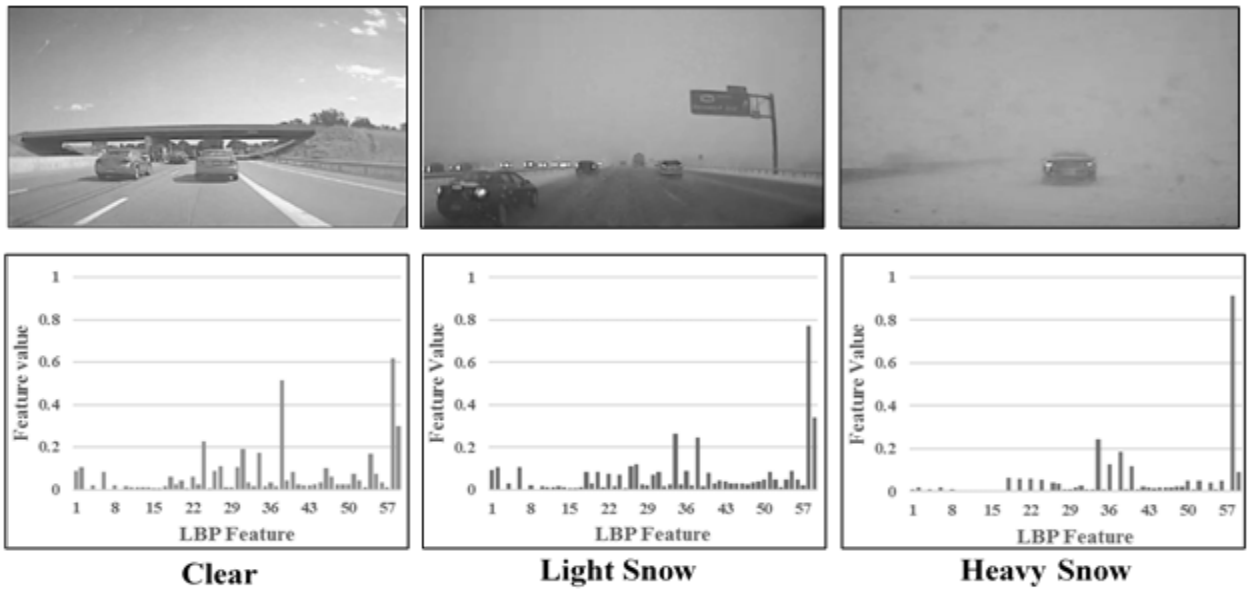

Figure 81 Sample LBP Feature Vectors for Clear, Light Snow, and Heavy Snow Images

As mentioned earlier, 59 $LBP_{8,1}$ feature vectors have been extracted from each image and were used as training parameters for classification algorithms. Figure 81 shows sample LBP feature vectors for three different image groups, which indicates that the values of the feature vectors vary significantly among the groups. For instance, most of the feature vectors of the heavy snow image have much lower values compared to the clear and light snow image. Overall, the figure indicates that the LBP features can be used as significant classification parameters to train the machine learning models.

Classification Algorithms

Three different classification methods including Support Vector Machine (SVM), K-Nearest Neighbor (K-NN), and Random Forest (RF) have been used in this study to classify the image groups based on the GLCM and LBP features.

An SVM is a discriminate classifier capable of constructing an optimal hyperplane, which can be used to categorize new samples. SVM classifies data by finding the best hyperplane that separates data points of one class from those of the other class. The best hyperplane for an SVM means the one with the largest margin between the two classes. Margin means the maximal width of the slab parallel to the hyperplane that has no interior data points. The support vectors are the data points on the boundary of the slab that is closest to the separating hyperplane (*185*, *271*). Figure 82 illustrates the concept of SVM classifier.

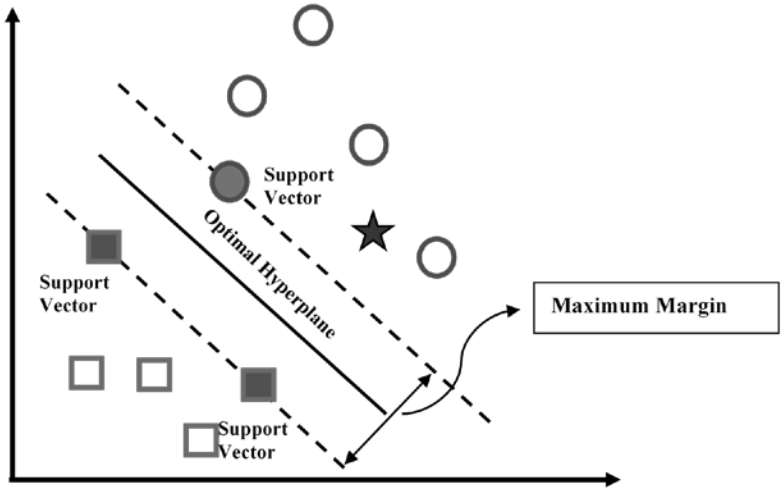

Figure 82 Support Vector Machine (SVM) Classification

K-NN classifier is a memory-based model that stores all available cases and classifies new cases based on their distance to points in a training dataset. k in KNN algorithm is the number of neighbors considered. The concept of KNN classifier has been illustrated in Figure 83. A large value of k increases the number of neighbors and in turn, increases model bias. Bias measures how far off the model predictions are from the correct value. Conversely, a small value of k will result in a large variance in predictions. The goal of any supervised machine learning algorithm including K-NN is to achieve low bias and low variance. However, the relationship between bias and variance is inversely related, meaning decreasing the bias will increase the variance. Therefore, k should be selected in such a way so that the model achieves the right balance between the variance and bias of the model (*185*).

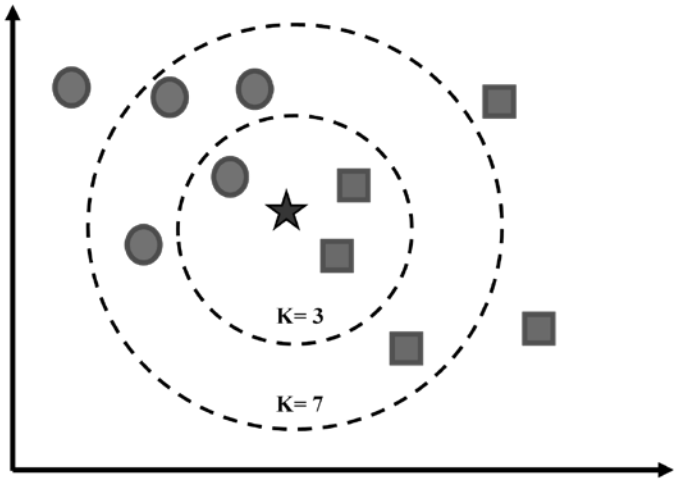

Figure 83 K-Nearest Neighbor (K-NN) Classification

RF algorithm is a supervised classification algorithm that builds multiple decision trees from a randomly selected subset of the training set and merges them to get more accurate and stable predictions. The RF algorithm creates a forest with a number of trees. In general, the higher the number of trees in the forest, the higher the prediction accuracy. The basic parameters of the RF

classifier are the total number of trees to be generated and decision tree-related parameters like minimum split, split criteria, etc. There are several advantages of RF over the decision tree. For instance, RF prevents overfitting by creating random subsets of the features and building smaller trees using these subsets. Another great advantage of the RF algorithm is that it can be used to measure the relative importance of each feature on the prediction (*272*).

Deep Learning

To develop weather detection systems, in addition to machine learning, the research team also experimented with several neural networks (NN) based deep learning methods. . The NN is a machine learning approach that has been extensively used in various fields of engineering for image classification, pattern recognition, and text categorization (*262*, *263*, *273*, *274*). Different variations of the traditional NN have been recently developed to serve specific purposes, e.g., RNN for time-series data analysis and CNN for image classification. This study explored the potential of the traditional NN as well as the RNN and CNN for real-time fog identification. The NN models can be developed using various machine learning libraries under different programming platforms, such as Python, Java, and C++. However, for this study, Python programming on the TensorFlow machine learning library has been used for image classification.

TensorFlow is a fast, flexible, and scalable open-source machine learning library that can be used to implement a wide variety of Machine Learning algorithms. TensorFlow was developed for conducting Machine Learning and Deep Learning research by the researchers and engineers working on Google's Machine Intelligence research organization. The official definition of TensorFlow is: *"TensorFlow is an open-source software library for numerical computation using data flow graphs. Nodes in the graph represent mathematical operations, while the graph edges represent the multidimensional data arrays (tensors) communicated between them. The flexible architecture allows you to deploy computation to one or more CPUs or GPUs in a desktop, server, or mobile device with a single API"*(*275*). The primary building block of any TensorFlow network is tensor, which is defined as a multi-dimensional array. The node inside a TensorFlow network can only accept data in a tensor form. Therefore, all the input data need to be converted into tensors before feeding them into the network.

As mentioned earlier, initially a traditional NN has been used to develop the fog detection model. A NN is a computational model inspired by the function and structure of the human brain. Like the human nervous system, a NN has the ability to receive, process, and transmit information in terms of computer science. A NN uses backpropagation to learn and train available weights and biases. In other words, a NN can improve the prediction accuracy of the model by using feedback from the previous iterations.

The basic unit of a NN is neuron, also called node, which receives input from some other neurons, or an external source and computes an output. Each input has an associated weight (W), which is assigned based on its relative importance to the other inputs. The node applies a function (a), called activation function, to the weighted sum of its inputs. The activation function takes a single number and performs a specific mathematical operation on it. The activation function, either returns one (neuron triggered) or zero (neuron not triggered) depending on the computations performed over the weights and biases. The neuron shown in Figure 84 has two numeric inputs X1 and X2 with weights W1 and W2, respectively. Additionally, there is another input 1 with weight B (called the bias) associated with it. Inside the neuron, the weighted sum

(S) of all the inputs has been calculated before passing it through an activation function (a) to generate the output for the next node.

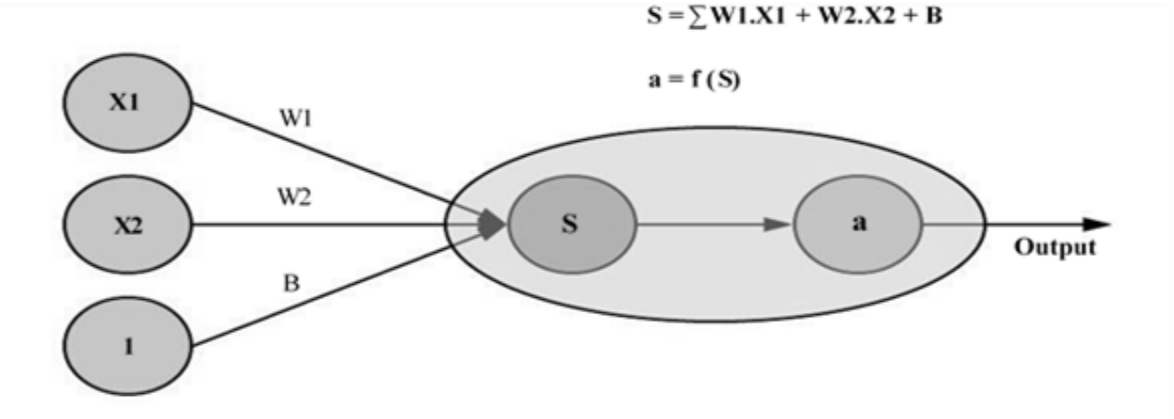

Figure 84 A Single Neuron

Another important parameter of a NN is cost, which captures the difference between the predicted and true class. The cost, also known as loss, is an overall measure of the performance of the trained model and is represented by a single value. The cost is a function of weights (W), biases (B), inputs of the training sample (I_T), and the desired output of the training sample (O_T) (*276*). The general form of a cost function is shown in the following equation.

Cost, $C = f(W, B, I_T, O_T)$ Equation 31

A cost function must satisfy two properties: first, it must represent the average deviation of the predicted class from the true class; second, it should be independent of any activation value of the NN except the output values. Although, various cost functions including, Quadratic, Cross-entropy, Exponential, Hellinger distance, Kullback-Leibler divergence, and Itakura-Satio are currently being used to determine the deviation of the predicted class from the true class, the most commonly used cost function for a NN model is Cross-entropy. The NN models proposed in this study also utilized the Cross-entropy as a cost function. The cost using cross-entropy can be defined by the following equation.

Cost, $C = -\sum_i [y_i \ln a_i + (1 - y_i)\ln(1 - a_i)]$ Equation 32

Here, y_i is the predicted probability value for class i and a_i is the true probability for that class (*277*).

In a NN model, the cost is minimized at every step using an optimizer, which alters the weights and biases at every iteration and feeds the value to the next iteration. The two most commonly used optimizers in a NN model are Gradient Descent Optimizer and Adam Optimizer. In this study, both optimizers have been used. The Gradient Descent minimizes the objective function, i.e., cost function by changing the model parameters, i.e., weight(W) and bias(B) in the opposite direction of the gradient of the objective function with respect to the parameters. The Gradient Descent can be described by the following equation.

$P_i = P_{i-1} - \gamma \nabla f(P_{i-1})$ Equation 33

Here, P_i represents the value of the parameters (W and B) for the next step, P_{i-1} represents the current value of the parameters, γ is a weighting factor, and the gradient term $\nabla f(P_{i-1})$ is the direction of the steepest descent (*278*). In order for the Gradient Descent to reach the optimum values of the parameter, an appropriate learning rate need to be selected. A large learning rate may not provide optimum value because it will bounce back and forth between the convex function of the Gradient Descent. Conversely, a small learning rate will significantly increase the training time. Therefore, the learning rate should be selected in such a way that the parameters achieve optimum values within the least possible time. While Gradient Descent maintains a constant learning rate for all the parameter updates, the Adam Optimizer, which was first proposed by Kingma et al., computes individual adaptive learning rates for different parameters. The Adam Optimizer combines the advantages of two optimizers including Adaptive Gradient Algorithm (AdaGrad) and Root Mean Square Propagation (RMSProp) (*279*).

Architecturally, a NN graph consists of three layers: the input layer that receives inputs such as images and vectorizes them to a mathematical representation that the neuron can interpret; one or multiple hidden layers that perform necessary numerical computations on the input data from the previous layer; and finally the output layer which is responsible for transferring information from the network to the outside world. A NN with more than one hidden layer is often called Deep Neural Network (DNN). In a NN model, the order of computation needs to be determined. Although the value of the nodes can be calculated separately, the common practice of calculating node values is to arrange the nodes into layers. This technique is called feedforward. A feedforward network takes the inputs in the lowest layer (input layer). Subsequently, the higher layer, i.e., hidden layers are calculated until the output is generated at the topmost layer. Figure 85 provides a graphical representation of a multilayer feedforward NN consisting of three inputs, three hidden layers, and one output layer.

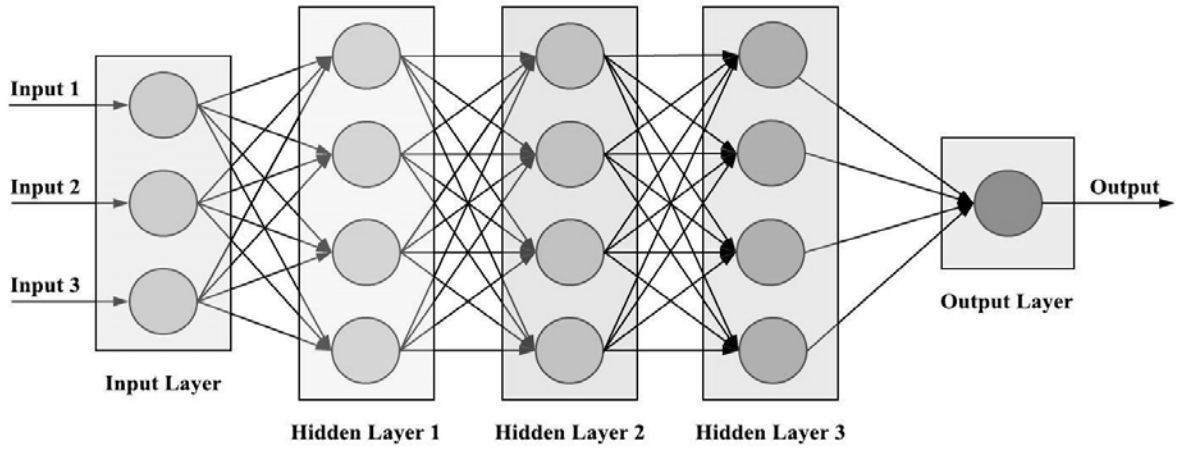

Figure 85 Fully Connected Multilayer Neural Network

The multilayer NN used in this study consists of one input layer, three hidden layers with five hundred nodes in each layer, and one output layer. The training of the NN model started with feeding the training data into the network. As mentioned earlier, the training dataset consists of 16,000 annotated images in three different weather conditions including clear, distant fog, and near fog. During the training process, the epoch, also called step, has been set to fifty to train the entire data in fifty iterations. Fifty epochs have been selected because the accuracy of the model became almost constant and no significant improvement was found after fifty steps. The sigmoid

function has been used as the activation function. For calculating the cost, Cross-entropy has been used. Two optimizers including Adam and Gradient Descent have been used to optimize the cost function. From the analysis result, it was found that the Adam optimizer performed marginally better than the Gradient Descent optimizer as can be seen in Figure 86**.**

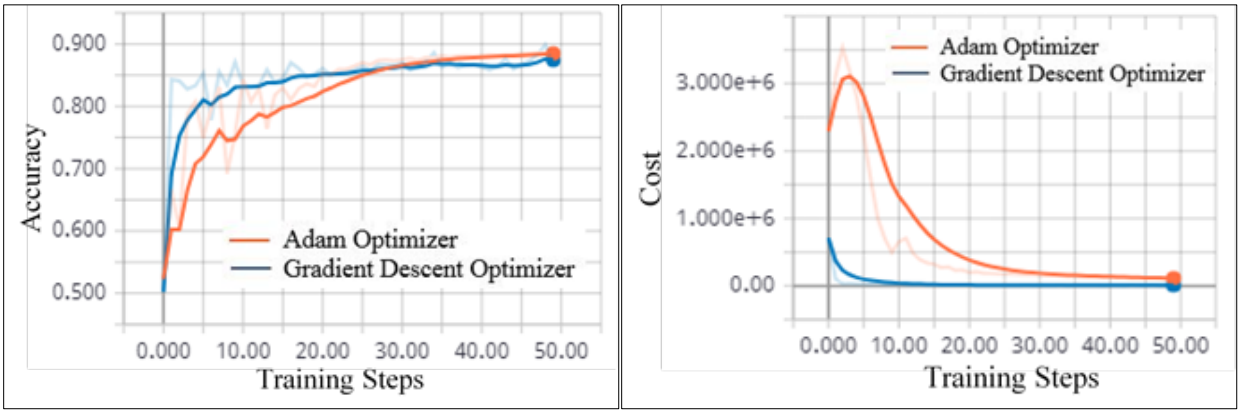

Figure 86 The Variation of Accuracy and Cost of the NN Models

Figure 86 illustrates the variation in accuracy and cost over the training steps. While the accuracy of the NN model using Adam optimizer gradually increased from 0.52 at the first step to 0.89 at the final step, the accuracy of the NN model using Gradient Descent optimizer increased from 0.50 to 0.87. It is worth mentioning that to determine the accuracy during the training process 20 percent of the training data have been used. Considering the cost, the NN using the Gradient Descent optimizer provided a continuous decrease until it reached a minimum value. On the other hand, the cost of the NN using Adam optimizer increased during the initial steps but eventually reached a minimum value at the final step.

One of the significant limitations of the traditional NN is that it does not consider the sequence of data, which is essential for time series and video data. Therefore, to leverage the sequential information, a modification of the NN, known as Recurrent Neural Network (RNN), has also been used in this study. The RNN treated data as a sequence using cyclic connections. The RNN stores information from the previous timestamp and uses the information as inputs to the network to compute the predictions at the current time step. At time t, hidden nodes with recurrent connection, collect inputs from the current data point $x_{t,}$ and from the hidden node values h_{t-1} of the previous step. The output y_t at time t is then calculated using the following equations.

$$y_t = \sigma\,(W_{yh}.\ h_t + b_y) \qquad \text{Equation 34}$$

$$h_t = \sigma\,(W_{hx}.\ x_t + W_{hh}.\ h_{t-1} + b_h) \qquad \text{Equation 35}$$

Here, σ is the activation function, h_t is the hidden node value at time t, W_{hx} is the conventional weight matrix based on the current input, W_{hh} is the recurrent weight matrix based on the previous hidden states, W_{hy} is the weight matrix based on hidden state and output, and b_h and b_y are the bias parameters (*280*). Figure 87 provides a simple representation of a RNN with three inputs, one hidden layer with recurrent nodes, and one output layer.

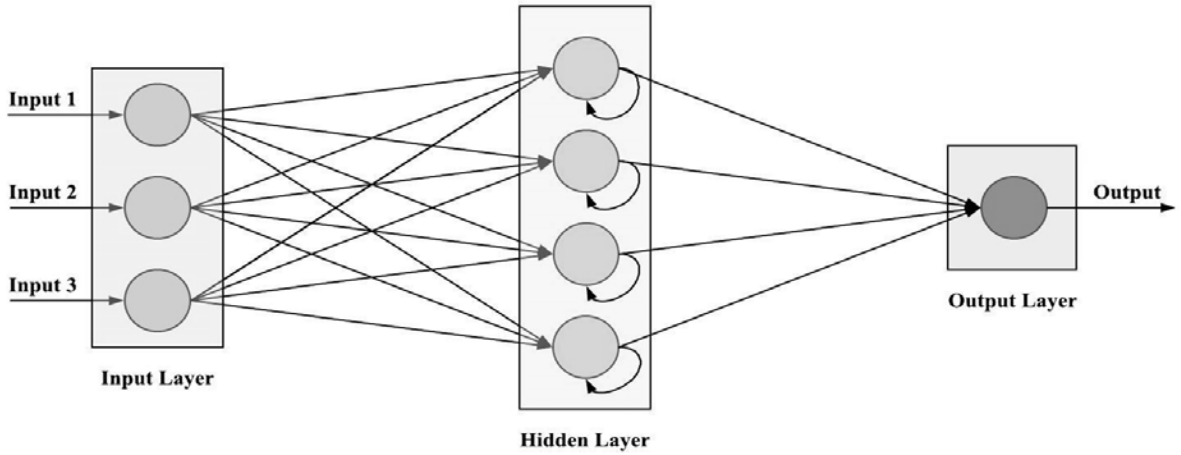

Figure 87 A Simple Representation of a Recurrent Neural Network (RNN)

To improve the traditional RNN, several modifications of the RNN including Bidirectional RNN, Long Short-Term Memory (LSTM) RNN, Independently RNN, Hopfield RNN have been developed. However, for this study, the LSTM RNN was used. The building block of an LSTM RNN is the LSTM which consists of a cell, an input gate, an output gate and a forget gate. The cell stores values over arbitrary time intervals, whereas the gates act as a neuron as well as a regulator of the flow of values that goes through the connections of the LSTM (*281*, *282*).

Like the traditional NN, the cross-entropy was used as a cost function, and both the Adam and Gradient Descent were used as optimizers during the training of the RNN models in every training step. Although the RNN model using the Adam optimizer provided excellent accuracy of 0.93 at the final step of the training, the RNN model using Gradient Descent performed worse than the Adam optimizer with a final accuracy of 0.77. The cost was also found to be much lower at every step of the training process for the RNN model trained with Adam optimizer compared to the RNN model trained with Gradient Descent as can be seen from Figure 88.

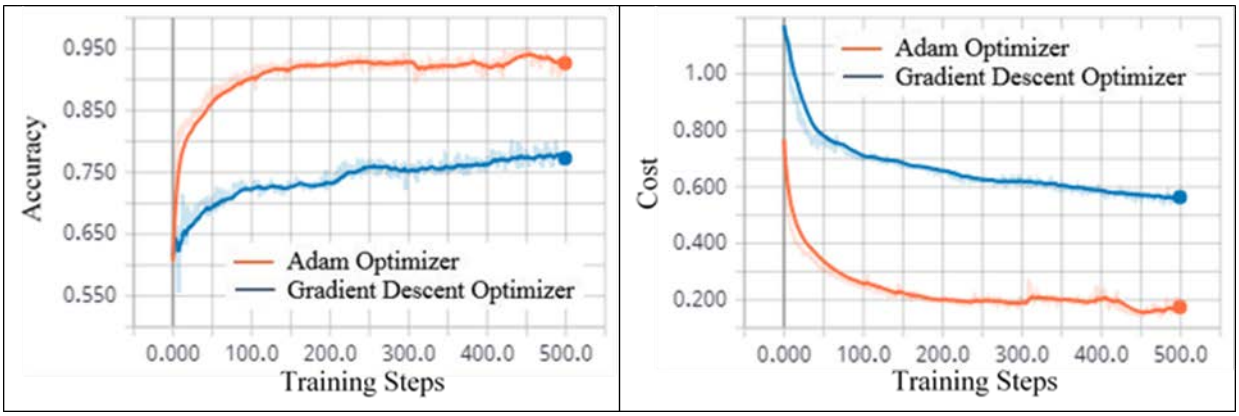

Figure 88 The Variation of Accuracy and Cost of the RNN Models

Another improvement of the traditional NN is the Convolutional Neural Network (CNN), which is developed primarily for image classification. Like other neural networks, a CNN consists of an

input layer, an output layer, and many layers in between. The in-between layers can be categorized into two types of layers: feature detection layers and classification layers.

The feature detection layer can perform three types of operation in the data including convolution, Rectified Linear Unit (ReLU), and pooling. Convolution operation can activate certain features from the images by passing them through a set of convolutional filters. The number of convolutional layers usually improves the performance of the model especially if the number of output categories of the training dataset is relatively high. However, the performance improvement is insignificant for the training dataset with a lower number of output categories (*283*). In this study, five convolutional layers were used during the training process. The first convolutional layer took the images as input and applied 32 filters, each with a height and width of 5 pixels. The second and the third convolutional layer applied 32 and 64 filters of the same size, respectively. For the next two convolutional layers, the same number of filters with the same filter size was applied. After each convolution layer, a ReLU layer was used to perform a threshold operation on each element of the input. ReLU layer maps negative values to zero to ensure faster and more accurate training. After each ReLU layer, a max-pooling layer was applied with pooling regions of 3×3 pixels. Pooling simplifies the output by performing nonlinear down-sampling which reduces the number of parameters that the network needs to learn.

After feature extraction, the architecture of a CNN moved to classification. The next layer was a Fully Connected (FC) layer that provided a vector of three dimensions, where three was the number of classes. Finally, the image dataset was passed into a softmax layer which is the final layer of the CNN model. The architecture of CNN has been shown in Figure 89.

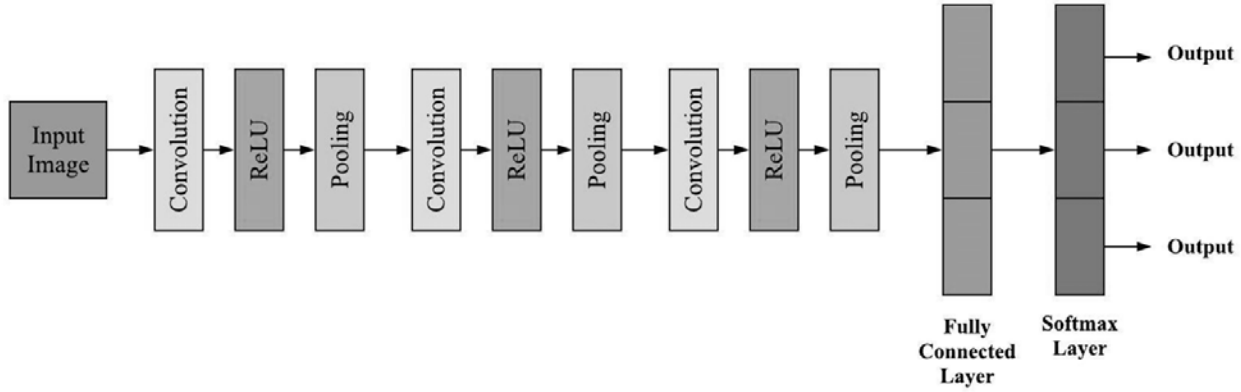

Figure 89 A Simple Representation of a Convolutional Neural Network (CNN)

Similar to the previous NN models, the cost was calculated using the cross-entropy, and the optimization of the cost function was performed by Adam and Gradient Descent optimizers. The Adam optimizer performed marginally better compared to the Gradient descent optimizer as can be seen from FIGURE 8. The prediction accuracy of the CNN model using Adam optimizer was about 0.78 at the first step which increased gradually and reached an accuracy of 0.97 at the last step. The CNN model using the Gradient Descent also produced similar results with an accuracy of 0.96 at the final step. The cost of the CNN model using Adam optimizer decreased gradually until it reached a minimum value. A similar trend was also found for the CNN model using Gradient Descent optimizer as can be seen from Figure 90.

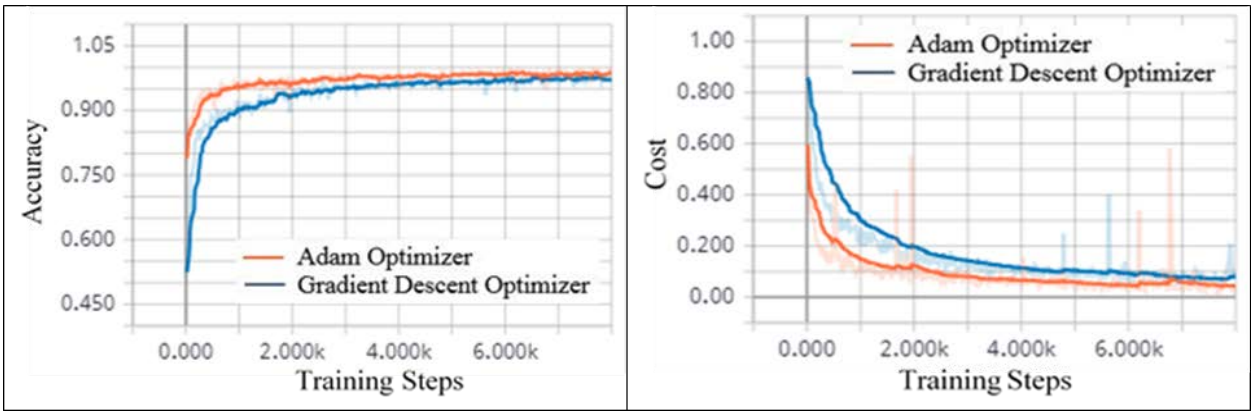

Figure 90 The Variation of Accuracy and Cost of the CNN Models

The prediction accuracy of the CNN models at the final training step was found to be much higher compared to the accuracies of the traditional NN and the RNN models. Previous image classification studies using CNN also indicated that CNN is capable of providing far better results than the other types of NN. For instance, Krizhevsky et al. used a subset of the ImageNet database to classify 1000 different classes. ImageNet is one of the largest image datasets designed for object recognition research and consists of over 15 million labeled high-resolution images belonging to roughly 22,000 categories. This study used five convolutional layers, followed by max-pooling layers, and three fully-connected layers. The results of this study showed that CNN is capable of achieving record-breaking results on a highly challenging dataset (*284*). Several other studies also adopted the CNN structure developed by Krizhevsky et al. with slight modification to classify the ImageNet dataset and found satisfactory results (*285*, *286*).

Development of the RoadweatherNet

Similar to other deep learning models, the architecture of a CNN can be broadly categorized into three types of layers, including an input layer, hidden layers, and an output layer. The primary purpose of the input layer is to receive the annotated input images and passes them to the subsequent hidden layers. The input layer of the RoadweatherNet was designed to receive seven weather categories with square image sizes. It is worth mentioning that with the increase in image size, the accuracy usually improves; however, it requires more computational power which results in a longer training time. Therefore, in order to select the optimum image size, a sensitivity analysis was performed, where the accuracy of the models was tested using different image sizes with 20 × 20 pixels increment at every iteration, as can be seen in Table 44 and Figure 91. In order to compare the performance of the models, all the parameters were kept constant and the default training options were used. The testing accuracy of the model with 20 × 20 pixels input image was around 83 percent, which improved gradually with the increase in image size and saturated at an accuracy of 92 percent for the model trained with 100 × 100 pixels. After that, no significant improvement in accuracy was observed. Although the computational time increased by 4.1 times for this model compared to the base model, the use of this image size was justified considering its significantly superior performance over the other models trained with smaller image sizes.

After taking the input images, the RoadweatherNet then passed the images to the subsequent hidden layers, where the majority of the computations occurred. Hidden layers can be grouped into three types of layers, including convolutional, Rectified Linear Unit (ReLU), and pooling

layer. The convolutional layer is the main building block of a CNN and consists of several filters. These filters are moved across the input image in such a way that all the pixels are covered at least once and the dot product between the filter and the input is generated at every special position of the image. The resulting outputs from all the filters are then piled along the depth dimension in order to get the output of the convolutional layer. The main purpose of the convolutional layer is to extract features from the input image. While the initial convolutional layers extract more generic features, as the network gets deep, the subsequent convolutional layers extract more refined features (*287*).

A higher number of convolutional layers usually improves the performance of a CNN model; however, it makes the network complex and deeper, which increases the training time. In addition, very deep neural networks are often subjected to overfitting (*288*). Therefore, to select the optimum number of convolutional layers, a sensitivity analysis was performed using 100 × 100 pixels input image and keeping all the parameters constant. The results are listed in Table 44 and are illustrated in Figure 92. It was found that the CNN model with only one convolutional layer could not learn at all and produced a very poor testing accuracy of only 14 percent. Adding an extra convolutional layer significantly improved the performance of the model with an overall testing accuracy of 84 percent. The performance of the models reached saturation after four convolutional layers, as can be seen in Figure 92. Therefore, four convolutional layers were selected for the development of the RoadweatherNet. The first convolutional layer took the images as input and applied 16 filters with a size of 3 × 3 pixels. The next three convolutional layers applied 32, 64, and 128 filters of the same size, respectively. The number of filters of the convolutional layers was chosen as powers of two in order to maximize the usage of the Graphics Processing Unit (GPU). It is worth mentioning that the size of the filter was also selected based on sensitivity analysis.

Table 44 Model Performance Under Different Input Image Size and Number of the Convolutional Layer

Parameter	Value	Testing Accuracy (%)	Validation Accuracy (%)	Relative Training Time (min)
Input Image Size	20	82.5	83.9	1.0
	40	84.4	85.2	1.4
	60	87.6	87.5	1.5
	80	88.2	89.0	2.3
	100	90.9	91.1	4.1
	120	91.4	91.7	5.3
	140	91.5	91.7	5.9
	160	91.2	91.8	7.7
Number of Convolutional Layer	1	14.2	14.5	1.0
	2	83.5	84.1	1.1
	3	88.9	89.8	1.2
	4	90.4	90.7	1.3
	5	88.3	89.0	1.4
	6	86.7	88.0	1.6

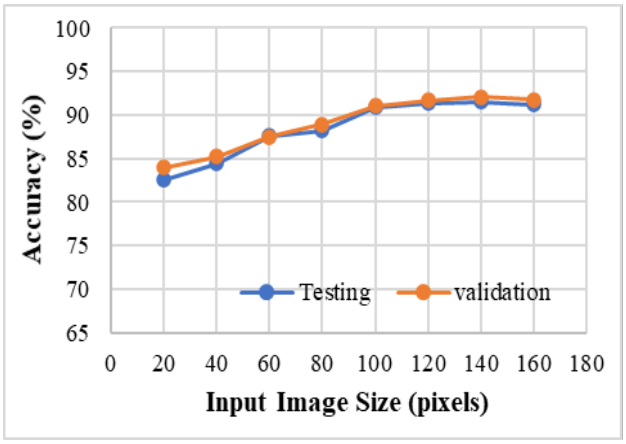

Figure 91 Selection of Input Image Size

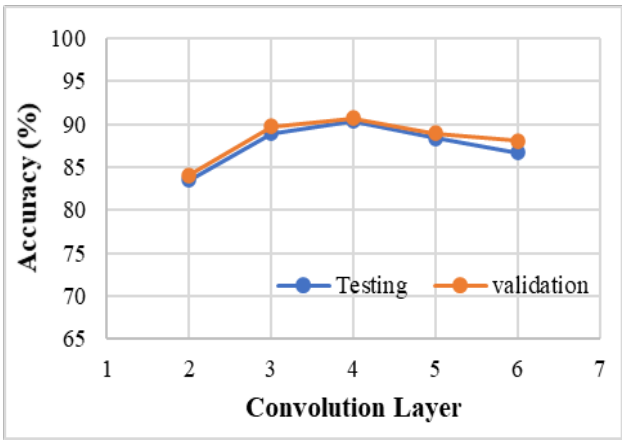

Figure 92 Selection of Number of Convolutional Layer

After each convolutional layer, a ReLU layer was applied to perform a threshold operation on each element of the inputs to ensure fast and consistent training of the RoadweatherNet. The ReLU layer applies a simple function that converts only the negative values to zero and keeps the positive value unchanged (*289*, *290*). Except for the last ReLU layer, all ReLU layers were followed by a pooling layer. This layer was applied to decrease the amount of information generated from the preceding convolutional layer to ensure the passing of only the most essential information to the next layers (*250*). The last ReLU layer was then linked to a fully connected layer to produce an output vector with seven dimensions based on the number of weather categories. The next layer of the RoadweatherNet was a softmax layer that assigns decimal probabilities to each of the output classes. Finally, the last layer of the RoadweatherNet was a classification layer, which provided the final weather condition based on the probabilities (*250*). The architecture of the RoadweatherNet is shown in Figure 93 and the description of each layer along with learnable parameters are listed in Table 45. It is worth mentioning that any parameter that needs to be optimized at each iteration during training is considered a learnable parameter. For CNN models, weights and biases at each layer of the network are the learnable parameters. (*291*). Using transfer learning, other researchers could use and test the capability of the proposed RoadweatherNet in detecting weather conditions using their image dataset.

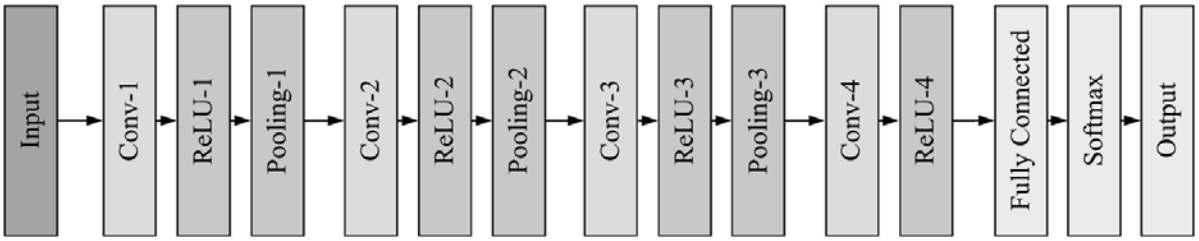

Figure 93 Architecture of the RoadweatherNet

Table 45 Parameters of the RoadweatherNet

Name	Description	Activations	Learnable Parameters	Total Learnable Parameters
Input	100×100×3 images with 'zero-centered' normalization	100×100×3	-	0
Conv-1	16 3×3×3 convolutions with stride [1 1] and padding [1 1 1 1]	100×100×16	W = 3×3×3×16 B = 1×1×32	448
ReLU-1	ReLU	100×100×16	-	0
Pooling-1	2×2 max pooling with stride [1 1] and padding [1 1 1 1]	50×50×16	-	0
Conv-2	32 3×3×16 convolutions with stride [1 1] and padding [1 1 1 1]	50×50×32	W = 3×3×3×32 B = 1×1×16	4640
ReLU-2	ReLU	50×50×32	-	0
Pooling-2	2×2 max pooling with stride [1 1] and padding [1 1 1 1]	25×25×32	-	0
Conv-3	64 3×3×32 convolutions with stride [1 1] and padding [1 1 1 1]	25×25×64	W = 3×3×32×64 B = 1×1×64	18496
ReLU-3	ReLU	25×25×64	-	0
Pooling-3	2×2 max pooling with stride [1 1] and padding [1 1 1 1]	12×12×64		0
Conv-4	128 3×3×32 convolutions with stride [1 1] and padding [1 1 1 1]	12×12×128	W = 3×3×64×128 B = 1×1×128	73856
ReLU-4	ReLU	12×12×128		0
Fully Connected	7 fully connected layers	1×1×7	W = 7×18432 B = 7×1	129031
Softmax	Softmax layer	11×1×7	-	0
Output	Classification Output	-	-	0

**W = Weights, B = Bias*

After the crafting of the RoadweatherNet architecture, the default parameters and training options were carefully updated by observing the training progress and validation accuracy. It is worth mentioning that 80 percent of the images were used for training and validation, and the remaining 20 percent were used to test the accuracy of the developed model. During validation, the cost of the RoadweatherNet was minimized using two optimizers: Stochastic Gradient Descent with Momentum (SGDM) and Root Mean Square Propagation (RMSProp); however, SGDM produced the best optimization. It is worth mentioning that cost is an overall measure of performance of a CNN model and is measured by calculating the difference between predicted

class and true class. The best performance of a CNN model is achieved only when the cost is properly optimized (*250*).

The hyperparameters and training options of the proposed model were carefully tuned utilizing one of the most commonly used methods named grid search. Grid search is an approach of tuning hyperparameters that searches and evaluates a model through a manually specified subset of hyperparameters (*166*, *292*). The subset used for grid search in this study was created by carefully observing the training progress and accuracy of the proposed model. It is worth mentioning that based on the initial observation, some of the parameters did not have a significant influence on the model performance, and therefore, were not included in the grid search to reduce the tuning time and computation resources. Table 46 listed the updated parameters for the developed weather detection model.

Table 46 Tuning of Hyperparameters of RoadweatherNet

Parameters	Initial/Default value	Final value after parameter tuning
Optimizer	SGDM	SGDM
Number of convolutional layers	4	4
Initial learning rate	0.01	0.0001
Learning rate drop period	10	5
Max epochs	30	15
Batch size	128	50
Factor for L2 regularization	0.0001	0.004

**SGDM = Stochastic Gradient Descent with Momentum*

Figure 4 illustrated the increase in accuracy and decrease in loss over the training iteration during validation using the best set of parameters, which shows that the overall validation accuracy of the RoadweatherNet was around 10 percent at the initial iteration which improved gradually until it reached a final overall validation accuracy of around 92.5 percent at the final iteration after 15 epochs of training. Similarly, the loss was also decreased until it reached a final value of around 0.1, as can be seen in Figure 94. The training and validation took about 41 minutes to complete using a computer with an Intel Core i7-7500U 2.70Ghz processor, 12 GB of RAM, and an NVIDIA GeForce 940MX GPU.

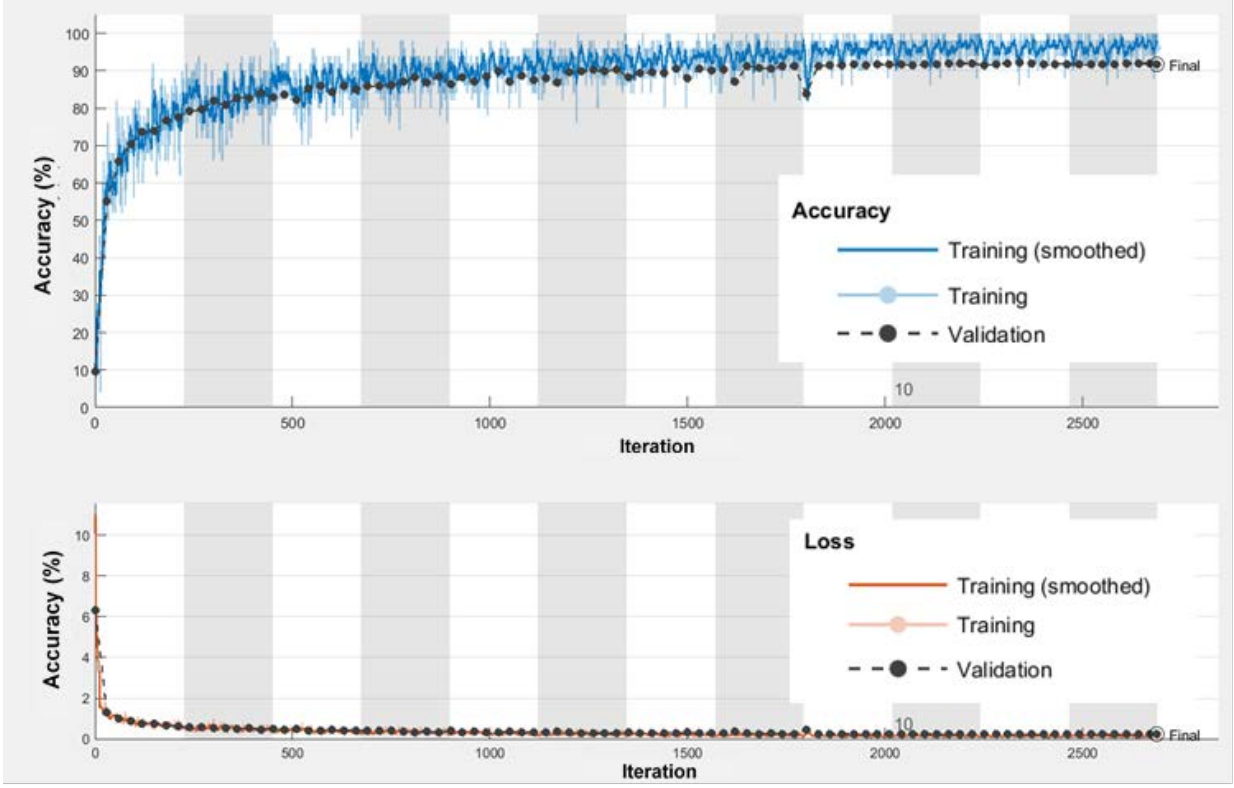

Figure 94 Training Progress of the RoadweatherNet

Results and Discussions

Performance of the Snow Detection Models

The prediction summary of the trained Machine Learning models (e.g. SVM, K-NN, and RF) using the GLCM based features has been shown in Table 47. Overall prediction accuracy of the trained SVM model was found to be 86.2 percent. Although various types of kernel functions including linear, quadratic, cubic, fine Gaussian, and coarse gaussian were used for the SVM-based classification, the fine Gaussian SVM produced the best result. It is worth mentioning that SVM performs very badly with datasets that are not linearly separable. For example, if two features of a classification problem are plotted in a two-dimensional space (e.g., x and y-axis), most of the time it will not be possible to separate the data points using a single straight line. Kernel function can overcome this problem by distributing the data points into three-dimensional space (e.g., x, y, and z-axis) by using different distributions (such as polynomial, quadratic, cubic, gaussian, etc.). Once the data points are distributed in the three-dimensional space, they can be separated using a two-dimensional plane. (*293*). It was found that the clear image group had the highest true positive rate (89 percent) and the lowest false negative rate (11 percent), which indicates that only 11 percent of the images have been misclassified by the trained SVM model. On the other hand, the heavy snow image group had the lowest prediction accuracy (83 percent) where 7 percent and 10 percent of the images were misclassified as clear and light snow images, respectively. In addition, the false positive rate of the clear, heavy snow, and light snow image group was found to be 12 percent, 17 percent, and 12 percent, respectively. It is worth noting that the high false positive rate of snowy weather will create frequent false alarms which may lead to disrespecting the warnings and may create compliance issues. However, from

a safety perspective, the false negative rate is more hazardous because it may lead drivers to get into snowy weather conditions without providing them any prior warnings. The Area Under Curve (AUC) is a measure of the overall quality of a classifier. AUC values of 0.5 to 0.7 represent poor accuracy, values between 0.7 to 0.9 represent moderate accuracy, whereas values over 0.9 indicate high accuracy (*190*). All the categories of the trained SVM models had AUC values greater than 0.9 which indicates high prediction accuracy. The overall prediction accuracy of the trained K-NN model using the GLCM based feature was found to be 85.6 percent as can be seen from Table 47. More specifically, about 89 percent, 83 percent, and 85 percent of the clear, heavy snow, and light snow images have been correctly classified. The highest false negative rate (17 percent) was found for the heavy snow image group, where 7 percent and 10 percent of the heavy snow images have been incorrectly identified as clear and light snow conditions, respectively. On the other hand, the false negative rate of the clear image group was found to be the lowest, where the trained K-NN model misclassified 4 percent and 7 percent of the clear images as heavy snow and light snow image, respectively. The highest false positive rate was found for the heavy snow image group where 17 percent of other images were classified as heavy snow. The false positive rate for both clear and light snow image groups was found to be 12 percent. It was found that the clear image group had the highest AUC (0.97), whereas the heavy snow image group had the lowest AUC (0.94). However, the AUC of all the image groups was found to be greater than 0.9, which indicates a high prediction accuracy of the trained K-NN model. The overall prediction accuracy of the RF model using the GLCM based feature was found to be 84.4 percent. Similar to the other two models, the highest true positive rate was found for the clear image group where 89 percent of the images were correctly classified. On the contrary, the heavy snow image group had the lowest true positive rate (82 percent) and the highest false negative rate (18 percent), which indicated that the trained RF model misclassified 18 percent of the heavy snow images as can be seen from Table 47. In addition, the AUC of all the image groups was found to be greater than 0.9.

Table 47 Prediction Summary of the Trained Models Using GLCM Based Features

Model	Weather	True Positive (%)	False Negative (%)	True Negative (%)	False Positive (%)	AUC	Overall Accuracy (%)
SVM	Clear	89	11	88	12	0.97	86.2
	Light Snow	87	13	88	12	0.95	
	Heavy Snow	83	17	83	17	0.95	
K-NN	Clear	89	11	88	12	0.97	85.6
	Light Snow	85	15	83	17	0.95	
	Heavy Snow	83	17	86	14	0.94	
RF	Clear	89	11	85	15	0.97	84.4
	Light Snow	83	17	81	19	0.94	
	Heavy Snow	82	18	86	14	0.95	

The prediction accuracies of the trained machine learning models using LBP-based features were found to be much higher compared to the accuracies of the trained models using GLCM features as can be seen from Table 48. The SVM model based on LBP features produced an outstanding overall accuracy of 95.9 percent. More specifically, 99 percent, 93 percent, and 95 percent of the clear, heavy snow, and light snow images, respectively, have been classified correctly. The false negative rate of the clear image group was only 1 percent. The heavy snow and light snow image groups also had a small false negative rate of 7 percent and 5 percent, respectively. In addition,

the AUC values of the trained SVM model were also found to be exceptionally high (close to 1) which indicates high prediction accuracy of the trained SVM model. The trained K-NN model based on the LBP feature produced marginally lower, but still impressive overall prediction accuracy of 93.1 percent. The lowest false negative rate was found for the clear image group where only 3 percent of the images have been misclassified. However, the highest false negative rate was found for the heavy snow image group where 12 percent of the images were incorrectly classified. The AUC values of the trained K-NN model were also found to be very high. The overall prediction accuracy of the RF model was found to be 94 percent. More clearly, 98 percent, 91 percent, and 93 percent of the clear, heavy snow, and light snow images, respectively, have been classified correctly. It is mentionable that the texture of a clear image is more prominent, making it easier to identify. On the contrary, the texture of a foggy image is more uniform which makes it difficult to differentiate between near fog and distant fog images. Because of the above-mentioned reason, the lowest false negative rate (2 percent) was found for the clear image group whereas the highest false negative rate (9 percent) was found for the heavy snow image group.

Table 48 Prediction Summary of the Trained Models Using LBP Based Features

Model	Weather	True Positive (%)	False Negative (%)	True Negative (%)	False Positive (%)	AUC	Overall Accuracy (%)
SVM	Clear	99	1	94	6	1.00	95.9
	Light Snow	95	5	95	5	0.99	
	Heavy Snow	93	7	98	2	0.99	
K-NN	Clear	93	7	98	2	0.99	93.1
	Light Snow	94	6	87	13	0.98	
	Heavy Snow	88	12	94	6	0.99	
RF	Clear	98	2	99	1	1.00	94.0
	Light Snow	93	7	90	10	0.94	
	Heavy Snow	91	9	93	7	0.95	

Performance of the Fog Detection Models

Once training of the different NN models was completed, the performance of the models was evaluated using a test dataset, which consisted of 4,000 images in different weather conditions. The overall detection accuracy of the trained DNN, RNN, and CNN models was found to be 85.1 percent, 77.4 percent, and 97.3 percent, respectively using Gradient Descent optimizer, as shown in TABLE 2. The highest true positive (TP) rate was found for the clear image group, where 95.1 percent of the images were correctly classified. On the other hand, the lowest TP rate was found for the distant fog image group was 73.7 percent of the images were correctly classified. Considering the RNN model, the highest TP and the lowest false negative (FN) rate were found for the clear image group, where 9.5 percent of the clear images were wrongly classified to other images. Similarly, the TP rate of the distant fog image group was found to be 73.2 percent, meaning 73.2 percent of the distant fog images were correctly classified. Interestingly, the CNN model provided significantly better results compared to the other models, the overall detection accuracy was found to be 98.4 percent, 98 percent, and 86.5 percent for clear, distant fog, and near fog image groups, respectively. The lowest FN rate was found for the clear image group, where only 1.6 percent of the images were misclassified as can be seen in Table 49.

Table 49 Detection Summary of the Trained Neural Network Models using Gradient Descent Optimizer

Model	Weather	TP Rate (%)	FN Rate (%)	TN Rate (%)	FP Rate (%)	Overall Accuracy
DNN	Clear	95.1	4.9	92.1	7.9	85.1
	Distant Fog	73.7	26.3	90.8	9.2	
	Near Fog	84.5	15.5	46.1	53.9	
RNN	Clear	90.5	9.5	81.0	19.0	77.4
	Distant Fog	73.2	26.8	74.7	25.3	
	Near Fog	9.2	90.8	31.7	68.3	
CNN	Clear	98.4	1.6	99.0	1.0	97.3
	Distant Fog	98.0	2.0	95.5	4.5	
	Near Fog	86.5	13.5	95.8	4.2	

The performance of the neural network models using the Adam optimizer is provided in Table 50, which shows that the models using this optimizer performed better than the models using Gradient Descent optimizer. The overall detection accuracy of the DNN, RNN, and CNN models was found to be 88.4 percent, 93 percent, 98.1 percent, respectively. The highest TP rate and the lowest FN rate were found for the clear image group with only 6 percent misclassification. More specifically, 4 percent and 2 percent of the clear images were misclassified as distant fog and near fog images, respectively. Similarly, the TP rate of the distant fog and near fog image groups were found to be 86.7 percent and 61.1 percent, respectively. Considering the RNN model, the highest TP rate was found for the distant fog image group where 95.2 percent of the distant fog images were correctly classified. As expected, the detection accuracy of the trained CNN models was found to be much higher compared to the other neural network models. The trained CNN model provided an outstanding prediction accuracy of 99.8 percent, 97.6 percent, and 89.1 percent for clear, distant fog, and near fog image groups, respectively, as can be seen in TABLE 3. The false positive (FP) rate of the clear image group using the trained CNN model was found to be only 1.4 percent, meaning that 1.4 percent of the other images were classified as clear images. It is worth noting that a high FP rate of clear weather is more hazardous since in such conditions drivers will be exposed to adverse weather without any warnings. On the other hand, a high FN rate of clear weather will provide frequent adverse weather warnings in clear roadway conditions, which might affect the compliance rate. The FN rate of the trained CNN model for the clear image group was found to be only 0.2 percent, meaning only 0.2 percent of the clear images were misclassified as other images.

Table 50 Detection Summary of the Trained Neural Network Models using Adam Optimizer

Model	Weather	TP Rate (%)	FN Rate (%)	TN Rate (%)	FP Rate (%)	Overall Accuracy
DNN	Clear	94.0	6.0	93.7	6.3	88.4
	Distant Fog	86.7	13.3	87.6	12.4	
	Near Fog	61.1	38.9	58.0	42.0	
RNN	Clear	93.3	6.7	97.6	2.4	93.0
	Distant Fog	95.2	4.8	89.3	10.7	
	Near Fog	77.5	22.5	84.0	16.0	
CNN	Clear	99.8	0.2	98.6	1.4	98.1
	Distant Fog	97.6	2.4	97.8	2.2	
	Near Fog	89.1	10.9	96.3	3.7	

Overall, the prediction accuracy of the CNN models was found to be significantly higher compared to the accuracy of the DNN and the RNN models. This finding is in line with previous studies. Previous image classification studies using CNN also indicated that CNN is capable of providing far better results than the other types of NN. For instance, Krizhevsky et al. used a subset of the ImageNet database to classify 1000 different classes. ImageNet is one of the largest image datasets designed for object recognition research and consists of over 15 million annotated images belonging to approximately 22,000 categories. The results of this study showed that CNN is capable of achieving record-breaking results in a highly challenging dataset (*284*). Several other studies also adopted the CNN structure developed by Krizhevsky et al. with a slight modification to classify the ImageNet dataset and found satisfactory results (*285*, *286*).

Performance of the RoadweatherNet

After training and validation, the performance of the RoadweatherNet was evaluated using a test dataset, consisted of 20 percent of the original images. Performance indices were calculated for each class, as listed in Table 51, and visualized using a confusion matrix, as illustrated in Figure 95. The RoadweatherNet provided an impressive overall detection accuracy of 92.5 percent, which is in accordance with the accuracy (91.9 percent) found during validation. The highest recall value was found for the heavy rain image group were, where out of 500 test images, 95.4 percent of the images were correctly classified. The heavy snow and near fog image group also had a high degree of recall with values of 95.2 percent and 94.8 percent, respectively. The highest precision value of 96 percent was also found for the heavy snow image group, which indicated that out of 496 predicted snowy images, 96 percent were actually snow. One of the interesting observations is that the precision, as well as recall values, were found to be superior for extreme adverse weather conditions, such as heavy rain, heavy snow, and near fog. Driver behavior and vehicle performance, as well as visibility and road surface frictions, are impacted more in such extreme weather conditions; therefore, a high degree of recall and precision under such conditions is crucial for developing reliable safety countermeasures. The lowest performance in terms of recall was found for the light rain image group with a value of 86.8 percent, where out of 500 test light rain images, 53 were wrongly classified as other images, as can be seen from Figure 95.

The lowest FPR was found for the clear image group with a value of only 0.7 percent. Considering the safety-related practical applications, a high degree of FPR of the clear image

group is particularly hazardous because it would increase the risk by exposing drivers to adverse weather without warnings. The RoadweatherNet produced a negligible amount of such hazardous misclassification, especially for extreme adverse weather. More specifically, only one heavy rain image was classified as clear weather and other extreme adverse weather (e.g., heavy snow and near fog) did not have any such hazardous classification, as can be seen from Figure 5. Considering the FNR, the lowest value (4.8 percent) was found for heavy snow, and the highest value (13.2 percent) was found for light rain. The FNR of the clear image group was also reasonably low with a value of 6.8 percent. It is worth mentioning that a high FNR of clear weather will provide frequent false warnings, which might lead to disrespect for the warning systems and might decrease the compliance rate.

Table 51 Performance Measure of the Trained RoadweatherNet

Image Category	Recall (%)	Precision (%)	Specificity (%)	FPR (%)	FNR (%)	F-1 Score	Overall Accuracy (%)
Clear	93.2	95.5	99.3	0.7	6.8	94.3%	
Light rain	86.8	93.5	99.0	1.0	13.2	90.0%	
Heavy Rain	95.4	88.3	97.3	2.7	4.6	91.7%	
Light Snow	93.0	92.6	98.7	1.3	7.0	92.8%	92.57
Heavy Snow	95.2	96.0	99.3	0.7	4.8	95.6%	
Distant Fog	89.6	88.7	98.1	1.9	10.4	89.2%	
Heavy Fog	94.8	93.9	99.0	1.0	5.2	94.3%	

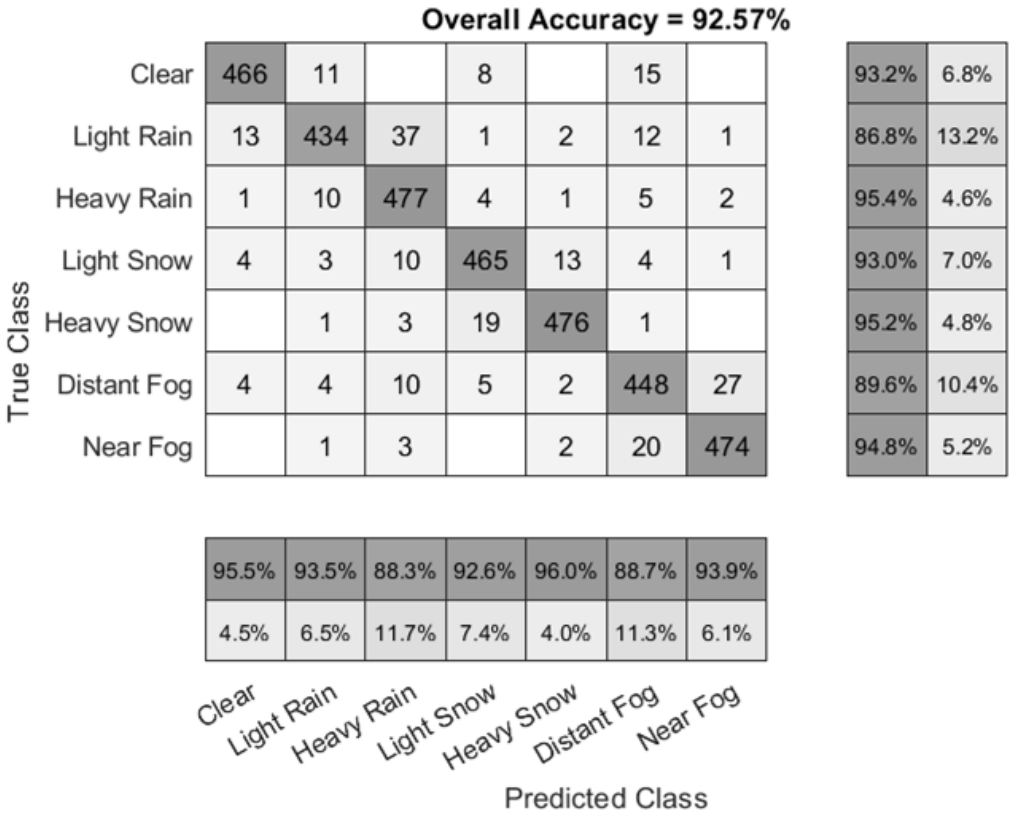

Figure 95 Confusion Matrix of the Trained RoadweatherNet

One of the major objectives of this study was to develop a weather detection model that is easy to implement and requires less computational power with a high degree of detection accuracy. In order to effectively implement trajectory-level weather detection models in an emerging CV environment, it is extremely important to reduce the computational requirements considering the fact that such weather detection will be applied mainly on a smartphone/tablet platform. Keeping this research need in mind, this study devised a simple CNN architecture (RoadweatherNet) capable of training and running on a computer with relatively less computational power such as a smartphone. The performance of the proposed RoadweatherNet was compared with some existing pre-trained CNN models, including AlexNet, ResNet18, Resnet50, GoogLeNet, ShuffleNet, and SqueezeNet, which revealed that the proposed RoadweatherNet required significantly less time to train compared to the existing pre-trained CNN models, as shown in Table 52. It is worth mentioning that most of the pre-trained networks have lots of layers with complex structures and require a relatively large input image size (*284*, *294–297*), whereas the proposed RoadweatherNet has only 15 layers with an input image size of 100 × 100 pixels. Although the pre-trained models provided marginally better performance, the simple structure of the RoadweatherNet significantly reduced the training time. Relative training time was also determined by dividing the training time of the pre-trained models with the training time of the RoadweatherNet, which revealed that the training times of AlexNet, ResNet18, ResNet50, GoogLeNet, ShuffleNet, and SqueezeNet were about 1.5, 4.9, 15.4, 6.8, 4.1, and 2.1 times higher than the RoadweatherNet, respectively. It is worth mentioning that after the training, the proposed RoadweatherNet can detect weather conditions instantaneously. Keeping the practical aspects in mind, such as applications in a CV environment, this study suggests the use of RoadweatherNet when the weather detection model needs to train and run on a smartphone platform. However, for other cases, when the weather detection model could be trained and applied off-road, such as in the Traffic Management Center (TMC), ResNet50 is suggested due to its relatively higher detection performance compared to the other models.

Table 52 Comparison of the RoadweatherNet with Other Pre-Trained CNN Models

Name	Number of layers	Input Image Size (Pixels)	Validation Accuracy (percent)	Testing Accuracy (percent)	Training Time (mins)	Relative Training Time
RoadweatherNet (Proposed CNN Architecture)	15	100-by-100	91.9	92.5	41.2	1
AlexNet	25	227-by-227	92.7	93.1	61.7	1.5
ResNet18	71	224-by-224	93.1	94.1	201.3	4.9
ResNet50	50	224-by-224	94.3	94.6	632.5	15.3
GoogLeNet	144	224-by-224	93.2	93.9	278.4	6.8
ShuffleNet	172	224-by-224	92.4	93.1	168.9	4.1
SqueezeNet	68	227-by-227	92.5	92.8	85.5	2.1

The performance of the RoadweatherNet was evaluated against other existing methods of weather detection, as shown in Table 53. The proposed RoadweatherNet achieved an overall detection accuracy of about 93 percent, which is higher than most of the previous weather detection models. However, previous research from the same author group achieved marginally higher detection performance. For instance, a snow detection system based on texture-based

image features combined with machine learning techniques was proposed by the research team, which achieved 96 percent accuracy in detecting two levels of snow (*167*). Another study of the research team leveraged various neural network methods to develop a fog detection system and achieved an impressive overall accuracy of 98 percent (*250*). The reason for getting a high degree of accuracy of these two studies is that it considered only two categories of adverse weather, whereas the proposed RoadweatherNet is capable of detecting seven levels of weather conditions.

Table 53 Evaluation of RoadweatherNet Against Weather Detection Methods

Study	Data Source	Method	Weather Categories	Overall Accuracy (percent)
Mori et al., 2007 (*298*)	In-vehicle camera, radar	Extinction coefficient	Light fog, moderate fog, and dense fog	84
Roser and Moosmann, 2008 (*299*)	In-vehicle camera	SVM	Clear, light rain, heavy rain	85
Yan et al., 2009 (*249*)	In-vehicle vision system	AdaBoost	Sunny, cloudy, rainy	85
Chu et. al., 2016 (*246*)	Image2weather dataset, EC1M dataset, Flickr, Google Maps	RF	Sunny, cloudy, snowy, rainy, foggy	70
Qian et al., 2016 (*251*).	Roadside camera, in-vehicle camera	Nearest Neighbor, Naive Bayes Boost, SVM, AdaBoost, DT	Dry, wet, Iced, snow-covered, snow-packed	88
Lu et. al., 2017 (*300*)	Stationary camera	CNN	Sunny, cloudy	91
Guerra et al., 2018 (*247*)	Flickr, Pixabay, Wikimedia, RFS dataset	Pre-trained CNN	Sunny, cloudy, snowy, rainy, foggy	80
Ozcan et. al., 2019 (*243*)	Roadside CCTV, mobile camera, NDS	VGG16	Clear, rainwet, snow	77
Gbeminiyi Oluwafemi and Zenghui, 2019 (*301*)	Google, Flickr, Gettyimages, Yahoo	Said Ensemble Method	Cloudy, sunshine, rainy, sunrise	86
Zhao et al., 2019 (*302*)	Open source images from the internet	CNN-LSTM	Sunny, cloudy, foggy, rainy, snowy	91
Ibrahim et. al., 2019 (*245*)	Google image	ResNet50, WeatherNet	Clear, rain, snow	93
Khan and Ahmed, 2019 (*167*)	SHRP2 NDS trajectory-level video data	SVM, KNN, RF	Clear, light Snow, heavy snow	96
Ali et al., 2020 (*303*)	SHRP2 NDS trajectory-level video data	ANN, DT, RF, GBT	Clear, snowy	89
Khan and Ahmed, 2020 (*250*)	SHRP2 NDS trajectory-level video data	DNN, RNN, LSTM, CNN	Clear, distant Fog, near Fog	98
RoadweatherNet	**SHRP2 NDS trajectory-level video data**	**CNN, Pre-trained CNN**	**Clear, light rain, heavy rain, light snow, heavy snow, distant fog, and near fog**	**93**

**SVM = Support Vector Machine, RF = Random Forest, GBT = Gradient Boosted Trees, DT = Decision Tree CNN = Convolution Neural Network, RNN = Recurrent Neural Network, DNN = Deep Neural network, ANN = Artificial Neural Network, LSTM = Long Short-Term Memory, EC1M = European City 1 Million, RFS = Rain Fog Snow, NDS = Naturalistic Driving Study*

Chapter 7. Integration of SHRP2 NDS Findings: Weather-based Microsimulation Modeling and Variable Speed Limit System

Literature Review

Development of Weather-based Microsimulation Model

Prevailing weather conditions impact the safety and mobility of the transportation network. Decades of experience and research illustrate that limited visibility and adverse road surface conditions increase travel time and decrease network capacity (*304*). In efforts to reduce the effect of adverse weather conditions on travelers and roadway infrastructure, transportation agencies dedicate resources to predictive, real-time, and responsive countermeasures. Recent developments in technology have enabled the introduction of intelligent transportation system (ITS) applications used for network planning, safety assessments, countermeasure evaluation, and roadway operations. Among these applications, microsimulation modeling is a powerful tool used to emulate traffic flow by predicting individual vehicle movements throughout a roadway network. Microsimulation is currently used as a forecasting tool to assess the safety and mobility impacts of proposed roadway designs or alterations. More recently, transportation agencies have started using microsimulation applications in their traffic management centers for online forecasting, in which traffic data are collected in real-time and used to make short-term predictions (*305*).

The development of a microsimulation model requires three primary components: roadway configuration, travel demand, and driving behavior. The third input requirement refers to the portrayed behavior of the individual vehicles in the model. Microsimulation models predict the behavior of individual drivers at sub-second intervals using designated driving behavior models. Different microsimulation tools use various behavioral models derived from different theories and data sources. The classic driving models were developed from the concept of traffic flow theory, while others were developed considering a driver's psychological nature and perception of their environment (*133*, *306*). Each behavioral model is controlled by a set of input parameters that dictate the predicted vehicle response. While default values are available for most models, numerous studies have shown that realistic predictions require these parameters to be tuned to match local conditions (*307–310*).

Researchers have investigated methods for calibrating driving behavior models using both macroscopic data (e.g., loop detector data) and microscopic data (e.g., individual vehicle trajectories, collecting driving speed, acceleration, following distance, and so forth, at a minimum resolution of 1 s) (*311–316*). Calibration with macroscopic data is attractive because of the availability of data and the decreased computational complexity; however, researchers hypothesize that this procedure of calibration may not be sufficient for realistic characterization of driving behavior as the resolution of the calibration data should be equivalent to that of the model's predicted behavior (*131*, *317*). Recently available sources of microscopic trajectory-level data have introduced new possibilities for testing this hypothesis and assessing the importance of using high resolution data for driving behavior model calibration (*318*, *319*).

Transportation agencies are interested in using microsimulation to forecast the impact of different adverse weather conditions on their roadway network. While microsimulation analyses are becoming increasingly commonplace, a consensus of how to develop a weather dependent microsimulation model is missing. Dozens of studies have evaluated macroscopic traffic data

(i.e., traffic counts, average travel speeds, headways) to study the influence of weather conditions on driving behavior (*320–322*). For instance, Rakha et al. (*320*) used freeway loop detector data from three geographic locations to evaluate traffic flow (i.e., free flow speed, speed at capacity, capacity, and jam density) in different weather conditions. Their findings indicated that in snow conditions, free flow speed and capacity are reduced more severely than in rain conditions. Lastly, the authors note that free flow speed and speed at capacity decrease as rain intensifies, but roadway capacity stays constant. As a result of these findings, the authors presented weather adjustment factors (WAFs) for computing traffic stream parameters as a function of weather type and intensity (*320*). This study and many others with similar goals and findings served as the motivation to compile WAFs in the 2016 edition of the U.S. Highway Capacity Manual (HCM) (*323*)

Other studies have aimed to calibrate microsimulation models using driving data in different weather conditions (*320, 324–326*). However, most of these efforts have been conducted using macroscopic traffic data and only a few research groups have calibrated driving models with weather-influenced trajectory-level driving data (*137, 327, 328*). To this end, this paper contributes a methodology for calibrating car-following models—a fundamental driving behavior model required for successful development of microsimulation models—using trajectory-level data captured in various weather conditions. The research was completed using data from the SHRP2 Naturalistic Driving Study (NDS) to capture realistic driving behavior from a diverse population of drivers.

Microsimulation of Weather-based Variable Speed Limit

Though the traditional before-after field evaluations of VSL applications provide the most direct insight into the effectiveness of VSL, it was found to be costly and time-consuming to collect traffic performance data from field. Another concern is that the effects of speed changes might not control for confounding factors that are not linked to the VSL system, such as changes in traffic volumes (*329*).

With consideration of these challenges and limitations of field tests, numerous researchers have employed microsimulation approach to assess the benefits of VSL. Lee et al. (*330*) developed a real-time crash prediction model to estimate the reduction of crash potential through simulating the changes in short-term speed variation before and after implementing VSL. The authors determined the threshold of crash potential at which VSL should be applied. Based on microsimulation, it was found that VSL reduced crash potential by 5 to 17 percent. Abdel-Aty et al. (*331*) employed PARAMICS microsimulation approach to evaluate the effects of VSL in term of reduction of crash likelihood. Simulations results showed that safety benefit was achieved when freeway speed was high. When freeway was congested (i.e., low-speed situation), the safety benefit of VSL was not significant. Hellinga and Mandelzys (*332*) employed PARAMICS simulation method to evaluate the sensitivity of the safety impacts of VSL to driver compliance rate. Simulation results indicated that safety was shown to be positively correlated with the level of compliance; the safety benefits of VSL under very high compliance scenario (i.e., greater than 70 percent) were more than four times the benefits obtained under low compliance scenario (i.e., lower than 1 percent). Lee et al. (*333*) examined the performance of VSL for addressing freeway recurring traffic congestion. A 5-mile freeway section was coded in VISSIM and calibrated using INRIX speed data and historical traffic counts from Virginia DOT. A VSL algorithm developed by California PATH was adopted in VISSIM to be used for determining optimum speed adjustments at three specific locations along the freeway section. Hadiuzzaman et al. (*334*) found

that the safety benefits of VSL were positively correlated with increasing compliance levels. The collision probability was improved when compliance level reached 50 to 60 percent. Muller et al. (*335*) applied a local feedback Mainstream Traffic Flow Control (MTFC) in microscopic simulation for an on-ramp merge bottleneck with VSL control. The authors pointed out that a more realistic VSL application at specific points instead of along an entire freeway section might produce a slower traffic response to speed limit changes. In addition, the nonlinear flow-variable speed limit relation observed in the microscopic model is more appropriate than that observed at the macroscopic level. Sadat and Celikoglu (*336*) analyzed the performance of VSL system using VSSIM and MATLAB simulation techniques on a 5.2-kilometer section in Istanbul, Turkey. Traffic volume, occupancy and average speed from the Remote Traffic Microwave Sensor (RTMS) were used to calibrate VISSIM. Results show reduction in Total Travel Time (TTT) and occupancy level along with improvement in average speed and volume. Conran (*337*) developed a two-state microscopic model and calibrated it using driving-simulation trajectory data. The microscopic model was implemented within VISSIM and utilized for a safety-mobility performance assessment of an incident-responsive VSL control algorithm implemented in a MATLAB COM interface. It was recommended that safety and mobility performance of VSL system indicated an inverse relationship, thus the selection of VSL control design parameters needs to balance the trade-offs between safety and mobility.

Microsimulation of Weather-Responsive VSL

For VSL under adverse weather conditions, Rama (*338*) investigated the effects of VSL on driver behavior under adverse weather conditions using historical traffic flow data. In summary, it was found that the weather-controlled VSL system decreased both the mean speed and the variance of speeds. In addition, statistical results showed that though the speed patterns were different in winter and in summer seasons, under both seasons VSL increased the homogeneity of driver behavior and reduced speed variance. Robinson (*339*) summarized the VSL applications throughout the world. The author noted that weather-responsive VSL is effective at reducing speeds and speed variability during poor weather in several locations. VSL on several rural areas in Germany has reduced crash rates by 20 to 30 percent; a VSL system on the M-25 highway near London contributed to a 10 to 15 percent reduction in crashes; and a VSL system in Netherlands led to an 8 to 10 kilometers per hour drop in mean speeds during foggy weather conditions. Another VSL system that primarily aimed at addressing foggy conditions in Utah led to a reduction in the average standard deviation of vehicle speeds by 22 percent (*340*). Rama and Schirokoff (*338*) found that a weather-responsive VSL system in Finland reduced crashes by 13 percent during the winter and 2 percent during the summer and reduced the overall injury crash risk by 10 percent. In 2012, the U.S. Department of Transportation issued the "*Guidelines for the Design of Wet Weather Variable Speed Limit Systems*" (*341*) which provided guidance on the use of VSL systems in wet weather at locations where the operating speed exceeds the design speed and the stopping distance exceeds the available sight distance. The report recommended to take into account traffic volume, operating speeds, weather information, sight distance, and roadway surface condition when posted speed limits.

A number of studies employed microsimulation approach for the development and evaluation of weather-responsive VSL. Buddemeyer et al. (*342*) developed a VSL control strategy based on speed and weather data collected on a segment of the Interstate-80 (I-80) corridor in Wyoming. The VSL control strategy was tested using a simulation of an actual storm event on the corridor. Results show that speed compliance increased from 64 percent to 79 percent with the new

recommended speed limit. Young et al. (*343*) and Sabawat and Young (*344*) pointed out that the primary purpose of weather-responsive VSL system is to reduce speed variation during winter storms because it provided drivers guidance as to an appropriate reduced speed. The authors developed a methodology to support speed posting decisions based on the real-time observed vehicle speeds and weather variables. Based on simulation, it was found that there was a significant increase in speed compliance and reduced speed variation with the implementation of automated control strategy. Kim et al. (*345*) developed and assessed a simulation framework to support weather-responsive traffic management (WRTM) strategies, including advisory and control variable message signs (VMSs). Various strategies are demonstrated with locally calibrated network simulation-assignment model capabilities. The analysis results illustrated the benefits of WRTM under inclement weather conditions. Li et al. (*346*) developed a VSL control strategy to reduce the risks of secondary collisions under adverse weather conditions. Based on microsimulation, the authors concluded that VSL reduced the risks of secondary collisions in terms of time-to-collision under various weather types. In comparison with weather conditions of rain and light fog, the safety benefits were more significant under moderate fog and snow weather conditions. Saha et al. (*347*) evaluated the effectiveness of VSL system on crash frequency in adverse weather conditions. Through a traditional safety analysis, the VSL system was found to be significant in reducing crashes. Choi and Oh (*348*) proposed a proactive VSL strategy that employed visibility distance, safe stopping distances, and average speeds to reduce the potential of crashes under fog weather conditions. Simulation results indicated that with VSL control, traffic conflicts reduced by approximately 19 and 27 percent under moderate and severe fog weather conditions, respectively.

Microsimulation of VSL in a Connected Autonomous Vehicle Environment

With the booming of Connected Vehicle (CV) technology, a number of studies have been conducted to investigate the potential of incorporating CV data in the development of VSL algorithms and assessing the benefits of VSL in a CV environment.

Pisano (*349*) indicated the advantage of CV is that it is able to collect and transmit real-time weather information at precise locations. With these data, local transportation management center could assess, forecast, and determine the suitable speed limits to address the impacts of the prevailing weather on roads and vehicles. Later on, Hill (*350*) pointed out that the emergence of new sources of road weather information from CVs opens opportunities to dramatically enhance existing freeway management strategies, tools, and systems that are focused on the needs of the traffic and maintenance management community to respond to the impacts of adverse weather on the roadways. Hammit and Young (*351*) pointed out that for rural freeways, the real-time weather and roadway information obtained from CVs could benefit the development of VSL algorithms. While the standardization of CV data between different vehicle makes and models will be required when developing weather-responsive VSL algorithms. Li et al. (*352*) pointed out that the successful operation of VSL relies on drivers compliance to the displayed speed limits and their interaction with other vehicles. The authors explored ways to implement VSL under a mixed Connected Autonomous Vehicles (CAVs) and regular vehicles condition. It was assumed that CAVs automatically followed the displayed speed limits. Simulation results showed that when CAV penetration rate was high, vehicle speed well aligned with the displayed speed limit. Later on, another study made by Li et al. (*353*) developed control strategy of an integrated system of cooperative adaptive cruise control (CACC) VSL to reduce rear-end collision risks near freeway bottlenecks. A feedback control algorithm was then

developed for the proposed vehicle to infrastructure system of CACC and VSL. Simulation results indicated that the VSL control plays an important role in reducing rear-end collision risks when the penetration rate of CACC is low; the combination of CACC and VSL controls mitigates the negative effects of the mixed traffic flow of the manual and CACC vehicles.

Paikari et al. (*354*) explored a low-cost modeling approach to provide guidelines for improving safety and mobility on freeways, specifically by using advisory speed and re-routing guidance in Vehicle-to-Vehicle (V2V) and Vehicle-to-Infrastructure (V2I) systems. The study tested fifteen scenarios differentiated by the V2V percentage penetration (0 percent, 10 percent, 20 percent, 30 percent, and 40 percent), and demand loading (60 percent, 80 percent, and 100 percent) implicitly representing peak and off-peak traffic, the study demonstrated that CV technology can enhance traffic safety on freeways, if the percentage of CVs is significant (e.g. 30-40 percent) and when it is accompanied by advisory speed reflected on VMSs not only upstream but also downstream of the incident location. Grumert et al. (*355*) studied the potential benefits of introducing infrastructure-to-vehicle (I2V) communication, autonomous vehicle control, and individualized speed limits in VSL systems. Communication between infrastructure and vehicles was used to transmit variable speed limits to upstream vehicles before the VSL signs were visible to the drivers. Microsimulation was employed to evaluate the performance of the I2V-based VSL system. Results showed that the I2V-based VSL system systems resulted in lower acceleration rates and thereby harmonized traffic flow. Khondaker and Kattan (*356*) employed microsimulation approach and used Time-to-Collision (TTC) as a Surrogate Measure of Safety (SMoS) to assess the safety benefits of VSL in a CV environment. Real-time driver compliance to the posted speed limit was used to adjust the optimal speed limits. It was concluded that with 100 percent CV penetration rate, VSL resulted in up to 11 percent of safety improvements. A comprehensive simulation framework to model driver behavior in a connected driving environment was presented by Talebpour et al. (*357*). The framework consists of a microscopic traffic simulator integrated with a discrete-event communications network simulator, Network Simulator 3, forms a basis for exploration of the properties of the resulting traffic systems and assessment of the system-level impacts of the CV technology. Furthermore, the connectivity of a vehicle-to-vehicle and vehicle-to-infrastructure communications network was investigated with the FHWA Next Generation Simulation: US-101 Highway dataset. Smith and Razo (*358*) have established a methodology to develop a regional traffic microsimulation model. The methodology includes the following steps: (a) converted the existing network planning model for the Ann Arbor area to a regional microsimulation model, (b) developed a method to identify the numbers, origins, and destinations of trips using equipped vehicles, and (c) developed post-processing code to track all equipped vehicles from the second-by-second microsimulation vehicle snapshot data and to identify interactions between equipped vehicles. Wang et al. (*359*) designed and tested a VSL control system that connected a traffic controller with in-vehicle controllers via vehicle-to-infrastructure communication. The link-level traffic controller regulates traffic speeds through VSL. The effectiveness of the connected VSL control was tested with simulation on a two-lane freeway stretch with connected vehicles randomly distributed among regular vehicles. Simulation shows that the connected VSL and vehicle control system improves traffic efficiency and sustainability. Li et al. (*360*) developed an I2V integrated system that incorporated VSL and Adaptive Cruise Control (ACC) system to reduce rear-end collision on freeways. Simulation results indicated that the proposed method reduced the potential rear-end collisions by up to 77.3 percent. Grumert, and Tapani (*361*) indicated that the real-time speed and location information from CV provided detailed information about the traffic state,

which has the potential to identify bottlenecks on a freeway and adjust speed limits. A recent study presented a thorough microscopic simulation investigation of a recently proposed methodology for highway traffic estimation with mixed traffic, i.e., traffic comprising both connected and conventional vehicles, which employs only speed measurements stemming from connected vehicles and a limited number (sufficient to guarantee observability) of flow measurements from spot sensors (*362*). The estimation scheme is tested using the commercial traffic simulator AIMSUN under various penetration rates of connected vehicles, employing a traffic scenario that features congested as well as free-flow conditions. Rahman et al. (*363*) evaluated the effectiveness of CV technologies in adverse visibility conditions using VISSIM microsimulation model. This study analyzed two types of CV approaches: CVs without platooning (CVWPL) and connected vehicles with platooning (CVPL). Simulation results showed that both CV approaches improved safety significantly in fog conditions, particularly when market penetration rate of CV was greater than 30 percent. Generally speaking, both safety and mobility benefits of CVPL significantly outperformed CVWPL when market penetration rates were equal to or higher than 50 percent.

Microsimulation and Surrogate Measure of Safety

Using microsimulation for safety evaluation, the most commonly used method is the Surrogate Safety Assessment Model (SSAM), which was first introduced by Gettman et al. (*364*, *365*). One of the advancements of the traffic conflict techniques combined with the micro-simulation is that it offers an innovative way of conducting safety assessment of traffic systems even before safety improvements are actually implemented. After the conception of Surrogate Measure of Safety (SMoS) was proposed, several researches were conducted to validate the simulation traffic conflicts using SMoS. Among various surrogate measures of safety used in the literature, time-to-collision (TTC) was found to be an efficient surrogate safety measure. Ozbay et al. (*366*) developed and validated an analytically derived Crash Index (CI) and Modified Time-to-Collision (MTTC) as new safety indicators based on the extension of the traditional TTC safety index. Preliminary results indicate that there was a strong relationship between the proposed surrogate safety measures and real accident data. Dijkstra et al. (*367*) found that there is a quantitative relationship between the detected conflicts at intersections in the PARAMICS microsimulation model and recorded crashes at the same locations in the real world. The number of conflicts at intersections and the number of passing motor vehicles appeared to be statistically related to the number of observed crashes for all the intersections. Huang et al. (*368*) compared the conflicts generated by the VISSIM simulation model and identified by SSAM to the traffic conflicts measured at ten signalized intersections in China. Similarly, Essa and Sayed (*369*) investigated the relationship between field-measured and simulated conflicts at an urban signalized intersection in Canada. Results from both studies showed that there was a reasonable goodness-of-fit between the simulated and the observed conflicts, and both researches highlighted the importance of the calibration of VISSIM model to match the existing traffic conditions and the actual driver behavior parameters. Young et al. (*370*) summarized the developments of road safety simulation models and proposed new research areas to direct the further work of simulating safety. The suggested developments mainly include: using crash as the measure of performance; investigate the theory behind driver behavior in crashes; present a more detailed representation of the vehicle and conflict situations, and a generalization of the models to look at more crash and vehicle types.

To date, there has been a number of studies that adopted surrogate measure of safety and SSAM for traffic safety assessment. Habtemichael and Santos (*371*) employed VISSIM and SSAM simulation models to assess the safety benefits of VSL under various traffic conditions and driver compliance levels. It was found that the safety benefits were highest during highly congested conditions and a higher compliance level led to more significant benefits. Fan et al. (*372*) developed a procedure that using VISSIM and SSAM for safety assessment at freeway merge areas. The authors employed a two-stage procedure to calibrate and validate the VISSIM simulation models. Data analysis results from Linear regression models and the Spearman rank correlation coefficient indicated that there was a reasonable consistency between the simulated and the observed conflicts. Olia et al. (*373*) attempted to quantify potential safety benefits of deploying a Connected Vehicle system through microscopic traffic simulation modeling. PARAMICS was used to model Connected Vehicles, construction zones, and incidents associated with work zones. The result of this research clearly demonstrates the effectiveness of Connected Vehicle systems to improve network safety. The percentage of Connected Vehicles within the network is the most significant factor to increase network safety and can be explained by re-routing to alternate routes and increased driver awareness with improvements of up to 50 percent in network safety. Another study evaluated the impact of connected vehicle on work zone safety (*374*). A dynamic route guidance system ,based on decaying average-travel-time and shortest path routing, was developed and tested in a microscopic traffic simulation environment to avoid routes with work zones. To account for the unpredictable behavior and psychology of driver's response to information, three behavior models, in the form of multinomial distributions, are proposed and studied in this research. The surrogate safety measure improved Time to Collision was used to gauge network safety at various market penetrations of connected vehicles. Results show that higher market penetrations of connected vehicles decrease network safety due to increased average travel distance, while the safest conditions, 5 percent -10 percent reduction in critical Time to Collision events, were observed at market penetrations of 20 percent -40 percent connected vehicle, with network safety strongly influenced by behavior model. Genders and Raviza (*375*) evaluated the potential safety benefits of deploying a connected vehicle system on a traffic network in the presence of a work zone. The modeled connected vehicle system in the study uses vehicle-to-vehicle (V2V) communication to share information about work zone links and link travel times. Vehicles which receive work zone information will also modify their driving behavior by increasing awareness and decreasing aggressiveness. Traffic microsimulation software was used to model the network and a C plugin was developed to implement connected vehicle in the simulation. The surrogate safety measure improved time to collision (TTC) is used to assess the safety of the network. Various market penetrations of connected vehicles were utilized along with three different behavior models to account for the uncertainty in driver response to connected vehicle information. The results show that network safety is strongly correlated with the behavior model used; conservative models yield conservative changes in network safety. The results also show that market penetrations of connected vehicles under 40 percent contribute to a safer traffic network, while market penetrations above 40 percent decrease network safety. The decrease in safety when rerouting more than 40 percent of traffic on a work zone is attributed to longer average trip distances (*375*). This also could be explained by the fact that more traffic will be diverted to other alternate routes resulting in more exposure to higher traffic volumes and increased crash risks. Fyfe and Sayed (*376*) combined VISSIM and SSAM with the application of the cumulative travel time (CTT) algorithm to evaluate the safety under CV environment. The study showed a 40 percent

reduction of rear-end conflict frequency at a signalized intersection with the application of CV. Abdel-Aty and Wang (*377*) tested several variable speed limit (VSL) strategies in a well-calibrated and validated microsimulation (VISSIM). The crash odds were calculated based on a real-time safety analysis model for weaving segments, and the conflicts were obtained by processing VISSIM vehicle trajectory file in the Surrogate Safety Assessment Model (SSAM). The results showed that both the location and the speed value of VSL were important. The VSL installed at the upstream of the weaving segment better enhanced the safety than the VSL set at downstream. Hence, the reduction of upstream speed is the key to improve the safety of weaving segment. Furthermore, lower upstream variable speed limit would better improve the safety of the whole weaving segment. Li et al. (*353*) developed a microsimulation testbed to assess the safety benefits of an integrated system of cooperative adaptive cruise control (CACC) and variable speed limit (VSL); surrogate safety measures of the time exposed time-to-collision (TET) and time integrated time-to-collision (TIT) were used. The simulation results showed that the proposed integration system with 100 percent CACC penetration rate can reduce the rear-end collision risks effectively, with the TIT and TET declined by 98 percent . Rahman et al. (*363*) employed the standard deviation of speed, the standard deviation of headway, and rear-end crash risk index (RCRI) as surrogate measures of safety in a microsimulation environment to assess the safety effectiveness of CV technologies. Simulation results indicated that CV improved traffic safety significantly in fog conditions as market penetration rates of CV increase.

In addition to the microsimulation based analysis of SMoS, Peng et al. (*378*) employed time-to-collision, speed variance and headway variance as surrogate measures of safety to assess the impact of reduced visibility on traffic crash risk based on field collected microscopic traffic flow data. Log-Inverse Gaussian regression modeling was used to explore the relationship between time-to-collision and visibility together with other traffic parameters. It was concluded that reduced visibility would significantly increase the traffic crash risk especially rear-end crashes and the impact on crash risk was different for different vehicle types and for different lanes.

Tools Available and Data Needed for VSL microsimulation

In summary, findings from several representative research revealed that safety benefits of freeway countermeasure, including VSL, were mostly stemmed from speed harmonization and reductions in speed variance. The emerging connected and autonomous vehicle technologies create opportunities to collect real-time road weather and traffic information, which has the possibility to dramatically enhance existing freeway management strategies, tools, and systems. Also, a well-calibrated microsimulation model will be a useful tool in analyzing the mobility and safety of various traffic systems. A number of simulation tools have been used for safety simulation, including but not limited to VISSIM, PARAMICS, AIMSUM, MATLAB, and SSAM, etc., as well as driving simulators. Tools and data used for microsimulation study from previous research works are summarized in Table 54.

Table 54 Tools and Data Used for Microsimulation of VSL

Reference	Tool(s) for Simulation	Data used for Simulation	Measure of Performance
Lee et al., 2013, (*333*)	VISSIM	Speed, Traffic Volume, Driver Behavior, Driver Compliance	Travel Time
Habtemichael and Santos, 2013, (*371*)	VISSIM, SSAM	Traffic Flow, Driver Compliance Level	Travel Time, Traffic Conflict
Sabawat and Young, 2013, (*344*)	N/A	Weather, Speed, Traffic volume	Speed Compliance and Speed Variation
Li, Z. et al., 2014, (*346*)	MATLAB	Accel/Decel, Driver Behavior, Weather	SMoS (TET, TIT)
Grumert et al, 2015, (*355*)*	SUMO – Simulation of Urban MObility, CMEM	Accel/Decel, Driver Imperfection, Reaction, Headway, Vehicle Length	Speed Harmonization, Emission
Hadiuzzaman et al., 2015, (*334*)	VISSIM, MATLAB	Traffic Density Dynamics, Speed Dynamics, Driver Compliance Level	Travel Time, Throughput Collision Probability, Speed Variance
Khondaker and Kattan, 2015, (*356*)*	VISSIM, MATLAB, VT-Micro	Traffic Flow, Density, Speed, Driver Compliance	Total Travel Time, SMoS (Time-To-Collision) Fuel Consumption
Kim et al., 2015, (*345*)	TrEPS (Traffic Estimation and Prediction System)	Weather, Traffic Flow, O-D Pattern, Driver Reaction and Behavior	Travel Time
Muller et al., 2015, (*335*)	AIMSUN	Acceleration, Reaction Time, Speed, Traffic Flow	Travel Time
Choi and Oh, 2016, (*348*)	VISSIM	Weather, Visibility, Speed, Traffic Flow	S.D. of Speed, Traffic Conflict
Li, Y. et al., 2016, (*352*)*	MATLAB	Traffic Flow, Headway, Speed Change Rate	SMoS (TET- Time Exposed To Collision, and TIT – Time Integrated Time To Collision), Travel Time
Wang et al., 2016, (*359*)*	MOTUS, MATLAB	Traffic Flow, Speed, Driver Behavior, Penetration Rate	Travel Time, Fuel Consumption
Abdel-Aty and Wang, 2017, (*377*)	VISSIM , SSAM	Crash, Traffic, Weather, Geometry	Crash Odds, Traffic Conflicts
Conran, 2017, (*337*)	VISSIM, MATLAB	Driver Compliance, Driver Behavior	Coefficient Of Variation of Speed, Travel Time
Grumert and Tapani, 2017, (*361*)*	SUMO	Speed And Position of Each CV	Travel Time
Li, D. et al., 2018, (*360*)	AISUN	Drive Compliance, Speed, Driver Behavior, Penetration Rate of Cavs	Speed And Speed Difference
Li, Y. et al., 2017, (*353*)*	MATLAB	Traffic Flow, Speed, Accel/Decel, Headway, Penetration of CV	TIT, TET, Travel Time
Sadat and Celikouglu, 2017, (*336*)	VISSIM, MATLAB	Traffic Flow, Speed, Driver Compliance Level	Traffic Volume, Average Speed and Occupancy,

Reference	Tool(s) for Simulation	Data used for Simulation	Measure of Performance
			Travel Time, Fuel Consumption, Emission
Rahman et al., 2018, (*363*)*	VISSIM	Weather, Traffic Flow, Driver Behavior, CV Penetration Rate	Smos (S.D. of Speed, S.D. of Headway, Rear-End Crash Risk Index (RCRI))
Yang et al.,2019, (*379*)*	Driving Simulator	Truck Driver Behavior, Weather, CV-VSL Warnings	Comparisons of Participants' Speeds under Baseline and CV Scenarios
Yang et al., 2020, (*380*)*	Driving Simulator	CV Pilot's Traveler Information Messages (TIMs), Driver Behavior, Weather, Road Surface	SMoS (TTC, Modified Deceleration to Avoid Crash (MDRAC))
Yang et al., 2020, (*381*)*	VISSIM, Driving Simulator, SSAM	Traffic Flow, Driver Behavior, SHRP 2, Penetration of CV	TTC
Ahmed et al., 2020, (*382*)*	Driving Simulator	Survey Response, Human–Machine Interface (HMI), Weather, CV Applications	Effectiveness of CV Technology
Subedi et al., 2020, (*383*)*	Driving Simulator	Driver Behavior of Highway Patrol Troopers, TIMs, Forward Collision Warning, Spot Weather Warnings, Work Zone Warnings	Evaluation of E-Training, Evaluation of Driving Simulator Training
Yang et al., 2020, (*384*)*	Driving Simulator	Truck Driver Behavior, Driver Preference Survey, Vehicle Dynamics	Effectiveness of CV Warnings
Raddaoui et al., 2020, (*385*)*	Driving Simulator	Driver Behavior of Truck Drivers, Weather, Work Zones	Effectiveness of CV Weather and Work Zone Warnings
Raddaoui et al., 2020, (*386*)*	Driving Simulator	Eye Glance Behavior of Truck Drivers, Weather, Work Zones	Comparison of the Visual/Cognitive Workload Demands of the CV Applications, Effects of Exposure to the CV Warnings on Participants' Visual/Cognitive Workload
Bakhshi et al., 2021, (*387*)*	Driving Simulator	Truck Driver Behavior, Vehicle Dynamics form Driving Simulator	Kinematic-based Surrogate Measures of Safety (K-SMoS), including deviation from the pathway, instantaneous acceleration, lateral speed, and steering angle.
Gaweesh et al., 2021, (*387*)*	Driving Simulator	Truck Driver Behavior, Vehicle Dynamics form Driving Simulator	Longitudinal Speed, Lateral Speed, Longitudinal Acceleration, Lateral Acceleration, Steering Angle, Pitch, Roll, Yaw
Adomah et al., 2021, (*388*)*	VISSIM, Driving Simulator, SSAM	Driver Behavior, Weather, CV Work Zone Warning	SMoS (TTC, TET, TIT, MDRAC)
Bakhshi and Ahmed, 2021, (*389*)*	Driving Simulator	Driver Behavior, CV Work Zone Warning	TTC, Four hierarchical Negative Binomial

Reference	Tool(s) for Simulation	Data used for Simulation	Measure of Performance
			Regressions Under Bayesian Inference

Note: * Connected Vehicle Environment

Data Processing

Development of Weather-based Microsimulation Model

Reliable and systematic data processing procedures are crucial when handling large datasets; the quality of even the most novel analysis is limited by the quality of the provided input data. The WYDOT SHRP2 NDS dataset comprises 1,284 trips (i.e., equivalent to 1,212h of driving data). In the SHRP2 NDS, a trip is defined by a single driving event captured continuously from a vehicle start (i.e., activation of the DAS) until the vehicle is turned off. To evaluate car-following behavior, the authors developed a radar-vision algorithm to identify the presence of a preceding or lead vehicle from the SHRP2 NDS post-processed radar data. Details about the formulation and verification of this radar-vision algorithm can be found in Hammit et al. (*390*). After processing each of the trips through the radar-vision algorithm to identify continuous segments of car-following, a moving average filter with a window size of 1.4s was applied to the radar range rate, that is, relative velocity, to smooth the resulting measurements. The window size was identified from a sensitivity analysis, as it provided optimal smoothing while maintaining the original data trends.

To evaluate car-following behavioral changes between different weather conditions, each adverse weather trip was manually clustered based on the most prevalent weather conditions observed in the front-facing video feed. Detailed descriptions of each cluster were clearly defined and a single video reviewer performed all observations to reduce bias in the manual processing (*89*). Trips with missing radar data or other erroneous values were removed, which resulted in 1,206 trips, as summarized in Table 1. The number of trips classified in each condition are provided, alongside their average total driving time, average driving time while influenced by a leading vehicle (i.e., car following), and the average travel speed during these periods of car-following behavior. A significantly greater distribution of weather intensity was observed in precipitation, specifically trips in rain conditions, therefore, these trips were further separated into categories: very light rain, light rain, moderately heavy rain, and heavy rain. These categories were defined by a review of the available data and by referencing existing classifications of rain, such as those provided in the HCM. Fog and snow conditions were identified to be more homogeneous than rain; however, larger datasets with greater exposure to these conditions would enable more detailed categorization.

Microsimulation of Variable Speed Limit

During VISSIM calibration stage, the VISSIM simulation models will be calibrated to reproduce performance measures collected by WYDOT's Wavetronix speed sensors and RWIS sensors. The key traffic performance data used for model calibration are 2-min traffic volume counts and spot speed at each speed sensor. Based on the available dataset, traffic performance data from two speed sensors were selected: Sensor #2146 (nearest RWIS sensor: WY28) and Sensor #2178 (nearest RWIS sensor: KVDW). In VISSIM model, data collection points were added at the same location to report the simulated traffic flow and speed data. Locations of the speed and RWIS sensors and VISSIM data collection points are illustrated in Figure 96.

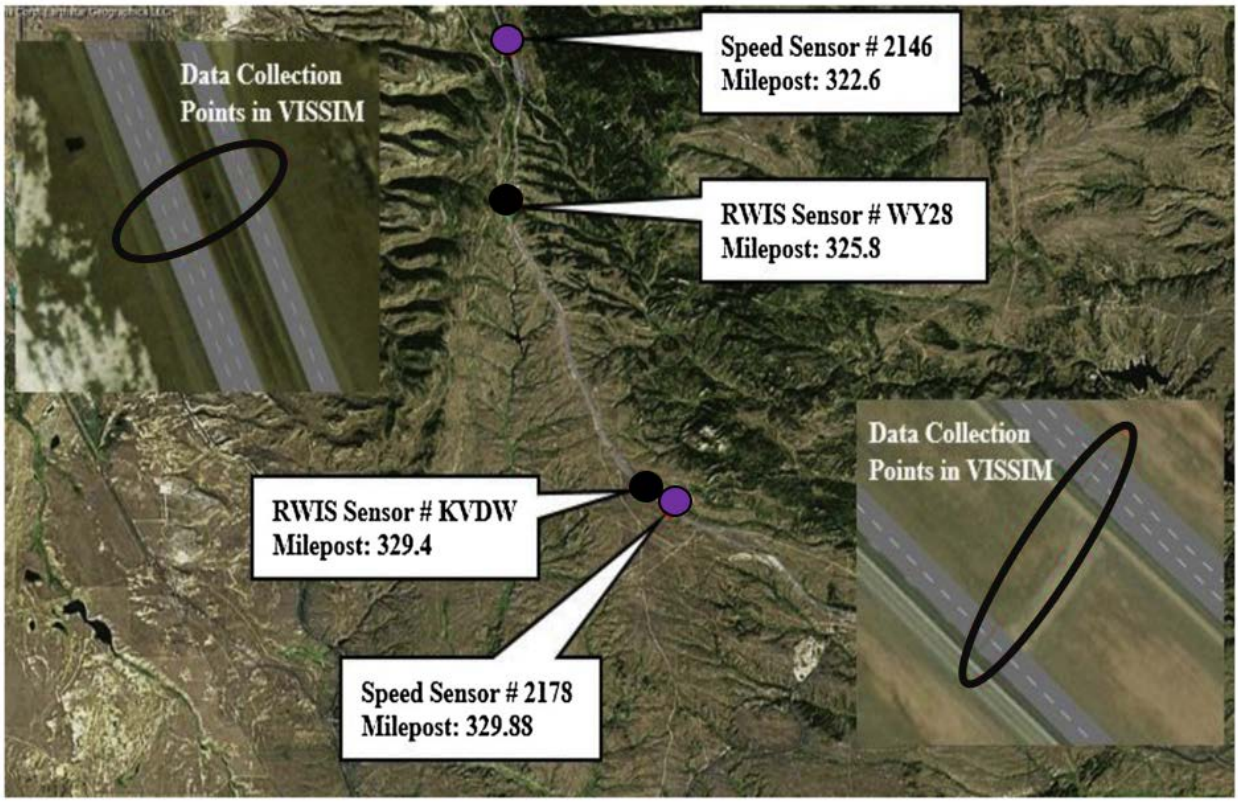

Figure 96 Location of Data Collection Points in VISSIM (Source: WYDOT)

Methodology

Development of Weather-based Microsimulation Model

Optimal Car-Following Model Parameter Sets

This analysis uses the W99 car-following model, as it is one of the two car following models available in PTV's VISSIM microsimulation software which is widely used in research and practice (*391*). The W99 model was selected over the W74 model as its use is recommended for freeway facilities. Limited documentation is available for this model; however, the fundamental logic was gathered from the original source code (*392*) and Liu's W99 Demo source code (*393*). The W99 model is a psychophysical car-following model derived to predict a driver's response (i.e., their acceleration) to leading vehicles at varying perception thresholds. The model contains four regimes which capture different car-following behavior in free flow, approaching, following, and danger zones. These regimes are defined in the psychophysical plane, which describes the relationship between the following distance and relative speed between an ego-vehicle and its preceding or leading vehicle (shown in Figure 97). A driver enters a regime by passing through a defined perception threshold (i.e., SDXC, SDXO, SDVC, SDVO, and SDXV) which indicates a shift in how the driver perceives his or her relationship with the leading vehicle. In accordance with this perception, different acceleration response equations are used to predict the ego-vehicle's (i.e., following vehicle) response in each regime. The model is calibrated by tuning 11 parameters which dictate the placement of the regime thresholds and the produced acceleration behavior.

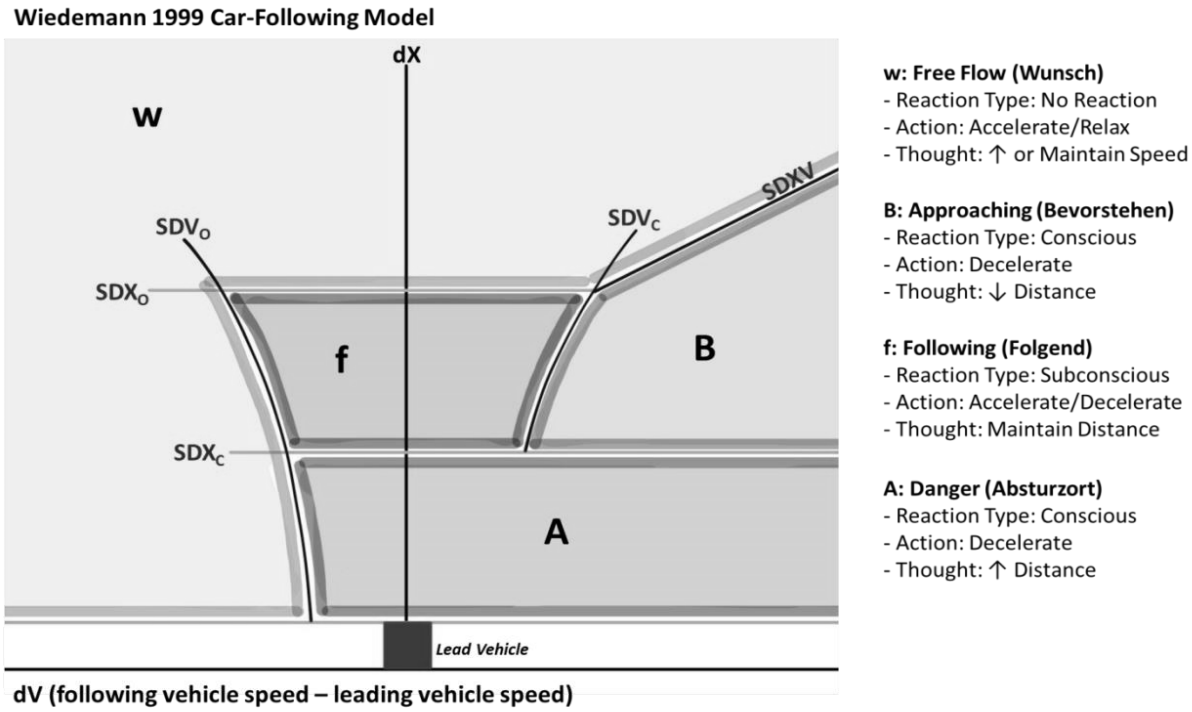

Figure 97 Wiedemann 1999 Car-Following Model Psychophysical Plane Regime Diagram.

Numerous research groups have calibrated car following models using trajectory-level driving data (*137*, *311*, *313–315*, *328*). A calibration optimization problem was developed through a synthesis of best practices found in the literature. In this paper, the model parameters were calibrated using the leader–follower driving trajectories from the SHRP2 NDS. The W99 model logic was used to predict the behavior of the following vehicle, and the resulting trajectory was compared with the actual trajectory by measuring the root mean squared error (RMSE) between the two following distance profiles. The optimization problem was designed to calibrate the W99 model parameters using a genetic algorithm in which the average RMSE of all leader–follower trajectories extracted from a single trip is minimized. Additional details related to the identified best practices and calibration implementation can be found in Hammit et al. (*394*). Using this calibration protocol, each individual NDS trip is calibrated, and optimal car-following model parameters are collected.

Concurrent research conducted by the authors considers various methodologies for selecting optimal car following parameter values to describe a set of SHRP2 NDS trips from a specific driver population or driving condition. Details about these methodologies will be available in James and Hammit (*395*), where a methodology is identified for obtaining a representative parameter set for a specific driving condition which achieves reasonable validation results while balancing practical implementation challenges; specifically for W99, it was recommended to sample the median value from each parameter independently. This sampling methodology was verified as the method that achieved the lowest error estimate, subject to computation constraints, using a 10-fold cross-validation procedure. Using this procedure, optimal car-following parameter values are presented for each weather condition and discussed based on their defined physical interpretation.

Comparison of Predicted and Expected Network-Wide Impacts Using Optimal Car-Following Model Parameter Sets

The next task applies the optimal W99 car following model parameter values—attained by the first analysis—in PTV's VISSIM microsimulation software and evaluates their performance on a simple freeway weaving segment (taken from the HCM). The freeway weaving segment is illustrated in Figure 98, and includes four lanes in one direction with three on-ramps and three off-ramps. A demand profile with increasing input volumes at each of the four inlet positions (denoted as A, B, C, and D in Figure 98) was used to load the network over a one-hour simulated time period. Data were then collected at 20-s time intervals to extrapolate networkwide fundamental diagrams, describing the speed, density, and flow rate throughout the network.

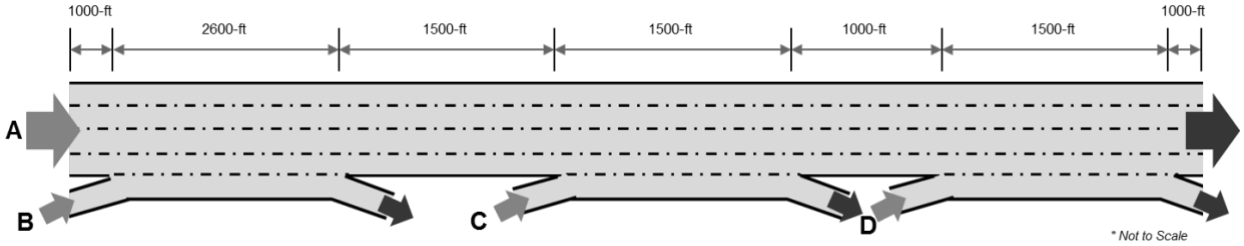

Figure 98 Simple Freeway Weaving Segment Constructed in VISSIM to Assess Calibrated Parameter Sets Representing Different Weather Conditions

In practice, when generating a microsimulation model, driving behavior is typically the last priority, as the development of the roadway configuration and appropriate representation of travel demand is extremely time intensive. In this analysis, however, all other simulation variables are held constant, and the driving behavior is modified to reflect the calibrated results from the SHRP2 NDS data in each weather condition. In the W99 model, 11 parameters are calibrated. The first ten values—CC0 through CC9—can be adjusted directly in VISSIM, as shown in Figure 99. The final calibrated parameter represents the desired travel speed. For the purpose of this analysis, the desired travel speed was associated with the 85th percentile free flow speed and the desired speed distribution in VISSIM was adjusted accordingly. Figure 100 shows the methodology used to construct the desired speed distribution, assigning the calibrated desired speed value as the free flow speed.

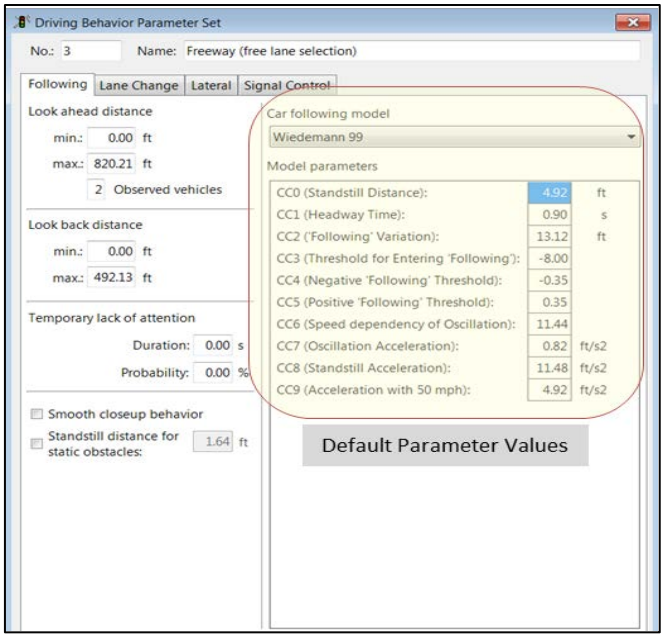

Figure 99 Snapshot of Driving Behavior Parameter Set in VISSIM

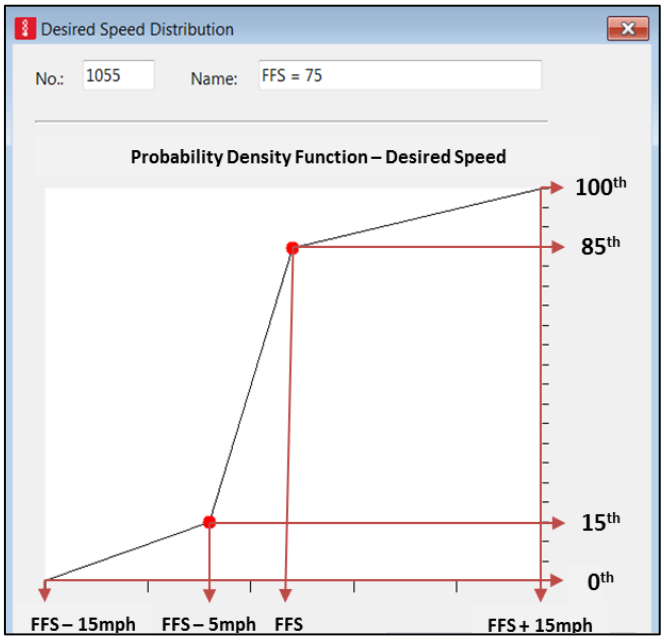

Figure 100 Snapshot of Desired Speed Distribution Graphical User Interfaces in VISSIM

Using this methodology, the VISSIM simulation model is created for each weather condition and data from each run were collected to compile fundamental diagrams representing network-wide traffic flow in each weather condition.

Microsimulation of Variable Speed Limit

Adjustment of VISSIM Parameters

The desired speed distribution has been updated based on the finding from the speed selection behavior investigation, as already described in Chapter 2. It was found that speeds followed normal distribution in clear weather and Weibull distribution in adverse weather. The range of

the speed distribution, i.e., the minimum and maximum speed in a particular weather condition were selected based on the spot speed data from WYDOT's Wavetronix detectors. Considering the input requirement of VISSIM, cumulative speed distribution curves were generated based on the above-mentioned distributions and used for the microsimulation modeling instead of using the default VISSIM speed distribution, as shown in Figure 101.

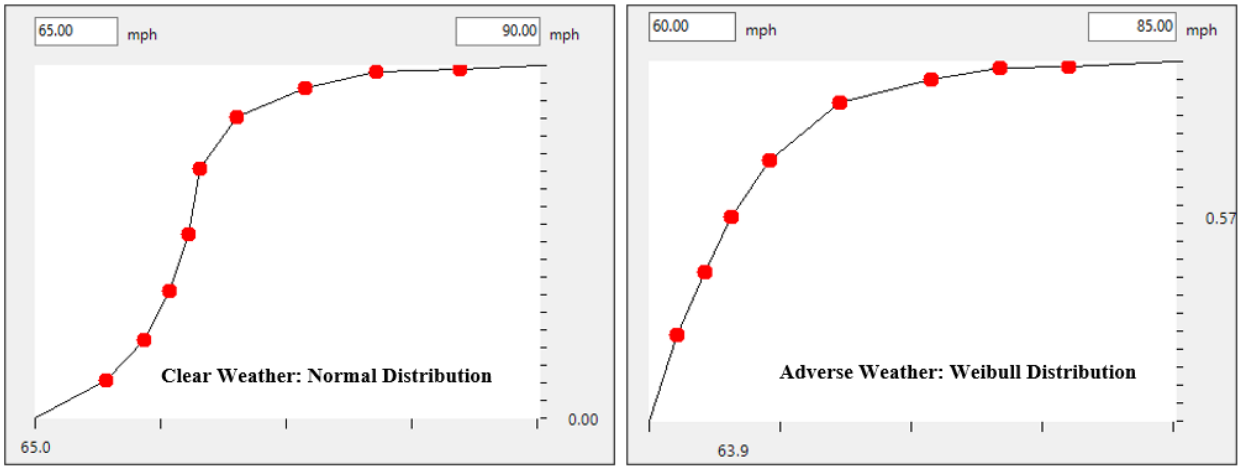

Figure 101 Adjusted Cumulative Speed Distribution

In VISSIM microsimulation the weather and traffic conditions are represented via various driver behavioral models, such as look-ahead distance, desired following gap, and desired velocity. However, parameters in driver behavior models cannot be linked to weather and road surface conditions directly. Therefore, driver behavior parameters should be calibrated based on different weather conditions to represent real-world driving behavior. The research team calibrated 10 car-following parameters for different weather conditions, as shown in Table 55.

Table 55 Calibrated Car-Following Parameters for Different Weather Conditions

W99 Parameters	Clear	Fog	Rain	Snow
CC0: Standstill Distance [m]	4.2	4.2	4.3	2.8
CC1: Spacing Time [s]	0.7	1.0	0.8	1.2
CC2: Following Variation, Max Drift [m]	12.7	12.9	12.8	11.7
CC3: Threshold for Entering Following [s]	-24.6	-21.9	-23.4	-25.9
CC4: Negative Following Threshold [m/s]	0.0	0.0	-0.1	-0.1
CC5: Positive Following Threshold [m/s]	0.9	1.1	0.9	0.4
CC6: Speed Dependency of Oscillation [10^{-4} rad/s]	1.7	2.2	1.9	1.7
CC7: Oscillation Acceleration [m/s2]	1.0	1.6	1.2	0.7
CC8: Standstill Acceleration [m/s2]	1.4	2.9	1.4	1.3
CC9: Acceleration at 80kph [m/s2]	0.1	0.2	0.1	0.1
Desired Velocity [m/s]	32.7	31.5	31.9	27.6

The definitions of CC0 through CC9 are as follows (*396*):

CC0 (Standstill Distance) defines the desired rear-bumper to front-bumper distance (feet) between stopped vehicles.
CC1 (Headway Time) defines the gap (seconds) which a driver wants to maintain at a certain speed. The higher the value, the more cautious the driver is.
CC2 (Following Variation) defines the longitudinal oscillation during following conditions. It defines the additional distance (feet) from the desired safety distance a driver allows before he intentionally moves closer to the car in front.
CC3 (threshold for entering following) defines the start (in seconds) of the deceleration process, i.e., the time in seconds, when the driver recognizes a slower moving preceding vehicle, and starts to decelerate.
CC4 (negative following threshold) and CC5 (positive following threshold) define the speed difference (in m/s) during the following process. CC4 controls speed differences during closing process, and CC5 controls speed differences in an opening process.
CC6 (speed dependency of oscillation) defines the influence of distance on speed oscillation during following condition.
CC7 (oscillation acceleration) defines the actual acceleration during oscillation in a following process.
CC8 (standstill acceleration) defines the desired acceleration when starting from a standstill.
CC9 (acceleration at 80 km/h) defines the desired acceleration when at 80km/h. However, it is limited by maximum acceleration for the vehicle type.

In addition to car following parameters, the research team also calibrated the default lane change parameters in VISSIM. The parameters were calibrated based on the trajectory SHRP2 time series data and associated lane change events, as well as engineering judgments. Note that the lane change events were identified based on an automated algorithm developed by the research team. More details of the algorithm can be found in (*235*). VISSIM classified the lane changes into two categories: necessary lane change and free lane change. In VISSIM, necessary lane change is described by the following most important parameter:

- Maximum Deceleration (Own/Trailing): Refers to the upper bound of deceleration for own vehicle and tailing vehicle for a lane change.
- Accepted Deceleration (Own/Trailing): Refers to the lower bound of deceleration for own vehicle and tailing vehicle for a lane change.

However, for free lane changes the following most important parameters are used in VISSIM.

- Minimum Headway (Front/Rear): The minimum distance between two vehicles that must be available after a lane change, so that the change can take place.
- Safety Distance Reduction Factor: During the lane change Vissim reduces the safety distance to the value that results from the multiplication between original safety distance and safety distance reduction factor.
- Maximum Deceleration for Cooperative Breaking: Refers to cooperative deceleration of a trailing vehicle that allows an own vehicle to change lanes.

The calibrated necessary and free lane change parameters in VISSIM for own vehicle and trailing vehicle are presented in Table 56 and Table 57, respectively.

Table 56 Calibrated Necessary Lane Change Parameters for Own Vehicle and Trailing Vehicle

Parameters	Necessary Lane Change			
	Own Vehicle			
	Clear	Rain	Snow	Fog
Maximum Deceleration (ft/s²)	-11.38	-8.32	-17.84	-17.43
Accepted Deceleration (ft/s²)	-0.11	-0.06	-0.11	-0.06
	Trailing Vehicle			
Maximum Deceleration (ft/s²)	-1.78	-1.61	-0.65	-1.21
Accepted Deceleration (ft/s²)	-0.09	-0.09	-0.08	-0.09

Table 57 Calibrated Free Lane Change Parameters

Parameters	Free Lane Change			
	Clear	Rain	Snow	Fog
Minimum Headway (Rear) (ft)	104.41	127.98	136.90	97.17
Safety Distance Reduction Factor	0.6	0.58	0.51	0.59
Maximum Deceleration for Cooperative Breaking (ft/s²)	-1.70	-0.93	-1.80	-1.26

Model Calibration and Validation

After running the simulation using the calibrated parameters, simulation results were compared against field observed data to check the errors between simulation inputs and outputs. One reliable measure to compare traffic volume inputs and outputs is the Geoffrey E. Havers (GEH) statistics that can be described using the following equation (*381*).

$$GEH = \sqrt{\frac{2(M-C)^2}{(M+C)}} \qquad \text{Equation 36}$$

Where:

M = hourly traffic volume output from the simulation model (vph)

C = real-world hourly traffic volume input (vph)

To determine if an acceptable fit is achieved, this report employed the GEH interpretation guide presented in Table 58 (*381*). The GEH test results using the updated parameters for all sensor locations were found to be within an acceptable range indicating that the microsimulation models were calibrated successfully.

Table 58 GEH Interpretation Guide

GEH Statistic Result	Reference
GEH < 5.0	Acceptable fit
5.0 <= GEH <= 10.0	Caution: possible model error or bad data
GEH>10.0	Unacceptable

Safety Evaluation Using SSAM

During the VISSIM simulation, the default settings were modified to generate the vehicle trajectory files for each simulation run. Note that it is not possible to evaluate traffic safety within VISSIM. Therefore, Surrogate Safety Assessment Model (SSAM) software was used. The generated vehicle trajectory data were processed in SSAM for identifying the simulated conflicts. Although SSAM can provide various SMoSs, including TTC, Post Enchroachment Time (PET), etc., the research team assessed the safety performance of VSL using TTC considering its applicability in rural freeway corridors. TTC is defined as the time required for two vehicles to collide if they continue at their present speeds on the same path, as shown in the following equation (*381*).

$$TTC = \begin{cases} \frac{D_{1-2}}{V_2 - V_1}, if\ V_2 > V_1 \\ \infty, Otherwisr \end{cases} \quad \text{Equation 37}$$

Where D_{1-2} represents the gap distance between the leading and the following vehicle, V_1 and V_2 are the speeds of the leading and following vehicles, respectively.

Results and Discussions

Development of Weather Based Microsimulation Model

As described in the Methodology section, calibrated W99 parameters were produced with each trip and descriptive parameter sets representing each weather condition were collected by taking the median value from the distribution of calibrated parameter values. The calibrated parameters for the W99 car-following model are shown in Table 59.

The calibrated parameters for each weather condition are described in Figure 102 through Figure 107. The most well-known parameters tuned in the W99 model are CC0 and CC1. Combined, these parameters represent the average following distance the ego-vehicle attempts to maintain throughout the following segment. Typically, these values are adjusted independently; however, their relationship with one another and the vehicle's travel speed are critical for understanding their impact on the resulting driving behavior. Figure 102 illustrates the average following distance for each weather condition derived from the CC0, CC1, and desired travel speed parameters. As shown, the shortest standstill distance is reported for snow conditions; however, its average following distance is the largest. The calibrated results indicate that the average following distance for moderate rain and heavy rain conditions are slightly shorter or the same as in clear conditions, while the average following distance in fog, very light rain, and light rain are slightly higher.

Table 59 Calibrated Model Parameters

W99 Parameters	Clear	Fog	Very Light Rain	Light Rain	Moderate Rain	Heavy Rain	Snow
CC0: Standstill Distance [m]	4.2	4.2	4.6	4.2	3.8	4.4	2.8
CC1: Spacing Time [s]	0.7	1.0	0.9	0.8	0.7	0.7	1.2
CC2: Following Variation, Max Drift [m]	12.7	12.9	13.5	11.7	13.5	12.4	11.7
CC3: Threshold for Entering Following [s]	-24.6	-21.9	-23.5	-24.8	-24.4	-21.0	-25.9
CC4: Negative Following Threshold [m/s]	0.0	0.0	-0.1	0.0	-0.1	-0.1	-0.1
CC5: Positive Following Threshold [m/s]	0.9	1.1	1.1	0.9	0.7	1.0	0.4
CC6: Speed Dependency of Oscillation [10-4 rad/s]	1.7	2.2	2.0	1.5	1.5	2.4	1.7
CC7: Oscillation Acceleration [m/s2]	1.0	1.6	1.1	1.2	1.4	1.2	0.7
CC8: Standstill Acceleration [m/s2]	1.4	2.9	1.5	1.1	1.0	1.8	1.3
CC9: Acceleration at 80kph [m/s2]	0.1	0.2	0.2	0.1	0.1	0.1	0.1
Desired Velocity [m/s]	32.7	31.5	31.5	31.8	31.9	32.4	27.6

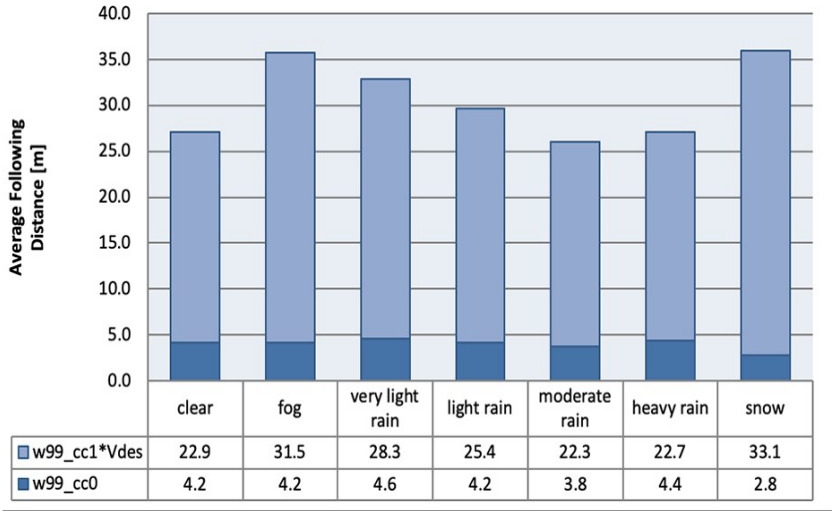

Figure 102 Investigation of Calibrated CC0, CC1, and Desired Velocity Parameters from W99

Figure 103 illustrates the minimum, average, and maximum following distance for each condition using the aforementioned average following distance and the following variation or maximum drift threshold (CC2). This drift defines the height of the following regime illustrated in Figure 97 by the SDXC and SDXO thresholds. These values can be interpreted as the largest and smallest following distances which a driver subconsciously aims to maintain while following a leading vehicle. Once these thresholds are passed and the ego-vehicle enters a new regime, different acceleration equations are used.

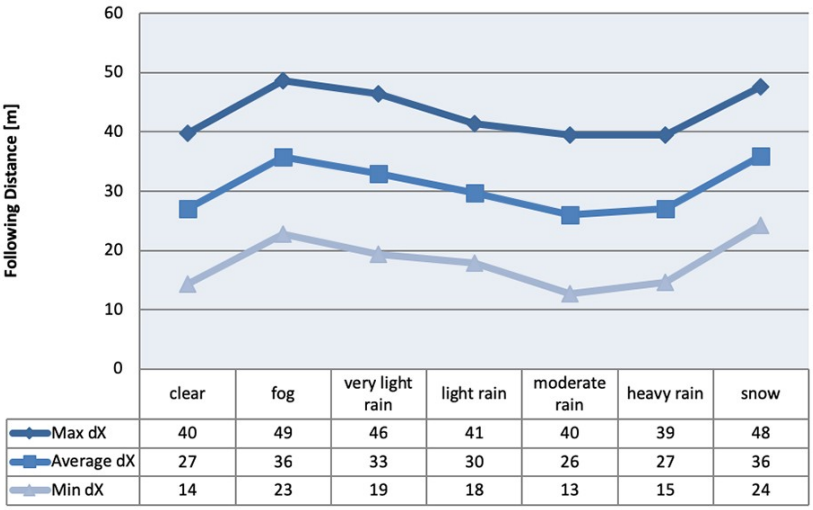

Figure 103 Investigation of Calibrated CC1, Desired Velocity, and CC2 Parameters from W99

The widest drift was calibrated for very light rain and moderate rain conditions, and the smallest drift is seen in light rain and snow conditions. The largest maximum following distance is associated with fog conditions, and the smallest minimum following distance is attributed to moderate rain conditions. While the trends illustrated by the maximum and minimum following distances are similar to the computed average following distance is shown in Figure 102, their subtle differences reinforce the relationship between CC0, CC1, CC2, and the current travel speed in defining perception thresholds surrounding the following regime.

Figure 104 shows CC4 and CC5 parameter values, the negative and positive following thresholds, respectively. These parameters are used in computing the SDVC and SDVO thresholds shown in Figure 97; the parameters describe the range of relative velocity values a driver subconsciously aims to stay within while following a lead vehicle. The larger the absolute value of the following threshold, the greater the acceptable difference in relative velocity. The positive following threshold dictates how quickly the ego-vehicle reacts when separating from the lead vehicle; conversely, the negative following threshold dictates how quickly the ego-vehicle reacts when approaching the lead vehicle. The results clearly indicate that in all scenarios drivers react much faster when gaining speed on the lead vehicle than they do when falling behind from the lead vehicle. The calibration results indicate that in fog, very light rain, and heavy rain conditions, drivers' subconscious following behavior allowed for longer periods of separation, while drivers traveling in snow conditions reacted much more quickly. Conversely, the fastest reaction to approaching a leading vehicle is seen for clear, fog, and light rain conditions, followed closely by the remaining weather conditions.

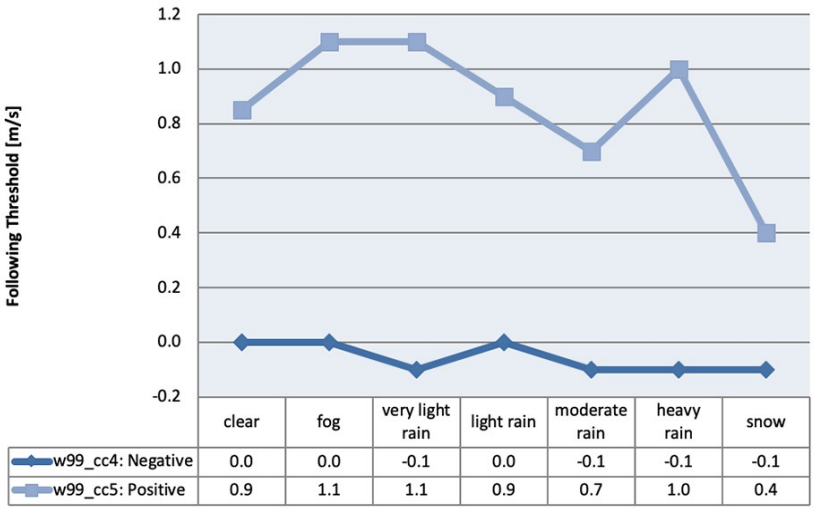

	clear	fog	very light rain	light rain	moderate rain	heavy rain	snow
w99_cc4: Negative	0.0	0.0	-0.1	0.0	-0.1	-0.1	-0.1
w99_cc5: Positive	0.9	1.1	1.1	0.9	0.7	1.0	0.4

Figure 104 Investigation of Calibrated CC4 and CC5 Parameters from W99.

Figure 105 presents the calibration results from CC6, speed dependency of oscillation. This parameter is used in conjunction with CC4 and CC5 to compute the SDVC and SDVO thresholds shown in Figure 97. One key aspect of psychophysical car-following models is the observation of oscillating subconscious behavior made visible in the psychophysical plane. This behavior is hypothesized to occur within the car-following regime, as defined by the aforementioned thresholds; however, the magnitude of this oscillation is dependent on the CC6 parameter; a larger magnitude represents wider oscillation, while a smaller magnitude represents narrower oscillation. The findings indicate that the narrowest range of oscillatory behavior is attributed to light and moderate rain conditions, while the widest range is associated with heavy rain conditions. Similar to the complex relationship exhibited between parameters defining following distance thresholds, the relationship between CC4, CC5, and CC6 is equally complex and difficult to interpret individually.

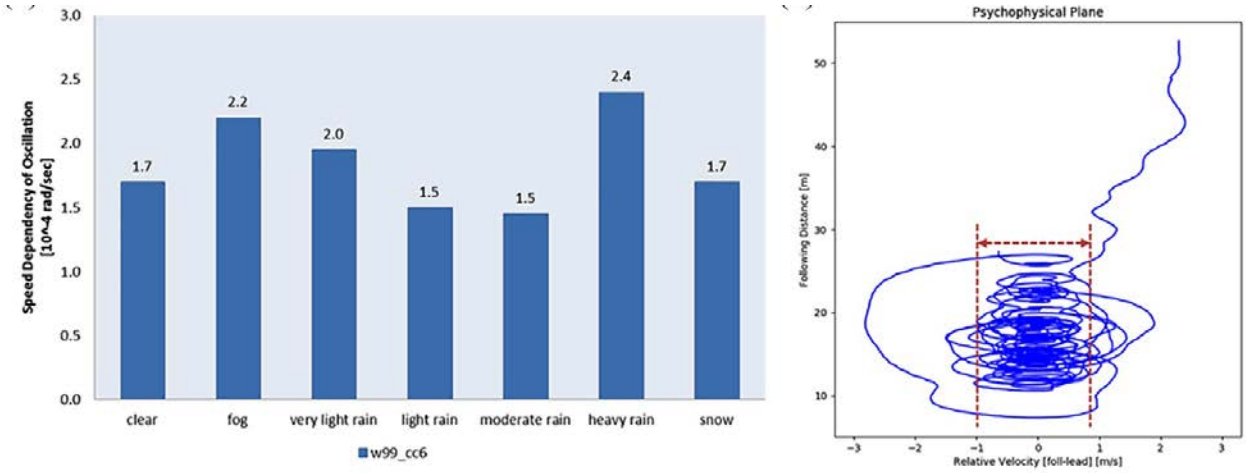

Figure 105 Calibration Outputs from CC6

Figure 106 illustrates the calibrated values for CC3, the threshold for entering. This parameter is used in the computation of the perception threshold SDXV separating the free flow and approaching regimes in Figure 97; it is a parameter representing when a vehicle ‘‘enters’’ the

approaching regime and begins to adjust its response in reaction to the lead vehicle. As the magnitude of the CC3 parameter decreases, the perception-reaction threshold for approaching a lead vehicle increases. Therefore, since the minimum threshold for entering is seen in snow conditions, this means that a driver traveling in snow conditions perceives and reacts to the leading vehicle more quickly than in the other conditions. The largest entering threshold, representing the slowest perception-reaction time is attributed to heavy rain conditions, followed by fog and very light rain. In reality, multiple factors contribute to a driver's perception and subsequent reaction to a lead vehicle. When considering behavior in adverse weather conditions, limited visibility can restrict the driver's line of sight to a leading vehicle increasing the entering threshold, while increased awareness and caution as a result of the adverse conditions can simultaneously cause a decrease in the entering threshold. The complexity in the definition of this parameter reinforces the need for calibrating its value concurrently with the other model parameters using trajectory-level data, as this behavior is nearly impossible to measure in isolation.

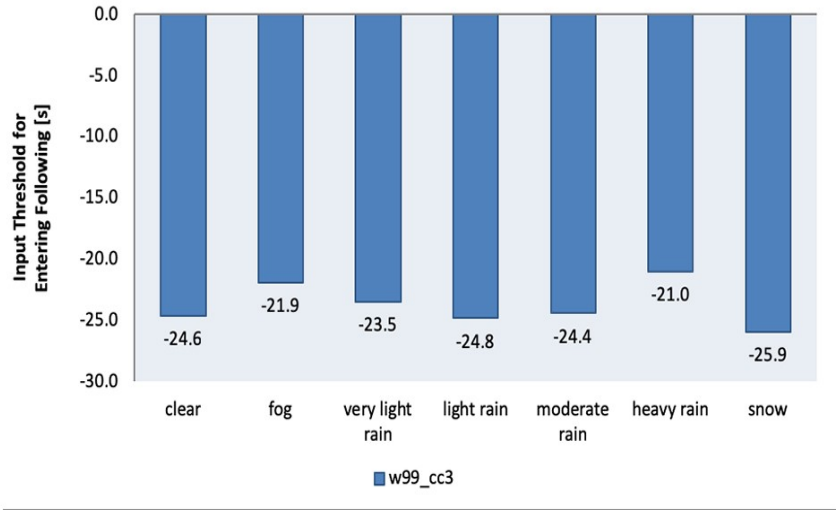

Figure 106 Investigation of the Calibrated W99 CC3 Parameter

The first seven W99 parameter values are used to construct the framework defining the regions of the psychophysical plane associated with each regime. The final parameters, CC7, CC8, and CC9, shown in Figure 107, are used in the calculation of driver response. CC7 represents the maximum acceleration during oscillation, CC8 represents the maximum acceleration from a standstill, and CC9 represents the maximum acceleration at 80 km/ h. In the W99 model, the negative inverses of these values are used for maximum deceleration thresholds. The largest acceleration for most conditions is the standstill acceleration, with the exception of light and moderate rain conditions, and the acceleration at high speeds is significantly lower than either of the other acceleration parameters in each scenario. An investigation of the oscillatory acceleration parameter, CC7—which controls acceleration behavior in both the danger and following regimes—shows that all rain conditions have greater oscillatory acceleration than clear conditions. In addition, the least aggressive behavior is demonstrated in snow conditions and the most aggressive behavior in fog conditions. The magnitude of acceleration in fog compared with precipitation conditions may be interpreted as overconfidence stemming from dry pavement conditions, while simultaneously eliciting more severe reactions than clear conditions because of the reduced visibility.

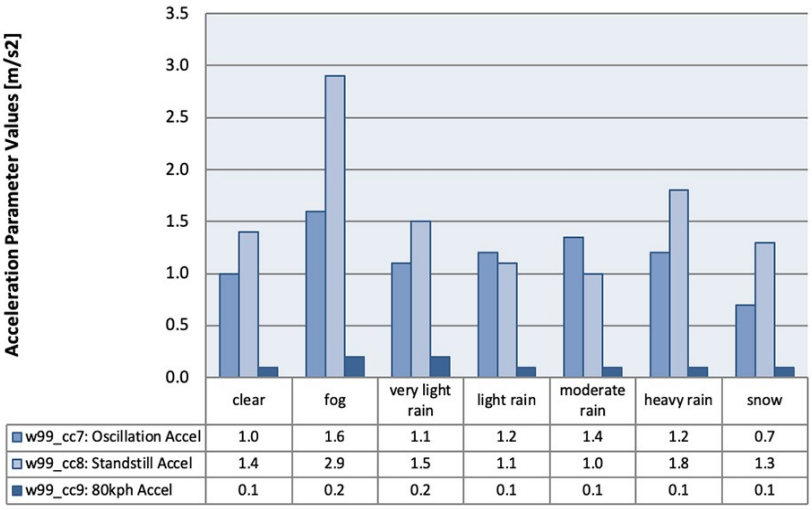

Figure 107 Investigation of the Calibrated CC7, CC8, and CC9 Parameters from W99.

While behavioral trends can be identified from the calibrated parameter values, it is critical to review the predicted behavior of the model using the complete parameter set to fully understand the behavioral differences attributed to each weather condition through the calibration of the car-following model. Figure 108 shows a basic simulated roadway segment controlled by a reduced speed area. Identical demand was given to each segment representing the behavior from each weather condition. Investigation of the queue lengths for each weather condition in comparison with the isolated calibration parameter values raises some unexpected findings. For example, snow conditions were associated with the largest average following distance; however, the simulated queue is shorter than the other conditions. On the other hand, a close look at the reduced speed area (i.e., shaded rectangles in Figure 108) for light and moderate rain conditions shows uniform following distances, which is supported by the low CC6 parameter value. Assessment of each individual parameter and the parameter set as a cohesive unit reinforces the importance of the relationships between the parameter values—dictated by the parameter interactions in the underlying model logic—in computing the driver response predicted for each weather condition.

The simulation results from the VISSIM network presented in the Methodology section are provided in Table 60, Figure 109, and Figure 110. The purpose of this discussion is to validate and compare the simulated traffic flow resulting from the calibrated models with expected traffic flow characteristics represented in the literature and in macroscopic field data.

Eight different cases were tested: (i) default W99 parameter values with the desired speed computed from clear weather conditions and (ii–viii) calibrated W99 parameter values and desired speeds from each weather condition identified from the SHRP2 NDS data. The capacity was calculated as the maximum flow rate observed during the simulation; therefore, the speed and density at capacity were derived from their fundamental relationship with flow rate (i.e., speed observed at the maximum flow rate and density computed from the maximum flow rate divided by the optimal speed).

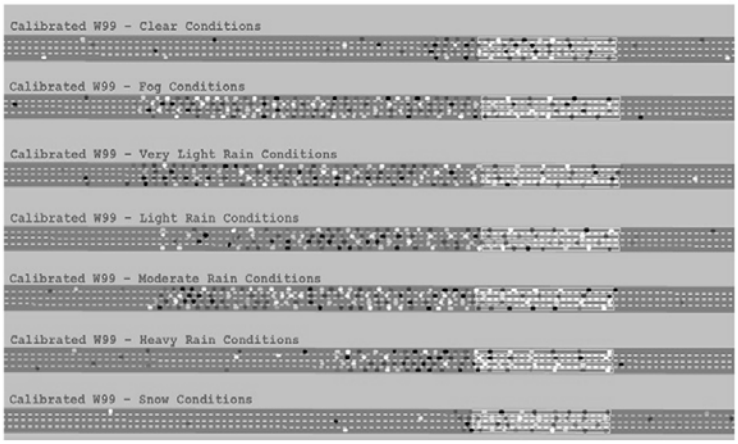

Figure 108 Application of Optimal W99 Parameters for Each Weather Condition in VISSIM

According to the 2010 HCM, the capacity of a basic segment in baseline conditions is 2,400 pcphpl (passenger cars per hour per lane) and 45 pcpmpl (passenger cars per mile per lane). Capacity reductions from these baseline conditions are expected in the simulated network illustrated in Figure 98 because of the sequence of weaving segments increasing the frequency of lane changes at merge and diverge points. Investigation of the results illustrates that when using the default parameters, the flow rate and density at capacity are substantially higher than the calibrated values. Moreover, interesting results are seen when investigating the calibrated behaviors. Intuitively, it is expected that the maximum capacity would be associated with clear conditions; however, capacity improvements are shown in moderate and heavy rain conditions and no capacity change is computed for very light and light rain. In clear conditions, the speed at capacity is 50 mph. In fog, very light rain, and light rain, this speed is shown to increase by approximately 22 percent and in moderate rain, heavy rain, and snow conditions, the speed at capacity decreases by approximately 11 percent. Further, the density at capacity is measured to be 38 pcphpl in clear conditions. Following the same pattern as the speed at capacity, a density reduction is evident in fog, very light rain, and light rain conditions, and an increase in density is shown in moderate rain, heavy rain, and snow conditions.

Table 60 Simulated Network Flow Characteristics: Flow, Speed, and Density at Capacity, and Jam Density

Condition	Flow Rate at Capacity [pc/hr/ln]		Speed at Capacity [mph]		Density at Capacity [pc/mi/ln]		Jam Density [pc/mi/ln]	
	Measured	%Change from Clear	Measured	%Change from Clear	Measured	%Change from Clear	Measured	%Change from Clear
Default	2475	-31.0%	34.1	31.8%	73	-92.0%	97	-14.1%
Clear	1890		50.0		38		85	
Fog	1845	2.4%	60.3	-20.5%	31	19.0%	74	12.9%
Very Light Rain	1890	0.0%	61.8	-23.5%	31	19.0%	71	16.5%
Light Rain	1890	0.0%	61.4	-22.8%	31	18.6%	71	16.5%
Moderate Rain	1980	-4.8%	45.7	8.6%	43	-14.6%	69	18.8%
Heavy Rain	2070	-9.5%	44.3	11.4%	47	-23.6%	73	14.1%
Snow	1845	2.4%	44.0	12.0%	42	-10.9%	79	7.1%

* A negative percent change means the capacity is larger for the measured condition compared with the baseline clear conditions.

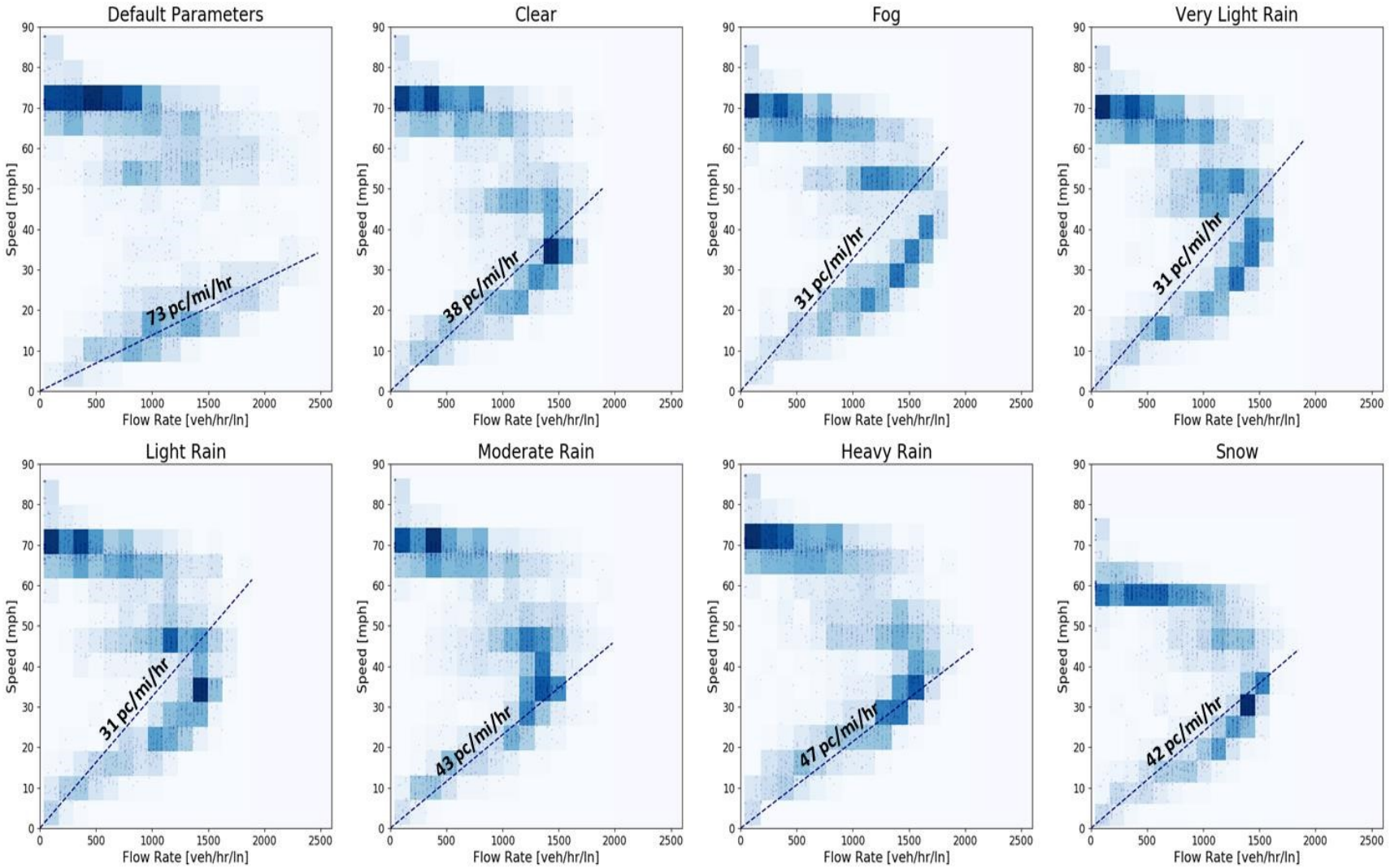

Figure 109 Simulated Speed – Flow Rate Relationship for Driving Behavior Calibrated from Each Weather Condition

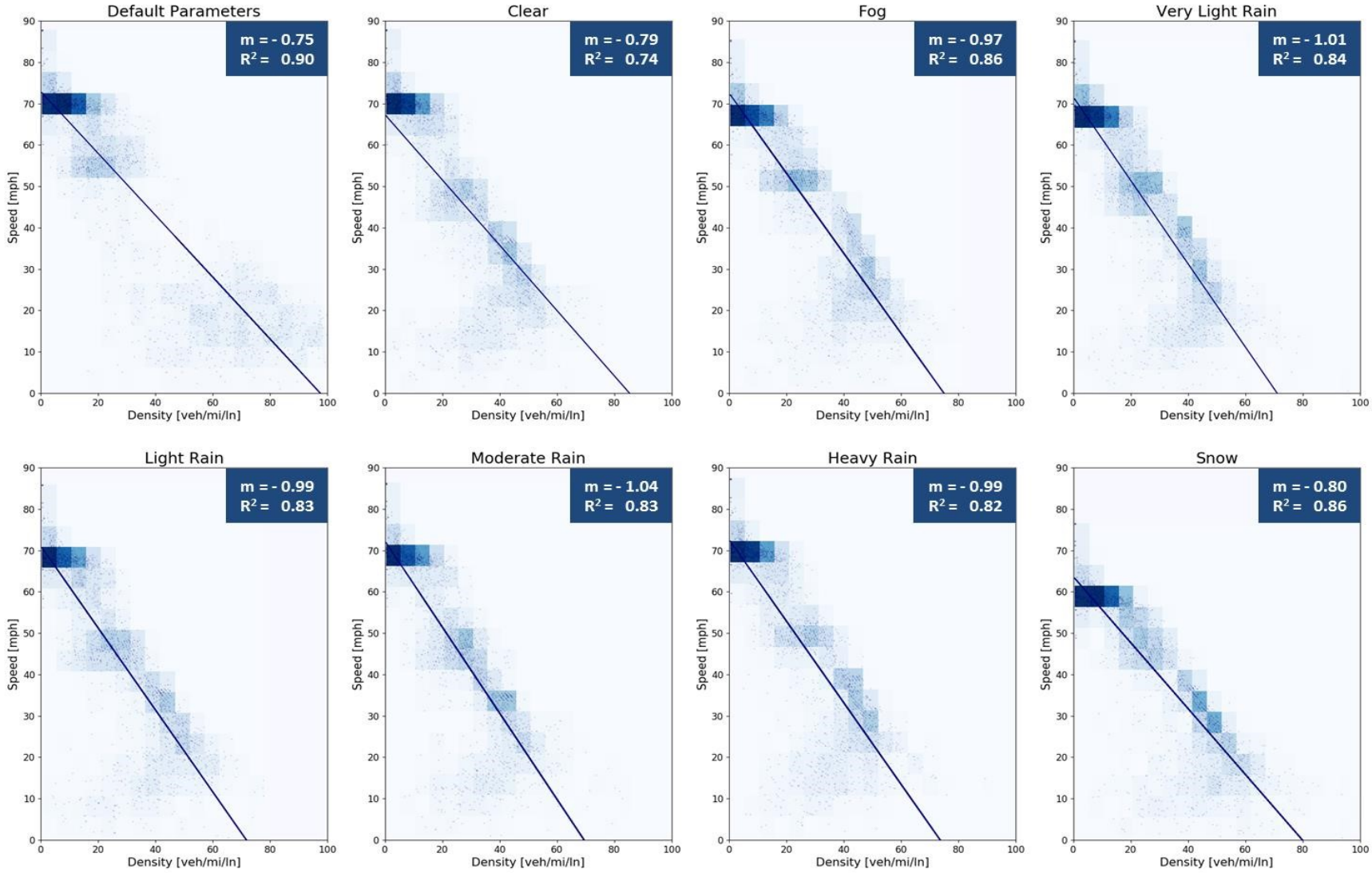

Figure 110 Simulated Speed – Density Relationship for Driving Behavior Calibrated from Each Weather Condition

The projection of jam density—estimated from Greenshield's hypothesis of a linear relationship between speed and density (*397*) shown in Figure 110—shows that the default parameters predicted a jam density of 97 pcpmpl. In calibrated clear conditions, the jam density is shown as 85 pcpmpl. Contrary to the traffic flow characteristics at capacity, when comparing all weather conditions, the jam density is highest in clear conditions and reduced for all adverse conditions.

Exploration of the predicted traffic flow in moderate and heavy rain conditions—the conditions that experienced an increase in capacity from the baseline clear conditions—shows a decrease in speed at capacity of approximately 10 percent. Similarly, they demonstrate a nearly 20 percent increase in optimal density. Further, this suggests that the predicted response of drivers in different weather conditions do not uniformly reduce the capacity; rather, these behaviors cause a shift in driver behavior which results in a change in traffic flow evident in the way traffic flow destabilizes. This phenomenon is illustrated in the fundamental diagrams in Figure 109 and Figure 110.

Initial inspection of Figure 109 and Figure 110 shows that traffic flow exhibited from the default parameters not only projects substantially higher flow rate and density values, but also forms a less defined pattern (i.e., greater spread in values resulting in less uniformity) than any of the calibrated parameter sets. The dark color on the upper edge of the default histogram indicates that the simulated vehicles traveled at their desired speed with larger flow rates compared with other conditions, indicating that the drivers' behavior was less affected by the surrounding traffic.

The speed–flow relationships for moderate and heavy rain conditions indicate that the maximum flow rate occurred at a lower speed than most other conditions, facilitating a density that bisects the oversaturated flow at the bottom of the curve. Comparatively, in clear conditions, in fog, very light rain, and light rain, the maximum flow rate occurs at a higher travel speed, indicating greater instability in the queue discharge flow (i.e., the flow located between undersaturated—top of curve— and oversaturated—bottom of curve). While very light and light rain conditions did not result in a change in capacity from clear conditions, Figure 109 illustrates that the simulated driving behavior was not the same for these three conditions.

In both very light rain and light rain conditions, the density is smaller because the speed at capacity is higher; this could be caused by a more rapid decline in traffic flow caused by the adverse weather conditions and drivers' reluctance to change their behaviors. In moderate and heavy rain conditions, however, drivers appeared to be more proactive in adjusting their behavior, that is, exhibiting a quicker speed reduction, which in turn resulted in greater roadway capacity.

Investigation of the calibrated weather conditions showed that the steepest slope—interpreted as the steepest decline from free flow to jam density—is associated with moderate rain conditions followed by very light rain, light rain, and heavy rain conditions. Intuitively, the steeper the slope, the quicker the traffic flow deteriorates; this results in a lower jam density. Clear conditions exhibited the most gradual decline of all simulations with calibrated parameters, followed closely by snow conditions.

Microsimulation of Variable Speed Limit

Preliminary Analysis

Currently, Wyoming has four VSL corridors on Interstate-80 covering approximately 145 miles. These VSL corridors have VSL signs spaced on average between 5 and 7 miles and have speed radar and RWIS equipment installed at each VSL sign location. The current VSL logic is primarily based on several weather-related variables, including surface condition, relative humidity, visibility, surface temperature, and wind speed. Although previous studies revealed that the current VSL logic has improved the operational and safety performance on the corridors, it lacks the integration of one of the most important factors that are "human factors" (*347*). The SHRP2 NDS has opened up unprecedented opportunities to investigate driver behaviors in naturalistic settings. The research team thoroughly investigated driver behavior using this unique dataset and found many insightful findings which could be useful to update current VSL algorithm. More details of the investigated driver behaviors are already discussed in Chapter 2. However, one major question is whether the current algorithm needs any further improvements. To answer this question, the research team thoroughly investigated the effectiveness of the VSL logic in terms of safety, operation, and speed compliance under various weather conditions. Based on previous literature drivers are considered in compliance with the posted speed limit if they are traveling at no more than 5 mph over the posted speed (*398*).

Figure 111 and Figure 112 shows the speed compliance and variation by speed limit in different road surface condition and visibility levels. It is worth mentioning the categories of the road surface and visibility were selected based on WYDOT guidelines (*398*). These figures provided the following important findings:

- Truck compliance was always higher than passenger car compliance.
- Drivers were more compliant with higher posted speed limits. In other words, it was found that driver compliance rate, in general, was lower in lower speed limit.
- Considering road surface conditions, overall drivers are more compliant in adverse surface conditions (e.g., snowy, wet, and icy) compared to dry surface conditions.
- Considering visibility levels, similarly, drivers were more compliant in moderate and poor visibility compared to good visibility. These results are not surprising considering the fact that drivers expect the post speed limits to be higher in clear conditions and therefore if lower speed limits are posted in such conditions, they disregard the posted speed limits. These findings indirectly show that the current algorithm is not always representative and hence needs to be updated.

In order to further investigate the effectiveness of the existing algorithms, the research team also selected a storm event that occurred on January 9, 2017. The findings are reported in Table 61 and Figure 113, which revealed that driver compliance varied significantly over spatial dimensions. Drivers were less compliant in some locations on the VSL corridor, for instance, the compliance rate at milepost 11.86 near sensor "2359" was found to be only around 46 percent. These results indirectly indicate that weather sensors in some locations might provide erroneous weather data which resulted in posted speed limits that were not consistent with the actual weather condition. Further, the research team also investigated driver speed compliance temporally. As an example, Figure 114 demonstrates the temporal speed profile at milepost 329.88 near sensor "2178". As observer previously, drivers were found to be less compliant at lower speed limits.

Table 61 Speed Compliance during a Storm Event (January 9, 2017)

Sensor	Lat	Long	Milepost	Compliance
2359	41.267286	-110.836625	11.86	**45.9 percent**
2372	41.273333	-110.807992	13.45	93.2 percent
3296	41.524088	-109.437853	91.99	74.4 percent
1269	41.587455	-106.179183	273.85	84.1 percent
2146	41.246296	-105.441189	322.6	62.1 percent
2178	41.152375	-105.395392	329.88	83.6 percent

Figure 111 Speed Compliance and Variation by Speed Limit in Different Road Surface

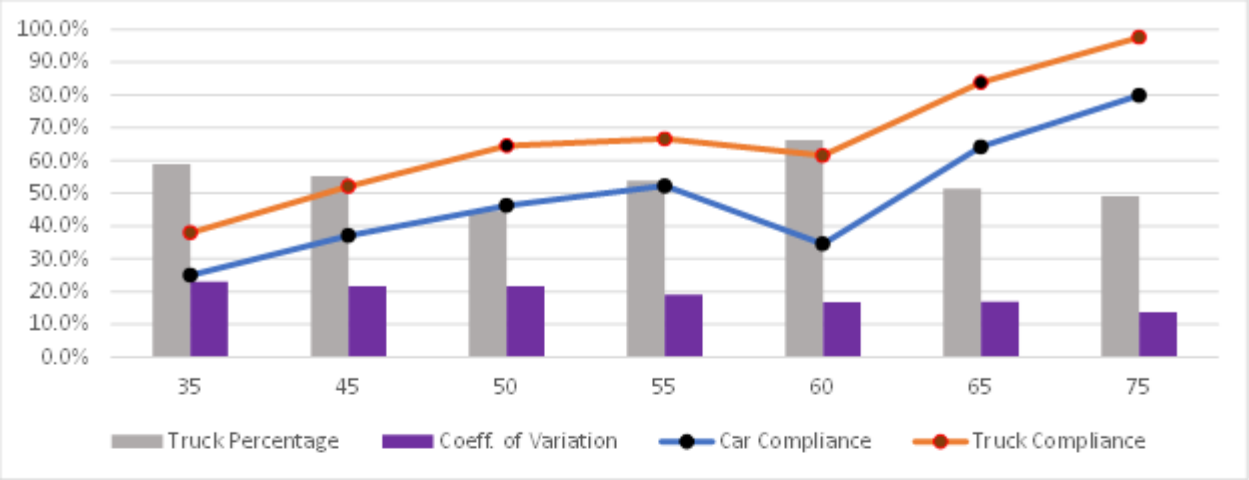

Good (Visibility>0.95 miles)

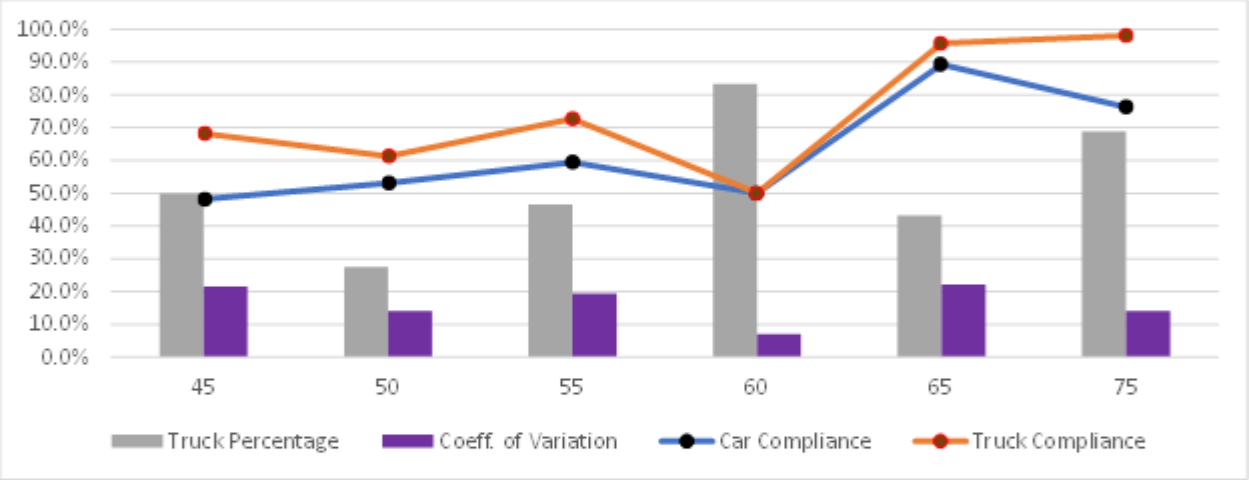

Modarate (Visibility between 0.57 and 0.95 miles)

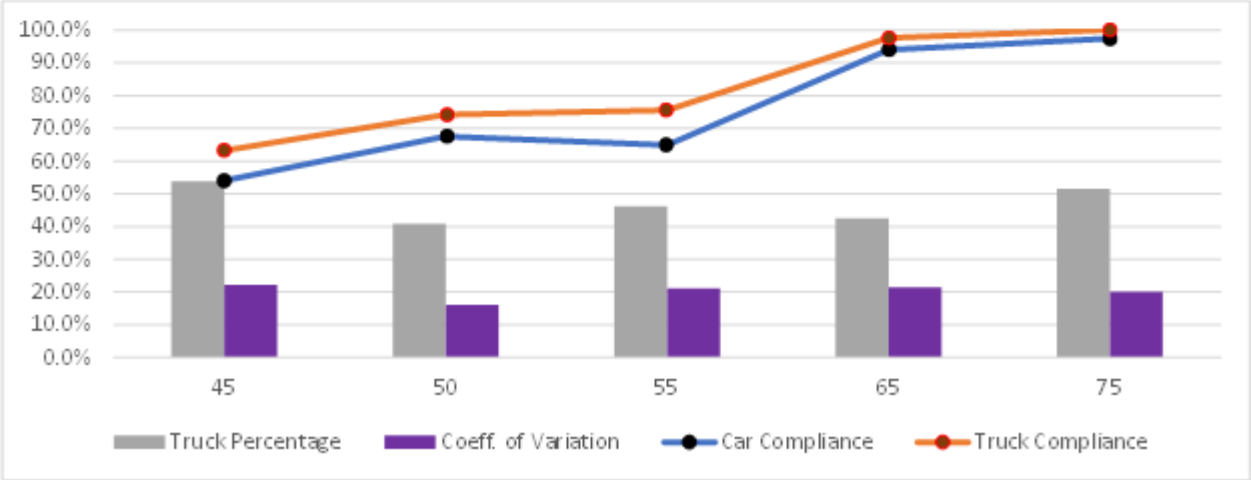

Poor (Visibility<0.57 miles)

Figure 112 Speed Compliance and Variation by Speed Limit in Different Visibility Levels

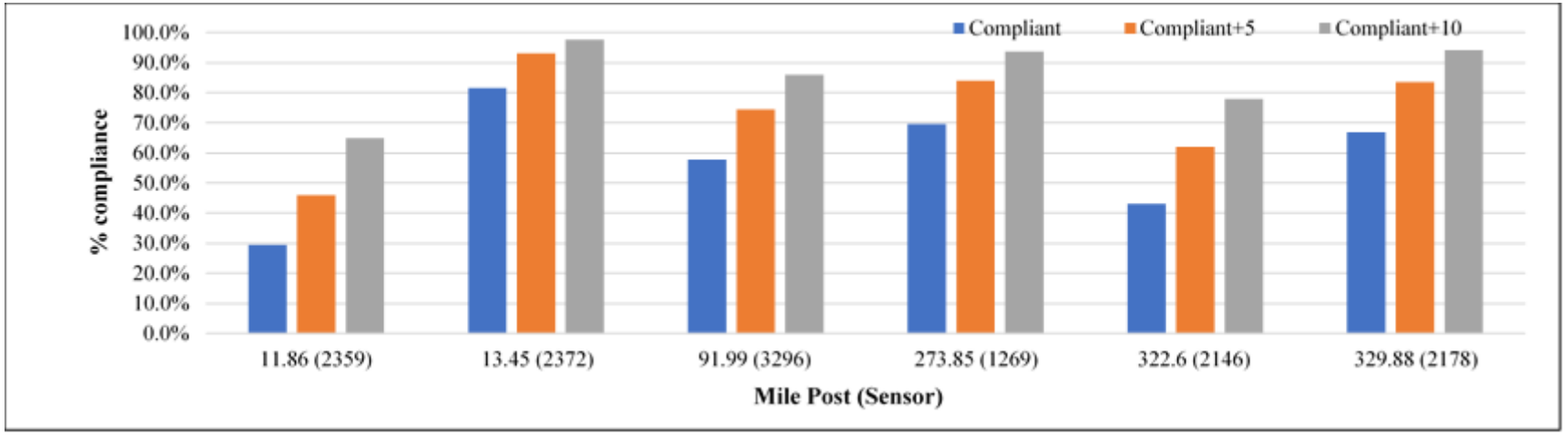

Figure 113 Speed Compliance at Various Sensor Locations During a Strom Event (January 9, 2017)

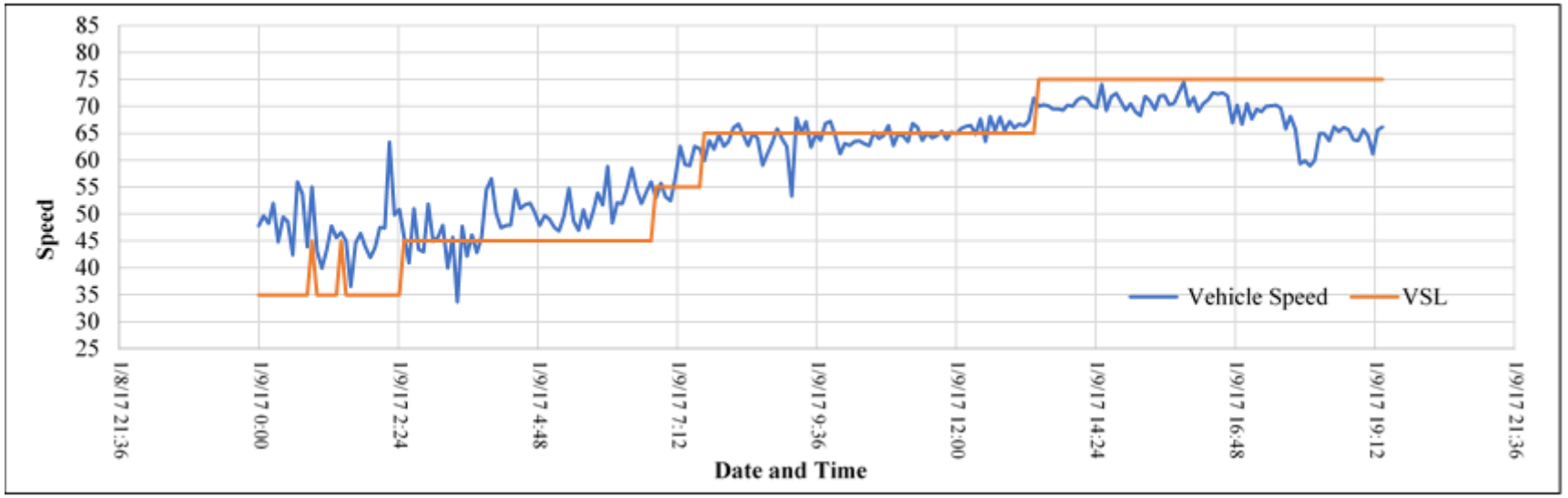

Figure 114 Speed Profile During a Strom Event at Sensor 2178 (January 9, 2017)

Updated VSL Algorithm

Considering the findings from preliminary analysis, the research team updated the current VSL algorithm that has two modules, namely weather module and driver behavior/ compliance module. The weather module is mainly based on the current VSL logic, as illustrated in Figure 115. The weather module considered five weather-based variables: surface condition, relative humidity, visibility, surface temperature, and wind speed. In-depth descriptions of the current VSL logic can be found in (*343*). The next module is the compliance module which takes the final speed limits from the first module (weather module) and updates it based on real-time driver behavior. Figure 116 illustrates the detailed logic of the compliance module. The primary steps of the compliance module are described below:

- First, the algorithm will define the maximum and minimum VSL. The VSL_{min} is the final speed limit from the weather module and VSL_{max} is the maximum speed that is allowed to be posted. The research team used a 10 mph increment for the VSL_{max}, however, this increment could be modified based on engineer judgment, real-time traffic and weather data, as well as driver behavior.
- Next, the algorithm will flag a location on the corridor if the speed compliance in less than 50 percent and the co-efficient of speed variation is more than 20 percent. These thresholds were selected based on engineering judgment and preliminary analysis.
- Consequently, the algorithm will check the quality of the VSL data at the flagged location based on several matrices, as listed in Table 62 (*399*). The VSL database consists of data from speed sensors, RWIS, and webcams.

Table 62 Metrics to Measure Data Quality

	Metric	Definition	How to calculate
1	Ratio of Data to Errors	How many errors do you have relative to the size of your data set?	Divide the total number of errors by the total number of items.
2	Number of missing Values	Empty values indicate information is missing from a data set.	Count the number of fields that are empty within a data set.
3	Data Transformation Error Rates	How many errors arise as you convert information into a different format?	How often does data fail to convert successfully?
4	Amounts of Dark Data	How much information is unusable due to data quality problems?	Look at how much of your data has data quality problems.
5	Data Time-to-Value	How long does it take to get value from its information?	Decide what “value” means to your firm, then measure how long it takes to achieve that value.

- If the data quality is good, instead of updating the posted speed limit, the algorithm will focus on increasing enforcement and providing speeding alerts via DMS and 511 apps.
- However, if there is some problem with the data, the algorithm will update the speed limit based on real-time driver speed behavior until the issue with the data at a location on the VSL corridor is fixed.
- Finally, the posted speed limits will be updated at a 5 mph increment up to VSL_{max} following the logic shown in Figure 116.

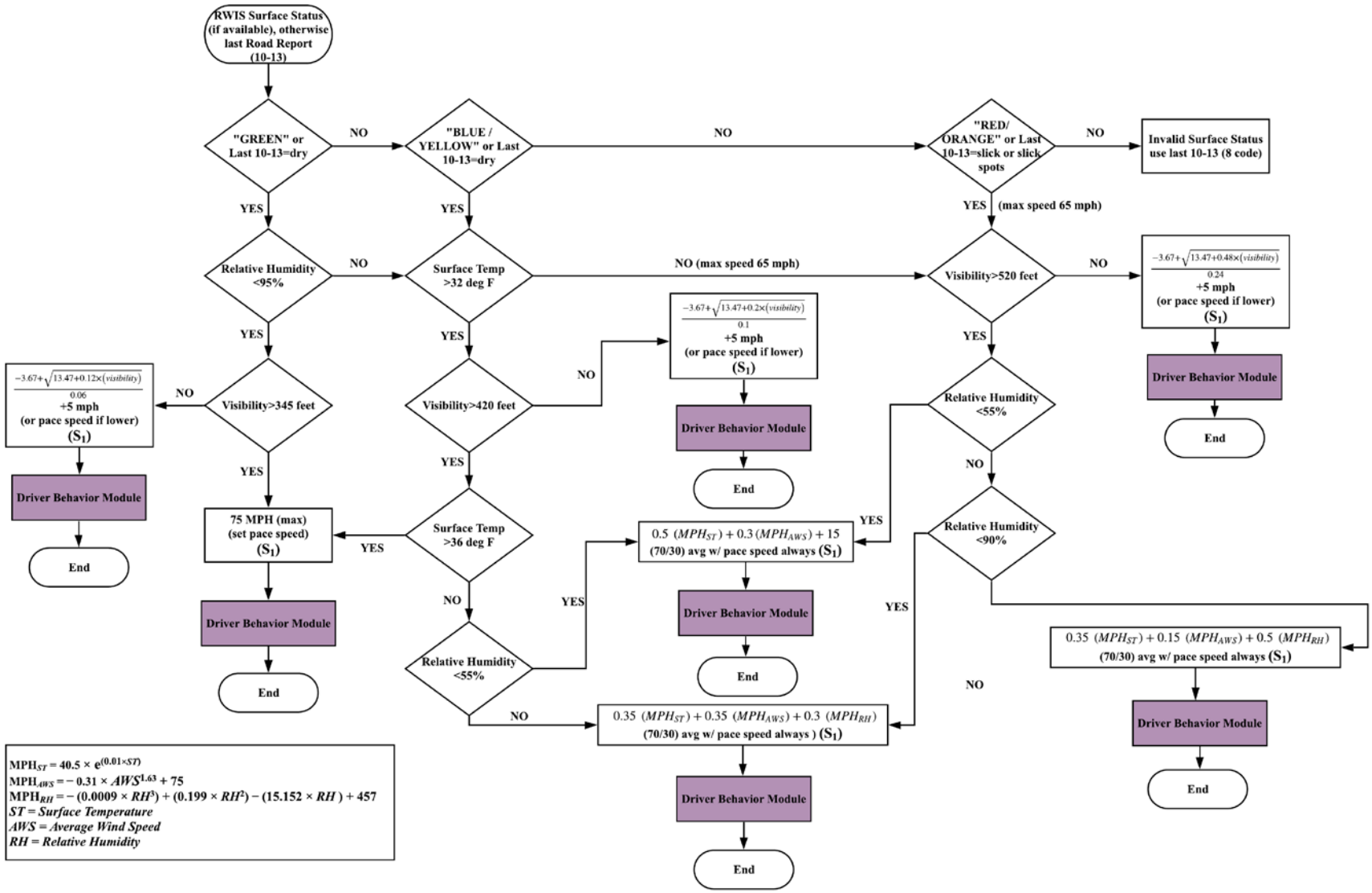

Figure 115 Updated VSL Algorithm (Weather Module)

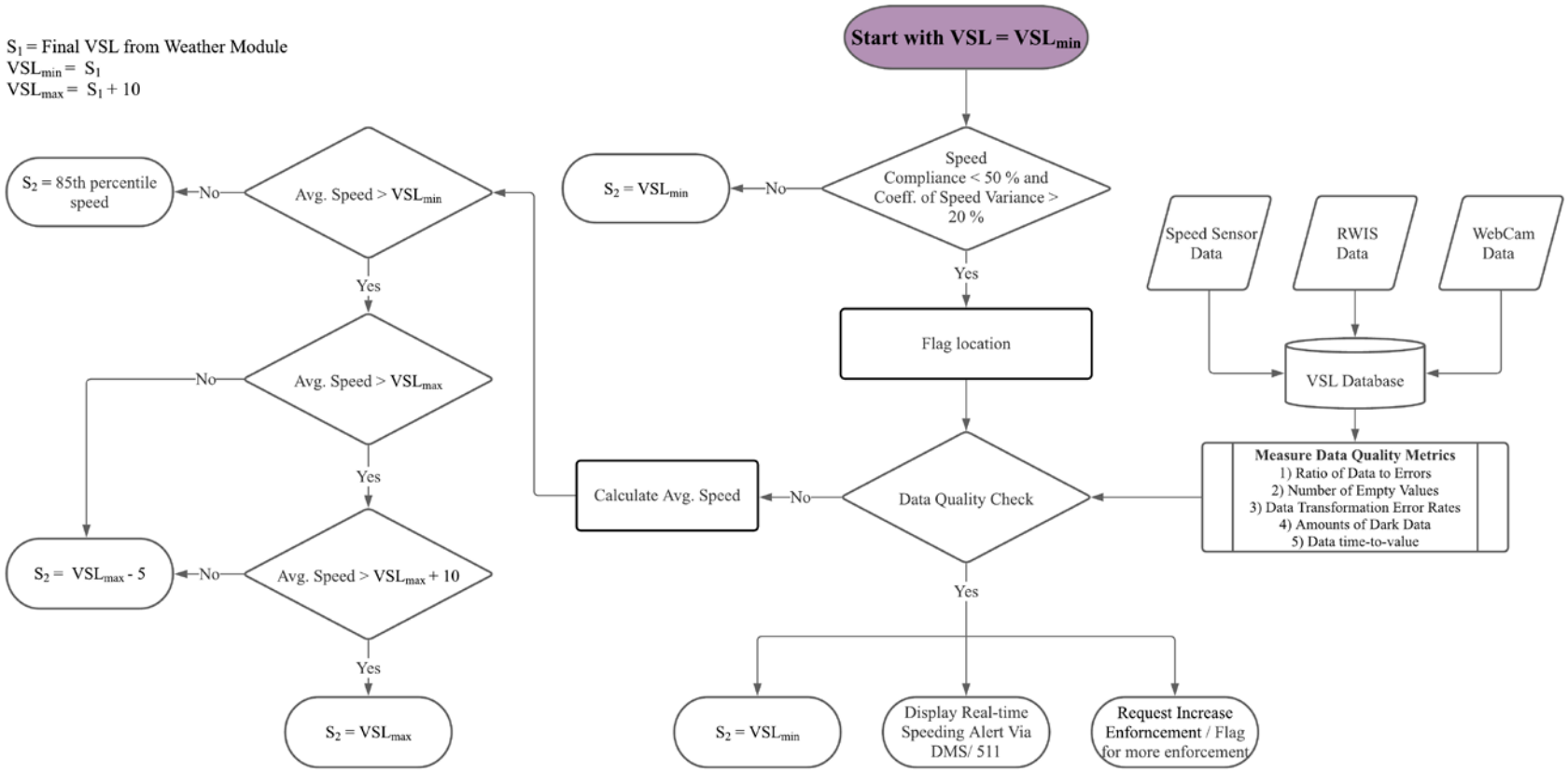

Figure 116 Updated VSL Algorithm (Compliance Module)

Performance Evaluation

The effectiveness of the updated VSL algorithm was examined from operational and safety perspectives. Various performance measures including total travel time, average delay, and average speed were utilized to analyze and compare the operational characteristics of the current and updated VSL algorithms. Figure 117 to Figure 119 and Figure 122 to Figure 124 illustrate the operational evaluation of the existing and updated VSL in snow and rain conditions, respectively. As for the snow conditions, it was observed that total travel and average delay were lower for the updated algorithm compared to the existing algorithm. More specifically, the travel time was reduced from around 6.3 to 4.9 hours and the average delay per vehicle was reduced from around 1 to 0.6 seconds. For the average speed, it was found that drivers' speed increased from about 34 to 49 mph considering the updated algorithm. Similar trends were also observed for rain conditions where travel time and average delay per vehicle were found to be lower and average speed was higher after implementing the updated VSL algorithm.

As mentioned earlier, this study considered SSAM to identify the probable conflicts during simulations. To evaluate the safety effectiveness of the updated VSL, this study adopted three different levels of TTC threshold: high risk (1.5 s), medium risk (3.5 s), and low risk (9 s) to qualitatively compare the simulated conflicts under various weather condition on the VSL corridor. The results of the simulated number of conflicts based on three TTC thresholds for the existing and updated algorithm in snow are provided in Figure 120 and Figure 121. In addition, the corresponding results for rain conditions are provided in Figure 125 and Figure 126. It was observed that conflicts in all TTC thresholds were found to be lower for the updated algorithm compared to the existing algorithm in snow conditions, as shown in Figure 120. For instance, the high-risk conflicts per hour per vehicle were reduced from 3 to 2.2 using the updated algorithm. Similarly, total number of conflicts was reduced for medium and low-risk scenarios when considering the updated algorithm. In addition, rear-end and lane change conflicts were found to be lower for the updated algorithm, as observed in Figure 121. Considering the rain conditions, overall conflicts per hour per vehicle were found to be lower after incorporating updated algorithm similar to snow conditions. More precisely, the rear-end conflicts were reduced from 28.3 to 13.8, and lane change conflicts were reduced from 29.5 to 9.8, respectively.

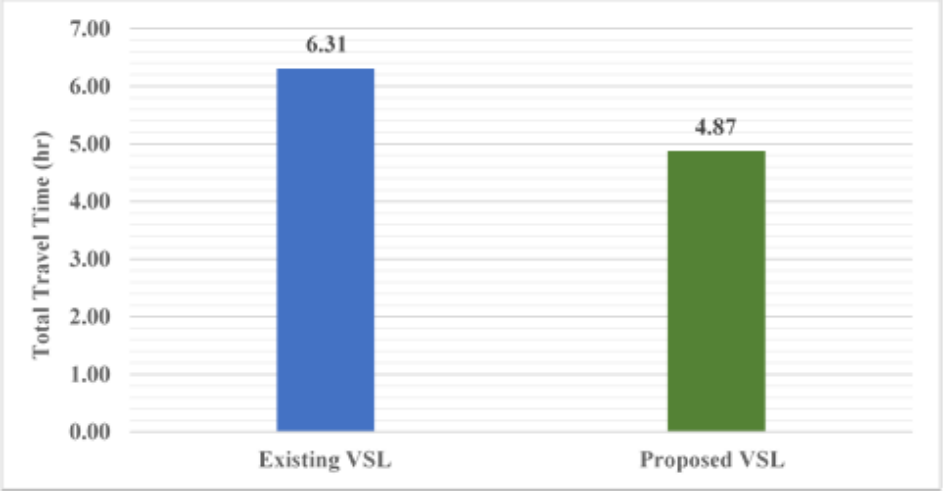

Figure 117 Evaluation of Total Travel Time in the Existing and Updated VSL in Snow

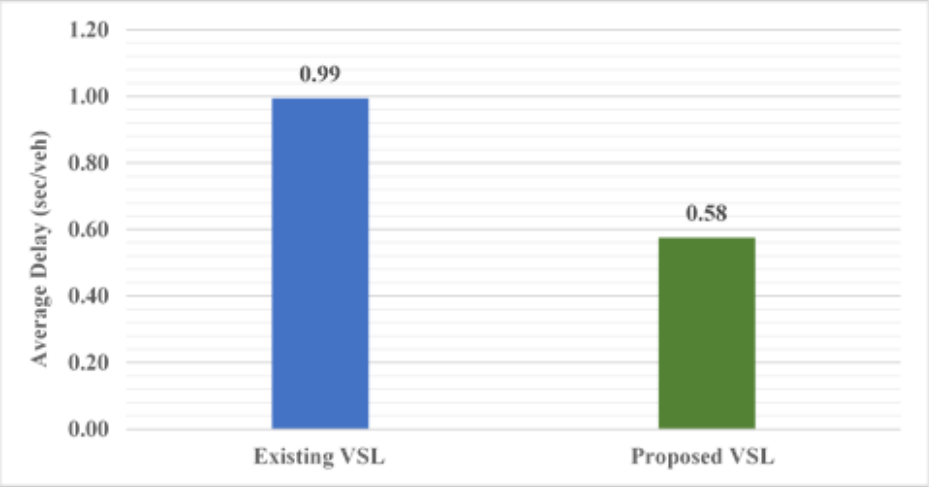

Figure 118 Evaluation of Average Delay in the Existing and Updated VSL in Snow

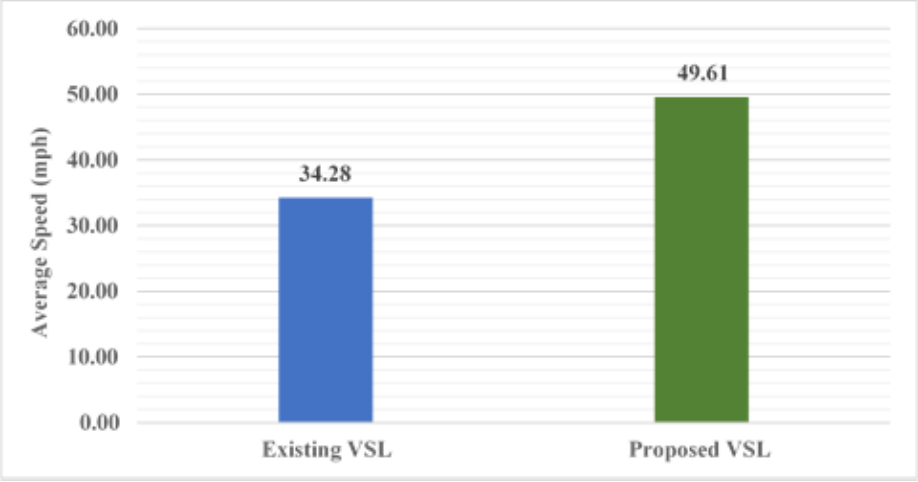

Figure 119 Evaluation of Average Speed in the Existing and Updated VSL in Snow

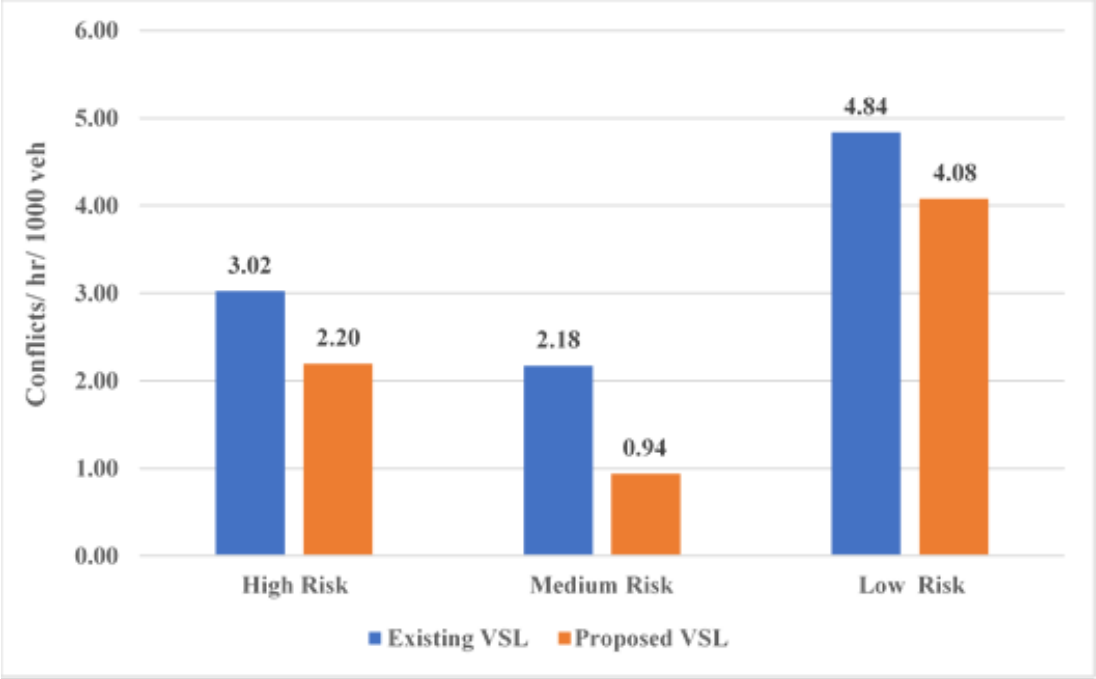

Figure 120 Safety Evaluation of the Existing and Updated VSL in Snow Based on Risk Level

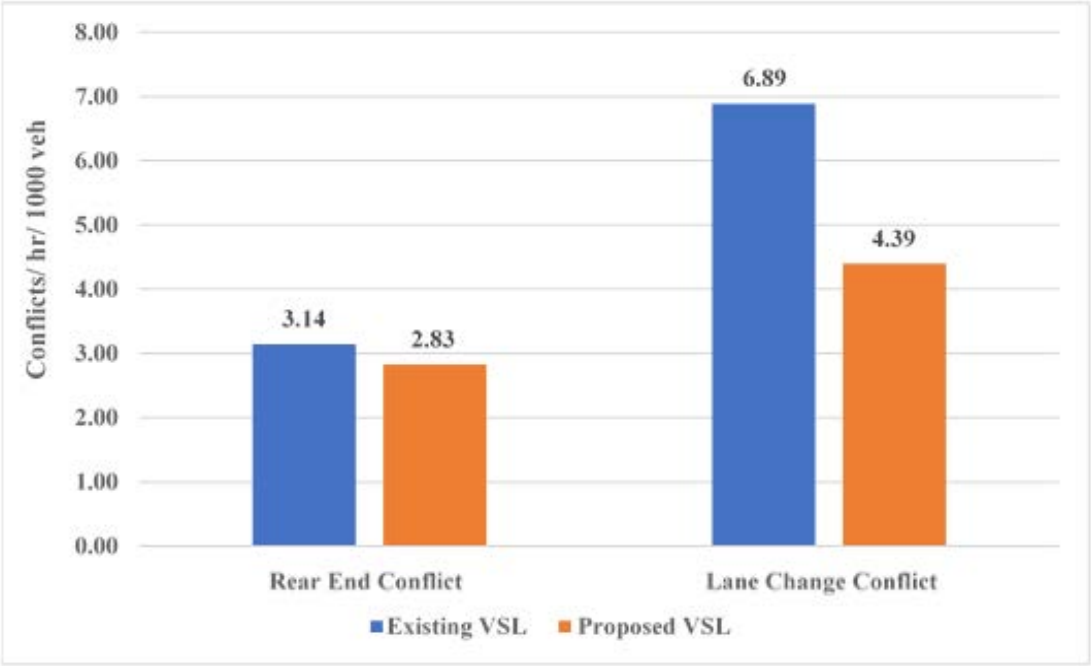

Figure 121 Safety Evaluation of the Existing and Updated VSL in Snow Based on Conflict Type

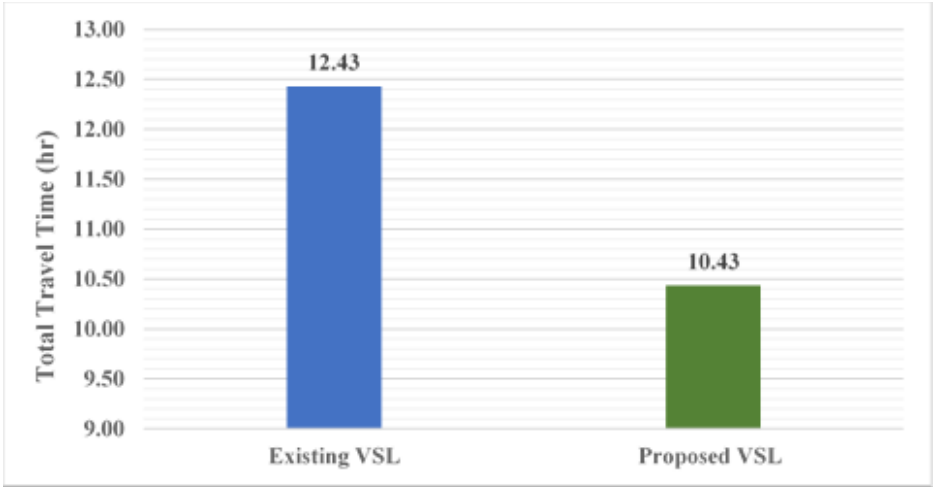

Figure 122 Evaluation of Total Travel Time in the Existing and Updated VSL in Rain

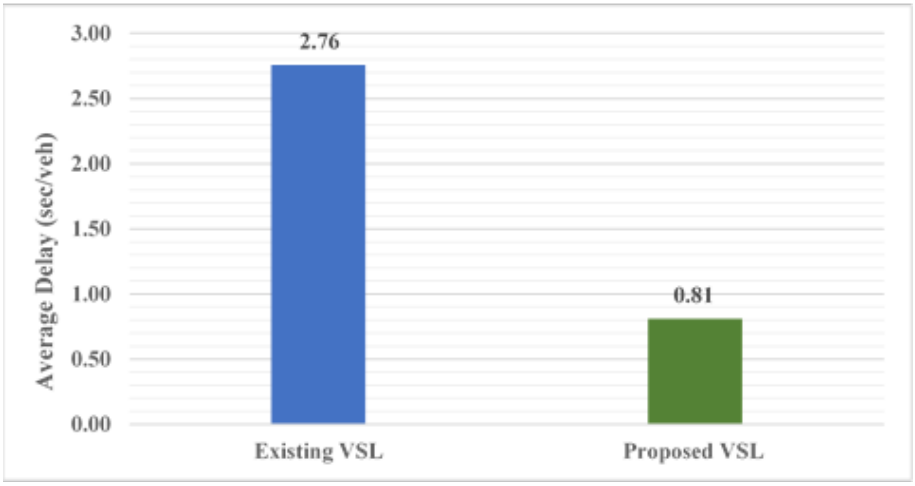

Figure 123 Evaluation of Average Delay in the Existing and Updated VSL in Rain

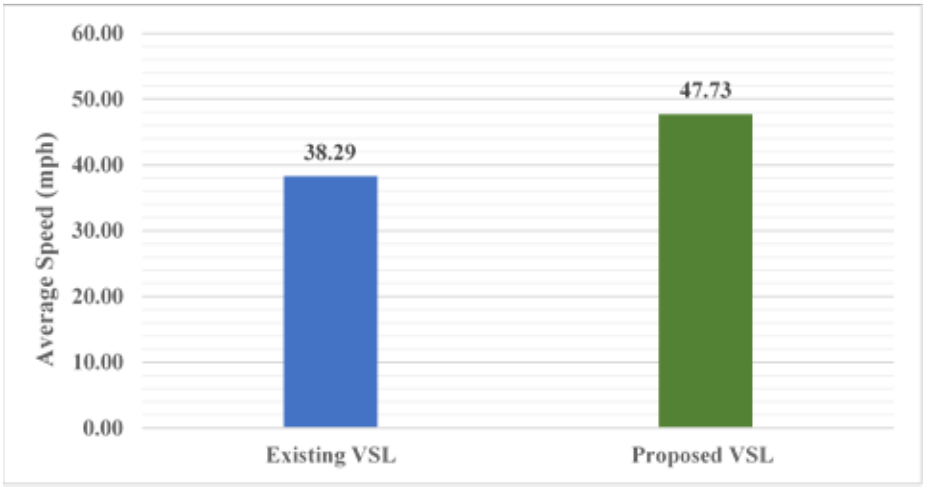

Figure 124 Evaluation of Average Speed in the Existing and Updated VSL in Rain

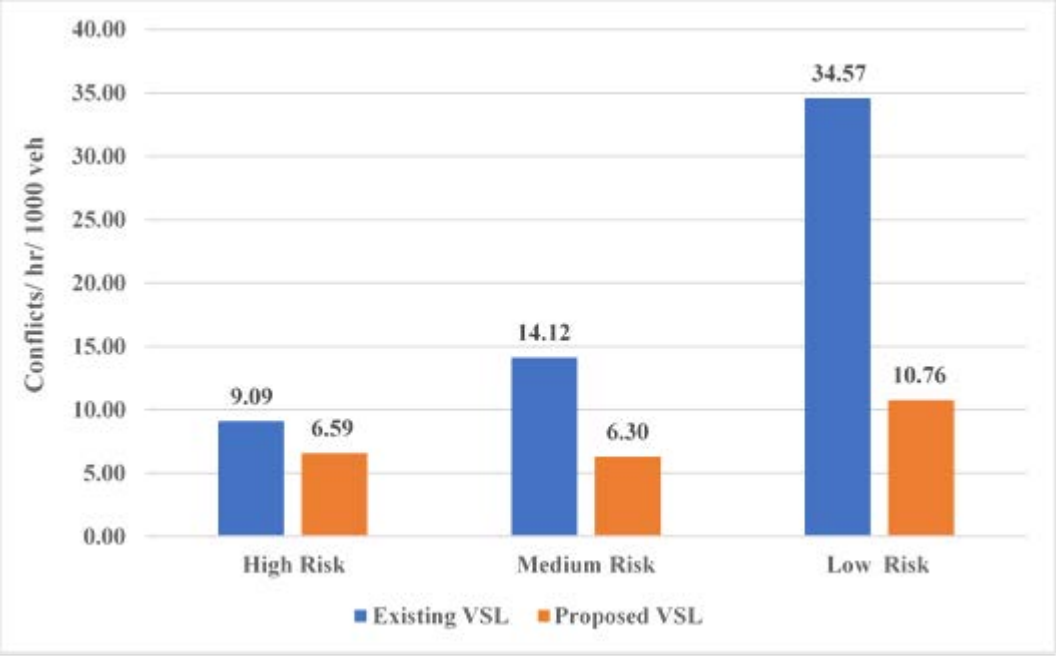

Figure 125 Safety Evaluation of the Existing and Updated VSL in Rain by Risk Levels

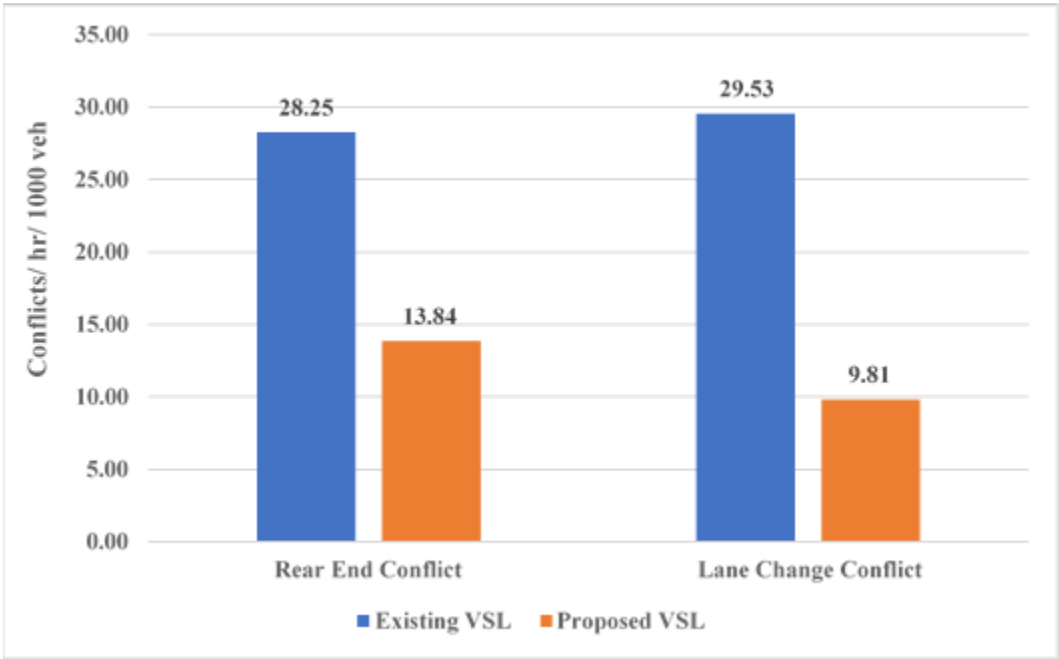

Figure 126 Safety Evaluation of the Existing and Updated VSL in Rain by Conflict Types

Chapter 8. Conclusions and Recommendations

Research Summary and Key Findings

Driver Behavior Investigation

Several driver behaviors, including lane keeping, lane changing characteristics, gap acceptance, and speed selection, have been thoroughly investigated. First, a lane-keeping model was calibrated to assess the factors contributing to the driver lane-keeping behavior in different weather conditions. Different environmental, traffic, driver, and roadway characteristics with some of the interaction terms were found to be significant in the developed ordered logistic regression model. Based on the developed lane-keeping model, drivers in affected visibility conditions were 1.37 times more likely to have higher SDLP (poor lane keeping) than drivers who were driving in good visibility conditions. Drivers in congested traffic conditions had better lane-keeping ability than drivers who were driving in free-flow conditions. Additionally, it was found that experienced drivers were 68 percent more likely to have better lane-keeping ability than inexperienced drivers in wet surface conditions. To enhance the modeling approach, association rules mining was performed to analyze driver lane-keeping performance under foggy weather conditions. Keeping SDLP as a consequent, some interesting findings were observed by mining association rules among a set of environmental, roadway geometry, traffic and driver demographics. It was found that affected visibility was associated with poor lane-keeping performance in several rules. Male drivers were found to be dominant in the rules for having poor lane-keeping performance compared to female drivers. In addition, a higher number of lanes and presence of curve were found to be significant factors for having higher proportions of poor lane-keeping performance. On the other hand, rules from the good lane-keeping performance indicated that visibility had no/little effect on good lane-keeping performance. However, drivers who drove equal or more than 12,000 miles were found to have better lane keeping.

After investigating lane-keeping ability, this research further analyzed lane changing characteristics based on aggressiveness. According to the several hypotheses tested in fog and clear weather under various traffic conditions, it was found that the mean of lane-changing durations in heavy fog was significantly higher than clear weather in mixed-flow conditions, which indicated that drivers were more cautious in heavy fog conditions under mixed-flow than clear weather. In addition, no significant differences were observed between the mean durations of mixed-flow lane changes to the left and right in both fog and clear weather, which might imply the cooperative behavior of driver to avoid vehicle collisions. All the lane-changing durations followed lognormal distribution except distant fog under mixed-flow conditions, which fitted gamma distribution. The range of the lane-changing durations was observed from 1.69 to 15.87 s with a mean of 4.86 to 5.47 s in lane-changing analysis. The k-means clustering analysis was utilized to identify various driver types (i.e., conservative and aggressive) based on their number of lane-changing events per mile and speed differences from speed limits in fog and clear weather under different traffic conditions. The clustering results showed that aggressive drivers in all weather and traffic condition had higher speed differences in comparison with conservative drivers. In addition, significant differences in number of lane-changing events and speed differences were observed between aggressive and conservative drivers. Drivers' questionnaire responses collected by SHRP2 were compared with the cluster analysis results. It was observed that drivers' responses related to foggy weather were more consistent with survey

questionnaires compared to their responses in clear weather during free-flow conditions. The results of the mean lane-changing durations of the two driver types concluded that both conservative and aggressive drivers in heavy fog conditions had longer lane-changing durations than in clear weather, which might indicate that drivers' lane-changing durations were affected by the reduced visibility in heavy fog conditions.

Next, the research provided valuable insights into lane-changing gap acceptance behavior. Summary statistics of lead and lag gaps showed that several statistics of lead gaps (i.e., mean and maximum) are relatively higher than lag gaps indicating that the perception of lag gaps are inconsistent compared to their lead gaps. Additionally, it was observed that drivers lead and lag gap acceptance followed gamma and lognormal distributions, respectively. The MARS models of lead and lag gap were developed to account for complex relationship between variables affecting gap acceptance behavior. Different factors that would affect gap acceptance were identified under several conditions using the developed knots in the MARS model. Considering all the explanatory variables in both models, relative speed between lane-changing vehicle (LCV) and lead vehicle (LV), as well as LCV speed turned out to be the most important variables affecting lead and lag gap acceptance, respectively. In addition, traffic conditions, acceleration of LCV and FV, and roadway geometric characteristics had significant effects on gap acceptance behavior.

Finally, the research investigated speed selection behavior in different adverse weather conditions. The preliminary analysis revealed that speeds follow Weibull distribution in adverse weather and normal distribution in clear weather. In addition, it was found that drivers reduced their speeds by 5.95 percent, 15.89 percent, and 3.91 percent due to the presence of rain, snow, and fog, respectively. The results from the association rule mining indicated that speeds more than 5 mph were highly associated with clear weather conditions, dry road surface, clear visibility, less experienced and young drivers; whereas a speed reduction of more than 5 mph was highly associated with snowy weather, affected visibility, snowy road surfaces, and middle-aged and older drivers. The results of ordered logistic regression were also in line with the findings from the association rules mining. It was found that drivers were 1.45. 4.57, and 1.77 times more likely to reduce their speeds in rain, snow, and fog respectively, compared to their speeds in clear weather conditions. Several other weather-related factors, such as surface conditions and visibility, were also found to have a significant effect on driver speed selection.

Radar-Vision Algorithms to Process the Trajectory-Level Driving Data

This research presents a novel methodology that leverages forward-facing radar data to continuously predict driving state, identify homogeneous driving segments with the same driving state, and estimate events that caused the transition between driving states. A thorough understanding of driver behavior is necessary to forecast and operate a safe and reliable transportation network. Driver behavior models have historically used traffic simulations to inform planning decisions; however, more recently these models have been incorporated into Active Traffic Management Decision Support Systems housed in transportation agency Traffic Management Centers. Realistic depiction of driver behavior is critical to the success of these applications, and while many researchers have focused effort on developing, calibrating, and validating driver behavior, their research is limited in scope due to a lack of trajectory-level data. The SHRP2 NDS introduces a new opportunity to investigate driver behavior with a surplus of trajectory-level driving data that could be used to broaden the transferability and emphasize the importance of research findings for practical application. When used in parallel with its

complementary RID database, researchers can gather hundreds of trips from hundreds of drivers traversing specific roadway sections or in specific roadway conditions. In order to fully reap the benefits of this massive database, systematic processing procedures are needed to transform the available SHRP2 NDS data into a format in which driver behavior can easily be analyzed.

Detection and Prediction of Lane Change Maneuvers

The research also focused on developing trajectory-level lane change detection and prediction models. Through cutting-edge Machine Learning techniques, this research developed trajectory-level lane change detection models based on features from vehicle kinematics, machine vision, roadway characteristics, and driver demographics under different weather conditions with promising detection accuracy. With respect to all features, the RF model provided the highest overall detection accuracy of around 91.5 percent and 88.9 percent during validation and testing, respectively. In addition, the highest detection accuracy of 81.8 percent during validation and 79.9 percent during testing were observed in the RF model while excluding features based on machine vision. Moreover, it was found that the trained ANN model provided the highest accuracy of 80.1 percent and 77.1 percent during validation and testing, respectively, utilizing features based on only vehicle kinematics, indicating that the vehicle kinematics features have the potential to detect lane change maneuver with reasonable accuracy. Considering the results from the detection models, the study recommends to use RF model if all the data from different sensors are available and in absence of machine vision-based data (e.g., lane position offset), and ANN model if only vehicle kinematics data are available.

Similarly, considering different data availability, the subsequent study developed reliable and efficient machine learning based lane change prediction models utilizing a data fusion approach. Considering the Feature Set 1 (i.e., vehicle kinematics, machine vision, driver, and roadway geometric characteristics), the XGBoost model outperformed all other models with respect to its overall accuracy (97.0 percent during validation and 96.7 percent during testing) and F1-score (95.5 percent during validation and 94.9 percent during testing). In addition, the highest overall accuracy and F1-score of 97.3 percent and 95.9 percent during validation and 96.5 percent and 94.6 percent during testing, respectively, were observed in the XGBoost model based on features from vehicle kinematics (i.e., Feature Set 6). Moreover, XGBoost was found to be the only model that achieved a reliable and balanced prediction performance across all six feature sets. Furthermore, it has been observed that the tree-based models performed better compared to other models. Considering the detailed performance evaluation from the prediction models, the study recommends to use XGBoost model at predicting lane change maneuvers.

Detection of Surrogate Measures of Safety in Adverse Weather Conditions

Detecting near-crash events on freeways using continuous naturalistic data could be one of the essential approaches to enhance traffic safety in the era of CV. This research aimed to use the NDS data for an early investigation of SMoS on freeways that could be collected from CV in the future. So, this work attempts to identify those measures that would be helpful in assessing traffic safety using the wealth of vehicle kinematic data collected from CV. This research showed that continuous vehicle kinematics dataset could be used to understand the effect of rainfall on increasing the likelihood of near-crash events through variation in driver behavior and vehicle kinematics. Also, the research presented the change in vehicle kinematics signatures due to the change in weather condition and how far the driving patterns were different according to having a safe or risky driving event. It was shown in this study that speed, acceleration and deceleration rate, and yaw rate could be used as SMoS indicators to distinguish between normal

driving and near-crash events. The time chunking technique attempted in this study might help future studies in defining the interest zone of vehicle kinematics used as indicators of risk for near-crash events. The significant time zone was determined to be the 11-seconds preceding the event timestamp using a parametric model and 23-seconds using non-parametric models. Therefore, the time zone of interest resulted from non-parametric models is more accurate in detecting near-crash events compared to the logistic regression model.

Weather Detection

To ensure safe driving in adverse weather, it is essential to detect and provide real-time weather and road surface conditions to road users. This study proposes some unique techniques based on machine learning and SHRP2 NDS trajectory-level video data to enhance the reliability of real-time weather detection. First, a snow detection system was developed using the in-vehicle video camera from the SHRP2 NDS dataset capable of detecting clear, light snow, and heavy snow conditions. To train the snow detection models two texture-based image features including Grey Level Co-occurrence Matrix (GLCM) and Local Binary Pattern (LBP), and three classification algorithms including Support Vector Machine (SVM), K-Nearest Neighbor (K-NN), and Random Forest (RF) were used. The overall prediction accuracy of the SVM, K-NN, and RF models based on the GLCM based features was found to be around 86 percent, 85 percent, and 84 percent, respectively. After that, the same technique was applied considering the LBP-based features, which improved the prediction accuracy significantly with overall prediction accuracies of 96 percent, 93 percent, and 94 percent for SVM, K-NN, and RF models, respectively.

After the effective development of snow detection systems, this research explored the possibility of detecting fog using the SHRP2 NDS dataset. To enhance the classification accuracy, the next study utilized several promising deep learning techniques, including Deep Neural Network (DNN), Recurrent Neural Network (RNN), Long Short-Term Memory (LSTM), and Convolutional Neural Network (CNN), to detect the levels of fog. Python programming on the TensorFlow Machine Learning library was used for training the deep learning models. During the training process, two optimizers, including Adam and Gradient Descent, were used. The overall prediction accuracy of the DNN, RNN, LSTM, and CNN using the Gradient Descent optimizer was found to be around 85 percent, 77 percent, 84 percent, and 97 percent, respectively. Much improved overall prediction accuracy of 88 percent, 91 percent, 93 percent, and 98 percent for the DNN, RNN, LSTM, and CNN, were observed considering the Adam optimizer, respectively.

The research then experimented with more refined categories of adverse weather and defined seven levels of adverse weather: clear, light rain, heavy rain, light snow, heavy snow, distant fog, and near fog. Extensive data reduction steps were taken to identify and classify the levels of adverse weather conditions to form a unique ground truth dataset from the massive SHRP2 NDS. To further improve the detection accuracy, this study then crafted a novel CNN-based weather detection algorithm and named it RoadweatherNet. The evaluation results revealed that the RoadweatherNet can provide a high degree of performance in detecting seven weather categories with an overall detection accuracy of around 93 percent.

Integration of SHRP2 NDS Findings: Weather-based Microsimulation and VSL

The research seeks to contribute to the state-of-practice in microsimulation modeling by applying a methodology to use the SHRP2 NDS data to calibrate car-following models as a function of specific weather conditions. The Wiedemann 1999 model was calibrated using 1,206 SHRP2

NDS trips and optimal parameter values were derived to represent each observed weather condition. These parameter values were investigated in relation to their physically interpretable meaning, which underscored the existence of parameter interaction in predicting driver response. In other words, driving behavior in various weather conditions can be characterized as unique simply by investigating the calibrated parameter values; however, a complete under- standing of the produced behavior requires that these parameters be used in simulation for their true representations of driving behavior to be realized. Next, a realistic microsimulation network was modeled in VISSIM, and the calibrated W99 parameters representing each weather condition were used to simulate traffic flow. Each of the calibrated parameter sets resulted in substantially lower capacity predictions and more uniform traffic flow-as illustrated on the fundamental diagram-than the default parameter values. Further, the predictions of capacity, speed at capacity, and density at capacity for clear weather conditions sat in-between the predictions for each of the adverse weather conditions, contrary to expectations that capacity decreases linearly with the level of weather adversity. A detailed synthesis of the fundamental diagram suggests, however, that these descriptive values may not tell the full story of how drivers adjusted their behavioral tendencies.

Practical Implications: Next Generation of Traffic Management

Driver Behavior Investigation

A better understanding of lane-keeping behavior could provide a more practical and realistic threshold for Lane Departure Warning (LDW) systems, especially under reduced visibility during foggy conditions. More specifically, integrating the findings into LDW systems would improve their capability to distinguish between a lane departure event due to behavior (i.e., inattention, fatigued driving, etc.) vs poor ability to maintain a lane due to limited visibility conditions. Additionally, differentiating poor lane keeping due to reduction in visibility and fatigue might be helpful in identifying the best driving mode in Autonomous Vehicles (AVs). Having affected visibility as one of the contributing factors for occurring poor lane keeping recommends implementing safety countermeasures, such as Changeable Message Signs (CMSs) to disseminate safety messages at roadway segments with limited visibility due to fog. Male drivers showed greater propensity towards poor lane-keeping, therefore necessary training, educational programs, and campaigns are needed to improve their lane-keeping ability.

The findings from lane-changing characteristics based on aggressiveness could provide perceptions into integrating driver aggressiveness behavior into Connected Vehicle (CV) technology and microsimulation modeling. In the future, with similar data like NDS, the analysis results could be used to classify drivers as conservative or aggressive based on their lane-changing behavior in a vehicle-to-vehicle (V2V) or CV environment in real-time. The outcome of the analysis related to the distributions of lane-changing durations could be used as inputs in microsimulation model calibration and validation related to lane-change in reduced visibility under various weather and traffic conditions.

The results of the analysis of gap acceptance behavior can help contribute to the calibration of traffic microsimulation. The distributions of lead and lag gaps using naturalistic data could be used as input in microsimulation lane-changing models to generate simulated values of lead and lag gaps. Using similar data to NDS, the developed automatic identification algorithm could be used to extract necessary gap acceptance parameters in real-time in a Connected and Autonomous Vehicles (CAV) environment. As the developed models provided overall

perception into gap acceptance behavior with several variables, the models have important implications for safety improvements in CAV. More specifically, the developed models can help with assessing and ameliorating active safety systems in CAV (8).

Investigating driver speed behavior at a trajectory level using the NDS data unlocked new opportunities to overcome the unpredictable behavioral trends of drivers, especially in adverse weather under various traffic conditions. With the rapid advancement in CV technologies and real-time crowdsourcing, trajectory-level data similar to NDS will be available soon. With this similarity in data, this study presented early insights into statistical methodologies to examine trajectory-level Basic Safety Messages data collected from CV. In a connected vehicle environment, speed data, as well as other driver demographics, traffic, and weather data, could be shared in real-time with other users and with the Traffic Management Centers (TMCs). If any unusual traffic patterns are observed, especially due to the presence of adverse weather conditions, these locations can be flagged to provide appropriate mitigation strategies in a timely manner.

Radar-Vision Algorithms to Process the Trajectory-Level Driving Data

Fusion of the developed "radar vision" procedure with "video vision" algorithms is suggested as the most promising method for streamlining the detection of driving state for efficient analysis of driver behavior using a large sample of the SHRP2 NDS database. Development of video-vision algorithms that can be used to complement the radar-vision algorithms in verifying the presence of a leading vehicle and adding additional context to trips systematically without the need for manual video observation. The developed radar vision algorithms hold great promise for the SHRP2 NDS dataset towards presenting a solution to achieve value from this massive dataset as a whole. These algorithms could also be applied to other Instrumented Research Vehicle (IRV) and Instrumented Personal Vehicle (IPV) datasets.

Detection and Prediction of Lane Change Maneuvers: Development of Advanced Driver Assistance Systems

The developed lane change detection models could be applied to monitor and control driver behavior in a CV environment. If unusual traffic patterns are detected in terms of lane changes under the CV environment, these roadway segments could be flagged, and appropriate countermeasures could be provided in a timely manner to reduce/prevent the risk of crashes. However, the proposed lane change prediction model could help in trajectory planning for AVs and could be used to develop more reliable Advanced Driver Assistance Systems (ADAS) in a Cooperative Connected and Automated Vehicles (CAV) environment. To be specific, the prediction information can help in improving cooperative driving through behavior cloning and enhancing the safety and mobility of CAVs.

Detection of Surrogate Measures of Safety in Adverse Weather Conditions

The SHRP2 NDS data is similar to Basic Safety Messages (BSM) collected in a CV environment. In the future, the results from this study might be used in Advanced Driver Warning Systems. It is worth mentioning that any early change in the vehicle kinematics might be a reason for an aggressive driving accumulation and would result in changing other vehicle kinematics. This might be a direct reason for a near-crash event occurrence. In addition, this reflects the accumulation of vehicle kinematics change from normal driving to aggressive diving in near-crash scenarios. Therefore, providing an early warning would help in inhibiting aggressive driving early according to the driver response to overcome any unexpected risky

event. So, based on the study results, an early warning message for aggressive driving behavior could be displayed to drivers starting from 23 to 5 seconds before the expected event. This early warring would help drivers take proper actions to overcome an unexpected risky event.

Integrating Weather Information into Active Traffic Management

The proposed trajectory-level weather detection systems based on SHRP2 NDS have numerous safety applications, especially in the context of active traffic management systems. The results can be effectively applied using the existing infrastructures and facilities. With the rapid advancement in connectivity, processing power, and camera quality of smartphones, the proposed weather detection model can be trained and integrated on smartphones of regular road users, thus making it an effective way for collecting real-time road weather information. Through crowdsourcing, weather data from regular road users can be shared with the TMCs, where data from all the vehicles from a road network can be weighted to get more representing and accurate real-time weather. The TMCs then can leverage this information to provide appropriate warnings back to the road users and to develop a more accurate and reliable Weather Responsive Traffic Management (WRTM), including weather-based Variable Speed Limit (VSL) system, especially on roadways with no RWISs. The methodology provided in this study could be extended to detect work zones, pedestrians, lane changes, motor vehicle crashes, and road closures. In a Connected Vehicle (CV) environment, this information can easily be shared with other road users and TMCs. Subsequently, based on the real-time road information, the TMCs can disseminate cautionary messages within Advanced Traveler Information Systems (ATIS), such as “Dense Fog 1-mile Ahead” over the DMS to warn drivers about any potentially hazardous weather on roadways where no RWIS is present. However, in extremely harsh weather conditions, such as snowstorms and blizzards, there might not be enough regular vehicles on the roads, which makes the above-mentioned concept for collecting weather data not always feasible. In such extreme weather conditions, maintenance vehicles, such as snowplows, can be equipped with smart devices to collect geocoded weather data that could be easily classified via mobile apps using the proposed weather detection system.

Integration of SHRP2 NDS Findings

The demonstrated procedure for collecting a single car-following model parameter set representing a specific weather condition is widely transferrable for investigation using other data sources and microsimulation tools to address additional research and practical questions. Using this methodology with trajectory-level data, such as the SHRP2 NDS, research questions seeking to characterize how different populations of drivers drive differently (e.g., age, gender, or geographic location) or how different drivers drive in varying conditions (e.g., weather conditions, work zones, or varying penetration rates of connected or automated vehicles) can be addressed and microsimulation models representing these different behaviors can be constructed. Human behavior is complex, stochastic, and often irrational; therefore, it is extremely difficult to interpret and summarize in a single metric (e.g., capacity, average speed, or average headway). Microsimulation offers an unprecedented platform to model unexplainable behavioral tendencies to more realistically predict traffic flow. While microsimulation tools have great potential, this research exemplifies the role that complex human behaviors have in traffic flow theory and the importance of using trajectory-level data to accurately calibrate driving behavior used in the microsimulation model.

Integrating Human Behavior Toward the Development of Cooperative Automated Transportation

The emergence of innovative transportation technologies comprises vehicle connectivity, autonomy, and personal mobility are accelerated by the rapid advancement in communication and information technologies along with advanced artificial intelligence on a large scale. Among the most comprehensively researched innovative technologies, Cooperative Automated Transportation (CAT), which includes Connected Vehicles (CV), Autonomous Vehicles (AV), and Connected and Automated Vehicles (CAV) received remarkable interest in recent years and recognized as "game-changer" in the current transportation system. With the booming of high-performance mobile processors, affordable and robust sensors/cameras, and high-speed connectivity, such as 5G technologies, CAT will likely emerge sooner than anticipated on the roadways. However, 100 percent market penetration rates (MPR) of CAT might not be achieved before long because it will be challenging to integrate CAT technologies into all the existing vehicles and roadway facilities. Despite the potential benefits of CAT, there is an increasing concern regarding the transition era of CAT where both CAT and HV will interact and share the same roadways in a mixed traffic environment. In terms of AV, we are far from level 5 implementation. Many car manufactures are experimenting with level 3/level 4 automation (e.g., partial/conditional automation), which frequently requires human override, continuous attention of the drivers, and might not work as intended due to poor visibility. Tesla® mentioned that "*Autopilot is a hands-on driver assistance system that is intended to be used only with a fully attentive driver. It does not turn a Tesla® into a self-driving car nor does it make a car autonomous* (*400*)." Therefore, CAT could introduce a variety of traffic problems caused by the complex behavior of human driving. If the CAT is not appropriately integrated and tested with human behavior, it might generate unexpected consequences. In order to overcome these limitations, the CAT equipped vehicle should mimic human driving to reduce variability and to ensure more harmonious traffic flow. However, mimicking human drivers requires driver behavior cloning, which is a popular approach where human behavior could be integrated into CAT so that it imitates the actions of human drivers. The findings from this study could provide valuable insights to incorporate complex human behavior from the naturalistic environment via behavior cloning for the development of realistic CAT and analyze their ability at different levels of MPR.

Development of Analysis, Modeling, and Simulation (AMS) Tools for Road Weather Connected Vehicle Applications

CV technologies would open up new opportunities for the state and local agencies to effectively mitigate the negative effects of adverse weather on traffic safety and operation. Implementation of WRTM requires representative analysis, modeling, and simulation frameworks. The findings from this study relevant to microsimulation provided valuable insights for developing AMS tools for road weather-connected vehicle applications.

Weather Responsive Traffic Management (WRTM)

FHWA WRTM is aimed at the development of implementable strategies for system management and operations in adverse weather conditions. I-80 was selected to apply AMS tools based on CV data to simulate three Weather Responsive Management Strategies (WRMS), including Traveler Information Messages (TIM), Connected Vehicle-Based Variable Speed Limit (CV–VSL), and snowplow pre-positioning. To ensure roadway safety on the roadways, Wyoming connected vehicle pilot (WYDOT CV Pilot) leveraged dedicated short-range communication (DSRC)

technologies to create V2V and vehicle-to-infrastructure (V2I) connectivity in an attempt to support an array of services, including advisories, roadside warnings, and active travel guidance for passenger and freight travels. CV–VSL can disseminate more VSL information to CV road users compared to traditional VSL. However, to evaluate the effectiveness of the CV–VSL, representative microsimulation modeling is required. Considering the fact that real-time CV data are not readily available, researchers have been using the findings from this study to develop representative microsimulation models in various driving scenarios, including adverse weather. This study captured driving behavior, including car following and lane changing, in various adverse weather conditions. The updated car-following parameters were integrated into various tools developed by FHWA to evaluate CV applications, including cooperative adaptive cruise control (CACC), signalized intersection approach and departure, cooperative merge, speed harmonization, and CV-VSL (*401*).

Safety Performance Assessment of the Wyoming Connected Vehicle Pilot

The USDOT selected Interstate-80 (I-80) in Wyoming to create, assess, and implement a suite of CV applications (WYDOT CV Pilot) (*379–381*, *388*, *398*, *402*, *403*). This program is aimed at enhancing safety and operations in inclement weather via generating innovative ways to connect not only the drivers but also the fleet managers with real-time road and travel information. Microsimulation modeling efforts were conducted to evaluate the safety performance of the WYDOT CV Pilot. Representative driving behavior models in various adverse weather were calibrated as part of this project. Observed behavioral changes identified from SHRP2 NDS were used to develop driving behavior models for the CV Pilot microsimulation modeling. Several studies under the WYDOT CV Pilot project extensively used the findings from SHRP2 to calibrate baseline microsimulation models by updating the default Wiedemann 99 car-following model and lane-changing parameters (*381*, *398*).

Future Research

Next Generation NDS

It is worth mentioning that no new comprehensive NDS has been conducted in the US after 2013. Considering numerous insightful findings from the previous NDS in the field of roadway safety and operations, it is of utmost importance to conduct a new NDS integrating updated technologies and sensors. Since SHRP2 NDS vehicles were instrumented with a single front-facing radar unit, it was not possible to include data related to all surrounding vehicles. Consequently, the lane change was considered as a single behavior of the subject vehicle. Future NDS studies could include 360-degree radar/ LiDAR that could provide better surrounding perception around vehicle for the analysis. In addition, future studies could consider rapidly emerging Artificial Intelligence and Machine Vision based technologies to collect more comprehensive driving data using advanced DAS systems. Moreover, the current NDS mainly used passenger cars, SUVs, and pickups without considering heavy vehicles including trucks. Trucks can negatively impact traffic flow by increasing speed variability on roadways with higher upgrades, taking longer time to stop in safety-critical situations, and by being more susceptible to rolling over and losing control in inclement conditions, especially on roadways with black eyes coupled with strong crosswinds. Hence, a dedicated naturalistic study considering only trucks could be introduced.

Development of Realistic Behavior Cloning

Behavior cloning is necessary for proper CAT deployment; however, it is extremely difficult to achieve due to the unpredictability and peculiar nature of individual human behaviors. In order to integrate heterogeneous nature of human behavior through behavior cloning approach, real-time trajectory-level naturalistic driving data is essential. Although SHRP2 NDS provided valuable initial insights for behavior cloning, more in-depth research/studies should be conducted to perfect the behavior cloning in order to facilitate the rapid development and deployment of CAV.

Expanding the Current Research

The study datasets were mainly limited to freeways. Future studies could consider all roadway facility types from the SHRP2 NDS to investigate driving behavior. A significant effort of this study was given in data preparation and manual image annotation. Therefore, to reduce the data processing time, future studies could also investigate the possibility of using unsupervised learning techniques, including clustering analysis, to automatically annotate and train images in various weather conditions. Additionally, future studies could investigate other driver behaviors, such as acceleration, and deacceleration, in different adverse weather conditions. Moreover, this study investigated driver behavior without considering age groups. In the future, speeding behavior of young drivers will be assessed and analyzed. In addition, an in-depth investigation of safety-critical events will also be conducted using the SHRP2 NDS data.

References

1. Singh, S. Critical Reasons for Crashes Investigated in the National Motor Vehicle Crash Causation Survey. *Traffic Safety Facts - Crash Stats, Report No. DOT HS 812 115, National Highway Traffic Safety Administration*, 2015, pp. 2–3.
2. Federal Highway Administration. How Do Weather Events Impact Roads? - FHWA Road Weather Management. http://www.ops.fhwa.dot.gov/weather/q1_roadimpact.htm. Accessed Sep. 20, 2019.
3. Andrey, J., B. Mills, M. Leahy, and J. Suggett. Weather as a Chronic Hazard for Road Transportation in Canadian Cities. *Natural Hazards*, Vol. 28, 2003, pp. 319–343.
4. Transportation Research Board. *Highway Capacity Manual, Chapter 22: Freeway Facilities*. 2000.
5. Fedschun, T. Wyoming Pileup Involved over 100 Vehicles in Crashes on Interstate 80, "rolling Closures" in Effect. *Fox News*, 2020.
6. Xu, C., W. Wang, and P. Liu. Identifying Crash-Prone Traffic Conditions under Different Weather on Freeways. *Journal of Safety Research*, Vol. 46, 2013, pp. 135–144.
7. El-tawab, S., and S. Olariu. FIRMS : A Framework for Intelligent Road Monitoring System Using Smart Sensors. *International Journal of Information Sciences and Computer Engineering*, Vol. 1, No. 2, 2010, pp. 1–6.
8. Files, T. Analyzing Driver Behavior Using Data from the SHRP 2 Naturalistic Driving Study. *SHRP 2 Safety Project Brief*, 2013.
9. Hankey, J. M., Miguel A. Perez, and J. A. McClafferty. *Description of the SHRP2 Naturalistic Database and the Crash, near-Crash, and Baseline Data Sets*. 2016.
10. FHWA's Safety Training and Analysis Center. https://www.fhwa.dot.gov/research/resources/stac/data.cfm. Accessed Apr. 16, 2018.
11. Ahmed, M. M., A. Ghasemzadeh, H. Eldeeb, S. Gaweesh, J. Clapp, K. Ksaibati, and R. Young. Driver Performance and Behavior in Adverse Weather Conditions: An Investigation Using the SHRP2 Naturalistic Driving Study Data—Phase 1. *Publication FHWA-WY-16/08F. Wyoming Department of Transportation*, No. 307, 2015, pp. 1–73.
12. Ahmed, M. M., A. Ghasemzadeh, B. Hammit, M. N. Khan, A. Das, E. Ali, R. K. Young, and H. Eldeeb. Driver Performance and Behavior in Adverse Weather Conditions: An Investigation Using the SHRP2 Naturalistic Driving Study Data-Phase 2. *FHWA-WY-18/05F*, 2018.
13. Ahmed, M. M., and A. Ghasemzadeh. Exploring the Impacts of Adverse Weather Conditions on Speed and Headway Behaviors Using the SHRP2 Naturalistic Driving Study Data. *Proceedings of the 96th Transportation Research Board Annual Meeting*, 2017.
14. Khattak, A., P. Kantor, and F. Council. Role of Adverse Weather in Key Crash Types on Limited-Access: Roadways Implications for Advanced Weather Systems. *Transportation Research Record: Journal of the Transportation Research Board*, Vol. 1621, No. 1621, 1998, pp. 10–19. https://doi.org/10.3141/1621-02.

15. Peterson, T. C., M. McGuirk, T. G. Houston, A. H. Horvitz, and M. F. Wehner. Climate Variability and Change with Implications for Transportation. *Transportation Research Board, Washington D.C., USA*, 2008, pp. 1–90.

16. Saha, S., P. Schramm, A. Nolan, and J. Hess. Adverse Weather Conditions and Fatal Motor Vehicle Crashes in the United States, 1994-2012. *Environmental Health: A Global Access Science Source*, Vol. 15, No. 1, 2016, pp. 1–9. https://doi.org/10.1186/s12940-016-0189-x.

17. Tefft, B. C. Motor Vehicle Crashes, Injuries, and Deaths in Relation to Weather Conditions, United States, 2010-2014. *AAA Foundation for Traffic Safety, Washington, D.C.*, No. January, 2016, pp. 1–16.

18. U.S. Department of Transportation. How Do Weather Events Impact Roads: FHWA Road Weather Management Program. *USDOT FHWA*.

19. Perry, A. H., and L. Symons. *Highway Meteorology*. Taylor & Francis Books, Inc, 2003.

20. NewYorkUpstate.com. The Fog of Autumn: Why Fog Is Most Dense (and Dangerous) Now in Upstate NY.

21. National Research Council. *Where the Weather Meets the Road: A Research Agenda for Improving Road Weather Services*. The National Academies Press, Washington, D.C., D.C., 2004.

22. The Fresno Bee. At Least 40 Vehicles Crash in Dense Fog on Highway 198.

23. Moore, R. L., and L. Cooper. *Fog and Road Traffic*. Crowthorne, 1972.

24. Abdel-Aty, M., A. A. Ekram, H. Huang, and K. Choi. A Study on Crashes Related to Visibility Obstruction Due to Fog and Smoke. *Accident Analysis and Prevention*, Vol. 43, No. 5, 2011, pp. 1730–1737. https://doi.org/10.1016/j.aap.2011.04.003.

25. Whiffen, B., P. Delannoy, and S. Siok. Fog : Impact on Road Transportation and Mitigation Options. 2004.

26. Hoogendoorn, R. G., G. Tamminga, S. P. Hoogendoorn, and W. Daamen. Longitudinal Driving Behavior under Adverse Weather Conditions: Adaptation Effects, Model Performance and Freeway Capacity in Case of Fog. 2010.

27. Kang, J. J., R. Ni, and G. J. Andersen. Effects of Reduced Visibility from Fog on Car-Following Performance. *Transportation Research Record: Journal of the Transportation Research Board*, Vol. 2069, 2008, pp. 9–15. https://doi.org/10.3141/2069-02.

28. Cavallo, V., M. Colomb, and J. Doré. Distance Perception of Vehicle Rear Lights in Fog. *Human factors*, Vol. 43, No. 3, 2001, pp. 442–451. https://doi.org/10.1518/001872001775898197.

29. Mueller, A. S., and L. M. Trick. Driving in Fog: The Effects of Driving Experience and Visibility on Speed Compensation and Hazard Avoidance. *Accident Analysis and Prevention*, Vol. 48, 2012, pp. 472–479. https://doi.org/10.1016/j.aap.2012.03.003.

30. Ni, R., Z. Bian, A. Guindon, and G. J. Andersen. Aging and the Detection of Imminent Collisions under Simulated Fog Conditions. *Accident Analysis and Prevention*, Vol. 49, 2012, pp. 525–531. https://doi.org/10.1016/j.aap.2012.03.029.

31. Ni, R., J. J. Kang, and G. J. Andersen. Age-Related Declines in Car Following Performance under Simulated Fog Conditions. *Accident Analysis and Prevention*, Vol. 42, No. 3, 2010, pp. 818–826. https://doi.org/10.1016/j.aap.2009.04.023.

32. Caro, S., V. Cavallo, C. Marendaz, E. R. Boer, and F. Vienne. Can Headway Reduction in Fog Be Explained by Impaired Perception of Relative Motion? *Human factors*, Vol. 51, No. 3, 2009, pp. 378–392. https://doi.org/10.1177/0018720809339621.

33. Saffarian, M., R. Happee, and J. C. F. de Winter. Why Do Drivers Maintain Short Headways in Fog? A Driving-Simulator Study Evaluating Feeling of Risk and Lateral Control during Automated and Manual Car Following. *Ergonomics*, Vol. 55, No. 9, 2012, pp. 971–985. https://doi.org/10.1080/00140139.2012.691993.

34. Hamilton, B., B. Tefft, L. Arnold, and J. Grabowski. Hidden Highways : Fog and Traffic Crashes on America's Roads. *AAA Foundation for Traffic Safety*, 2014.

35. Jalayer, M., H. Zhou, and C. Satterfield. Overview of Safety Countermeasures for Roadway Departure Crashes. *Proceedings of the 95th Transportation Research Board Annual Meeting*, 2015.

36. Engström, J., E. Johansson, and J. Östlund. Effects of Visual and Cognitive Load in Real and Simulated Motorway Driving. *Transportation Research Part F: Traffic Psychology and Behaviour*, Vol. 8, No. 2 SPEC. ISS., 2005, pp. 97–120. https://doi.org/10.1016/j.trf.2005.04.012.

37. Peng, Y., L. N. Boyle, and S. L. Hallmark. Driver's Lane Keeping Ability with Eyes off Road: Insights from a Naturalistic Study. *Accident Analysis and Prevention*, Vol. 50, No. November 2015, 2013, pp. 628–634. https://doi.org/10.1016/j.aap.2012.06.013.

38. Barham, P., L. Andreone, X. H. Zhang, and M. Vache. The "Darwin" Driver Vision Support System - Its Potential Impact on Driving Behaviour and Road Safety, In Conditions of Reduced Visibility. 2000.

39. Ghasemzadeh, A., and M. M. Ahmed. Driver's Lane Keeping Ability in Heavy Rain: Preliminary Investigation Using the SHRP2 Naturalistic Driving Study Data. *Transportation Research Record: Journal of the Transportation Research Board*, 2017. https://doi.org/DOI is 10.3141/2663-13.

40. Das, A., A. Ghasemzadeh, and M. M. Ahmed. A Comprehensive Analysis of Driver Lane-Keeping Performance in Fog Weather Conditions Using the SHRP2 Naturalistic Driving Study Data. *Proceeding of the 97th Transportation Research Board Annual Meeting*, 2018.

41. Ghasemzadeh, A., and M. M. Ahmed. Utilizing Naturalistic Driving Data for In-Depth Analysis of Driver Lane-Keeping Behavior in Rain : Non-Parametric MARS and Parametric Logistic Regression Modeling Approaches. *Transportation Research Part C*, Vol. 90, 2018, pp. 379–392. https://doi.org/10.1016/j.trc.2018.03.018.

42. Ahmed, M. M., and A. Ghasemzadeh. The Impacts of Heavy Rain on Speed and Headway Behaviors: An Investigation Using the SHRP2 Naturalistic Driving Study Data. *Transportation Research Part C: Emerging Technologies*, Vol. 91, No. February 2017, 2018, pp. 371–384. https://doi.org/10.1016/j.trc.2018.04.012.

43. Das, A., A. Ghasemzadeh, and M. M. Ahmed. Analyzing the Effect of Fog Weather Conditions on Driver Lane-Keeping Performance Using the SHRP2 Naturalistic Driving Study Data. *Journal of Safety Research*, Vol. 68, 2019, pp. 71–80. https://doi.org/10.1016/j.jsr.2018.12.015.

44. Ghasemzadeh, A., B. E. Hammit, M. M. Ahmed, and R. K. Young. Parametric Ordinal Logistic Regression and Non-Parametric Decision Tree Approaches for Assessing the Impact of Weather Conditions on Driver Speed Selection Using Naturalistic Driving Data. *Transportation Research Record*, Vol. 2672, No. 12, 2018, pp. 137–147. https://doi.org/10.1177/0361198118758035.

45. Yamamoto, T., R. Kitamura, and J. Fujii. Drivers' Route Choice Behavior: Analysis by Data Mining Algorithms. *Transportation Research Record: Journal of the Transportation Research Board*, Vol. 1807, No. 02, 2002, pp. 59–66. https://doi.org/10.3141/1807-08.

46. Mafi, S., Y. Abdelrazig, and R. Doczy. Analysis of Gap Acceptance Behavior for Unprotected Right and Left Turning Maneuvers at Signalized Intersections Using Data Mining Methods: A Driving Simulation Approach. *Transportation Research Record: Journal of the Transportation Research Board*, 2018, pp. 1–18. https://doi.org/10.1177/0361198118783111.

47. Meseguer, J. E., C. T. Calafate, J. C. Cano, and P. Manzoni. DrivingStyles: A Smartphone Application to Assess Driver Behavior. *Proceedings - International Symposium on Computers and Communications*, 2013, pp. 535–540. https://doi.org/10.1109/ISCC.2013.6755001.

48. Wu, C., C. Sun, D. Chu, Z. Huang, J. Ma, and H. Li. Clustering of Several Typical Behavioral Characteristics of Commercial Vehicle Drivers Based on GPS Data Mining. *Transportation Research Record: Journal of the Transportation Research Board*, No. 2581, 2016, pp. 154–163. https://doi.org/10.3141/2581-18.

49. Geurts, K., I. Thomas, and G. Wets. Understanding Spatial Concentrations of Road Accidents Using Frequent Item Sets. *Accident Analysis and Prevention*, Vol. 37, No. 4, 2005, pp. 787–799. https://doi.org/10.1016/j.aap.2005.03.023.

50. Pande, A., and M. Abdel-Aty. Discovering Indirect Associations in Crash Data Through Probe Attributes. *Transportation Research Record: Journal of the Transportation Research Board*, No. 2083, 2008, pp. 170–179. https://doi.org/10.3141/2083-20.

51. Mirabadi, A., and S. Sharifian. Application of Association Rules in Iranian Railways (RAI) Accident Data Analysis. *Safety Science*, Vol. 48, No. 10, 2010, pp. 1427–1435. https://doi.org/10.1016/j.ssci.2010.06.006.

52. Montella, A. Identifying Crash Contributory Factors at Urban Roundabouts and Using Association Rules to Explore Their Relationships to Different Crash Types. *Accident Analysis and Prevention*, Vol. 43, No. 4, 2011, pp. 1451–1463. https://doi.org/10.1016/j.aap.2011.02.023.

53. Das, S., and X. Sun. Investigating the Pattern of Traffic Crashes under Rainy Weather by Association Rules in Data Mining. *Proceedings of the 93rd Transportation Research Board Annual Meeting*, 2014, pp. 1–19.

54. Das, S., A. Dutta, R. Avelar, K. Dixon, X. Sun, and M. Jalayer. Supervised Association Rules Mining on Pedestrian Crashes in Urban Areas: Identifying Patterns for Appropriate Countermeasures. *International Journal of Urban Sciences*, Vol. 0, No. 0, 2018, pp. 1–19. https://doi.org/10.1080/12265934.2018.1431146.

55. Montella, A., and A. D. Ambrosio. Classification Trees and Association Rules for Exploratory Analysis of Powered Two-Wheeler Crashes. *Proceedings of the 90th Transportation Research Board Annual Meeting*, 2011.

56. Jeong, H., G. Gan, and E. Valdez. Association Rules for Understanding Policyholder Lapses. *Risks*, Vol. 6, No. 3, 2018, p. 69. https://doi.org/10.3390/risks6030069.

57. Mousa, S., S. Ishak, and O. A. Osman. Extracting Association Rules from the SHRP 2 Naturalistic Driving Data: A Market Basket Analysis. *10th SHRP 2 Safety Data Symposium: From Analysis to Results*, No. October, 2017, pp. 11–12.

58. Hill, C., L. Elefteriadou, and A. Kondyli. Exploratory Analysis of Lane Changing on Freeways Based on Driver Behavior. *Journal of Transportation Engineering*, Vol. 141, No. 2006, 2014, pp. 1–11. https://doi.org/10.1061/(ASCE)TE.1943-5436.0000758.

59. Sun, D. J., and L. Elefteriadou. Lane-Changing Behavior on Urban Streets: An "In-Vehicle" Field Experiment-Based Study. *Computer-Aided Civil and Infrastructure Engineering*, Vol. 27, No. 7, 2012, pp. 525–542. https://doi.org/10.1111/j.1467-8667.2011.00747.x.

60. Wang, Q., Z. Li, and L. Li. Investigation of Discretionary Lane-Change Characteristics Using next-Generation Simulation Data Sets. *Journal of Intelligent Transportation Systems: Technology, Planning, and Operations*, Vol. 18, No. 3, 2014, pp. 246–253. https://doi.org/10.1080/15472450.2013.810994.

61. Keyvan-Ekbatani, M., V. L. Knoop, V. Grébert, and W. Daamen. Lane Change Strategies on Freeways: A Microscopic Simulation Study. *Traffic and Granular Flow '15*, 2015, pp. 395–402. https://doi.org/10.1007/978-3-319-10629-8.

62. Lee, S. E., E. C. B. Olsen, and W. W. Wierwille. *A Comprehensive Examination of Naturalistic Lane-Changes*. 2004.

63. Chen, R., K. D. Kusano, and H. C. Gabler. Driver Behavior During Overtaking Maneuvers from the 100-Car Naturalistic Driving Study. *Traffic Injury Prevention*, Vol. 16, No. September, 2015, pp. 176–181. https://doi.org/10.1080/15389588.2015.1057281.

64. Chen, R., and R. Sherony. Predicting Driver Lane Change Maneuvers Using Vehicle Kinematic Data. *25th International Technical Conference on the Enhanced Safety of Vehicles (ESV)*, 2017, pp. 1–9.

65. Hetrick, S. Examination of Driver Lane Change Behavior and the Potential Effectiveness of Warning Onset Rules for Lane Change or "Side" Crash Avoidance Systems. *Virginia Polytechnic Institute and State University*, 1997.

66. Salvucci, D. D., and A. Liu. The Time Course of a Lane Change: Driver Control and Eye-Movement Behavior. *Transportation Research Part F: Traffic Psychology and Behaviour*, Vol. 5, No. 2, 2002, pp. 123–132. https://doi.org/10.1016/S1369-8478(02)00011-6.

67. Toledo, T., and D. Zohar. Modeling Duration of Lane Changes. *Transportation Research*

Record: Journal of the Transportation Research Board, Vol. 1999, 2007, pp. 71–78. https://doi.org/10.3141/1999-08.

68. Hou, Y., P. Edara, and C. Sun. Situation Assessment and Decision Making for Lane Change Assistance Using Ensemble Learning Methods. *Expert Systems with Applications*, Vol. 42, No. 8, 2015, pp. 3875–3882. https://doi.org/10.1016/j.eswa.2015.01.029.

69. Ahmed, K. I. Modeling Drivers ' Acceleration and Lane Changing Behavior. *Doctoral Thesis*, Vol. Ph.D, 1999, p. 189.

70. Toledo, T., H. N. Koutsopoulos, and M. E. Ben-akiva. Modeling Integrated Lane-Changing Behavior. *Transportation Research Record: Journal of the Transportation Research Board*, Vol. 1857, No. 03–3391, 2003, pp. 30–38.

71. Lee, J., M. Park, and H. Yeo. A Probability Model for Discretionary Lane Changes in Highways. *KSCE Journal of Civil Engineering*, Vol. 20, No. 7, 2016, pp. 2938–2946. https://doi.org/10.1007/s12205-016-0382-z.

72. Wang, X., M. Yang, and D. Hurwitz. Analysis of Cut-in Behavior Based on Naturalistic Driving Data. *Accident Analysis and Prevention*, Vol. 124, No. March 2018, 2019, pp. 127–137. https://doi.org/10.1016/j.aap.2019.01.006.

73. Das, A., and M. M. Ahmed. Exploring the Effect of Fog on Lane-Changing Characteristics Utilizing the SHRP2 Naturalistic Driving Study Data. *Journal of Transportation Safety & Security*, Vol. 13, No. 5, 2021, pp. 477–502. https://doi.org/10.1080/19439962.2019.1645777.

74. Das, A., M. M. Ahmed, and A. Ghasemzadeh. Using Trajectory-Level SHRP2 Naturalistic Driving Data for Investigating Driver Lane-Keeping Ability in Fog: An Association Rules Mining Approach. *Accident Analysis and Prevention*, Vol. 129, 2019, pp. 250–262. https://doi.org/10.1016/j.aap.2019.05.024.

75. Haleem, K., A. Gan, and J. Lu. Using Multivariate Adaptive Regression Splines (MARS) to Develop Crash Modification Factors for Urban Freeway Interchange Influence Areas. *Accident Analysis and Prevention*, Vol. 55, 2013, pp. 12–21. https://doi.org/10.1016/j.aap.2013.02.018.

76. Park, J., and M. Abdel-Aty. Assessing the Safety Effects of Multiple Roadside Treatments Using Parametric and Nonparametric Approaches. *Accident Analysis and Prevention*, Vol. 83, 2015, pp. 203–213. https://doi.org/10.1016/j.aap.2015.07.008.

77. Haleem, K., M. Abdel-Aty, and J. Santos. Multiple Applications of Multivariate Adaptive Regression Splines Technique to Predict Rear-End Crashes at Unsignalized Intersections. *Transportation Research Record: Journal of the Transportation Research Board*, Vol. 2165, No. 1, 2010, pp. 33–41. https://doi.org/10.3141/2165-04.

78. Chang, L. Y., H. C. Chu, D. J. Lin, and P. Lui. Analysis of Freeway Accident Frequency Using Multivariate Adaptive Regression Splines. *Procedia Engineering*, Vol. 45, 2012, pp. 824–829. https://doi.org/10.1016/j.proeng.2012.08.245.

79. Gaweesh, S. M., M. M. Ahmed, and A. V. Piccorelli. Developing Crash Prediction Models Using Parametric and Nonparametric Approaches for Rural Mountainous Freeways: A Case Study on Wyoming Interstate 80. *Accident Analysis and Prevention*,

Vol. 123, No. March 2018, 2019, pp. 176–189. https://doi.org/10.1016/j.aap.2018.10.011.

80. Xu, Y., Q. J. Kong, R. Klette, and Y. Liu. Accurate and Interpretable Bayesian MARS for Traffic Flow Prediction. *IEEE Transactions on Intelligent Transportation Systems*, Vol. 15, No. 6, 2014, pp. 2457–2469. https://doi.org/10.1109/TITS.2014.2315794.

81. Oduro, S. D., S. Metia, H. Duc, G. Hong, and Q. P. Ha. Multivariate Adaptive Regression Splines Models for Vehicular Emission Prediction. *Visualization in Engineering*, Vol. 3, No. 1, 2015. https://doi.org/10.1186/s40327-015-0024-4.

82. Chen, Y., L. Zhu, J. Gonder, S. Young, and K. Walkowicz. Data-Driven Fuel Consumption Estimation: A Multivariate Adaptive Regression Spline Approach. *Transportation Research Part C: Emerging Technologies*, Vol. 83, 2017, pp. 134–145. https://doi.org/10.1016/j.trc.2017.08.003.

83. Agarwal, M., T. H. Maze, and R. Souleyrette. *Impact of Weather On Urban Freeway Traffic Flow Characteristics And Facility Capacity*. 2006.

84. Rakha, H., M. Farzaneh, and S. Emily. Inclement Weather Impacts on Freeway Traffic Stream Behavior. *International Journal of Transportation Science and Technology*, Vol. 1, No. 1, 2012, pp. 25–48. https://doi.org/10.3141/2071-02.

85. Hogema, J., and R. van der Horst. Evaluation of A16 Motorway Fog-Signaling System with Respect to Driving Behavior. *Transportation Research Record*, Vol. 1573, No. 970227, 1994, pp. 63–67.

86. Liang, W. L., M. Kyte, F. Kitchener, and P. Shannon. Effect of Environmental Factors on Driver Speed: A Case Study. *Transportation Research Record*, Vol. 1635, No. 98, 1998, pp. 155–161.

87. Jr, J. P., P. T. Martin, and B. G. Hansen. Modifying Signal Timing during Inclement Weather. 2001.

88. Ahmed, M. M., M. Abdel-aty, and R. Yu. Assessment of Interaction of Crash Occurrence , Mountainous Freeway Geometry , Real-Time Weather , and Traffic Data. *Transportation Research Record*, 2012.

89. Ahmed, M. M., R. K. Young, A. Ghasemzadeh, B. Hammit, E. Ali, M. N. Khan, A. Das, and H. Eldeeb. Implementation of SHRP2 Results within the Wyoming Connected Vehicle Variable Speed Limit System. *U.S. Department of Transportation*, 2017.

90. Insight Website. SHRP2 NDS Data Access.

91. MathWorks. Fillmissing.

92. MathWorks. Smoothdata.

93. Bham, G. H. Estimating Driver Mandatory Lane Change Behavior on a Multi Lane Freeway. *Proceedings of the 88th Transportation Research Board Annual Meeting*, No. 573, 2009.

94. Ghasemzadeh, A., B. E. Hammit, M. M. Ahmed, and H. Eldeeb. Unlocking New Potentials of SHRP2 Naturalistic Driving Study Data: Complementary Methodologies to Supplement Real-Time Weather Conditions and Effective Frameworks for Data Reduction and Preparation. *Safety Science*, Vol. In Press, 2019.

https://doi.org/10.1016/j.ssci.2019.01.006.

95. Ahmed, M. M., and A. Ghasemzadeh. The Impacts of Heavy Rain on Speed and Headway Behaviors: An Investigation Using the SHRP2 Naturalistic Driving Study Data. *Transportation Research Part C: Emerging Technologies*, Vol. 91, 2018, pp. 371–384. https://doi.org/10.1016/j.trc.2018.04.012.

96. Agresti, A. *Analysis of Ordinal Categorical Data*. John Wiley & Sons, Hoboken, NJ, 2010.

97. Exarchos, T. P., C. Papaloukas, D. I. Fotiadis, and L. K. Michalis. An Association Rule Mining-Based Methodology for Automated Detection of Ischemic ECG Beats. *IEEE Transactions on Biomedical Engineering*, Vol. 53, No. 8, 2006, pp. 1531–1540. https://doi.org/10.1109/TBME.2006.873753.

98. Agrawal, R., T. Imielinski, and A. Swami. Mining Association in Large Databases. *Proceedings of the ACM SIGMOD International Conference on Management of Data-SIGMOD '93*, 1993, pp. 207–216. https://doi.org/10.1145/170036.170072.

99. Ding, J., J. Wang, C. Liu, M. Lu, and K. Li. A Driver Steering Behavior Model Based on Lane-Keeping Characteristics Analysis. *2014 17th IEEE International Conference on Intelligent Transportation Systems, ITSC 2014*, 2014, pp. 623–628. https://doi.org/10.1109/ITSC.2014.6957759.

100. Hahsler, M. ArulesViz: Interactive Visualization of Association Rules with R. *The R Journal*, Vol. 9/2, No. December, 2017, pp. 1–13.

101. Hahsler, M., B. Grün, and K. Hornik. Introduction to Arules – A Computational Environment for Mining Association Rules and Frequent Item Sets. *Journal of Statistical Software*, Vol. 14, No. 15, 2005, pp. 1–25. https://doi.org/10.1007/978-1-84800-201-2.

102. Brin, S., R. Motwani, J. D. Ullman, and S. Tsur. Dynamic Itemset Counting and Implication Rules for Market Basket Data. *ACM SIGMOD Record*, Vol. 26, No. 2, 1997, pp. 255–264. https://doi.org/10.1145/253262.253325.

103. Montella, A., M. Aria, A. D'Ambrosio, and F. Mauriello. Data-Mining Techniques for Exploratory Analysis of Pedestrian Crashes. *Transportation Research Record: Journal of the Transportation Research Board*, Vol. 2237, 2011, pp. 107–116. https://doi.org/10.3141/2237-12.

104. Guo, F., and Y. Fang. Individual Driver Risk Assessment Using Naturalistic Driving Data. *Accident Analysis and Prevention*, Vol. 61, 2013, pp. 3–9. https://doi.org/10.1016/j.aap.2012.06.014.

105. Higgs, B., and M. Abbas. A Two-Step Segmentation Algorithm for Behavioral Clustering of Naturalistic Driving Styles. 2013.

106. Musselwhite, C. Attitudes towards Vehicle Driving Behaviour: Categorising and Contextualising Risk. *Accident Analysis and Prevention*, Vol. 38, No. 2, 2006, pp. 324–334. https://doi.org/10.1016/j.aap.2005.10.003.

107. Zheng, Y., J. Wang, X. Li, C. Yu, K. Kodaka, and K. Li. Driving Risk Assessment Using Cluster Analysis Based on Naturalistic Driving Data. *17th IEEE International Conference on Intelligent Transportation Systems (ITSC)*, 2014, pp. 2584–2589.

https://doi.org/10.1109/ITSC.2014.6958104.

108. Macqueen, J. Some Methods for Classification and Analysis of Multivariate Observations. *Proceedings of the Fifth Berkeley Symposium on Mathematical Statistics and Probability*, Vol. 1, No. 233, 1967, pp. 281–297. https://doi.org/citeulike-article-id:6083430.

109. Trevino, A. Introduction to K-Means Clustering. *Datascience.com*.

110. Alsabti, K., S. Ranka, and V. Singh. An Efficient K-Means Clustering Algorithm. *Electrical Engineering and Computer Science. Paper*, Vol. 43, 1997.

111. Jain, A. K. Data Clustering: 50 Years beyond K-Means. *Pattern Recognition Letters*, Vol. 31, No. 8, 2010, pp. 651–666. https://doi.org/10.1016/j.patrec.2009.09.011.

112. Tibshirani, R., G. Walther, and T. Hastie. Estimating the Number of Clusters in a Data Set via the Gap Statistic. *Journal of the Royal Statistical Society: Series B (Statistical Methodology)*, Vol. 63, No. 2, 2001, pp. 411–423. https://doi.org/10.1111/1467-9868.00293.

113. SAS. How Can I Tell How Many Clusters Are in My Data Set?

114. Friedman, J. H. Multivariate Adaptive Regression Splines. *The Annals of Statistics*, Vol. 11, No. 2, 1991, pp. 416–431.

115. Osei-Bryson, K.-M., and O. Ngwenyama. *Advances in Systems Research for Information Research Methods*. 2014.

116. Hahsler, M., C. Buchta, B. Gruen, A. Michael, C. Buchta, B. Gruen, K. Hornik, and I. Johnson. Arules: Mining Association Rules and Frequent Itemsets.

117. Brooks, J. O., M. C. Crisler, N. Klein, R. Goodenough, R. W. Beeco, C. Guirl, P. J. Tyler, A. Hilpert, Y. Miller, J. Grygier, B. Burroughs, A. Martin, R. Ray, C. Palmer, and C. Beck. Speed Choice and Driving Performance in Simulated Foggy Conditions. *Accident Analysis and Prevention*, Vol. 43, No. 3, 2011, pp. 698–705.

118. Kondyli, A., and L. Elefteriadou. Modeling Driver Behavior at Freeway-Ramp Merges. *Transportation Research Record: Journal of the Transportation Research Board*, Vol. 2249, No. 2249, 2011, pp. 29–37. https://doi.org/10.3141/2249-05.

119. Li, Q., F. Qiao, and L. Yu. Socio-Demographic Impacts on Lane-Changing Response Time and Distance in Work Zone with Drivers' Smart Advisory System. *Journal of Traffic and Transportation Engineering (English Edition)*, Vol. 2, No. 5, 2015, pp. 313–326. https://doi.org/10.1016/j.jtte.2015.08.003.

120. Gurupackiam, S., S. Jones, and D. Turner. *Characterization of Arterial Traffic Congestion Through Analysis of Operational Parameters (Gap Acceptance and Lane Changing)*. 2010.

121. American Automobile Association. Aggressive Driving: Research Update. *American Automobile Association Foundation for Traffic Safety*, 2009, pp. 202–638.

122. He, Y., Z. Shu, Y. Ge, and J. Daniel. Drivers' Lane Change Maneuver and Speed Behavior in Freeway Work Zones. *Proceedings of SAE-China Congress 2015*, Vol. 364, 2016, pp. 229–241. https://doi.org/10.1007/978-981-287-978-3.

123. Maryland Motor Vehicle Administration. Maryland Driver's Manual. Maryland Department of Transportation, , 2016, pp. 1–47.

124. Zhang, J., Y. Liao, S. Wang, and J. Han. Study on Driving Decision-Making Mechanism of Autonomous Vehicle Based on an Optimized Support Vector Machine Regression. *Applied Sciences*, Vol. 8, No. 1, 2017, p. 13. https://doi.org/10.3390/app8010013.

125. Balal, E., R. Cheu, T. Gyan-Sarkodie, and J. Miramontes. Analysis of Discretionary Lane Changing Parameters on Freeways. *International Journal of Transportation Science and Technology*, Vol. 3, No. 3, 2014, pp. 277–296. https://doi.org/10.1260/2046-0430.3.3.277.

126. Yang, M., W. Xuesong, and M. Quddus. Examining Lane Change Gap Acceptance, Duration, and Impact Using Naturalistic Drivining Data. *Proceedings of the 98th Transportation Research Board Annual Meeting*, 2019.

127. Khan, M. N., A. Ghasemzadeh, and M. M. Ahmed. Investigating the Impact of Fog on Freeway Speed Selection Using the SHRP2 Naturalistic Driving Study Data. *Transportation Research Record: Journal of the Transportation Research Board*, Vol. 2672, No. 16, 2018, pp. 93–104. https://doi.org/10.1177/0361198118774748.

128. Das, S., A. Dutta, R. Avelar, K. Dixon, and X. Sun. Supervised Association Rules Mining on Pedestrian Crashes in Urban Areas : Identifying Patterns for Appropriate Countermeasures. *International Journal of Urban Sciences*, Vol. 23, No. 1, 2019, pp. 30–48.

129. Hahsler, M., and S. Chelluboina. Visualizing Association Rules : Introduction to the R-Extension Package ArulesViz. *R project module*, 2011.

130. Myers, R. H. *Classical and Modern Regression with Applications*. Duxbury press, Belmont, CA, 1990.

131. Ossen, S., and S. P. Hoogendoorn. Car-Following Behavior Analysis from Microscopic Trajectory Data. *Transportation Research Record: Journal of the Transportation Research Board*, Vol. 1934, 2005, pp. 13–21. https://doi.org/10.3141/1934-02.

132. Punzo, V., and F. Simonelli. Analysis and Comparison of Microscopic Traffic Flow Models with Real Traffic Microscopic Data. *Transportation Research Record: Journal of the Transportation Research Board*, Vol. 1934, 2005, pp. 53–63. https://doi.org/10.3141/1934-06.

133. Toledo, T. Driving Behaviour: Models and Challenges. *Transport Reviews*, Vol. 27, No. 1, 2007, pp. 65–84. https://doi.org/10.1080/01441640600823940.

134. Montanino, M., and V. Punzo. Trajectory Data Reconstruction and Simulation-Based Validation against Macroscopic Traffic Patterns. *Transportation Research Part B: Methodological*, Vol. 80, 2015, pp. 82–106. https://doi.org/10.1016/j.trb.2015.06.010.

135. Punzo, V., D. J. Formisano, and V. Torrieri. Traffic Flow Theory and Car Following: Nonstationary Kalman Filter for Estimation of Accurate and Consistent Car-Following Data. *Transportation Research Record: Journal of the Transportation Research Board*, Vol. 1934, 2005, pp. 1–12.

136. Neale, V. L., and T. Dingus. 100-Car Naturalistic Driving Study. *FOT-NET Data*.

137. Sangster, J., H. Rakha, and J. Du. Application of Naturalistic Driving Data to Modeling of Driver Car-Following Behavior. *Transportation Research Record: Journal of the Transportation Research Board*, Vol. 2390, 2013, pp. 20–33. https://doi.org/10.3141/2390-03.

138. Higgs, B., and M. Abbas. Segmentation and Clustering of Car-Following Behavior: Recognition of Driving Patterns. *IEEE Transactions on Intelligent Transportation Systems*, Vol. 16, No. 1, 2015, pp. 81–90. https://doi.org/10.1109/TITS.2014.2326082.

139. Gorman, T., L. Stowe, and J. Hankey. *S31: NDS Data Dissemination Activities, Task 1.6: Radar Post-Processing*. 2015.

140. Hooper G, K., and H. McGee W. Driver Perception-Reaction Time: Are Revisions to Current Specification Values in Order? *Transportation Research Record*, No. 904, 1983, p. pp 21--30.

141. Smadi, O. SHRP2 - Roadway Information Database. *Iowa State University CTRE*.

142. NHTSA. Traffic Safety Facts: A Compilation of Motor Vehicle Crash Data from the Fatality Analysis Reporting System and the General Estimates System. *U.S. Department of Transportation*, 2018.

143. Fitch, G. M., S. E. Lee, S. Klauer, J. Hankey, J. Sudweeks, and T. Dingus. *Analysis of Lane-Change Crashes and Near-Crashes*. 2009.

144. You, F., R. Zhang, G. Lie, H. Wang, H. Wen, and J. Xu. Trajectory Planning and Tracking Control for Autonomous Lane Change Maneuver Based on the Cooperative Vehicle Infrastructure System. *Expert Systems with Applications*, Vol. 42, No. 14, 2015, pp. 5932–5946. https://doi.org/10.1016/j.eswa.2015.03.022.

145. Xi, Y., and M. Crisler. A Review of Lane Change Definitions and Identification Methods. *Proceedings of the 92th Transportation Research Board Annual Meeting*, No. January, 2013.

146. Tijerina, L., W. Garrott, D. Stoltzfus, and E. Parmer. Eye Glance Behavior of Van and Passenger Car Drivers During Lane Change Decision Phase. *Transportation Research Record: Journal of the Transportation Research Board*, Vol. 1937, 2005, pp. 37–43. https://doi.org/10.3141/1937-06.

147. Bogard, S., and P. Fancher. *Analysis of Data on Speed-Change and Lane-Change Behavior in Manual and Acc Driving*. 1999.

148. Miller, R., and G. Srinivasan. Determination of Lane Change Maneuvers Using Naturalistic Driving Data. *Proceedings of the 19th International Technical Conference on the Enhanced Safety of Vehicles*, 2005, pp. 1–5.

149. Thiemann, C., M. Treiber, and A. Kesting. Estimating Acceleration and Lane-Changing Dynamics Based on NGSIM Trajectory Data. *Transportation Research Record: Journal of the Transportation Research Board*, 2008, pp. 90–101. https://doi.org/10.3141/2088-10.

150. Knoop, V. L., S. P. Hoogendoorn, Y. Shiomi, and C. Buisson. Quantifying the Number of Lane Changes in Traffic. *Transportation Research Record: Journal of the Transportation Research Board*, Vol. 2278, No. 1, 2012, pp. 31–41. https://doi.org/10.3141/2278-04.

151. Koziol, J., V. Inman, M. Carter, J. Hitz, W. Najm, S. Chen, A. Lam, M. Penic, M. Jensen, M. Baker, M. Robinson, and C. Goodspeed. Evaluation of the Intelligent Cruise Control System Volume II - Appendices. *Proceedings of the 78th Transportation Research Board Annual Meeting*, 1999.

152. Ayres, G., B. Wilson, and J. LeBlanc. Method for Identifying Vehicle Movements for Analysis of Field Operational Test Data. *Transportation Research Record: Journal of the Transportation Research Board*, No. 1886, 2004, pp. 92–100. https://doi.org/10.3141/1886-12.

153. Yiguang Xuan, and B. Coifman. Lane Change Maneuver Detection from Probe Vehicle DGPS Data. *IEEE Intelligent Transportation Systems Conference*, 2006, pp. 624–629. https://doi.org/10.1109/ITSC.2006.1706811.

154. Papathanasopoulou, V., and C. Antoniou. Identification of Lane Changes Manoeuvreson Mixed Traffic Trajectory Data. *Proceedings of the 97th Transportation Research Board Annual Meeting*, No. August 2017, 2018, pp. 1–17.

155. Hanowski, R. I., W. W. Wierwille, S. A. Garness, and T. A. Dingus. A Field Evaluation of Safety Issues in Local/Short Haul Trucking. *Proceedings of the Human Factors and Ergonomics Society Annual Meeting*, Vol. 44, No. September, 1999.

156. Yang, D., X. Qiu, Y. Liu, C. Wen, L. Zhu, and X. Hong. Modeling the Discretionary Lane-Changing Decision Behavior Using Random Forest Theory. *Proceedings of the 96th Transportation Research Board Annual Meeting*, 2017.

157. Bakhit, P. R., O. A. Osman, and S. Ishak. Detecting Imminent Lane Change Maneuvers in Connected Vehicle Environments. *Transportation Research Record: Journal of the Transportation Research Board*, Vol. 2645, No. 2645, 2017, p. 14p. https://doi.org/10.3141/2645-18.

158. Mandalia, H. M., and D. D. Salvucci. Using Support Vector Machines for Lane-Change Detection. *Proceedings of the Human Factors and Ergonomics Society*, 2005, pp. 1965–1969.

159. Kumar, P., M. Perrollaz, S. Lefevre, and C. Laugier. Learning-Based Approach for Online Lane Change Intention Prediction. *IEEE Intelligent Vehicles Symposium (IV)*, No. Iv, 2013, pp. 797–802.

160. Zheng, J., K. Suzuki, and M. Fujita. Predicting Driver's Lane-Changing Decisions Using a Neural Network Model. *Simulation Modelling Practice and Theory*, Vol. 42, 2014, pp. 73–83. https://doi.org/10.1016/j.simpat.2013.12.007.

161. Schmidt, K., M. Beggiato, K. H. Hoffmann, and J. F. Krems. A Mathematical Model for Predicting Lane Changes Using the Steering Wheel Angle. *Journal of Safety Research*, Vol. 49, No. February, 2014, pp. 85.e1-90. https://doi.org/10.1016/j.jsr.2014.02.014.

162. Morris, B., A. Doshi, and M. Trivedi. Lane Change Intent Prediction for Driver Assistance: On-Road Design and Evaluation. *IEEE Intelligent Vehicles Symposium, Proceedings*, No. Iv, 2011, pp. 895–901. https://doi.org/10.1109/IVS.2011.5940538.

163. Toledo-Moreo, R., and M. A. Zamora-Izquierdo. IMM-Based Lane-Change Prediction in Highways with Low-Cost GPS/INS. *IEEE Transactions on Intelligent Transportation*

Systems, Vol. 10, No. 1, 2009, pp. 180–185. https://doi.org/10.1109/TITS.2008.2011691.

164. Chen, R., H. C. Gabler, and R. Sherony. Predicting Driver Lane Change Maneuvers Using Vehicle Kinematic Data. *25th International Technical Conference on the Enhanced Safety of Vehicles (ESV)*, 2017, pp. 1–9.

165. Leonhardt, V., and G. Wanielik. Feature Evaluation for Lane Change Prediction Based on Driving Situation and Driver Behavior. *20th International Conference on Information Fusion, Fusion 2017 - Proceedings*, 2017. https://doi.org/10.23919/ICIF.2017.8009848.

166. Das, A., M. N. Khan, and M. M. Ahmed. Detecting Lane Change Maneuvers Using SHRP2 Naturalistic Driving Data: A Comparative Study Machine Learning Techniques. *Accident Analysis and Prevention*, Vol. 142, 2020, p. 105578. https://doi.org/10.1016/j.aap.2020.105578.

167. Khan, M. N., and M. M. Ahmed. Snow Detection Using In-Vehicle Video Camera with Texture-Based Image Features Utilizing K-Nearest Neighbor, Support Vector Machine, and Random Forest. *Transportation Research Record: Journal of the Transportation Research Board*, Vol. 2673, No. 8, 2019, pp. 221–232.

168. Osman, O. A., M. Hajij, P. R. Bakhit, and S. Ishak. Prediction of Near-Crashes from Observed Vehicle Kinematics Using Machine Learning. *Transportation Research Record: Journal of the Transportation Research Board*, Vol. 2673, No. 12, 2019, pp. 463–473.

169. Das, A., and M. M. Ahmed. Machine Learning Approach for Predicting Lane Change Maneuvers Using the SHRP2 Naturalistic Driving Study Data. *Transportation Research Record: Journal of the Transportation Research Board*, Vol. 2675, No. 9, 2021, pp. 574–594. https://doi.org/10.1177/03611981211003581.

170. Gao, K., D. Yan, F. Yang, J. Xie, L. Liu, R. Du, and N. Xiong. Conditional Artificial Potential Field-Based Autonomous Vehicle Safety Control with Interference of Lane Changing in Mixed Traffic Scenario. *Sensors*, Vol. 19, No. 19, 2019. https://doi.org/10.3390/s19194199.

171. Benterki, A., M. Boukhnifer, V. Judalet, and M. Choubeila. Prediction of Surrounding Vehicles Lane Change Intention Using Machine Learning. *Proceedings of the 2019 10th IEEE International Conference on Intelligent Data Acquisition and Advanced Computing Systems: Technology and Applications, IDAACS 2019*, Vol. 2, 2019, pp. 839–843. https://doi.org/10.1109/IDAACS.2019.8924448.

172. Hou, Y., P. Edara, and C. Sun. Modeling Mandatory Lane Changing Using Bayes Classifier and Decision Trees. *IEEE Transactions on Intelligent Transportation Systems*, Vol. 15, No. 2, 2014, pp. 647–655. https://doi.org/10.1109/TITS.2013.2285337.

173. Kenneth L. Campbell. The SHRP 2 Naturalistic Driving Study. *Tr News*, *282*, , 2012, pp. 31–35.

174. Hutton, J. M., K. M. Bauer, C. A. Fees, and A. Smiley. *Analysis of Naturalistic Driving Study Data: Offset Left-Turn Lanes*. 2014.

175. Center for Transportation Research and Education (CTRE). SHRP2-Roadway Information Database - Background.

176. Ghasemzadeh, A., B. E. Hammit, M. M. Ahmed, and H. Eldeeb. Complementary

Methodologies to Identify Weather Conditions in Naturalistic Driving Study Trips: Lessons Learned from the SHRP2 Naturalistic Driving Study & Roadway Information Database. *Safety Science*, Vol. 119, 2019, pp. 21–28. https://doi.org/10.1016/j.ssci.2019.01.006.

177. Zhou, Y. *Deterioration and Optimal Rehabilitation Modelling for Urban Water Distribution Systems*. 2018.

178. Peng, F., F. Feng, and A. Mccallum. Chinese Segmentation and New Word Detection Using Conditional Random Fields. *Proceedings of the 20th international conference on Computational Linguistics*, 2004.

179. InSight SHRP2 NDS. SHRP2 NDS Data Access.

180. Garg, S., K. Kaur, S. Batra, G. Kaddoum, N. Kumar, and A. Boukerche. A Multi-Stage Anomaly Detection Scheme for Augmenting the Security in IoT-Enabled Applications. *Future Generation Computer Systems*, Vol. 104, 2020, pp. 105–118. https://doi.org/10.1016/j.future.2019.09.038.

181. Kovalerchuk, B., and E. Vityaev. *Data Mining in Finance: Advances in Relational and Hybrid Methods*. 1997.

182. Breiman, L. Random Forest. *Machine Learning*, Vol. 45, No. 1, 2001, pp. 5–32.

183. Mousa, S. R., P. R. Bakhit, O. A. Osman, and S. Ishak. A Comparative Analysis of Tree-Based Ensemble Methods for Detecting Imminent Lane Change Maneuvers in Connected Vehicle Environments. *Transportation Research Record: Journal of the Transportation Research Board*, Vol. 2672, No. 42, 2018, pp. 268–279.

184. Ray, S. Quick Guide to Boosting Algorithms in Machine Learning.

185. Friedman, J., T. Hastie, and R. Tibshirani. *The Elements of Statistical Learning*. Springer, New York, US, 2008.

186. Hill, T., and P. Lewicki. *Statistics: Methods and Applications*. StatSoft, 2007.

187. Singh, V. Machine Learning K-Nearest Neighbors (KNN) Algorithm In Python.

188. Nick, T., E. Coersmeier, J. Geldmacher, and J. Goetze. Classifying Means of Transportation Using Mobile Sensor Data. *Proceedings of the International Joint Conference on Neural Networks*, 2010. https://doi.org/10.1109/IJCNN.2010.5596549.

189. FrontlineSolvers. Neural Network Classification.

190. McDowell, I. *Measuring Health: A Guide to Rating Scales and Questionnaires*. Oxford University Press, USA, 2006.

191. Goh, Y. M., and C. U. Ubeynarayana. Construction Accident Narrative Classification: An Evaluation of Text Mining Techniques. *Accident Analysis and Prevention*, Vol. 108, No. July, 2017, pp. 122–130. https://doi.org/10.1016/j.aap.2017.08.026.

192. Chin, H., and S. Quek. Measurement of Traffic Conflicts. *Safety Science*, Vol. 26, No. 3, 1997, pp. 169–185. https://doi.org/10.1016/S0925-7535(97)00041-6.

193. Datta, T. K., D. D. Perkins, J. I. Taylor, and H. T. Thompson. Accident Surrogates for Use in Analyzing Highway Safety Hazards. Volume III: Appendices A-G. Final Report. 175 p.

194. Parker, M. R., and J. and C. V. Zegeer. *Traffic Conflict Techniques for Safety Observers Manual and Operations*. 1989.

195. Zheng, L., K. Ismail, and X. Meng. Traffic Conflict Techniques for Road Safety Analysis: Open Questions and Some Insights. *Canadian Journal of Civil Engineering*, Vol. 41, No. 7, 2014, pp. 633–641. https://doi.org/10.1139/cjce-2013-0558.

196. Chin, H., S. Quek, and R. Cheu. Quantitative Examination of Traffic Conflicts. *Transportation Research Record*, Vol. 1376, No. 7, 1992, pp. 67–74.

197. Kloeden, C., G. Ponte, and A. McLean. Travelling Speed and the Risk of Crash Involvement. *Ponte*, Vol. 1, No. November, 2001, p. 61.

198. Shoarian-Sattari, K., and D. Powell. Measured Vehicle Flow Parameters As Predictors in Road Traffic Accident Studies. *Traffic Engineering and Control*, Vol. 28, No. 6, 1987, pp. 328–329, 331.

199. Minderhoud, M. M., and P. H. L. Bovy. Extended Time-to-Collision Measures for Road Traffic Safety Assessment. *Accident Analysis and Prevention*, Vol. 33, No. 1, 2001, pp. 89–97. https://doi.org/10.1016/S0001-4575(00)00019-1.

200. Allen, B., B. T. Shin, and P. Cooper. Analysis of Traffic Conflicts and Collisions. *Transportation Research Record*, No. 667, 1978, pp. 67–74.

201. USDOT. Road Weather Connected Vehicle Applications. *Research and Innovative Technology Administration*.

202. Ahmed, M., M. Hoque, and P. Pfeiffer. Comparative Study of Connected Vehicle Simulators. 2016.

203. Olia, A., H. Abdelgawad, B. Abdulhai, and S. N. Razavi. Assessing the Potential Impacts of Connected Vehicles: Mobility, Environmental, and Safety Perspectives. *Journal of Intelligent Transportation Systems*, Vol. 20, No. 3, 2016, pp. 229–243. https://doi.org/10.1080/15472450.2015.1062728.

204. NHTSA. Vehicle-to-Vehicle Communication.

205. FHWA. Analyzing Driver Behavior to Understand the Factors Contributing to Highway Crashes.

206. Guo, F., S. G. Klauer, M. T. McGill, and T. A. Dingus. Evaluating the Relationship Between Near-Crashes and Crashes: Can Near-Crashes Serve as a Surrogate Safety Metric for Crashes? *DOT HS 811 382*, 2010.

207. Rittho, O., R. Klinkenberg, S. Fischer, and I. Mierswa. Yale: Yet Another Learning Environment - Tutorial.

208. Hofmann, M., and R. Klinkenberg. *Data Mining and Knowledge Discovery Series : RAPID MINER Data Mining Use Cases and Business Analytics Applications*. 2014.

209. Al-Ghamdi, A. Using Logistic Regression to Estimate the Influence of Accident Factors on Accident Severity. *Accident Analysis and Prevention*, Vol. 34, No. 6, 2002, pp. 729–741. https://doi.org/10.1016/S0001-4575(01)00073-2.

210. Yau, K. K. W. Risk Factors Affecting the Severity of Single Vehicle Traffic Accidents in

Hong Kong. *Accident Analysis and Prevention*, Vol. 36, No. 3, 2004, pp. 333–340. https://doi.org/10.1016/S0001-4575(03)00012-5.

211. Li, Y., C. Xu, L. Xing, and W. Wang. Evaluation of Impacts of Different Car-Following Types on Rear-End Crash Risk at Freeway Weaving Sections Using Vehicle Trajectory Data. *Transportation Research Board 96th Annual Meeting*, No. January, 2017. https://doi.org/10.3969/j.issn.1003-7985.2017.03.013.

212. Kurtner, Nachtsheim, N. *Applied Linear Regression Models (4th Edition)*. McGraw-Hill, Boston, 2009.

213. SAS Institute Inc. SAS/STAT® 9.2 User's Guide: The LOGISTIC Procedure., Cary, NC.

214. Tan, P.-N., M. Steinbach, and V. Kumar. *Introduction to Data Mining*. Pearson Addison Wesley, 2005.

215. Abellán, J., G. López, and J. De Oña. Analysis of Traffic Accident Severity Using Decision Rules via Decision Trees. *Expert Systems with Applications*, Vol. 40, No. 15, 2013, pp. 6047–6054. https://doi.org/10.1016/j.eswa.2013.05.027.

216. Kumar, S., and D. Toshniwal. A Data Mining Approach to Characterize Road Accident Locations. *Journal of Modern Transportation*, Vol. 24, No. 1, 2016, pp. 62–72. https://doi.org/10.1007/s40534-016-0095-5.

217. Kumar, S., and D. Toshniwal. A Novel Framework to Analyze Road Accident Time Series Data. *Journal of Big Data*, Vol. 3, No. 1, 2016, p. 8. https://doi.org/10.1186/s40537-016-0044-5.

218. Jain, A. K., and R. C. Dubes. *Algorithms for Clustering Data*. Prentice Hall, 1988.

219. Witten, I., E. Frank, and M. Hall. *Data Mining Practical Machine Learning Tools And Techniques*. 2005.

220. Zaki, M. J., and M. J. Wagner. *Data Mining and Analysis: Fundamental Concepts and Algorithms*. 2014.

221. Operator Manual - RapidMiner Documentation.

222. Guo, G., H. Wang, D. Bell, Y. Bi, and K. Greer. KNN Model-Based Approach in Classification. 2003.

223. Basheer, I. A., and M. Hajmeer. Artificial Neural Networks: Fundamentals, Computing, Design, and Application. *Journal of Microbiological Methods*, Vol. 43, No. 1, 2000, pp. 3–31. https://doi.org/10.1016/S0167-7012(00)00201-3.

224. Lecun, Y., Y. Bengio, and G. Hinton. Deep Learning. *Nature*, Vol. 521, No. 7553, 2015, pp. 436–444. https://doi.org/10.1038/nature14539.

225. Schmidhuber, J. Deep Learning in Neural Networks: An Overview. *Neural Networks*, Vol. 61, 2015, pp. 85–117. https://doi.org/10.1016/j.neunet.2014.09.003.

226. Montgomery, D. C., G. C. Runger, and N. F. Hubele. *Engineering Statistics*. John Wiley & Sons, Inc, 2010.

227. SAS Institute Inc. *Getting Started with SAS® Enterprise Miner™ 13.1*. Cary, NC, 2013.

228. Hosmer, Jr., D. W., S. Lemeshow, and R. X. Sturdivant. *Applied Logistic Regression, Third Edition*. John Wiley & Sons, Inc., NJ, 2013.

229. Bollinger, G., D. A. Belsley, E. Kuh, and R. E. Welsch. Regression Diagnostics: Identifying Influential Data and Sources of Collinearity. *Journal of Marketing Research*, Vol. 18, No. 3, 1981, p. 392. https://doi.org/10.2307/3150985.

230. Midi, H., S. K. Sarkar, and S. Rana. Collinearity Diagnostics of Binary Logistic Regression Model. *Journal of Interdisciplinary Mathematics*, Vol. 13, No. 3, 2010, pp. 253–267. https://doi.org/10.1080/09720502.2010.10700699.

231. Mathworks. Machine Learning Challenges: Choosing the Best Model and Avoiding Overfitting. 2016, pp. 1–8.

232. Chen, Z., X. Qin, and M. R. R. Shaon. Modeling Lane-Change-Related Crashes with Lane-Specific Real-Time Traffic and Weather Data. *Journal of Intelligent Transportation Systems: Technology, Planning, and Operations*, Vol. 22, No. 4, 2018, pp. 291–300. https://doi.org/10.1080/15472450.2017.1309529.

233. Vlahogianni, E. I., M. G. Karlaftis, and F. P. Orfanou. Modeling the Effects of Weather and Traffic on the Risk of Secondary Incidents. *Journal of Intelligent Transportation Systems: Technology, Planning, and Operations*, Vol. 16, No. 3, 2012, pp. 109–117. https://doi.org/10.1080/15472450.2012.688384.

234. Khan, M. N., A. Das, and M. M. Ahmed. Non-Parametric Association Rules Mining and Parametric Ordinal Logistic Regression for an In-Depth Investigation of Driver Speed Selection Behavior in Adverse Weather Using SHRP2 Naturalistic Driving Study Data. *Transportation Research Record: Journal of the Transportation Research Board*, Vol. 2674, No. 11, 2020, pp. 101–119. https://doi.org/10.1177/0361198120941509.

235. Das, A., M. N. Khan, and M. M. Ahmed. Nonparametric Multivariate Adaptive Regression Splines Models for Investigating Lane-Changing Gap Acceptance Behavior Utilizing Strategic Highway Research Program 2 Naturalistic Driving Data. *Transportation Research Record: Journal of the Transportation Research Board*, Vol. 2674, No. 5, 2020, pp. 223–238. https://doi.org/10.1177/0361198120914293.

236. Hassan, H. M., M. A. Abdel-Aty, K. Choi, and S. A. Algadhi. Driver Behavior and Preferences for Changeable Message Signs and Variable Speed Limits in Reduced Visibility Conditions. *Journal of Intelligent Transportation Systems: Technology, Planning, and Operations*, Vol. 16, No. 3, 2012, pp. 132–146. https://doi.org/10.1080/15472450.2012.691842.

237. Jonsson, P. Road Condition Discrimination Using Weather Data and Camera Images. *IEEE Conference on Intelligent Transportation Systems, ITSC*, Vol. 4460318, 2011, pp. 1616–1621. https://doi.org/10.1109/ITSC.2011.6082921.

238. Carrillo, J., M. Crowley, G. Pan, and L. Fu. Comparison of Deep Learning Models for Determining Road Surface Condition from Roadside Camera Images and Weather Data. 2019.

239. Pan, G., L. Fu, R. Yu, and M. Muresan. Evaluation of Alternative Pre-Trained Convolutional Neural Networks for Winter Road Surface Condition Monitoring. 2019.

240. Lee, J., B. Hong, Y. Shin, and Y. J. Jang. Extraction of Weather Information on Road Using CCTV Video. *2016 International Conference on Big Data and Smart Computing, BigComp 2016*, 2016, pp. 529–531. https://doi.org/10.1109/BIGCOMP.2016.7425986.

241. Lee, J., B. Hong, S. Jung, and V. Chang. Clustering Learning Model of CCTV Image Pattern for Producing Road Hazard Meteorological Information. *Future Generation Computer Systems*, Vol. 86, 2018, pp. 1338–1350. https://doi.org/10.1016/j.future.2018.03.022.

242. Babari, R., N. Hautière, É. Dumont, N. Paparoditis, and J. Misener. Visibility Monitoring Using Conventional Roadside Cameras - Emerging Applications. *Transportation Research Part C: Emerging Technologies*, Vol. 22, 2012, pp. 17–28. https://doi.org/10.1016/j.trc.2011.11.012.

243. Ozcan, K., A. Sharma, S. Knickerbocker, J. Merickel, N. Hawkins, and M. Rizzo. Road Weather Condition Estimation Using Fixed and Mobile Based Cameras. *Advances in Computer Vision. CVC 2019. Advances in Intelligent Systems and Computing*, Vol. 943, 2020, pp. 192–204.

244. Khan, M. N., and M. M. Ahmed. Weather and Surface Condition Detection Based on Road-Side Webcams: Application of Pre-Trained Convolutional Neural Network. *International Journal of Transportation Science and Technology*, 2021. https://doi.org/10.1016/j.ijtst.2021.06.003.

245. Ibrahim, M. R., and J. Haworth. WeatherNet : Recognising Weather and Visual Conditions from Street-Level Images Using Deep Residual Learning. *International Journal of Geo-Information*, Vol. 8, No. 12, 2019, p. 549.

246. Chu, W. T., X. Y. Zheng, and D. S. Ding. Image2weather: A Large-Scale Image Dataset for Weather Property Estimation. *IEEE 2nd International Conference on Multimedia Big Data*, 2016, pp. 137–144. https://doi.org/10.1109/BigMM.2016.9.

247. Guerra, J. C. V., Z. Khanam, S. Ehsan, R. Stolkin, and K. McDonald-Maier. Weather Classification: A New Multi-Class Dataset, Data Augmentation Approach and Comprehensive Evaluations of Convolutional Neural Networks. *2018 NASA/ESA Conference on Adaptive Hardware and Systems (AHS)*, 2018, pp. 305–310.

248. Pomerleau, D. Visibility Estimation from a Moving Vehicle Using the RALPH Vision System. *Proceedings of IEEE Conference on Intelligent Transportation Systems*. 906–911.

249. Yan, X., Y. Luo, and X. Zheng. Weather Recognition Based on Images Captured by Vision System in Vehicle. *In International Symposium on Neural Networks*, 2009, pp. 390–398. https://doi.org/10.1007/978-3-642-01513-7_42.

250. Khan, M. N., and M. M. Ahmed. Trajectory-Level Fog Detection Based on in-Vehicle Video Camera with TensorFlow Deep Learning Utilizing SHRP2 Naturalistic Driving Data. *Accident Analysis and Prevention*, Vol. 142, 2020. https://doi.org/10.1016/j.aap.2020.105521.

251. Qian, Y., E. J. Almazan, and J. H. Elder. Evaluating Features and Classifiers for Road Weather Condition Analysis. *International Conference on Image Processing, ICIP*, 2016, pp. 4403–4407. https://doi.org/10.1109/ICIP.2016.7533192.

252. Kawai, S., K. Takeuchi, K. Shibata, and Y. Horita. A Smart Method to Distinguish Road Surface Conditions at Night-Time Using a Car-Mounted Camera. *IEEJ Transactions on Electronics, Information and Systems*, Vol. 134, No. 6, 2014, pp. 878–884. https://doi.org/10.1541/ieejeiss.134.878.

253. Bronte, S., L. M. Bergasa, and P. F. Alcantarilla. Fog Detection System Based on Computer Vision Techniques. *2009 12th International IEEE Conference on Intelligent Transportation Systems*, No. November, 2009. https://doi.org/10.1109/ITSC.2009.5309842.

254. Gallen, R., A. Cord, N. Hautière, and D. Aubert. Towards Night Fog Detection through Use of In-Vehicle Multipurpose Cameras. *IEEE Intelligent Vehicles Symposium*, 2011, pp. 399–404. https://doi.org/10.1109/IVS.2011.5940486.

255. Hautiére, N., R. Labayrade, and D. Aubert. Real-Time Disparity Contrast Combination for Onboard Estimation of the Visibility Distance. *IEEE Transactions on Intelligent Transportation Systems*, Vol. 7, No. 2, 2006, pp. 201–211.

256. Smadi, O., N. Hawkins, Z. Hans, B. A. Bektas, S. Knickerbocker, I. Nlenanya, R. Souleyrette, and S. Hallmark. Naturalistic Driving Study: Development of the Roadway Information Database. *SHRP 2 Report: S2-S04A-RW-1*, 2015.

257. Ahmed, M. M., M. Abdel-Aty, J. Lee, and R. Yu. Real-Time Assessment of Fog-Related Crashes Using Airport Weather Data : A Feasibility Analysis. *Accident Analysis and Prevention*, Vol. 72, 2014, pp. 309–317. https://doi.org/10.1016/j.aap.2014.07.004.

258. Agarwal, M., T. H. Maze, and R. Souleyrette. Impacts of Weather on Urban Freeway Traffic Flow Characteristics and Facility Capacity. *Proceedings of the 2005 mid-continent transportation research symposium.*, 2005.

259. Weng, J., L. Liu, and J. Rong. Impacts of Traffic Characteristics According to Snowy Weather Conditions on an Expressway. *Discrete Dynamics in Nature and Society*, Vol. 2013, 2013, pp. 1–6.

260. Mueller, F. H. History of Observational Instructions on Fog. *Key Meteorological Records Documentation No. 3.031*, 1959, pp. 1–8.

261. Murphy, R., R. Swick, B. A. Hamilton, and G. Guevara. *Best Practices for Road Weather Management. Version 3.0*. 2012.

262. Sebastiani, F. Machine Learning in Automated Text Categorization. *ACM computing surveys (CSUR)*, Vol. 34, No. 1, 2002, pp. 1–47.

263. Abadi, M., J. D. Paul Barham, Jianmin Chen, Zhifeng Chen, Andy Davis, M. K. Matthieu Devin, Sanjay Ghemawat, Geoffrey Irving, Michael Isard, P. T. Josh Levenberg, Rajat Monga, Sherry Moore, Derek G. Murray, Benoit Steiner, and Y. Y. X. Z. Vijay Vasudevan, Pete Warden, Martin Wicke. TensorFlow: A System for Large-Scale Machine Learning. *OSDI*, Vol. 16, 2016, pp. 265–283.

264. Bosch, A., A. Zisserman, and X. Munoz. Image Classification Using Random Forests and Ferns. *In Computer Vision, 2007. ICCV 2007. IEEE 11th International Conference.*, 2007. https://doi.org/10.1109/ICCV.2007.4409066.

265. Haralick, R., K. Shanmugam, and I. Dinstein. Textural Features for Image Classification.

IEEE Transactions on systems, man, and cybernetics, Vol. 6, 1973, pp. 610–621.

266. Gebejes, A., and R. Huertas. Texture Characterization Based on Grey-Level Co-Occurrence Matrix. *Proceedings in Conference of Informatics and Management Sciences*, 2013.

267. Ojala, T., M. Pietikäinen, and D. Harwood. A Comparative Study of Texture Measures with Classification Based on Featured Distributions. *Pattern Recognition*, Vol. 29, No. 1, 1996, pp. 51–59. https://doi.org/10.1016/0031-3203(95)00067-4.

268. Khan, M. N., A. Das, M. M. Ahmed, and S. S. Wulff. Multilevel Weather Detection Based on Images: A Machine Learning Approach with Histogram of Oriented Gradient and Local Binary Pattern Based Features. *Journal of Intelligent Transportation Systems: Technology, Planning, and Operations*, 2021. https://doi.org/10.1080/15472450.2021.1944860.

269. Ojala, T., M. Pietikäinen, and T. Mäenpää. Multiresolution Gray-Scale and Rotation Invariant Texture Classification with Local Binary Patterns. *IEEE Transactions on Pattern Analysis and Machine Intelligence*, Vol. 24, No. 7, 2002, pp. 971–987. https://doi.org/10.1109/TPAMI.2002.1017623.

270. Ahonen, T., A. Hadid, and M. Pietikäinen. Face Description with Local Binary Patterns: Application to Face Recognition. *IEEE Transactions on Pattern Analysis and Machine Intelligence*, Vol. 28, No. 12, 2006, pp. 2037–2041. https://doi.org/10.1109/TPAMI.2006.244.

271. Suthaharan, S. Support Vector Machine - Machine Learning Models and Algorithms for Big Data Classification., Springer, Boston, MA, pp. 207–235.

272. Saimadhu Polamuri. How the Random Forest Algorithm Works in Machine Learning. https://dataaspirant.com/2017/05/22/random-forest-algorithm-machine-learing/. Accessed Jul. 12, 2018.

273. Khan, M. N., and M. M. Ahmed. Development of a Novel Convolutional Neural Network Architecture Named RoadweatherNet for Trajectory-Level Weather Detection Using SHRP2 Naturalistic Driving Data. *Transportation Research Record: Journal of the Transportation Research Board*, 2021, pp. 1–15. https://doi.org/10.1177/03611981211005470.

274. Gaweesh, S. M., M. N. Khan, and M. M. Ahmed. Development of a Novel Framework for Hazardous Materials Placard Recognition System to Conduct Commodity Flow Studies Using Artificial Intelligence AlexNet Convolutional Neural Network. *Transportation Research Record: Journal of the Transportation Research Board*, Vol. In-Press, 2021, pp. 1–18.

275. Google. TensorFlow. https://opensource.google.com/projects/tensorflow. Accessed Jul. 26, 2018.

276. Karn, U. Introduction to Neural Networks. https://ujjwalkarn.me/2016/08/09/quick-intro-neural-networks/. Accessed Jul. 24, 2018.

277. TensorFlow. Cross-Entropy with Logit. https://www.tensorflow.org/api_docs/python/tf/nn/sigmoid_cross_entropy_with_logits.

Accessed Jul. 25, 2018.

278. Niklas Donges. Gradient Descent in a Nutshell – Towards Data Science. https://towardsdatascience.com/gradient-descent-in-a-nutshell-eaf8c18212f0. Accessed Jul. 25, 2018.

279. Kingma, D. P., and J. L. Ba. Adam: A Method for Stochastic Optimization. *arXiv:1412.6980*, 2014.

280. Lipton, Z. C., J. Berkowitz, and C. Elkan. A Critical Review of Recurrent Neural Networks for Sequence Learning. 2015, pp. 1–38. https://doi.org/10.1145/2647868.2654889.

281. Beaufays, F., H. Sak, and A. Senior. Long Short-Term Memory Recurrent Neural Network Architectures for Large Scale Acoustic Modeling Has. *Interspeech*, No. September, 2014, pp. 338–342. https://doi.org/arXiv:1402.1128.

282. Zaremba, W., I. Sutskever, and O. Vinyals. Recurrent Neural Network Regularization. No. 2013, 2014, pp. 1–8. https://doi.org/ng.

283. Chu, J. L., and A. Krzyżak. Analysis of Feature Maps Selection in Supervised Learning Using Convolutional Neural Networks, Springer, Cham, pp. 59–70.

284. Krizhevsky, A., I. Sutskever, and G. E. Hinton. ImageNet Classification with Deep Convolutional Neural Networks. *Advances in Neural Information Processing Systems*, 2012, pp. 1097–1105.

285. Simonyan, K., and A. Zisserman. Very Deep Convolutional Networks for Large-Scale Image Recognition. *arXiv preprint arXiv:1409.1556*, 2015.

286. Sermanet, P., D. Eigen, X. Zhang, M. Mathieu, R. Fergus, and Y. Lecun. OverFeat: Integrated Recognition, Localization and Detection Using Convolutional Networks. *In ICLR*, 2014.

287. Ke, Q., J. Liu, M. Bennamoun, S. An, F. Sohel, and F. Boussaid. Computer Vision for Human-Machine Interaction. In *Computer Vision For Assistive Healthcare*, Elsevier Inc., pp. 127–145.

288. Yeoh, Y. J., T. Morie, and H. Tamukoh. A Hardware-Oriented Dropout Algorithm for Efficient FPGA Implementation. *Neural Information Processing - ICONIP 2017*, Vol. 10639 LNCS, 2017, pp. 821–829. https://doi.org/10.1007/978-3-319-70136-3_87.

289. Goodfellow, I., Y. Bengio, and A. Courville. *Deep Learning*. MIT Press, 2016.

290. Nair, V., and G. E. Hinton. Rectified Linear Units Improve Restricted Boltzmann Machines. *27 th International Conference on Machine Learning*.

291. Deeplizard. Deep Learning & Deep Learning Fundamentals. https://deeplizard.com/learn/video/gZmobeGL0Yg. Accessed Nov. 30, 2020.

292. Chicco, D. Ten Quick Tips for Machine Learning in Computational Biology. *BioData Mining*, Vol. 10, No. 1, 2017, pp. 1–17. https://doi.org/10.1186/s13040-017-0155-3.

293. Patle, A., and D. S. Chouhan. SVM Kernel Functions for Classification. *2013 International Conference on Advances in Technology and Engineering (ICATE)*, 2013, pp.

1–9.

294. He, K., X. Zhang, S. Ren, and J. Sun. Deep Residual Learning for Image Recognition. *IEEE Computer Society Conference on Computer Vision and Pattern Recognition*, Vol. 2016-Decem, 2016, pp. 770–778. https://doi.org/10.1109/CVPR.2016.90.

295. Szegedy, C., W. Liu, Y. Jia, P. Sermanet, S. Reed, D. Anguelov, D. Erhan, V. Vanhoucke, and A. Rabinovich. Going Deeper with Convolutions. *IEEE Computer Society Conference on Computer Vision and Pattern Recognition*, 2015, pp. 1–9. https://doi.org/10.1109/CVPR.2015.7298594.

296. Zhang, X., X. Zhou, M. Lin, and J. Sun. ShuffleNet: An Extremely Efficient Convolutional Neural Network for Mobile Devices. *IEEE Computer Society Conference on Computer Vision and Pattern Recognition*, 2018, pp. 6848–6856. https://doi.org/10.1109/CVPR.2018.00716.

297. Iandola, F. N., S. Han, M. W. Moskewicz, K. Ashraf, W. J. Dally, and K. Keutzer. SqueezeNet: AlexNet-Level Accuracy with 50x Fewer Parameters and <0.5MB Model Size. *arXiv:1602.07360v4*, 2016.

298. Mori, K., T. Takahashi, I. Ide, H. Murase, T. Miyahara, and Y. Tamatsu. Fog Density Recognition by In-Vehicle Camera and Millimeter Wave Radar. *International Journal of Innovative Computing, Information and Control*, Vol. 3, No. 5, 2007, pp. 1173–1182.

299. Roser, M., and F. Moosmann. Classification of Weather Situations on Single Color Images. *IEEE Intelligent Vehicles Symposium*, 2008, pp. 798–803. https://doi.org/10.1109/IVS.2008.4621205.

300. Lu, C., D. Lin, J. Jia, and C. K. Tang. Two-Class Weather Classification. *IEEE Transactions on Pattern Analysis and Machine Intelligence*, Vol. 39, No. 12, 2017, pp. 2510–2524. https://doi.org/10.1109/TPAMI.2016.2640295.

301. Ajayi, G. O., and Z. Wang. Multi-Class Weather Classification from Still Image Using Said Ensemble Method. *2019 Southern African Universities Power Engineering Conference/Robotics and Mechatronics/Pattern Recognition Association of South Africa*, 2019, pp. 135–140. https://doi.org/10.1109/RoboMech.2019.8704783.

302. Zhao, B., X. Li, X. Lu, and Z. Wang. A CNN–RNN Architecture for Multi-Label Weather Recognition. *Neurocomputing*, Vol. 322, 2018, pp. 47–57. https://doi.org/10.1016/j.neucom.2018.09.048.

303. Ali, E. M., M. N. Khan, and Mohamed Ahmed. Real-Time Snowy Weather Detection Based on Machine Vision and Vehicle Kinematics: A Non-Parametric Data Fusion Analysis Protocol. *99th Transportation Research Board Annual Meeting*, 2020.

304. FHWA. How Do Weather Events Impact Roads?

305. US Department of Transportation Federal Highway Administration. Integrated Corridor Management (ICM) Demonstration Sites. *Fact Sheet*.

306. Brackstone, M., and M. McDonald. Car-Following: A Historical Review. *Transportation Research Part F: Traffic Psychology and Behaviour*, Vol. 2, No. 4, 1999, pp. 181–196. https://doi.org/10.1016/S1369-8478(00)00005-X.

307. Aghabayk, K., M. Sarvi, W. Young, and L. Kautzsch. A Novel Methodology for Evolutionary Calibration of Vissim by Multi-Threading. *Proceedings of the Australasian Transport Research Forum, ATRF 2013*, No. October, 2013, pp. 1–15.

308. Toledo, T., M. E. Ben-Akiva, D. Darda, M. Jha, and H. N. Koutsopoulos. Calibration of Microscopic Traffic Simulation Models with Aggregate Data. *Transportation Research Record*, No. 1876, 2004, pp. 10–19. https://doi.org/10.3141/1876-02.

309. Henclewood, D., W. Suh, M. O. Rodgers, R. Fujimoto, and M. P. Hunter. A Calibration Procedure for Increasing the Accuracy of Microscopic Traffic Simulation Models. *Simulation*, Vol. 93, No. 1, 2017, pp. 35–47. https://doi.org/10.1177/0037549716673723.

310. Dowling, R., A. Skabardonis, J. Halkias, G. McHale, and G. Zammit. Guidelines for Calibration of Microsimulation Models: Framework and Applications. *Transportation Research Record*, No. 1876, 2004, pp. 1–9. https://doi.org/10.3141/1876-01.

311. Ossen, S., and S. P. Hoogendoorn. Validity of Trajectory-Based Calibration Approach of Car-Following Models in Presence of Measurement Errors. *Transportation Research Record: Journal of the Transportation Research Board*, Vol. 2088, 2008, pp. 117–125. https://doi.org/10.3141/2088-13.

312. Rakha, H., and Y. Gao. Calibration of Steady-State Car-Following Models Using Macroscopic Loop Detector Data. *Final Report: VT-2008-01*, 2010, pp. 1–24.

313. Ciuffo, B., V. Punzo, and M. Montanino. *The Calibration of Traffic Simulation Models: Report on the Assessment of Different Goodness of Fit Measures and Optimization Algorithms*. Luxembourg, 2012.

314. Treiber, M., and A. Kesting. Microscopic Calibration and Validation of Car-Following Models – A Systematic Approach. *Procedia - Social and Behavioral Sciences*, Vol. 80, 2013, pp. 922–939. https://doi.org/10.1016/j.sbspro.2013.05.050.

315. Punzo, V., B. Ciuffo, and M. Montanino. Can Results of Car-Following Model Calibration Based on Trajectory Data Be Trusted? *Transportation Research Record: Journal of the Transportation Research Board*, Vol. 2315, 2012, pp. 89–99. https://doi.org/10.3141/2315-02.

316. Hamdar, S. H., H. S. Mahmassani, and M. Treiber. From Behavioral Psychology to Acceleration Modeling: Calibration, Validation, and Exploration of Drivers' Cognitive and Safety Parameters in a Risk-Taking Environment. *Transportation Research Part B: Methodological*, Vol. 78, 2015, pp. 32–53. https://doi.org/10.1016/j.trb.2015.03.011.

317. Reiter, U. Empirical Studies as Basis for Traffic Flow Models. *Proceedings of the Second International Symposium on Highway Capacity*, Vol. 2, 1994, pp. 493–502.

318. U.S. Department of Transportation. Next Generation Simulation (NGSIM). *Traffic Analysis Tools*.

319. Hedlund, J. SHRP2 Naturalistic Driving Study: The First Data Analysis Studies. *Journal of Safety Research*, Vol. 54, 2015, pp. 3–4. https://doi.org/10.1016/j.jsr.2015.06.002.

320. Rakha, H., M. Farzaneh, M. Arafeh, and E. Sterzin. Inclement Weather Impacts on Freeway Traffic Stream Behavior. *Transportation Research Record*, No. 2071, 2008, pp. 8–18. https://doi.org/10.3141/2071-02.

321. Rahman, A., and N. E. Lownes. Analysis of Rainfall Impacts on Platooned Vehicle Spacing and Speed. *Transportation Research Part F: Traffic Psychology and Behaviour*, Vol. 15, No. 4, 2012, pp. 395–403. https://doi.org/10.1016/j.trf.2012.03.004.

322. Hamdar, S. H., L. Qin, and A. Talebpour. Weather and Road Geometry Impact on Longitudinal Driving Behavior: Exploratory Analysis Using an Empirically Supported Acceleration Modeling Framework. *Transportation Research Part C: Emerging Technologies*, Vol. 67, 2016, pp. 193–213. https://doi.org/10.1016/j.trc.2016.01.017.

323. Kittelson, W., and M. Vandehey. *Incorporating Travel Time Reliability into the Highway Capacity Manual*. 2014.

324. Jung, S., X. Qin, and D. A. Noyce. Modeling Highway Safety and Simulation in Rainy Weather. *Transportation Research Record: Journal of the Transportation Research Board*, No. 2237, 2011, pp. 134–143. https://doi.org/10.3141/2237-15.

325. Hou, T., H. Mahmassani, R. Alfelor, J. Kim, and M. Saberi. Calibration of Traffic Flow Models under Adverse Weather and Application in Mesoscopic Network Simulation. *Transportation Research Record*, No. 2391, 2013, pp. 92–104. https://doi.org/10.3141/2391-09.

326. Golshan Khavas, R., B. Hellinga, and A. Zarinbal Masouleh. Identifying Parameters for Microsimulation Modeling of Traffic in Inclement Weather. *Transportation Research Record: Journal of the Transportation Research Board*, Vol. 2613, No. 1, 2017, pp. 52–60. https://doi.org/10.3141/2613-07.

327. Hoogendoorn, R. G., S. P. Hoogendoorn, K. A. Brookhuis, and W. Daamen. Longitudinal Driving Behavior under Adverse Conditions: A Close Look at Psycho-Spacing Models. *Procedia - Social and Behavioral Sciences*, Vol. 20, 2011, pp. 536–546. https://doi.org/10.1016/j.sbspro.2011.08.060.

328. Soria, I. S., and L. Elefteriadou. Assessment of Car-Following Models Using Field Data. 2011.

329. Milliken, J. G., F. M. Council, T. W. Gainer, N. J. Garber, K. M. Gebbie, J. W. Hall, C. Lave, J. M. Mason, F. Mosteller, and R. P. Weaver. Managing Speed: Review of Current Practice for Setting and Enforcing Speed Limits. Transportation Research Board. Committee for Guidance on Setting and Enforcing Speed Limits, , 1998.

330. Lee, C., B. Hellinga, and F. Saccomanno. Evaluation of Variable Speed Limits to Improve Traffic Safety. *Transportation research part C: emerging technologies*, Vol. 14, No. 3, 2006, pp. 213–228.

331. Abdel-Aty, M., J. Dilmore, and L. Hsia. Applying Variable Speed Limits and the Potential for Crash Migration. *Transportation Research Record: Journal of the Transportation Research Board*, Vol. 1953, No. 1953, 2006, pp. 21–30. https://doi.org/10.3141/1953-03.

332. Hellinga, B., and M. Mandelzys. Impact of Driver Compliance on the Safety and Operational Impacts of Freeway Variable Speed Limit Systems. *Journal of Transportation Engineering*, Vol. 137, No. 4, 2011, pp. 260–268.

333. Lee, J., D. J. Dailey, J. Bared, and B. Park. Variable Speed Limit System for Elk Mountain Corrido. *British Journal of Clinical Pharmacology*, Vol. 76, No. 5, 2013, pp.

776–786. https://doi.org/10.1111/bcp.12106.

334. Hadiuzzaman, M., J. Fang, M. A. Karim, Y. Luo, and T. Z. Qiu. Modeling Driver Compliance to VSL and Quantifying Impacts of Compliance Levels and Control Strategy on Mobility and Safety. *Journal of Transportation Engineering*, 2015. https://doi.org/10.1061/(ASCE)TE.1943-5436.0000795.

335. Müller, E. R., R. C. Carlson, W. Kraus, and M. Papageorgiou. Microsimulation Analysis of Practical Aspects of Traffic Control with Variable Speed Limits. *IEEE Transactions on Intelligent Transportation Systems*, 2015. https://doi.org/10.1109/TITS.2014.2374167.

336. Sadat, M., and H. B. Celikoglu. Simulation-Based Variable Speed Limit Systems Modelling: An Overview and A Case Study on Istanbul Freeways. 2017.

337. Conran, C. A., and C. A. Conran. Modeling Microscopic Driver Behavior under Variable Speed Limits: A Driving Simulator and Integrated MATLAB-VISSIM Study. 2017.

338. RAMA, P., and T. R. Board. EFFECTS OF WEATHER-CONTROLLED VARIABLE SPEED LIMITS AND WARNING SIGNS ON DRIVER BEHAVIOR. *Transportation Research Record*, 1999. https://doi.org/10.1097/OGX.0000000000000256.Prenatal.

339. Robinson, M. D. Examples of Variable Speed Limit Applications. *speed management workshop*.

340. Perrin, J., P. T. Martin, and B. Coleman. Testing the Adverse Visibility Information System Evaluation (ADVISE) - Safer Driving in Fog. *TRB 81st Annual Meeting Compendium of Papers*, 2002. https://doi.org/10.1016/S0277-5387(00)81478-3.

341. Katz, B., C. ODonnell, K. Donoughe, J. Atkinson, M. Finley, K. Balke, B. Kuhn, and D. Warren Brudis. Guidelines for the Use of Variable Speed Limit Systems in Wet Weather. *FHWA Safety Program, Report No.: FHWA-SA-12-022 Technical*, 2012.

342. Buddemeyer, J., R. Young, V. Sabawat, and E. Layton. Variable Speed Limit System for Elk Mountain Corridor. *FINAL REPORT: FHWA-WY-10/04F*, No. October, 2010.

343. Young, R., V. Sabawat, P. Saha, and Y. Sui. Rural Variable Speed Limits: Phase II. *FINAL REPORT: FHWA-WY-13/03F*, No. May, 2012.

344. Sabawat, V., and R. Young. Control Strategy for Rural Variable Speed Limit Corridor. *Transportation Research Record: Journal of the Transportation Research Board*, 2013. https://doi.org/10.3141/2329-05.

345. Kim, J., H. Mahmassani, R. Alfelor, Y. Chen, T. Hou, L. Jiang, M. Saberi, Ö. Verbas, and A. Zockaie. Implementation and Evaluation of Weather-Responsive Traffic Management Strategies. *Transportation Research Record: Journal of the Transportation Research Board*, 2013. https://doi.org/10.3141/2396-11.

346. Li, Z., Y. Li, P. Liu, W. Wang, and C. Xu. Development of a Variable Speed Limit Strategy to Reduce Secondary Collision Risks during Inclement Weathers. *Accident Analysis & Prevention*, Vol. 72, 2014, pp. 134–145.

347. Promothes Saha, Mohamed M. Ahmed, and Rhonda Kae Young. Safety Effectiveness of Variable Speed Limit System in Adverse Weather Conditions on Challenging Roadway Geometry. *Transportation Research Record: Journal of the Transportation Research*

Board, No. 2521, 2015, pp. 45–53. https://doi.org/10.3141/2521-05.

348. Choi, S., and C. Oh. Proactive Strategy for Variable Speed Limit Operations on Freeways under Foggy Weather Conditions. *Transportation Research Record*, 2016. https://doi.org/10.3141/2551-04.

349. Pisano, P. Road Weather and the Connected Vehicle: Improving Road Weather Awareness. 2011, p. 2.

350. Hill, C. J. Concept of Operations for Road Weather Connected Vehicle Applications. 2013, p. 170.

351. Hammit, B., and R. Young. Connected Vehicle Weather Data for Operation of Rural Variable Speed Limit Corridors. 2015.

352. Li, Y., H. Wang, W. Wang, S. Liu, and Y. Xiang. Reducing the Risk of Rear-End Collisions with Infrastructure-to-Vehicle (I2V) Integration of Variable Speed Limit Control and Adaptive Cruise Control System. *Traffic Injury Prevention*, 2016. https://doi.org/10.1080/15389588.2015.1121384.

353. Li, Y., C. Xu, L. Xing, and W. Wang. Integrated Cooperative Adaptive Cruise and Variable Speed Limit Controls for Reducing Rear-End Collision Risks Near Freeway Bottlenecks Based on Micro-Simulations. *IEEE Transactions on Intelligent Transportation Systems*, 2017. https://doi.org/10.1109/TITS.2017.2682193.

354. Paikari, E., S. Tahmasseby, and B. Far. A Simulation-Based Benefit Analysis of Deploying Connected Vehicles Using Dedicated Short Range Communication. 2014.

355. Grumert, E., X. Ma, and A. Tapani. Analysis of a Cooperative Variable Speed Limit System Using Microscopic Traffic Simulation. *Transportation Research Part C: Emerging Technologies*, 2015. https://doi.org/10.1016/j.trc.2014.11.004.

356. Khondaker, B., and L. Kattan. Variable Speed Limit: A Microscopic Analysis in a Connected Vehicle Environment. *Transportation Research Part C: Emerging Technologies*, Vol. 58, 2015, pp. 146–159. https://doi.org/10.1016/j.trc.2015.07.014.

357. Talebpour, A., H. S. Mahmassani, and F. E. Bustamante. Modeling Driver Behavior in a Connected Environment: Integrated Microscopic Simulation of Traffic and Mobile Wireless Telecommunication Systems. *Transportation Research Record*, 2016. https://doi.org/10.3141/2560-09.

358. Smith, S., and M. Razo. Using Traffic Microsimulation to Assess Deployment Strategies for the Connected Vehicle Safety Pilot. *Journal of Intelligent Transportation Systems: Technology, Planning, and Operations*, 2016. https://doi.org/10.1080/15472450.2014.889941.

359. Wang, M., W. Daamen, S. P. Hoogendoorn, and B. van Arem. Connected Variable Speed Limits Control and Car-Following Control with Vehicle-Infrastructure Communication to Resolve Stop-and-Go Waves. *Journal of Intelligent Transportation Systems: Technology, Planning, and Operations*, 2016. https://doi.org/10.1080/15472450.2016.1157022.

360. Li, D., Y. Zhao, P. Ranjitkar, H. Zhao, and Q. Bai. Hybrid Approach for Variable Speed Limit Implementation and Application to Mixed Traffic Conditions with Connected Autonomous Vehicles. *IET Intelligent Transport Systems*, 2018.

https://doi.org/10.1049/iet-its.2017.0090.

361. Grumert, E. F., and A. Tapani. Using Connected Vehicles in a Variable Speed Limit System. 2017.

362. Fountoulakis, M., N. Bekiaris-Liberis, C. Roncoli, I. Papamichail, and M. Papageorgiou. Highway Traffic State Estimation with Mixed Connected and Conventional Vehicles: Microscopic Simulation-Based Testing. *Transportation Research Part C: Emerging Technologies*, 2017. https://doi.org/10.1016/j.trc.2017.02.015.

363. Rahman, M. S., M. Abdel-Aty, L. Wang, and J. Lee. Understanding the Highway Safety Benefits of Different Approaches of Connected Vehicles in Reduced Visibility Conditions. *Transportation Research Record, ,* 2018. https://doi.org/10.1177/0361198118776113.

364. Gettman, D., and L. Head. Surrogate Safety Measures from Traffic Simulation Models. *Transportation Research Record: Journal of the Transportation Research Board*, 2003. https://doi.org/10.3141/1840-12.

365. Gettman, D., T. Sayed, L. Pu, and S. Shelby. Surrogate Safety Assessment Model and Validation. *Fhwa-Hrt-08--51*, No. June, 2008, p. 322. https://doi.org/10.3109/17453674.2011.581265.

366. Ozbay, K., H. Yang, B. Bartin, and S. Mudigonda. Derivation and Validation of New Simulation-Based Surrogate Safety Measure. *Transportation Research Record: Journal of the Transportation Research Board*, 2008. https://doi.org/10.3141/2083-12.

367. Dijkstra, A., P. Marchesini, F. Bijleveld, V. Kars, H. Drolenga, and M. van Maarseveen. Do Calculated Conflicts in Microsimulation Model Predict Number of Crashes? *Transportation Research Record: Journal of the Transportation Research Board*, 2010. https://doi.org/10.3141/2147-13.

368. Huang, F., P. Liu, H. Yu, and W. Wang. Identifying If VISSIM Simulation Model and SSAM Provide Reasonable Estimates for Field Measured Traffic Conflicts at Signalized Intersections. *Accident Analysis and Prevention*, 2013. https://doi.org/10.1016/j.aap.2012.08.018.

369. Essa, M., and T. Sayed. Simulated Traffic Conflicts: Do They Accurately Represent Field-Measured Conflicts? *Transportation Research Record: Journal of the Transportation Research Board*, 2015. https://doi.org/10.3141/2514-06.

370. Young, W., A. Sobhani, M. G. Lenné, and M. Sarvi. Simulation of Safety: A Review of the State of the Art in Road Safety Simulation Modelling. *Accident Analysis and Prevention*, 2014. https://doi.org/10.1016/j.aap.2014.01.008.

371. Habtemichael, F., and L. de Picado Santos. Safety and Operational Benefits of Variable Speed Limits Under Different Traffic Conditions and Driver Compliance Levels. *Transportation Research Record: Journal of the Transportation Research Board*, 2013. https://doi.org/10.3141/2386-02.

372. Fan, R., W. Wang, P. Liu, and H. Yu. Using VISSIM Simulation Model and Surrogate Safety Assessment Model for Estimating Field Measured Traffic Conflicts at Freeway Merge Areas. *IET Intelligent Transport Systems*, 2013. https://doi.org/10.1049/iet-

its.2011.0232.

373. Arash Olia, G. W., and S. N. Razavi. Microsimulation Based Impact Assessment of the Vehicle to Vehicle (V2V) System for Work Zone Safety. *CSCE 2013 General Conference*, No. June, 2013, pp. 0–10.

374. Genders, B. W., S. Faculty, E. C. Engineering, T. Submitted, D. Masters, and W. Genders. A Microsimulation Approach Assessing the Impact of Connected Vehicle on Work Zone Traffic Safety. No. October, 2014.

375. Genders, W., and S. N. Razavi. Impact of Connected Vehicle on Work Zone Network Safety through Dynamic Route Guidance. *Journal of Computing in Civil Engineering*, 2016. https://doi.org/10.1061/(ASCE)CP.1943-5487.0000490.

376. Fyfe, M., and T. Sayed. Safety Evaluation of Connected Vehicles for a Cumulative Travel Time Adaptive Signal Control Microsimulation Using the Surrogate Safety Assessment Model. *Transportation Research Board 96th Annual Meeting*, 2017.

377. Abdel-Aty, M., and L. Wang. Implementation of Variable Speed Limits to Improve Safety of Congested Expressway Weaving Segments in Microsimulation. *Transportation Research Procedia*, Vol. 27, 2017, pp. 577–584. https://doi.org/10.1016/j.trpro.2017.12.061.

378. Peng, Y., M. Abdel-Aty, Q. Shi, and R. Yu. Assessing the Impact of Reduced Visibility on Traffic Crash Risk Using Microscopic Data and Surrogate Safety Measures. *Transportation Research Part C: Emerging Technologies*, Vol. 74, 2017, pp. 295–305. https://doi.org/10.1016/j.trc.2016.11.022.

379. Yang, G., M. M. Ahmed, and S. Gaweesh. Impact of Variable Speed Limit in a Connected Vehicle Environment on Truck Driver Behavior under Adverse Weather Conditions: Driving Simulator Study. *Transportation Research Record*, Vol. 2673, No. 7, 2019, pp. 132–142. https://doi.org/10.1177/0361198119842111.

380. Yang, G., M. Ahmed, S. Gaweesh, and E. Adomah. Connected Vehicle Real-Time Traveler Information Messages for Freeway Speed Harmonization under Adverse Weather Conditions: Trajectory Level Analysis Using Driving Simulator. *Accident Analysis and Prevention*, Vol. 146, No. October 2019, 2020, p. 105707. https://doi.org/10.1016/j.aap.2020.105707.

381. Yang, G., M. Ahmed, and E. Adomah. An Integrated Microsimulation Approach for Safety Performance Assessment of the Wyoming Connected Vehicle Pilot Deployment Program. *Accident Analysis and Prevention*, Vol. 146, 2020, p. 105714.

382. Ahmed, M. M., G. Yang, and S. Gaweesh. Assessment of Drivers' Perceptions of Connected Vehicle–Human Machine Interface for Driving Under Adverse Weather Conditions: Preliminary Findings From Wyoming. *Frontiers in Psychology*, Vol. 11, No. August, 2020, pp. 1–12. https://doi.org/10.3389/fpsyg.2020.01889.

383. Subedi, B., S. M. Gaweesh, G. Yang, and M. M. Ahmed. Connected Vehicle Training Framework and Lessons Learned to Improve Safety of Highway Patrol Troopers. *Transportation Research Record*, Vol. 2674, No. 12, 2020, pp. 447–463. https://doi.org/10.1177/0361198120957309.

384. Yang, G., M. M. Ahmed, and B. Subedi. Distraction of Connected Vehicle Human–Machine Interface for Truck Drivers. *Transportation Research Record: Journal of the Transportation Research Board*, 2020, p. 036119812092969. https://doi.org/10.1177/0361198120929692.

385. Raddaoui, O., M. M. Ahmed, and S. M. Gaweesh. Assessment of the Effectiveness of Connected Vehicle Weather and Work Zone Warnings in Improving Truck Driver Safety. *IATSS Research*, Vol. 44, No. 3, 2020, pp. 230–237. https://doi.org/10.1016/j.iatssr.2020.01.001.

386. Raddaoui, O., and M. M. Ahmed. Evaluating the Effects of Connected Vehicle Weather and Work Zone Warnings on Truck Drivers' Workload and Distraction Using Eye Glance Behavior. *Transportation Research Record: Journal of the Transportation Research Board*, Vol. 2674, No. 3, 2020, pp. 293–304. https://doi.org/10.1177/0361198120910743.

387. Khoda Bakhshi, A., S. M. Gaweesh, and M. M. Ahmed. The Safety Performance of Connected Vehicles on Slippery Horizontal Curves through Enhancing Truck Drivers' Situational Awareness: A Driving Simulator Experiment. *Transportation Research Part F: Traffic Psychology and Behaviour*, Vol. 79, 2021, pp. 118–138. https://doi.org/10.1016/j.trf.2021.04.017.

388. Adomah, E., A. Khoda Bakhshi, and M. M. Ahmed. Safety Impact of Connected Vehicles on Driver Behavior in Rural Work Zones under Foggy Weather Conditions. *Transportation Research Record: Journal of the Transportation Research Board*, 2021, p. 036119812110491. https://doi.org/10.1177/03611981211049147.

389. Khoda Bakhshi, A., and M. M. Ahmed. Accounting for Human-Related Unobserved Heterogeneity in the Safety Performance of Connected Vehicles: An Incorporation of Bayesian Hierarchical Negative Binomial into Simulated Work Zone Warning Application. *IATSS Research*, No. xxxx, 2021. https://doi.org/10.1016/j.iatssr.2021.06.005.

390. Hammit, B., R. James, and M. Ahmed. Radar-Vision Algorithms to Process the Trajectory-Level Driving Data in the SHRP2 Naturalistic Driving Study. *IEEE Conference on Intelligent Transportation Systems, Proceedings, ITSC*, Vol. 2018-Novem, 2018, pp. 2126–2133. https://doi.org/10.1109/ITSC.2018.8569688.

391. Das, A., and M. M. Ahmed. Adjustment of Key Lane Change Parameters to Develop Microsimulation Models for Representative Assessment of Safety and Operational Impacts of Adverse Weather Using SHRP2 Naturalistic Driving Data. *Journal of Safety Research*, Vol. In-Press, 2022.

392. Wiedemann, R. Original Code of W99.

393. Liu, G. W99 Car Following Model – How It Works.

394. Hammit, B., R. James, and M. Ahmed. A Case for Online Traffic Simulation: Systematic Procedure to Calibrate Car-Following Models Using Vehicle Data. *IEEE Conference on Intelligent Transportation Systems, Proceedings, ITSC*, Vol. 2018-Novem, 2018, pp. 3785–3790. https://doi.org/10.1109/ITSC.2018.8569684.

395. James, R. M., B. E. Hammit, and S. D. Boyles. Methods to Obtain Representative Car-

Following Model Parameters from Trajectory-Level Data for Use in Microsimulation. *Transportation Research Record: Journal of the Transportation Research Board*, Vol. 2673, No. 7, 2019, pp. 62–73. https://doi.org/10.1177/0361198119849401.

396. Ma;, J., H. Mahmassani;, J. K. Garrett;, E. Kim;, and M. Neuner. Implementation of Analysis, Modeling, and Simulation Tools for Road Weather Connected Vehicle Applications. *FHWA-HOP-20-060*, 2021.

397. Greenshields, B. D., J. R. Bibbins, W. S. Channing, and H. H. Miller. A Study of Traffic Capacity. *Proceedings of the 14th Annual Meeting of the Highway Research Board*, 1935.

398. Kitchener, F., R. Young, M. Ahmed, G. Yang, S. Gaweesh, T. English, V. Garcia, A. Ragan, N. Urena Serulle, and D. Gopalakrishna. Connected Vehicle Pilot Deployment Program : Phase 2 Final System Performance Report, Baseline Conditions – WYDOT CV Pilot. *FHWA-JPO-17-474*, 2018.

399. Christopher Tozzi. How to Measure Data Quality – Metrics to Assess Your Data. https://www.precisely.com/blog/data-quality/how-to-measure-data-quality-7-metrics. Accessed Sep. 16, 2021.

400. Tesla. Autopilot and Full Self-Driving Capability . https://www.tesla.com/support/autopilot. Accessed Sep. 25, 2020.

401. Ma, J., H. Mahmassani, J. K. Garrett, E. Kim, and M. Neuner. Implementation of Analysis, Modeling, and Simulation Tools for Road Weather Connected Vehicle Applications. *FHWA-HOP-20-060*, 2020.

402. Yang, G., and M. M. Ahmed. Analysis, Modeling and Simulation Framework for Performance Evaluation of the Wyoming Connected Vehicle Pilot Deployment Program. *Advances in Transportation Studies*, Vol. 2, No. Special Issue, 2020, pp. 1–14.

403. Gaweesh, S. M., A. Khoda Bakhshi, and M. M. Ahmed. Safety Performance Assessment of Connected Vehicles in Mitigating the Risk of Secondary Crashes: A Driving Simulator Study. *Transportation Research Record: Journal of the Transportation Research Board*, Vol. 80, 2021, p. 036119812110278. https://doi.org/10.1177/03611981211027881.

Acknowledgment

The research work was conducted under the second Strategic Highway Research Program (SHRP2), which is administrated by the Transportation Research Board of the National Academies of Sciences, Engineering, and Medicine, and it was sponsored by the Federal Highway Administration in cooperation with the American Association of State Highway and Transportation Officials (AASHTO) and the Wyoming Department of Transportation (WYDOT).